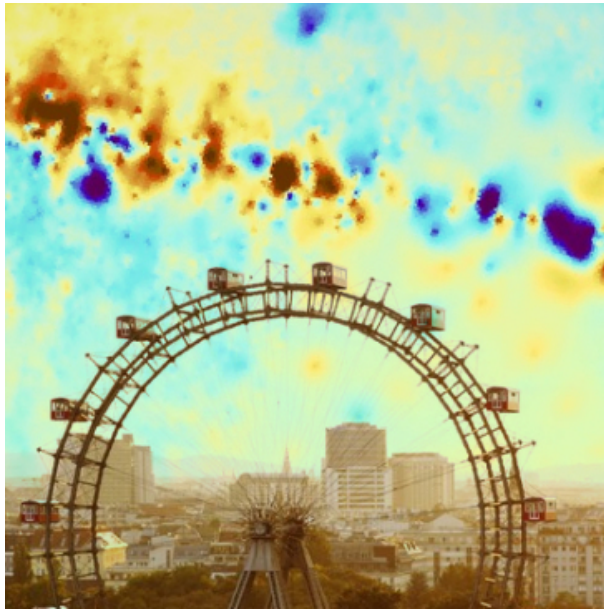


Proceedings of IAU Focus Meeting 8:

New Insights in Extragalactic Magnetic Fields

XXXth General Assembly of the
International Astronomical Union, Vienna 2018



L. Feretti, F. Govoni, G. Heald, *Editors*

**Invited and Contributed Talks
included in IAU Volume
“Astronomy in Focus”**

Content

L. Feretti, F. Govoni, G. Heald, L. Rudnick, M. Johnston-Hollitt, <i>New Insights in Extragalactic Magnetic Fields</i>	5
K. Subramanian, <i>Origins of Cosmic Magnetism</i>	9
T. Kahniashvili, A. Brandenburg, A. Kosowsky, S. Mandal, A. Roper Pol, <i>Magnetism in the Early Universe</i>	13
A. Bonafede, C. Stuardi, F. Savini, F. Vazza, M. Brüggen, <i>Constraining magnetic fields in galaxy clusters</i>	17
M. Brüggen, S. O’Sullivan, A. Bonafede, F. Vazza, <i>Magnetic fields in the intergalactic medium and in the cosmic web</i>	21
S. A. Mao, <i>Magnetism in the Square Kilometre Array Era</i>	25
J. M. Stil, <i>Capabilities of next generation telescopes for cosmic magnetism</i>	29
R.-J. Dettmar, V. Heesen, and the CHANG-ES Team, <i>A fresh view of magnetic fields and cosmic ray electrons in halos of spiral galaxies</i>	33
M. Kierdorf, S.A. Mao, A. Fletcher, R. Beck, M. Haverkorn, A. Basu, F. Tabatabaei, J. Ott, <i>The Magnetized Disk-Halo Transition Region of M51</i>	37
V. Vacca, F. Govoni, M. Murgia, T. Enßlin, N. Oppermann, L. Feretti, G. Giovannini, J. Jasche, H. Junklewitz, F. Loi, <i>Techinques and algorithmic advances in the SKA era</i>	41

Contributed Talks and Posters included in IAU Online Supplementary Material

Content

D.G. Yamazaki, <i>CMB weak lensing with the primordial magnetic field</i>	45
M. Langer, J.-B. Durrive, <i>Magnetizing the Intergalactic Medium during Reionization</i>	49
D. Sokoloff, <i>Small-scale dynamo as a mechanism for excitation of extragalactic mag- netic fields</i>	53
P. Barai, E.M. de Gouveia Dal Pino, (on behalf of CTA Collaboration), <i>Large-Scale Diffuse Intergalactic Magnetic Fields Constraints With the Cherenkov Telescope Array</i>	57
R.A. Batista, E. M. de Gouveia Dal Pino, K. Dolag, S. Hussain, <i>Cosmic-Ray propa- gation in the turbulent intergalactic medium</i>	61
A. Seta, A. Shukurov, P.J. Bushby, T.S. Wood, <i>On energy equipartition between cosmic rays and magnetic fields</i>	65
F. Loi, M. Murgia, F. Govoni, V. Vacca, I. Prandoni, H. Li, L. Feretti, G. Giovannini, <i>Simulations of the polarized sky for the SKA</i>	69
Y.K. Ma, S.A. Mao, J. Stil, A. Basu, J. West, C. Heiles, A. S. Hill, S. K. Betti, <i>From the NVSS RM Catalogue to Future Polarisation Surveys</i>	73
L. Chamandy, A. Shukurov, A.R. Taylor, <i>New Insights on Galactic Dynamos</i>	77
F.S. Tabatabaei, <i>The Role of Magnetic Fields in The Evolution of Galaxies</i>	81
C.L. Sarazin, R. Vijayaraghavan, P.M. Ricker, <i>Magnetic Fields and Ram Pressure Stripping of Galaxies in Clusters</i>	85
M. Ramos-Martínez, G. Gómez, <i>Magnetic fields in simulations of ram pressure stripped galaxies</i>	89
A. Basu, S.A. Mao, A. Fletcher, N. Kanekar, A. Shukurov, D. Schnitzeler, V. Vacca, H. Junkewitz, <i>Statistical properties of Faraday rotation measure from large-scale magnetic fields in intervening disc galaxies</i>	93
L. Rudnick, <i>Optimizing Faraday Background Grids</i>	97
B. Ruiz-Granados, E. Battaner, E. Florido, J.A. Rubiño-Martín, <i>Magnetic fields at the epoch of Reionization</i>	101

S. Hackstein, F. Vazza, M. Brüggen, J.G. Sorce, S. Gottlöber, <i>Propagation of UHECRs in the local Universe and origin of cosmic magnetic fields</i>	103
M. Cau, G. Giovannini, A. Ignesti, <i>Statistics and new detections of diffuse radio sources in galaxy clusters</i>	105
P. Domínguez-Fernández, F. Vazza, M. Brüggen, <i>Spectral analysis of magnetic fields in simulated galaxy clusters</i>	107
J.M. Stil, on behalf of the CHANG-ES collaboration, <i>CHANG-ES: an overview</i>	109
G. Heald, and the QUOCKA Team, <i>The QUOCKA Survey: Early Results</i>	111
M. Zajaček, V. Karas, <i>Magnetized stars embedded in AGN accretion disks and tori</i>	113
A. Janiuk, J. Mortier, K. Sapountzis, <i>Variability of magnetically-dominated jets in blazars and gamma ray bursts</i>	115
R. Beck, E. M. Berkhuijsen, <i>Magnetic Fields and Cosmic Ray Diffusion in M 31</i>	117
C. Horellou, A. Neld, D.D. Mulcahy, R. Beck, S. Bourke, T.D. Carozzi, K.T. Chyży, J.E. Conway, J.S. Farnes, A. Fletcher, M. Haverkorn, G. Heald, A. Horneffer, B. Nikiel-Wroczyński, R. Paladino, S.S. Sridhar, C.L. Van Eck, <i>Reliable detection and characterization of low-frequency polarized sources in the LOFAR M 51 field</i>	119
L.F.S. Rodrigues, L. Chamandy, A. Shukurov, C. M. Baugh, A.R. Taylor, <i>The evolution of large scale magnetic fields in spiral galaxies</i>	121
J.F. Hollins, G.R. Sarson, A. Shukurov, A. Fletcher, F.A. Gent, <i>The supernova-regulated ISM. Space- and time-correlations</i>	123
A. Shukurov, C.C. Evirgen, A. Fletcher, P.J. Bushby, F.A. Gent, <i>Magnetic field effects on the ISM structure and galactic outflows</i>	125
M. Krause, S.C. Mora-Partiarroyo, P. Schmidt, <i>Magnetic fields and CR propagation in the halos of spiral galaxies</i>	127
E. Lopez, J. Armijos, M. Llerena, F. Aldaz, <i>Magnetic field constraint in the outskirts of spiral galaxies</i>	129
Y. Stein, R.-J. Dettmar, J. Irwin, and the CHANG-ES Team <i>The CHANG-ES Galaxy NGC 4666</i>	131
S. Sur, <i>Faraday rotation from magnetic fields in young galaxies</i>	133

New Insights in Extragalactic Magnetic Fields

Luigina Feretti¹, Federica Govoni², George Heald³, Lawrence Rudnick⁴, and Melanie Johnston-Hollitt^{5,6}

¹INAF - Istituto di Radioastronomia, Via Gobetti 101, I-40129 Bologna, Italy

²INAF - Osservatorio Astronomico di Cagliari, Via della Scienza 5, I-09047 Selargius (CA), Italy

³CSIRO Astronomy and Space Science, PO Box 1130, Bentley WA 6102, Australia

⁴Minnesota Institute for Astrophysics, University of Minnesota, 116 Church St. SE, Minneapolis, MN 55455, USA

⁵International Centre for Radio Astronomy Research, Curtin University, Bentley, WA 6102, Australia

⁶Peripety Scientific Ltd., PO Box 11355 Manners Street, Wellington 6142, New Zealand

Abstract. In this contribution we introduce the motivation and goals of IAU Focus Meeting 8, “New Insights in Extragalactic Magnetic Fields”. We provide a background for the nine contributions included in these proceedings, as well as the online contributions. A recap of the meeting is provided in the form of audience feedback that was collected during the wrap-up session at the conclusion of FM8.

1. Introduction

Magnetic fields are a key ingredient of the extragalactic Universe on many different spatial scales, from individual galaxies and active galactic nuclei (AGN) to clusters of galaxies and the cosmic web. They play an important role in the process of large-scale structure formation and enrichment of the intergalactic medium, having effects on turbulence, cloud collapse, large-scale motions, heat and momentum transport, convection, viscous dissipation, etc. They are of utmost importance in the growth of radio galaxies and AGN and are crucial for the formation of spiral arms in spiral galaxies, outflows and star formation processes.

Despite their importance and ubiquity, magnetic fields remain poorly understood components of the Universe. The origin of the fields that are currently observed remains largely uncertain. A commonly accepted hypothesis is that they result from the amplification of much weaker pre-existing “seed” fields via shock/compression and/or turbulence/dynamo amplification during merger events, and different magnetic field scales survive as the result of turbulent motions. The origin of “seed” fields is unknown. They could be either “primordial”, i.e. generated in the early Universe prior to recombination, or produced locally at later epochs of the Universe, in early stars and/or (proto)galaxies, and then injected in the interstellar and intergalactic medium. The cosmic origin of magnetic “seed fields” and the subsequent processes through which they are amplified give us critical information on the growth of structure in the universe. The history of these processes can be uncovered through accurate knowledge of the strength and structure of magnetic fields in clusters, in the intergalactic medium, at the boundary of galaxy clusters, in the filamentary cosmic web, and in the relation of magnetic fields to gas flows in spiral galaxies, radio galaxies and AGN.

The coming years and decades will see a burst in our capacity to collect information

and to develop our understanding of extragalactic magnetic fields. This change is due to the next generation of radio astronomy facilities, especially the SKA and its pathfinders and precursors, as well as major advances in MHD numerical simulations and algorithmic improvements to extract magnetism information from the databases. The Focus Meeting brought together the scientific community to discuss the challenges and opportunities for understanding the magnetized Universe from scales of galaxies to the cosmic web and to connect information from across the spectrum, to address the fundamental questions that remain unanswered:

- How did magnetic fields form and evolve, and how are they maintained?
- How do they control the acceleration and dynamics of relativistic particles in astrophysical plasmas?
- How do magnetic fields affect the evolution of thermal plasma in galaxies and clusters?
- How do magnetic fields illuminate otherwise invisible processes in the thermal plasma?
- How do the insights from magnetic field studies contribute to the larger questions about origins and evolution of structures in the Universe, from galactic to cosmic web scales?

Most of what is known about magnetic fields in the Universe comes from sensitive observations at radio frequencies, which directly prove the existence of relativistic electrons gyrating around magnetic field lines. In addition, measurements of the Faraday rotation effect on the polarized emission of radio galaxies provide information on both the magnetic field strength and its structure. Beside studies at cm and mm wavelengths, magnetism can be investigated at a broader range of other wavelengths. Indeed, the density of the cluster thermal gas obtained from X-ray data is a crucial parameter for the interpretation of Rotation Measure data. In addition, upper bounds to the magnetic fields in voids and large scale structure can be obtained from studies of the Cosmic Microwave Background radiation anisotropies and dust polarization, and from studies of the multi-TeV gamma-ray flux of distant blazars, whose emission is deflected by the extragalactic magnetic fields.

Given the huge shift in processing capacity that will be required by the observational facilities seeking to provide new breakthroughs, the time was ripe to take stock of the state of the field and to understand our successes and opportunities. This Focus Meeting engaged the observational and theoretical communities to consider the results already in hand, to present new algorithms and numerical techniques for the interpretation of the observations, and to address underlying theoretical issues. With this approach, we hoped to accelerate our ability both to explore the massive volumes of data that will be delivered by next-generation instruments, toward our ultimate quest to obtain a deeper understanding of the magnetized Universe.

2. Selected Highlights

The aim of the Focus Meeting was to develop a diverse scientific program, covering a large range of topics related to extragalactic magnetic fields. The collection of papers presented in *Astronomy in Focus* is representative of the diversity of the contributions that animated the meeting. The meeting started with a welcome by L. Feretti and was structured around a series of invited talks, as well as a rich collection of contributed oral and poster presentations. The meeting concluded with a final discussion lead by L. Rudnick. Readers are encouraged to peruse all the contributions, but we present here some of the highlights identified by the attendees themselves at the conclusion of the meeting. During the final discussion, audience members were invited to provide short written de-

scriptions of what they found most interesting and exciting. They were admonished to cite work other than their own, and sometimes they even did that. Note that the citations provided here refer to these proceedings; where relevant, references to the original work are found in the individual contributions. So, with a modicum of editorializing, here's what they identified:

Early Universe, Cosmology

- Standard picture for the origin involves turbulent dynamo amplification in the interstellar or intracluster medium (*Subramanian's talk, these proceedings*).
- Primordial magnetic fields could have a measurable effect on the $B - modes$ of the CMB at low l : good news for magnetic field aficionados, but for disentangling inflation signatures, not so much! (*Yamazaki's talk, online*).
- MHD turbulence accompanying primordial fields might be capable of distorting the gravitational wave spectrum at levels accessible to LISA (*Kahniashvili's talk, these proceedings*).
- During the period of reionization, magnetic fields create Faraday rotation which can be observed in the CMB. Current estimates of $10^{-8} \text{ rad m}^{-2}$ at $z = 10$ are very encouraging for seeding the dynamos for later amplification in galaxies and clusters (*Ruiz-Granados's poster, online*).
- In the ongoing quest to identify the origins of primordial magnetic fields, a mechanism invoking photoionization in an inhomogeneous IGM around Pop III stars, primeval galaxies and quasars might do the job (*Langer's talk, online*).

Field amplification and large scale structures

Progress continues on a number of fronts to understand how the μG fields that we see today were amplified from much weaker seed fields. Recent insights include:

- It isn't clear that we can always generate the large scale coherence we need (*Sur's poster, online*), whether we can align the magnetic fields post-shock in cluster "relics" (*Ryu's talk*), and whether we can distinguish between astrophysical and primordial field origins in clusters (*Dominguez-Fernandez's poster, online*).
- Magnetic fields can suppress turbulence in the ICM, homogenize both temperature and density fluctuations (*Shukurov's poster, online*), and affect galaxy evolution and star formation (*talks by Tabatabaei, and Ramos-Martinez, online*).
- Power spectra do not sufficiently capture the structure of fields, which might form as filaments, ribbons, sheets, etc. (*Shukurov's talk, see online contribution by Seta; Jones' poster*)

Fast Radio Bursts

- The combination of Dispersion Measures and Rotation Measures for Fast Radio Bursts suggests that there are at least two different types. Contributions can be either local to the source or indicators of cosmological magnetic fields at levels $< 20 \text{ nG}$ (*Johnston's talk*).

Extragalactic radio sources

- Exquisite fine structure in Rotation Measures and magnetic fields is now being revealed by LOFAR (*talk by Hoeft, poster by Heesen*).
- ALMA is in the polarization business! including the discovery of RMs $> 10^5 \text{ rad m}^{-2}$ in 3C273's jet (*talk by Nagai*), and progress is being made in reconstruction of 3D fields in jets (*talk by Laing*).

- The first indicators of the relation between turbulence in the thermal plasma in clusters and the resulting fields are emerging (*talk by Bonafede, these proceedings*).

Normal Galaxies

- Progress continues on the challenge of dynamos on various scales (*talks by Chamandy, and Sokoloff, online*).
- On the observational side, field reversal now seen outside of Milky Way in the axisymmetric spiral NGC 4666 (*poster by Stein, online*), and even the pitch angle of the fields with respect to the spiral arms can be measured with good accuracy in M31 (*poster by Beck, online*).
- Large scale dynamos are sometimes sub-critical and will not generate strong coherent fields; causes are under investigation (*poster by Rodrigues, online*).
- Among many highlights from the CHANG-ES survey (*poster by Stil, online*), the Virgo galaxy NGC4388 has magnetized outflows extending to 5 kpc above the plane (*poster by Damas-Segovia*).
- Surprisingly, the small group of galaxies in Stephan's Quintet hosts an intergalactic field of strengths comparable to those seen in clusters (*talk by Nikiel-Wroczyński*).

Techniques and the Future

- Signatures of the primordial field can be decoded from local structure if we're clever enough to overcome a factor of 10^{24} confusion from other fields (*talk by Enßlin*).
- An incredible variety of new polarization information, including circular polarization, is coming in the next few to 10 years, new telescopes, surveys and techniques to exploit them: LoTSS, MWA, VLASS, POSSUM, MeerKAT, QUOCCA, SKA and even SOFIA in the far IR (*talks and posters by Mao, these proceedings; Loi, Ma, Rudnick, Heald, Horellou, Lopez, online; Gaensler, Hoeft, McKimven, Zinneker*).

Acknowledgements

The organisers of this Focus Meeting (LF, FG, GH, MJH) would like to extend our gratitude to the organizers of the IAU General Assembly and to the LOC for their hard work and support. We would also like to thank the contributors to the Focus Meeting: those who delivered invited talks, contributed talks or posters, and all of those who participated in the discussions and provided input to the collection of highlights that directly led to this contribution. Our particular thanks go to those of the speakers and poster presenters who delivered contributions to our proceedings.

Partial support for LR comes from U.S. National Science Foundation grant AST1714205 to the University of Minnesota.

Origins of Cosmic magnetism

Kandaswamy Subramanian

¹IUCAA, Post Bag 4, Ganeshkhind, Pune 411007, India
email: kandu@iucaa.in

Abstract. The standard picture for the origin of magnetic fields in astrophysical systems involves turbulent dynamo amplification of a weak seed field. Dynamos convert kinetic energy of motions to magnetic energy. While it is relatively easy for magnetic energy to grow, explaining the observed degree of coherence of cosmic magnetic fields generated by turbulent dynamos, remains challenging. We outline potential resolution of these challenges. Another intriguing possibility is that magnetic fields originated at some level from the early universe.

Keywords. magnetic fields, galaxies: magnetic fields, galaxies: clusters: general, early universe

1. Introduction

The universe is magnetized from planets, stars, nearby and high redshift galaxies, the plasma in galaxy clusters and perhaps even the inter galactic medium in void regions devoid of galaxies! Understanding the coherence of magnetic fields detected in these astronomical systems presents an outstanding challenge of modern astrophysics. The general paradigm for extragalactic magnetogenesis involves dynamo amplification of a seed magnetic field due to electromagnetic induction by motions of a conducting plasma. The seed itself could be due to a cosmic battery effect or more intriguingly primordial. We briefly review the dynamo paradigm and then touch upon a possible primordial scenario.

Plasma in all astrophysical systems are turbulent. In galaxies, turbulence is driven by supernovae explosions and in galaxy clusters during its formation by collapse and mergers. Turbulence combined with large scale shearing motions in a highly conducting fluid of galaxies and clusters, generically leads to dynamo action, a process referred to as a turbulent dynamo. Turbulent dynamos are conveniently divided into the small-scale (or fluctuation) dynamos and large-scale (or mean-field) dynamos. The distinction depends respectively on whether the generated magnetic field is ordered on scales smaller or larger than the scale of the turbulent motions. The small-scale dynamos would be relevant for the magnetization of galaxy clusters and young galaxies, while the large-scale dynamo for understanding the system scale magnetic fields in disk galaxies.

2. Small-scale dynamos

In a highly conducting plasma, magnetic flux through any area moving with the fluid is conserved. Consider a flux tube containing plasma of density ρ , magnetic field strength B , area of cross section A and going through fluid parcels separated by a length l . Flux conservation implies $BA = \text{constant}$. Mass conservation in the flux tube gives $\rho Al = \text{constant}$, which implies $B/\rho \propto l$. In any turbulent flow, fluid parcels random walk away from each other and l increases due to random stretching, and if ρ is roughly constant, then B increases. This of course comes at the cost of $A \propto 1/\rho l \propto 1/B$ decreasing, the field being concentrated on smaller and smaller scales l_B at least in one direction, till decay rate due to resistive diffusion, η/l_B^2 is of same order as growth rate due to random stretching v/l . Here v and l are the velocity and coherence scale respectively of turbulent

eddies, while η is the resistivity of the plasma. This gives $l_B \sim lR_m^{-1/2}$ where the magnetic Reynolds number $R_m = vl/\eta$ is typically very large in astrophysical systems, which also implies a resistive scale $l_B \ll l$.

Kazantsev (1967) first showed that a specialized short correlated random flow can be a dynamo and cause net magnetic field growth on the very rapid eddy turn over time l/v , provided the R_m exceeds a very modest critical value $R_c \sim 100$. This growth due to the small scale dynamo has since been verified by many direct numerical simulations where a seed field is introduced into a turbulent flow (Haugen et al., (2004), Schekochihin et al., (2004), Bhat and Subramanian (2013)). Thus generically turbulence in the interstellar or intra cluster medium, which have $R_m \gg R_c$, is expected to rapidly amplify magnetic fields on a timescale $l/v \sim 10^7$ yr in galaxies (with $v \sim 10$ km s $^{-1}$ and $l \sim 100$ pc) and $l/v \sim 3 \times 10^8$ yr in galaxy clusters (with $v \sim 300$ km s $^{-1}$ and $l \sim 100$ kpc), much smaller than their age. However as $l_B \ll l$, the field in the growing phase is extremely intermittent and concentrated in to the small resistive scales. The big challenge is then whether these fields can become coherent enough on dynamo saturation to explain for example observations of the Faraday rotation inferred in galaxy clusters and young galaxies.

We have used direct numerical simulations of fluctuation dynamos in forced compressible turbulence with various values of R_m , fluid Reynolds number R_e and up to rms Mach number of $\mathcal{M} = 2.4$, to directly measure the resulting Faraday rotation measure (RM) and the degree of coherence of the magnetic field (Subramanian et al., (2006), Bhat and Subramanian (2013), Sur et al. (2018)). The measured values of a normalized RM, $\bar{\sigma}_{RM}$, normalized by that expected in a model where fields with the rms strength B_{rms} are assumed to be coherent on the forcing scale of turbulence, are shown in Fig. 1 for some of these runs. At dynamo saturation, for a range of parameters, we find $\bar{\sigma}_{RM} \sim 0.40 - 0.55$, or an rms RM contribution which is about half the value expected if the field is coherent on the turbulent forcing scale. This arises in spite of the highly intermittent nature of the field. The left panel of Fig. 1, also shows that when regions with the field above $2B_{rms}$ are excluded from the RM computation for the subsonic case, there is only a modest 20% decrease of $\bar{\sigma}_{RM}$ (Bhat and Subramanian (2013)). Thus the dominant contribution to the RM in this case (and also when the flow is transonic) comes from the general sea of volume filling fields, rather than from the rarer, strong field structures. However, in the

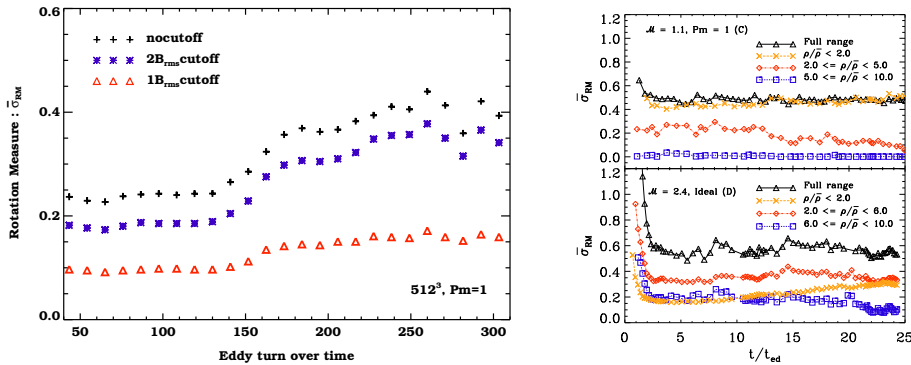


Figure 1. Left panel shows the time evolution $\bar{\sigma}_{RM}$ for a 512^3 subsonic run with $\mathcal{M} = 0.14$, $R_m = R_e = 622$ from Bhat and Subramanian (2013). The stars and triangles show respectively the result of excluding regions with field above $2B_{rms}$ and B_{rms} while the crosses correspond to not imposing any cutoff. The right panel shows the corresponding results from Sur et al. (2018) of higher Mach number flows, with also overdensity cuts as indicated in the figure.

supersonic case, strong field regions as well as moderately overdense regions contribute significantly to RM. The density dependence is illustrated in the right panel of Fig. 1, where the $\bar{\sigma}_{RM}$ contribution by various overdensity ranges is shown for the cases with $\mathcal{M} = 1.1$ and 2.4 (Sur et al. (2018)). Our results can account for the observed RMs in galaxy clusters and in young galaxies just as due to fluctuation dynamo action. We also find that the coherence scale of the generated intermittent field is about 1/3 to 1/4 of the velocity coherence scale for the parameters so far explored, and so not too small.

3. Mean-field dynamos

Magnetic fields with coherence scales larger than that of the stirring can be amplified if the turbulence is helical. In disk galaxies, supernovae drive turbulent motions which become helical due to the rotation and vertical stratification of the disk. Helical turbulent motions of the gas draw out any toroidal field in the galaxy into a loop and twists it to look like a twisted Omega (called the α -effect). These lead to the generation of poloidal magnetic fields from toroidal fields. The shear due to galactic differential rotation winds up radial component of the poloidal field to generate a toroidal component. The combination of these two effects lead to a mean-field dynamo generation of disk galaxy magnetic fields on the differential rotation time scales of about $10^8 - 10^9$ yr.

This idea faces two important challenges. First, magnetic fluctuations due to the fluctuation dynamo in a disk galaxy grow on small scales much faster ($10^7 yr$) than the growth time of the mean field. Lorentz forces can then become important to saturate the field growth much before the mean field has grown significantly. Can the large-scale field then grow at all? Bhat et al. (2016) examined this issue using direct simulations of magnetic field amplification due to fully helical turbulence in a periodic box. The results of one such run where both the fluctuation and mean-field dynamos arise in a unified manner is shown in Fig. 2. We find that initially scales both larger and much smaller than the stirring scale grow together as an eigenfunction dominated by small scales. But crucially on saturation of small scales due to the Lorentz force, larger and larger scales come to dominate due to the mean-field dynamo action. Finally system scale fields (here the scale of the box) develop provided small-scale magnetic helicity can be efficiently removed (see below), which in this simulation is due to resistive dissipation.

The second challenge is that in the highly conducting galactic plasma, magnetic he-

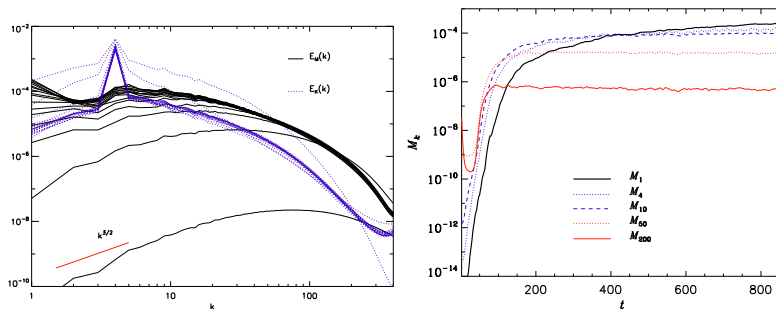


Figure 2. Left panel: time evolution of the magnetic spectra $E_M(k)$ and kinetic spectra $E_K(k)$ from Bhat et al. (2016) for a 1024^3 simulation of helically forced (at $k = 4$), turbulence with $\mathcal{M} = 0.135$, $R_m = 10R_e = 3375$. Right panel: The time evolution of different modes of the magnetic spectra $M_k(t)$ for $k = 1, 4, 10, 50$, and 200. Initially all scales grow together, with magnetic power peaked on small scales. Lorentz forces act to order the field on larger and larger scales as the dynamo saturates.

licity which measures the linkages between field lines, is nearly conserved. Then when helical motions writhe the toroidal field to generate a poloidal field, an oppositely signed twist develops on smaller scales, to conserve magnetic helicity and Lorentz forces due to this twist try to unwind the field and quench the dynamo. Large-scale dynamos only work by shedding this small-scale magnetic helicity. This can happen due to resistivity, but on a time scale that exceeds the age of the universe! It can also happen if the small-scale helicity is transported out of the system by helicity fluxes. One such flux is simply advection of the gas and its magnetic field out of the disk. Such advection can be larger from the optical spiral region, where star formation and galactic outflows are expected to be enhanced. Chamandy et al. (2015) solved the mean-field dynamo equation incorporating both such an advective flux and a diffusive flux. The helicity fluxes allow the mean-field dynamo to survive, but stronger outflow along spiral arms led to a suppression of mean field generation there and an interlaced pattern of magnetic and gaseous arms develops, as seen in the galaxy NGC6946 (Beck & Hoernes (1996)). Interestingly a wide spread magnetic spiral only results if the optical spiral is allowed to wind up and thus here we are constraining spiral structure theory using magnetic field observations!

4. Primordial magnetic fields

An intriguing possibility is that magnetic fields are an early Universe relic, arising during inflation along with density fluctuations, or being generated in QCD or electroweak phase transitions (for a review see Subramanian (2016)). A number of problems have been raised about inflationary magnetogenesis. A model by Sharma et al. (2018) which addresses these, predicts a blue magnetic field spectrum $d\rho_B/d\ln k \propto k^4$ and requires a low energy scale of inflation and reheating. The field is also helical and so orders itself considerably as it decays. A scenario with reheating at a temperature of 100 GeV leads to present day field strengths of order $B_0 = 4 \times 10^{-11}$ G with a coherence scale of 70 kpc. Such models can be constrained by space gravitational wave detectors like LISA in the future.

In summary the origin of cosmic magnetism on galactic and extragalactic scales is still an area of active research with many interesting ideas which will continue to fascinate astronomers of the future.

Acknowledgements

I thank Pallavi Bhat, Axel Brandenburg, Luke Chamandy, T. R. Seshadri, Ramkishor Sharma, Sharanya Sur and Anvar Shukurov for the enjoyable collaborations reported here and the FM8 organisers and IAU for financial support to attend this meeting.

References

- Beck, R., & Hoernes, P. 1996, *Nature*, 379, 47
 Bhat, P., and Subramanian, K. 2013, *MNRAS*, 429, 2469–2481.
 Bhat, P., Subramanian, K., & Brandenburg, A. 2016, *MNRAS*, 461, 240
 Chamandy, L., Shukurov, A., & Subramanian, K. 2015, *MNRAS*, 446, L6
 Haugen, N. E., Brandenburg, A., and Dobler, W. 2004, *PRE*, 70 (1), 016308.
 Kazantsev, A. P. 1967, *JETP*, 53, 1807 (English translation: Sov. Phys. JETP, 26, 1031, 1968).
 Schekochihin, A. A., Cowley, S. C., Taylor, S. F., Maron, J. L., and McWilliams, J. C. 2004, *ApJ*, 612, 276
 Sharma, R., Subramanian, K., & Seshadri, T. R. 2018, *PRD*, 97, 083503
 Subramanian, K., Shukurov, A., and Haugen, N. E. L. 2006, *MNRAS*, 366, 1437
 Subramanian, K. 2016, *Reports on Progress in Physics*, 79, 076901
 Sur, S., Bhat, P., & Subramanian, K. 2018, *MNRAS*, 475, L72

Magnetism in the Early Universe

Tina Kahniashvili^{1,2}, Axel Brandenburg^{3,4,1}, Arthur Kosowsky⁵,
Sayan Mandal¹, Alberto Roper Pol^{4,6}

¹Department of Physics, Carnegie Mellon University, USA

²Abastumani Astrophysical Observatory, Iliia State University, Georgia

³Nordita, KTH Royal Institute of Technology & Stockholm University; Department of Astronomy, Stockholm University, Sweden; and JILA, University of Colorado at Boulder, USA

⁴Laboratory for Atmospheric and Space Physics, University of Colorado at Boulder, USA

⁵Department of Physics and Astronomy and PITT PACC, University of Pittsburgh, USA

⁶Department of Aerospace Engineering, University of Colorado at Boulder, USA

Abstract. Blazar observations point toward the possible presence of magnetic fields over intergalactic scales of the order of up to ~ 1 Mpc, with strengths of at least $\sim 10^{-16}$ G. Understanding the origin of these large-scale magnetic fields is a challenge for modern astrophysics. Here we discuss the cosmological scenario, focussing on the following questions: (i) How and when was this magnetic field generated? (ii) How does it evolve during the expansion of the universe? (iii) Are the amplitude and statistical properties of this field such that they can explain the strengths and correlation lengths of observed magnetic fields? We also discuss the possibility of observing primordial turbulence through direct detection of stochastic gravitational waves in the mHz range accessible to LISA.

Keywords. Early Universe, Cosmic Magnetic Fields, Turbulence, Gravitational Waves

1. Introduction

Magnetic fields of strengths of the order of $\sim 10^{-16}$ G are thought to be present in the voids between galaxy clusters; see Neronov & Vovk (2010) for the pioneering work and Durrer & Neronov (2013) for a review and references therein. These are thought to be the result of seed magnetic field amplification, with two scenarios of the origin currently under discussion; see Subramanian (2016) for a review: a bottom-up (astrophysical) scenario, where the seed is typically very weak and magnetic field is transferred from local sources within galaxies to larger scales, and a top-down (cosmological) scenario where a magnetic field is generated prior to galaxy formation in the early universe on scales that are large at the present epoch. We discuss two different primordial magnetogenesis scenarios: inflationary and cosmological phase transitions. We address cosmic magnetohydrodynamic (MHD) turbulence, in order to understand the magnetic field evolution. Turbulent motions can also affect cosmological phase transitions. We argue that even a small total energy density in turbulence (less than 10% of the total thermal energy density), can have substantial effects because of strong nonlinearity of the relevant physical processes; see also Vazza et al. (2017).

2. Overview

The evolution of a primordial magnetic field is determined by various physical processes that result in amplification as well as damping. Complexities arise in the problem due to the strong coupling between magnetic field and plasma motions (Kahniashvili et al. 2010), producing MHD turbulence, which then undergoes free decay after the forcing is switched off (Brandenburg et al. 1996; Dimopoulos & Davis 1997; Jedamzik et al. 1998;

Subramanian & Barrow 1998); see Kahniashvili et al. (2016) for a recent overview. The presence of initial kinetic and/or magnetic helicity strongly affects the development of turbulence. In several models of phase transition magnetogenesis, parity (mirror symmetry) violation leads to a non-zero chirality (helicity) of the field (Cornwall 1997; Giovannini & Shaposhnikov 1998; Field & Carroll 2000; Giovannini 2000; Vachaspati 2001). We also underline the importance of possible kinetic helicity: our recent simulations have shown that through the decay of hydromagnetic turbulence with initial kinetic helicity, a weak nonhelical magnetic field eventually becomes fully helical (Brandenburg et al. 2017).

The anisotropic stresses of the resulting turbulent magnetic and kinetic fields are a source of gravitational waves, as already pointed out by Deryagin et al. (1986). The amplitude of the gravitational wave spectrum depends on the strength of the turbulence, and its characteristic wavelength depends on the energy scale at which the phase transition occurs (Gogoberidze et al. 2007).

3. Results

Understanding the mechanisms for generating primordial turbulence is a major focus of our investigation. Turbulence may be produced during cosmological phase transitions when the latent heat of the phase transition is partially converted to kinetic energy of the plasma as the bubbles expand, collide, and source plasma turbulence (Christensson et al. 2001). The two phase transitions of interest in the early universe are (i) the electroweak phase transition occurring at a temperature of $T \sim 100$ GeV, and (ii) the QCD phase transition occurring at $T \sim 150$ MeV. Turbulence at the electroweak phase transition scale is more interesting for the gravitational wave detection prospects, since the characteristic frequency of the resulting stochastic gravitational wave background, set by the Hubble length at the time of the phase transition, falls in the Laser Interferometer Space Antenna (LISA) frequency band; see Kamionkowski et al. (1994), and Kosowsky et al. (2002) for pioneering studies, and Caprini & Figueroa (2018) for a recent review.

Since the electroweak phase transition is probably a smooth crossover in the Standard Model of particle physics, it would not proceed through bubble collisions and follow up turbulence. Our knowledge of electroweak scale physics is incomplete; at least two lines of reasoning point toward a first-order phase transition in the very early universe. First, such a transition can provide the out-of-equilibrium environment necessary for successful baryogenesis; see, e.g., Morrissey & Ramsey-Musolf (2012). Secondly, as discussed above, turbulence induced in a first-order transition naturally amplifies seed magnetic fields which can explain the magnetic fields that might be present in cosmic voids; see Fig. 1 and Brandenburg et al. (2017). Arguments in favor of a primordial origin of such fields were also given by Dolag et al. (2011).

If significant magnetic fields exist after the phase transitions, they can source turbulence for long durations, extending even until recombination. For these sources, the damping due to the expansion of the universe cannot be neglected. Numerical simulations show only a slow decay of turbulent energy, especially at the large-scale end of the spectrum, along with the generation of significant energy density in velocity fields; see Fig. 4 of Kahniashvili et al. (2010), and Brandenburg & Kahniashvili (2017). Turbulence in the early universe can also be generated during inflation, whereby the magnetic field energy is injected into primordial plasma ensuring a strong coupling between the magnetic field and fluid motions. The correlation scale of induced turbulent motions is limited by the Hubble scale, as required by causality; see Kahniashvili et al. (2012) for the non-helical case and Kahniashvili et al. (2017) for the helical case, while the magnetic field stays frozen-in at superhorizon scales. The strength of the turbulent motions is determined by

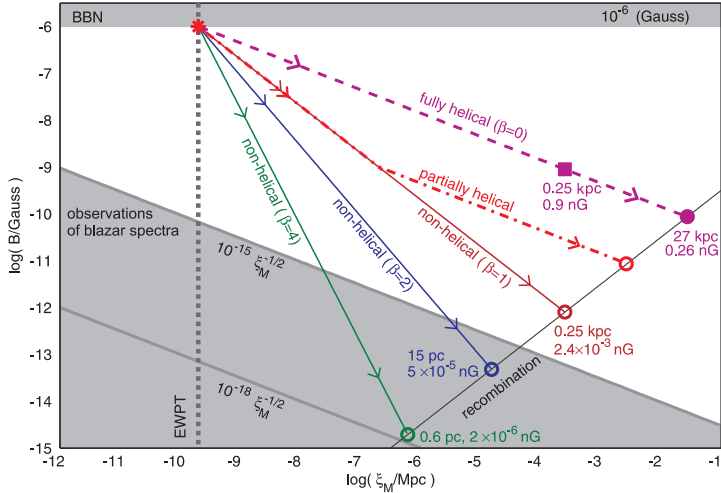


Figure 1. Turbulent evolution of the strength B_{rms} and correlation length ξ_M of the magnetic field starting from their upper limits given by the Big Bang Nucleosynthesis (BBN) bound and the horizon scale at the electroweak phase transitions (from Brandenburg et al. (2017), Fig. 11).

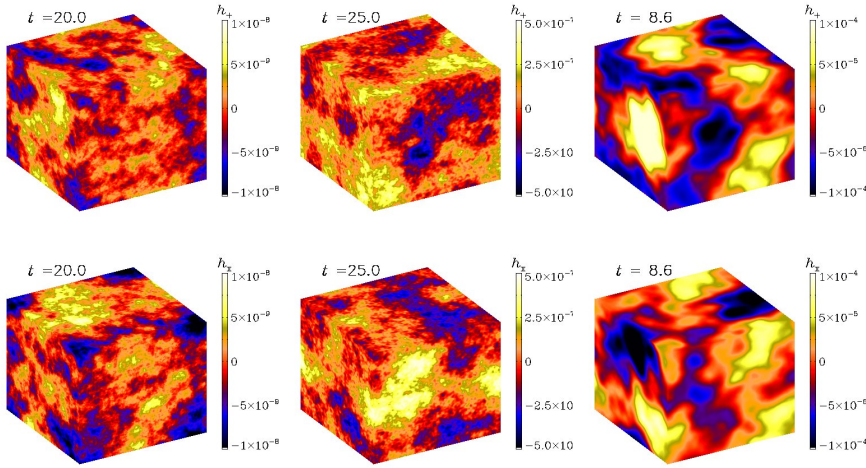


Figure 2. Visualizations of h_+ (top) and h_\times (bottom) on the periphery of the computational domain for different positions of the initial turbulent spectrum peak frequency $k_f/k_H = 300, 60, 2$ from left to right respectively. (in press)

the total energy density of the magnetic field; a sufficiently strong field can lead to a detectable gravitational wave signal (Kahniashvili et al. 2008).

The PENCIL CODE (Brandenburg & Dobler 2002) is a general public domain toolbox to solve sets of partial differential equations on large, massively parallel platforms. It has recently been applied to early universe simulations of mesh size up to 2304^3 (Brandenburg & Kahniashvili 2017), which was necessary for modeling turbulence at the phase transitions (Brandenburg et al. 2017) and the inflationary stage (Kahniashvili et al. 2017). We have recently added a module to evolve the gravitational waves in the simulation domain from the dynamically evolving MHD stresses. Details of the numerical simulations can be found in Roper Pol et al. (2018). Our first preliminary results are

presented in Fig. 2, where we plot the gravitational wave strain components h_+ and h_\times sourced by fully helical hydromagnetic turbulence. It must be highlighted that the presence of initial magnetic helicity significantly affects the detection prospects. However, the detection of the circular polarization degree by LISA seems to be problematic (Smith & Caldwell 2017).

Acknowledgements

It is our pleasure to thank the organizers, in particular Luigina Feretti and Federica Govoni of IAU XXX FM8 “New Insights in Extragalactic Magnetic Fields”. Partial support through the NSF Astrophysics and Astronomy Grant Program (AAG) (1615940 & 1615100) is gratefully acknowledged.

References

- Brandenburg, A., Enqvist, K. & Olesen, P. 1996, *Phys. Rev. D*, **54**, 1291
- Brandenburg, A. & Kahniashvili, T. 2017, *Phys. Rev. Lett.*, **118**, 055102
- Brandenburg, A. & Dobler, W. 2002, *Comput. Phys. Commun.*, **147**, 471
- Brandenburg, A., Kahniashvili, T., Mandal, M., Roper Pol, A., Tevzadze, A. & Vachaspati, T. 2017, *Phys. Rev. D*, **96**, 123528
- Caprini, C. & Figueroa, D. G. 2018, *Class. Quant. Grav.*, **35**, 163001
- Cornwall, J. M. 1997, *Phys. Rev. D*, **56**, 6146
- Christensson, M., Hindmarsh, M. & Brandenburg, A. 2001, *Phys. Rev. E*, **64**, 056405
- Deryagin, D., Grigoriev, D., Rubakov, V. & Sazhin, M. 1986, *Mod. Phys. Lett. A*, **1**, 593
- Dimopoulos, K. & Davis, A. C. 1997, *Phys. Lett. B*, **390**, 87
- Dolag, K., Kachelriess, M., Ostapchenko, S. & Tomas, R. 2011, *Astrophys. J.*, **727**, L4
- Durrer, R. & Neronov, A. 2013, *Astron. Astrophys. Rev.*, **21**, 62
- Field, G. B. & Carroll, S. M. 2000, *Phys. Rev. D*, **62**, 103008
- Giovannini, M. & Shaposhnikov, M. E. 1998, *Phys. Rev. D*, **57**, 2186
- Giovannini, M. 2000, *Phys. Rev. D*, **61**, 063004
- Gogoberidze, G., Kahniashvili, T. & Kosowsky, A. 2007, *Phys. Rev. D*, **76**, 083002
- Jedamzik, K., Katalinic, V. & Olinto, A. V. 1998, *Phys. Rev. D*, **57**, 3264
- Kahniashvili, T., Kosowsky, A., Gogoberidze, G. & Maravin, Y. 2008, *Phys. Rev. D*, **78**, 043003
- Kahniashvili, T., Brandenburg, A., Tevzadze, A. G. & Ratra, B. 2010, *Phys. Rev. D*, **81**, 123002
- Kahniashvili, T., Brandenburg, A., Campanelli, L., Ratra, B. & Tevzadze, A. 2012, *Phys. Rev. D*, **86**, 103005
- Kahniashvili, T., Brandenburg, A. & Tevzadze, A. 2016, *Phys. Scripta*, **91**, 104008
- Kahniashvili, T., Brandenburg, A., Durrer, R., Tevzadze, A. & Yin, W. 2017, *JCAP*, **1712**, 002
- Kamionkowski, M., Kosowsky, A. & Turner, M. S. 1994, *Phys. Rev. D*, **49**, 2837
- Kosowsky, A., Mack, A. & Kahniashvili, T. 2002, *Phys. Rev. D* **66**, 024030
- Morrissey, D. E. & Ramsey-Musolf, M. J. 2012, *New J. Phys.*, **14**, 125003
- Neronov, A. & Vovk, I. 2010, *Science*, **328**, 73.
- Roper Pol, A., Brandenburg, A., Kahniashvili, T., Kosowsky, A. & Mandal, S. 2018, *Geophys. Astrophys. Fluid Dynam.*, arXiv:1807.05479
- Smith, T. L. & Caldwell, R. 2017, *Phys. Rev. D*, **95**, 044036
- Subramanian, K. & Barrow, J. D. 1998, *Phys. Rev. Lett.*, **81**, 3575
- Subramanian, K. 2016, *Rept. Prog. Phys.*, **79**, 076901
- Vachaspati, T. 2001. *Phys. Rev. Lett.*, **87**, 251302
- Vazza, F., Brüggen, M., Gheller, C., Hackstein, S., Wittor, D. & Hinz, P. M. 2017, *Class. Quant. Grav.*, **34**, 234001

Constraining magnetic fields in galaxy clusters

Annalisa Bonafede^{1,2,3}, Chiara Stuardi^{1,2}, Federica Savini³, Franco Vazza^{1,2,3}, and Marcus Brüggen³

¹Dipartimento di Fisica e Astronomia, Università di Bologna, via P. Gobetti 93/2, 40129, Bologna, Italy.

²INAF - Istituto di Radioastronomia, Via Gobetti 101, I-40129 Bologna, Italy.

³Hamburger Sternwarte, Universität Hamburg, Gojenbergsweg 112, 21029, Hamburg, Germany.

email: annalisa.bonafede@unibo.it

Abstract. Magnetic fields originate small-scale instabilities in the plasma of the intra-cluster medium, and may have a key role to understand particle acceleration mechanisms. Recent observations at low radio frequencies have revealed that synchrotron emission from galaxy clusters is more various and complicated than previously thought, and new types of radio sources have been observed. In the last decade, big step forwards have been done to constrain the magnetic field properties in clusters thanks to a combined approach of polarisation observations and numerical simulations that aim to reproduce Faraday Rotation measures of sources observed through the intra-cluster medium. In this contribution, I will review the results on magnetic fields reached in the last years, and I will discuss the assumptions that have been done so far in light of new results obtained from cosmological simulations. I will also discuss how the next generation of radio instruments, as the SKA, will help improving our knowledge of the magnetic field in the intra-cluster medium.

Keywords. Galaxy clusters, magnetic field, non-thermal phenomena

1. Introduction

Galaxy clusters host magnetic fields that are responsible for a variety of phenomena on a large range of spatial scales. The intra-cluster medium (ICM) is an almost perfect plasma, and the magnetic field originates small-scale instabilities that can amplify the field itself and modify the ICM microphysics. On Mpc scale, the magnetic field interacts with Cosmic Ray electrons (CRE) and produce diffuse emission such as radio halos, mini halos, and radio relics. Recent observations with the LOw Frequency ARray (LOFAR, van Haarlem, et al. 2013) have shown that the radio emission in the ICM is more complex than initially thought. In particular, Savini et al. (2018) have discovered that steep-spectrum emission on Mpc scale is observed also in clusters that do not show signs of major merger. In Fig. 1 (right panel), the radio emission from the galaxy cluster RXCJ1720.1+2638 is shown. This cluster is known to host a mini halo confined between two cold fronts, i.e. discontinuities in the X-ray surface brightness profile. It has been proposed that the cold fronts are formed during a minor merger, where the dense core of the cluster is perturbed and starts a sloshing motion in the dark matter potential well. LOFAR reveals that the radio emission extends well beyond the cold fronts. The radio emission inside and outside the core can be well separated both in brightness and in spectral index. The core emission (mini halo) is relatively flat ($\alpha \sim -1$) and the spectral index distribution is uniform. The emission SW and NE of the core emission, beyond the cold fronts, is steeper ($\alpha \sim -2$), suggesting either a different acceleration process and/or

a different magnetic field strength in the two regions.

New emission has also been observed by LOFAR in the cluster MACSJ0717.0+3745 (Bonafede et al. 2018). This massive ($M_{500} \sim 1.1 \times 10^{15} M_{\odot}$) high- z ($z=0.546$) cluster was known to host diffuse radio emission visible at GHz frequencies, which is not co-spatial with the X-ray emission from the gas. The radio emission is confined in the Eastern part of the cluster. LOFAR observations at 150 MHz have confirmed this asymmetry in the radio emission (see Fig. 1, left panel), and a new radio arc with a linear size of ~ 1.7 Mpc has been discovered at the NW of the cluster centre. The analysis of the power spectrum of the gas density fluctuations - performed following the method by Zhuravleva et al. (2014) - has shown that there is a correlation between the amplitude of the power spectrum and the presence of radio emission. This might indicate a higher ratio of kinetic versus thermal energy in the region with radio emission than in the region without.

Recently, theoretical studies have focussed on the role of magnetic fields to accelerate particles in the cluster outskirts. Radio relics are linked to low Mach number shocks, that have a low acceleration efficiency (e.g. Brüggen et al. 2011). Shock waves should also amplify the magnetic field, but only the magnetic field amplification in the relic of the Coma cluster has been analysed so far (Bonafede et al. 2013) and no net amplification in the shocked region has been found.

2. Constraints on magnetic fields and assumptions

The analysis of the Faraday effect from sources inside and in the background of clusters is the most used technique to constrain the magnetic field. Using this method, Bonafede et al. (2010) used the Rotation Measure (RM) of 7 sources in the background of the Coma cluster and the Faraday code (Murgia et al. 2004), and derived that the magnetic field strength in the cluster centre is $B_0 \sim 5 \mu\text{G}$, with a radial profile that scales with the square-root of the gas density profile (i.e. $B(r) \propto n^{0.5}$). To derive these values, assumptions need to be made on the magnetic field properties. In particular, the magnetic field is assumed to be a Gaussian random field, characterised by a single power law power spectrum. Thanks to the increasing resolution reached by recent cosmological simulations, it is now possible to compare observed and simulated RM. Using an adaptive

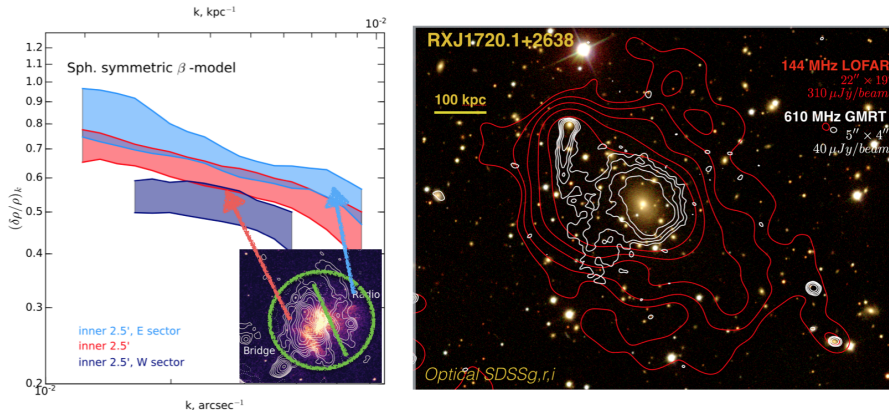


Figure 1. Left: power spectrum of the gas density fluctuations in the cluster MACSJ0717 in the regions with and without radio emission, as shown in the inset (Bonafede et al. 2018). Right: The cluster RXCJ1720.1+2638: optical emission and radio emission from GMRT at 610 MHz (white) and LOFAR at 150 MHz (red), from Savini et al (2018, in press).

mesh refinement method, Vazza et al. (2018) have performed MHD cosmological simulations reaching a resolution of ~ 4 kpc in the cluster centres. A primordial magnetic field $B_i = 0.1$ nG at $z=30$ is evolved, and its amplification is observed to be above the one predicted from a pure adiabatic compression. As the resolution increases, the magnetic field amplification increases as well, reaching $B \sim \mu\text{G}$ in the cluster centres. The magnetic field components show a departure from a Gaussian distribution, with a tail towards high values of the magnetic field. The amplitude of this tail depends on time, cluster dynamics, and resolution of the simulation. The net effect is that the RM profile for a Coma-like cluster can be reproduced with slightly lower values of B_0 than those derived by Bonafede et al. (2010). In the specific case analysed by Vazza et al. (2018), the average value of the magnetic field in the core is $B_{core} \sim 1.5\mu\text{G}$.

Cosmological simulations also predict that magnetic field power spectrum deviates from a simple power law. The relevant scales to understand the role of magnetic field in accelerating particles would be the injection scale ($L_{inj} \sim \text{few } 100$ kpc) and the viscous scale ($L_{visc} \sim \text{few kpc}$, or even lower if the Spitzer viscosity is suppressed in the ICM). The power spectrum can be approximated by a power law between L_{inj} and L_{visc} (see e.g. Ryu, this meeting, Xu et al. 2009).

However, it must be noted that the number of free parameters would increase if non-Gaussian magnetic fields and non power law power spectra were considered. The constraints on the magnetic fields that have been obtained so far are based on few sources per cluster (from 1 to 7), and the modelling done by the authors to reproduce mock RM images already have a total of 5 free-parameters. Hence, we conclude that - despite more complicated models for the magnetic field should be ideally considered - the limiting factor is the low number of sources per cluster. Considering more complicated models of magnetic field and increasing the number of free parameters will make sense only when future observations will be able to sample the RM through several tens of lines on sight per cluster.

3. New results with present instruments and future perspectives

The advent of spectro-polarimetric and wide-band receivers enables us to make an important step forward in the study of cluster magnetic fields. We started a project to constrain the magnetic field amplification by low Mach number shocks in clusters. To

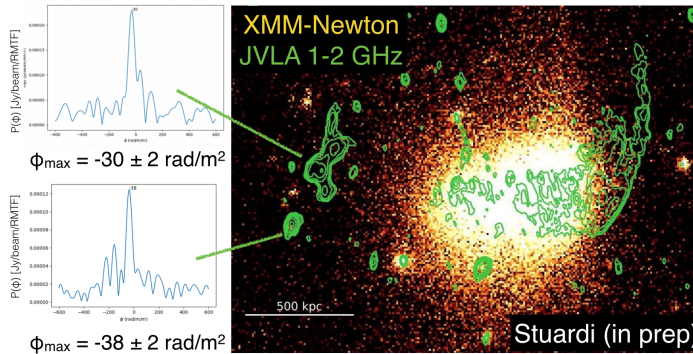


Figure 2. Radio emission from the cluster RXCJ1314 at 1-2 GHz (Stuardi et al, in prep.). The left panels show the Faraday spectra through one source in the relic (top) and in the pre-shock region (bottom). The Galactic foreground RM is $\phi \sim -30\text{rad}/m^2$, consistent with the values found for the two sources.

overcome the limit of few sources observed per cluster, we built up a sample of cluster with double relics, and obtained ~ 80 h observing time at the Jansky Very Large Array. In Fig. 2, we show the cluster RXCJ1314-2515 (Stuardi et al in prep). We analysed the Faraday spectrum of the emission using the Rotation Measure synthesis technique (Brentjens & de Bruyn 2005). So far, the regions that we have analysed seem consistent with the Galactic RM, suggesting little/no amplification of the magnetic field in the shocked region.

The next generation of radio instruments, i.e. the Square Kilometer Array (SKA) will permit a study of the magnetic field in individual clusters. The expected number density of polarised sources that SKA will observe is ~ 300 per square degree (Rudnick & Owen 2014). This means that we will be able to study the magnetic field in a Coma-like cluster using ~ 50 radio sources, i.e. a factor 7 higher than present-day studies. Bonafede et al. (2015) have analysed the RM grid that SKA will provide for clusters of different mass, finding that we will have enough sources to constrain the magnetic field in the background of low-mass galaxy clusters and galaxy groups. Having such a high number of RM samples through the line of sight, one may be able to investigate different configurations for the magnetic field, i.e. non-Gaussian distributions of the components and different functions for the power spectrum.

4. Conclusions

Obtaining constraints on the magnetic field in the ICM is crucial to understand particle acceleration mechanisms and the ICM microphysics. One must bear in mind that magnetic fields are not directly observable, and the constraints derived through observations rely on the assumptions that have been made. State-of-the-art instruments, such as the JVLA are very promising to obtain statistical constraints on the magnetic field using samples of clusters. Using this approach, Stuardi et al (in prep) are already investigating for the first time the magnetic field amplification by low Mach number shocks in radio relics. In the next years, the advent of the SKA will permit a detailed study on individual clusters, and will in principle allow us to investigate different model assumptions for the magnetic field structure.

Acknowledgments: AB and CS acknowledge financial support from the ERC-Stg DRA-NOEL, no 714245. FV acknowledges financial support from the ERC-Stg MAGCOW, no.714196.

References

- Bonafede A., et al., 2018, MNRAS, 478, 2927
 Bonafede A., et al., 2015, aska.conf, 95
 Bonafede A., Vazza F., Brügggen et al. 2013, MNRAS, 433, 3208
 Bonafede A., Feretti L., Murgia M., Govoni et al. 2010, A&A, 513, A30
 Brentjens M. A., de Bruyn A. G., 2005, A&A, 441, 1217
 Brügggen M., Bykov A., Ryu D., Röttgering H., 2011, SSR, p. 138
 Murgia M., Govoni F., Feretti L., et al., 2004, A&A, 424, 429
 Rudnick L., Owen F. N., 2014, ApJ, 785, 45
 van Haarlem M. P., Wise M. W., Gunst A. W., Heald G., et al 2013, A&A, 556, A2
 Savini F., et al., 2018, MNRAS, 478, 2234
 Vazza F., Brunetti G., Brügggen M., Bonafede A., 2018, MNRAS, 474, 1672
 Xu H., Li H., Collins D. C., Li S., Norman M. L., 2009, ApJ, 698, L14
 Zhuravleva I., Churazov E. M., Schekochihin A. A., et al. 2014, ApJ, 788, L13

Magnetic fields in the intergalactic medium and in the cosmic web

Marcus Brüggen¹ and Shane O’Sullivan¹ and Annalisa Bonafede^{1,2,3}
and Franco Vazza^{1,2,3}

¹University of Hamburg,
Gojenbergsweg 112, 21029 Hamburg, Germany
email: mbrueggen@hs.uni-hamburg.de

²Dipartimento di Fisica e Astronomia, Università di Bologna, via P. Gobetti 93/2, 40129,
Bologna, Italy.

³INAF - Istituto di Radioastronomia, Bologna Via Gobetti 101, I-40129 Bologna, Italy

Abstract. In these proceedings we discuss advances in the theory and observation of magnetic fields in the intergalactic medium and in the cosmic web. We make the point that, despite perhaps unsurmountable obstacles in simulating a small-scale dynamo, currently most cosmological magnetohydrodynamical simulations paint a similar picture of magnetic field amplification in the cosmos. However, observations of magnetic fields in the intergalactic medium turn out to be very difficult. As a case in point, we present recent work on Faraday rotation measurement in the direction of a giant galaxy with the Low Frequency Array (LOFAR). These observations demonstrate the currently unique capability of LOFAR to measure Faraday rotation at the high accuracy and angular resolution required to investigate the magnetisation of large-scale structure filaments of the cosmic web.

Keywords. (galaxies:) intergalactic medium, (cosmology:) large-scale structure of universe, magnetic fields, methods: numerical, (magnetohydrodynamics:) MHD

1. Introduction

Much has been written about the origin of cosmic magnetism, the processes that can seed fields in the early universe and the various mechanisms to amplify magnetic fields. Here we can refer to the review by J. Donnert et al. that has just been submitted. For want of clear indications to the contrary, it is almost always assumed that magnetohydrodynamics (MHD) is a good theory that describes the evolution of fields in the cosmos. Still one should mention some brave attempts to go beyond the simplest descriptions, e.g. by Schekochihin et al. (2004).

Under the set of equations of MHD, it appears that in the presence of turbulence a few percent of the kinetic energy is transferred to magnetic energy in a fast operating small-scale fluctuation dynamo (Miniati & Beresnyak 2015). Such a turbulent dynamo has been shown to operate in galaxy clusters (e.g. Jaffe 1980, Roland 1981, Ruzmaikin et al. 1989, De Young 1992, Goldshmidt & Rephaeli 1993, Kulsrud et al. 1997, Sanchez-Salcedo et al. 1998, Subramanian et al. 2006). In such dynamos, magnetic fields are amplified through an inverse cascade up until a scale, where the field starts to act back onto the fluid flow. Simulations seem to agree that field amplification is primarily caused by compression in cosmological filaments, whereas at higher overdensities such as in galaxy clusters, turbulence is increasingly solenoidal and there are a sufficient number of eddy turn-overs for a dynamo to cause a fast amplification beyond what you would get via compression. The initial exponential increase in magnetic field strength is followed by a non-linear growth phase. The timescale of exponential growth is set by the magnetic

Prandtl number and is determined by the spatial resolution and the algorithm. The real growth rate thus may never be determined by direct numerical simulations. Moreover, on smaller scales magnetic fields may get injected by galactic outflows and active galaxies. Galactic winds can transport magnetic fields into the circum-galactic medium where it can be stripped and enter the ICM (Donnert et al. 2009, Xu et al. 2009). The modelling of this is still in its infancy.

A recent example of such simulation work is presented in Vazza et al. (2018) where it was demonstrated how a small-scale dynamo develops (see Fig. 1). Interestingly but not unexpectedly, a significant non-Gaussian distribution of field components is found which results from the superposition of plasma that has gone through different amplification histories. Evidence for the presence of a dynamo is the anti-correlation of magnetic field strength and its curvature \vec{K} ,

$$\vec{K} = \frac{(\vec{B} \cdot \nabla) \vec{B}}{\vec{B}^2}, \quad (1.1)$$

so that $\vec{B} \vec{K}^{\frac{1}{2}} = \text{const}$ (Schekochihin et al. 2004) which can be tested in simulations of small-scale dynamos.

2. Observations of Faraday rotation from giant radio galaxy

On the observational side, progress has been fairly slow which is largely due to the fact that measuring extragalactic fields is unreasonably difficult. On scales of galaxies and beyond, magnetic fields are best traced via radio observations. Cluster magnetic fields were first inferred from upper limits on the diffuse synchrotron emission by Burbidge (1958). Later estimates based on the Rotation Measure (RM) of background sources to the Coma cluster obtain central magnetic fields of $3 - 7 \mu\text{G}$. Consequently, the ICM is a high $\beta = 8\pi n_{\text{th}} k_B T / B^2 \approx 100$ plasma, meaning that thermal pressure is much larger

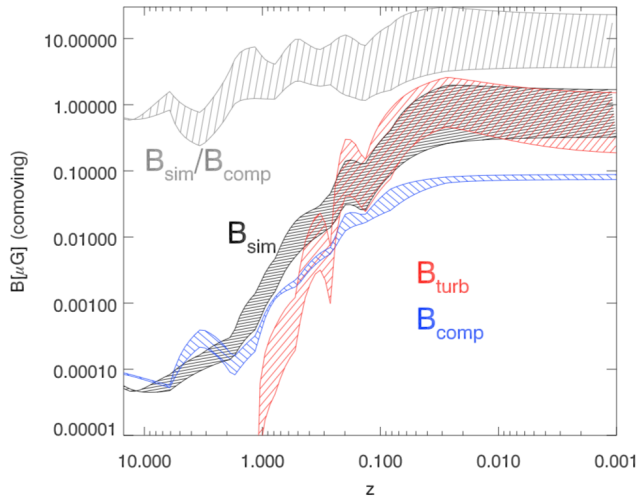


Figure 1. Magnetic field growth in a cosmological MHD simulation performed with the ENZO code. The black curve shows the magnetic field strength in innermost comoving Mpc^3 as a function of redshift. In comparison, there is the prediction from compression alone (blue) and from dynamo amplification (red) Beresnyak & Miniati (2016), assuming a 4% amplification efficiency. The grey curve shows the ratio between the simulated field and the expectation from compression alone. The dashed areas show the scatter. From Vazza et al. (2018)

than magnetic pressure. There are the attempts to measure the magnetic fields in cluster outskirts using Faraday rotation of the polarised emission from radio relics (e.g. Kierdorf et al. 2017). Radio relics or cluster radio shocks trace shock waves in merging galaxy clusters and sometime show large degrees of polarisation and μG magnetic fields.

In these proceedings, we would like to bring attention to a recent attempt by O’Sullivan et al. (in press) to analyse the FR II radio galaxy (J1235+5317) at redshift $z = 0.34$ with a linear size of 3.4 Mpc whose polarised emission may have been rotated by intergalactic magnetic fields. This work was conducted with the Low Frequency Array (LOFAR) whose broad bandwidth provides excellent precision to measure Faraday rotation and, at the same time, is sensitive to emission on large angular scales. On the downside, LOFAR observations suffer from Faraday depolarisation, which renders many sources undetectable in polarisation (Farnsworth et al. 2011). Figure 2 shows the RM distributions of this giant radio galaxy. The mean and standard deviations of the RM are $+7.42 \text{ rad m}^{-2}$ and 0.07 rad m^{-2} for the North-Western radio lobe, and $+9.92 \text{ rad m}^{-2}$ and 0.11 rad m^{-2} for the South-Eastern radio lobe.† The mean RM difference between the two lobes is $2.5 \pm 0.1 \text{ rad m}^{-2}$. Next, we relied on dynamical modelling of the radio lobes to infer the density of the ambient gas, which came out to be $n_e \sim 10^{-7} \text{ cm}^{-3}$. This suggests that the radio galaxy is expanding into a very underdense region. However, the observed Faraday depolarisation of $\sim 0.1 \text{ rad m}^{-2}$ which is most likely caused by plasma local to the source, requires $n_e \sim 10^{-5} \text{ cm}^{-3}$ with a turbulent magnetic field of strength $\sim 0.09 \mu\text{G}$ at a distance of about 1.5 Mpc from the host galaxy. Hence, we are either underestimating the density of the external medium or the depolarisation does not occur in the environment close to the source. Better models for the evolution of radio jets within a realistic cosmological environment may help refine these estimates in the future. With the current value, the estimated magnetic field strength is unable to account for the observed difference of the mean RM of 2.5 rad m^{-2} between the two lobes. We then searched a catalogue of cosmological filaments that is derived from optical spectroscopic

† The RM errors are 0.04 rad m^{-2} and 0.06 rad m^{-2} , for the NW and SE lobes, respectively.

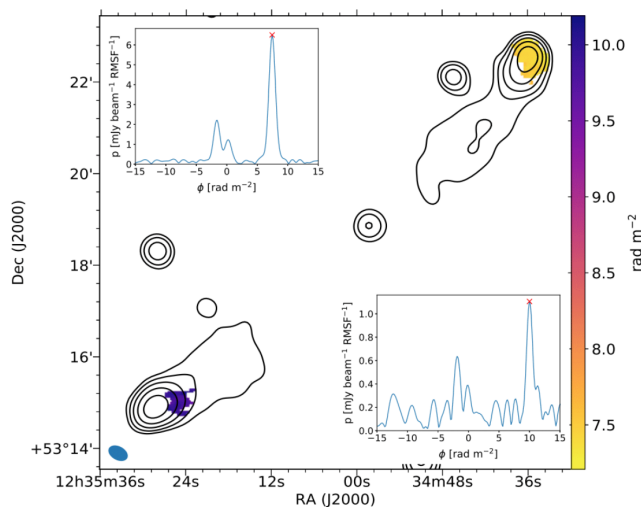


Figure 2. Faraday RM distribution of the NW and SE lobes, overlaid by the total intensity contours starting at 5 mJy/beam and increasing in factors of two. Insets: The absolute value of the Faraday dispersion function for the NW lobe (top) and SE lobe (bottom). From O’Sullivan et al. (in press).

observations and found an excess of filaments that intersect lines-of-sight towards the Northwestern lobe. If magnetised plasma in these filaments causes the RM difference between the lobes and assuming a path length through each filament of 3 Mpc, and a magnetic field coherence length of 300 kpc, this would imply a density-weighted magnetic field strength inside the filaments of $0.3 \mu\text{G}$.

We then compared this result with predictions from cosmological simulations and found that the probability of a RM contribution as large as 2.5 rad m^{-2} is only $\sim 5\%$. This estimate assumed magnetic field strengths in the cosmological filaments of 10 to 50 nG, as suggested from MHD simulations that started out with primordial magnetic fields of $\sim 1 \text{ nG}$, close to current upper limits from the CMB. Alternatively, the RM difference could come from variations in the Milky Way and finer observations of Milky Way RMs are needed to obtain better constraints.

3. Conclusions

There remains the hope that with the advent of the Square Kilometre Array (SKA) and the LOFAR upgrade this field will gain fresh momentum (e.g. Bull et al. 2018). Large samples of RMs from radio galaxies with known redshifts will permit more advanced statistical analyses, such as RM structure functions (e.g. Akahori et al. 2014). Only then will we be able to disentangle the effect of the Milky Way on RM measurements for filaments and the intergalactic space.

Acknowledgements

AB acknowledges financial support from the ERC-StG DRANOEL, no. 714245. FV acknowledges financial support from the ERC-StG MAGCOW, no. 714196.

References

- Akahori, T., Kumazaki, K., Takahashi, K., & Ryu, D. 2014, *Publications of the Astronomical Society of Japan*, 66, 65
- Beresnyak, A., & Miniati, F. 2016, *ApJ*, 817, 127
- Bull, P., Camera, S., Kelley, K., et al. 2018, arXiv:1810.02680
- Burbidge, G.R. 1958, *ApJ*, 128, 1
- De Young, D.S. 1992, *ApJ*, 386, 464–472
- Donnert, J., Dolag, K., Lesch, H., Müller, E. 2009, *MNRAS*, 392, 1008–1021,
- Farnsworth, D., Rudnick, L., & Brown, S. 2011, *ApJ*, 141, 191
- Goldshmidt, O., Rephaeli, Y. 1993, *ApJ*, 411, 518–528,
- Jaffe, W. 1980, *ApJ*, 241, 925–927
- Kierdorf, M., Beck, R., Hoeft, M., et al. 2017, *A&A*, 600, A18
- Kulsrud, R.M., Cen, R., Ostriker, J.P., Ryu, D. 1997, *ApJ*, 480, 481–491
- Miniati, F., Beresnyak, A. 2015, *Nature*, 523, 59–62
- Roland, J. 1981, *A&A*, 93, 407–410
- Ruzmaikin, A., Sokolov, D., Shukurov, A. 1989, *MNRAS*, 241, 1–14
- Sánchez-Salcedo, F.J., Brandenburg, A., Shukurov, A. 1998, *APSS*, 263, 87–90,
- Schekochihin, A.A., Cowley, S.C., Taylor, S.F., Maron, J.L., McWilliams, J.C. 2004, *ApJ*, 612, 276–307,
- Subramanian, K., Shukurov, A., Haugen, N.E.L. 2006, *MNRAS*, 366, 1437–1454,
- Vazza, F., Brunetti, G., Brüggen, M., Bonafede, A. 2018, *MNRAS*, 474, 1672–1687
- Xu, H., Li, H., Collins, D. C., Li, S., & Norman, M. L. 2009, *ApJL*, 698, L14

Magnetism in the Square Kilometre Array Era

S. A. Mao¹

¹Max Planck Institute for Radio Astronomy, Auf dem Hügel 69,
D-53121 Bonn, Germany
email: mao@mpifr-bonn.mpg.de

Abstract. The unprecedented sensitivity, angular resolution and broad bandwidth coverage of Square Kilometre Array (SKA) radio polarimetric observations will allow us to address many long-standing mysteries in cosmic magnetism science. I will highlight the unique capabilities of the SKA to map the warm hot intergalactic medium, reveal detailed 3-dimensional structures of magnetic fields in local galaxies and trace the redshift evolution of galactic magnetic fields.

Keywords. polarization, cosmology: large-scale structure of universe, galaxies: magnetic fields

1. Introduction

The Square Kilometre Array (SKA) will be the most powerful radio telescope in the world and it is currently in pre-construction phase. It will be hosted at two separate sites: SKA1-MID (350 MHz–24 GHz) with 133 15-m SKA dishes and 64 13.5-m MeerKAT dishes over a maximum baseline of 150 km will be located in the Karoo site in South Africa, while SKA1-LOW (50–350 MHz) with 130,000 antennas over a maximum baseline of 65 km will be located in the Boolardy site in Western Australia. The full SKA1-MID will have ~ 5 times better sensitivity and 4 times higher angular resolution than the Karl G. Jansky Very Large Array, while the full SKA1-LOW will be a factor of ~ 8 more sensitive than the Low Frequency Array. Science commissioning of SKA1 will commence in 2022 and full operation will begin in 2025[†]. The origin and evolution of cosmic magnetism is one of the five original SKA Key Science Projects (Gaensler, Beck & Feretti 2004). In the updated SKA science book *Advancing Astrophysics with the SKA*, the magnetism community continues to have a strong presence, contributing a total of 19 chapters. This proceedings will highlight selected topics covered in these chapters, as well as latest developments in the field which were not included in the science book.

Radio polarization observations encode rich information on particle densities and magnetic fields in the Universe on different scales: from Mpc down to sub-pc scales. Besides mapping the polarized synchrotron emission from the astrophysical object of interest, a key measurement of cosmic magnetism is the Faraday rotation towards polarized background extragalactic radio sources. These measurements, forming a so-called rotation measure (RM) grid, enable us to directly probe the magnetic field strength and direction, as well as the gas density in the foreground intervening medium.

Our knowledge of the rotation measure sky has improved significantly in the past 20 years. In the early 2000s, only $\sim 10^3$ extragalactic sources have Faraday rotation measurements (Johnston-Hollitt 2003). At present, the NRAO VLA Sky Survey rotation

[†] For the anticipated SKA1 science performance, see document number: SKA-TEL-SKO-0000818 (Braun, Bonaldi, Bourke, Keane & Wagg 2017). For the current timeline, see document number: SKA-TEL-SKO-0000822 (SKAO Science & Op Teams 2017). Both documents are available on <https://astronomers.skatelescope.org/documents/>.

measure catalog of Taylor *et al.* (2009) (1 source deg^{-2} at $\text{DEC} > -40^\circ$) along with the S-PASS/ATCA catalog of Schnitzeler *et al.* (2018) (0.2 source deg^{-2} at $\text{DEC} < 0^\circ$) provide us with $\sim 40,000$ extragalactic RMs across the entire sky, enabling magnetic field measurements in a range of different foreground astrophysical objects. In addition to the ever increasing density of the all-sky RM grid, the advent of broadband polarimetry — a more than 10-fold increase in the instantaneous observing bandwidth in frequency — have brought revolution to our field in the recent years as well. Precise and $n\pi$ -ambiguity free Faraday rotation (Ma *et al.* 2018) along with other properties of the magnetized gas can be derived using newly-developed broadband polarization analysis tools.

An all-sky full Stokes survey at $2''$ resolution with SKA1-MID (Band 2) down to $4 \mu\text{Jy beam}^{-1}$ will provide ~ 7 to 14 million extragalactic radio sources with Faraday rotations (Johnston-Hollitt *et al.* 2015). This dense RM grid will facilitate the characterization of astrophysical magnetic fields, gas densities and turbulence in unprecedented details.

2. Extragalactic Magnetism Science with the SKA

2.1. Revealing the elusive missing baryons and the magnetic fields in the cosmic web

Only about 50% of the expected baryons in the Universe can be accounted for, while the rest – missing baryons – are thought to reside in the warm-hot intergalactic medium (WHIM) in the form of shock-heated gas at 10^5 – 10^7K . The WHIM can be traced by absorption lines in X-ray and UV spectra, but extremely long integration time is required to produce high significance detection along a single sight line (Nicastro *et al.* 2018). Radio observations offer a highly complementary approach to characterize the particle density and magnetic fields in the cosmic web. Shocks produced by the accretion of baryonic matter as large-scale structures of the Universe form are sufficient to accelerate particles to relativistic energies, illuminating the cosmic web in synchrotron emission in the presence of intergalactic magnetic fields. The WHIM should also produce imprints on the RM of background sources if magnetic fields permeate the cosmic web.

Currently, limits on the surface brightness and the magnetic fields of the cosmic web can be placed by cross-correlating tracers of large-scale structures and diffuse synchrotron emission (e.g., Brown *et al.* 2017, Vernstrom *et al.* 2017). Intergalactic magnetic field strength can also be estimated by determining whether a difference in the number of large scale structure filaments intercepting the line-of-sight corresponds to a difference in Faraday rotation between two nearby sight lines (O’Sullivan *et al.* 2018). A potentially new population of radio sources in environments connecting galaxy clusters was discovered recently (Vacca *et al.* 2018). These sources have properties similar to those expected from the brightest patches of the diffuse emission associated with the WHIM.

With the advent of the SKA comes new methods to reveal the cosmic web. Direct imaging of the brightest filaments of the cosmic web will be possible with deep (>1000 hours) SKA1-LOW observations (Vazza *et al.* 2015), provided that confusion from Galactic foreground synchrotron emission and extragalactic point source emission are minimized and accurately removed. A dense ($>10^3$ sources deg^{-2}) and precise rotation measure grid (error $\sim 1 \text{ rad m}^{-2}$) towards filaments of the cosmic web and its structure function can probe the turbulent scale, gas densities and magnetic fields in the intergalactic medium (Akhori & Ryu 2011, Taylor *et al.* 2015). Performing a joint Faraday rotation and dispersion measure analysis of the $\sim 10^4$ localized fast radio bursts anticipated by the SKA (Macquart *et al.* 2015) can put tight limits on properties of the magnetized intergalactic medium if the *in situ* and host galaxy contributions can be reliably subtracted (Akhori *et al.* 2016, Johnston *et al.* this volume). The all-sky RM grid with redshift information

will enable the employment of new Bayesian algorithms (Vacca *et al.* 2016) to statistically isolate Faraday rotation produced by the cosmic web. These different approaches will yield densities and magnetic fields of the WHIM, addressing the missing baryon problem and ultimately distinguishing between different magnetogenesis scenarios.

2.2. Mapping the 3-dimensional magnetic fields in nearby galaxies

The leading theories of the amplification of magnetic fields in galaxies are the fluctuation dynamo and the large-scale α - Ω dynamo, but details of these processes remain poorly constrained observationally. Rigorous comparisons between theoretical predictions and observations of 3-dimensional magnetic fields in nearby galaxies are necessary to fully understand these dynamos. Magnetic fields in approximately 100 galaxies have been studied by measuring their diffuse polarized synchrotron emission at limited angular resolution with mostly narrowband data (Beck & Wielebinski 2013). Only 3 nearby large-angular extent galaxies, the Large and the Small Magellanic Clouds and M31, have had their magnetic fields probed via the RM-grid approach (Gaensler *et al.* 2005, Mao *et al.* 2008, Han *et al.* 1998). These studies have established some basic properties of galactic magnetic fields, such as the typical field strength and the dominant disk field symmetry, but a 3-dimensional picture of galactic magnetic fields is still lacking. Broadband radio polarimetry in combination with models of the magnetized interstellar medium (ISM) can be used to conduct tomography to characterize both large and small-scale galactic magnetic fields as a function of the line-of-sight depth, thus yielding 3-D pictures of galactic magnetic fields (Fletcher *et al.* 2011, Kierdorf *et al.* this volume).

While until now only a few galaxies have broadband polarization data that allow for tomography studies, the SKA will revolutionize this area. With the SKA, sensitive diffuse polarized synchrotron emission can be measured with excellent λ^2 coverage, specifically with SKA1-MID band 2, 4 and possibly 3 (Beck *et al.* 2015, Heald *et al.* 2015), which is ideal for magnetic field tomography. The SKA will have enough surface brightness sensitivity to map the polarized emission at extremely high angular resolution (1 kpc at $z \sim 0.04$). Moreover, at least 200 nearby galaxies will have enough polarized background sources for us to conduct RM-grid experiments on. A joint analysis of the broadband diffuse polarized emission and the RM grid of nearby galaxies will provide a complete 3-D view of their magnetic fields. The strength and structure of the disk and halo magnetic fields and their radial and vertical dependencies can be determined. The nature (isotropic vs. anisotropic) and the power spectrum of random magnetic fields can be derived. With much improved angular resolution, an extensive search for extragalactic large-scale magnetic field reversals will also be feasible. A clear link between galaxy properties and their magnetic fields will emerge from these SKA data and will allow us to constrain the field generation processes.

2.3. Tracing the redshift evolution of galactic magnetic fields

Since galactic magnetic fields play important roles in processes that are closely linked to galaxy evolution, it is crucial to understand how galaxies and their magnetic fields have co-evolved over cosmic time. Directly tracing the redshift evolution of galactic magnetic fields is a challenging task: polarized synchrotron emission from cosmologically distant galaxies is faint and Faraday rotation produced by these distant galaxies when seen against background polarized sources is subjected to redshift dilution and is difficult to isolate from other sources of Faraday rotation along the line of sight. As a result, measurements of magnetic fields in galaxies beyond the local Universe are scarce. Recently, Mao *et al.* (2017) have demonstrated that strong gravitational lensing of polarized background quasars by galaxies offers a clean and effective probe of the *in situ* magnetic

fields in individual cosmologically distant galaxies. Using differential polarization properties (Faraday rotation and fractional polarization) derived from broadband observations of a lensing system at $z=0.44$, the authors have derived both the magnetic field strength and geometry in the lensing galaxy as seen 4.6 billion years ago, making it the most distant galaxy with such a measurement.

At present, the number of systems for which this technique can be applied to is limited (Mao *et al.* in prep). With an expected discovery of $>10^4$ new radio-bright gravitational lenses (a factor of >100 more than the currently known systems, McKean *et al.* 2015), the SKA will provide significantly more lensing systems that are well-suited for magnetism studies, extending measurements of magnetic fields in cosmologically distant galaxies to a much wider range in redshift and in mass. Along with other tracers of galactic magnetic fields at high redshifts (e.g., Basu *et al.* 2018), the SKA will enable one to firmly establish the observational trend of galactic magnetic fields as a function of cosmic time.

3. Summary

The SKA will transform our understanding of the origin and evolution of cosmic magnetic fields. The dense, broadband all-sky RM-grid together with additional pointed observations of selected targets will greatly advance our knowledge on the magnetized WHIM, 3-D magnetic fields in galaxies and their redshift evolution.

References

- Akahori, T. & Ryu, D. 2011, *ApJ*, 738, 134
 Akahori, T., Ryu, D., & Gaensler, B. M. 2016, *ApJ*, 824, 105
 Basu, A., Mao, S. A., Fletcher, A., et al. 2018, *MNRAS*, 477, 2528
 Beck, R., & Wielebinski, R. 2013, in *Planets, Stars and Stellar Systems*, Vol. 5, ed. T. D. Oswlat & G. Gilmore (Dordrecht: Springer), 641, updated in 2018 (arXiv: 1302.5663)
 Beck, R., Bomans, D., Colafrancesco, S., et al. 2015, *PoS, AASKA14*, 94
 Brown, S., Vernstrom, T., Carretti, E., et al. 2017, *MNRAS*, 458, 4246
 Fletcher, A., Beck, R., Shukurov, A., Berkhuijsen, E. M., & Horellou, C. 2011, *MNRAS*, 412, 2396
 Gaensler, B. M., Beck, R., & Feretti, L. 2004, *New Astron. Revs*, 48, 1003
 Gaensler, B. M., Haverkorn, M., Staveley-Smith, L., et al. 2005, *Science*, 307, 1610
 Han, J. L., Beck, R., & Berkhuijsen, E. M. 1998, *A&A*, 335, 1117
 Heald, G., Beck, R., de Blok, W. J. G., et al. 2015, *PoS, AASKA14*, 106
 Johnston-Hollitt, M. 2003, *Phd Thesis*, University of Adelaide
 Johnston-Hollitt, M., Govoni, F., Beck, R., et al. 2015, *PoS, AASKA14*, 92
 Macquart, J. P., Keane, E., Grainge, K., et al. 2015, *PoS AASKA14*, 55
 Ma, Y. K., Mao, S. A., Stil, J., et al. 2018, *MNRAS*, submitted
 Mao, S. A., Gaensler, B. M., Stanimirović, S., et al. 2008, *ApJ*, 688, 1029
 Mao, S. A., Carilli, C., Gaensler, B. M., et al. 2017, *Nature Astronomy*, 1, 621
 McKean, J., Jackson, N., Vegetti, S., et al. 2015, *PoS, AASKA14*, 92
 Nicastro, F., Kaastra, J., Krongold, Y., et al. 2018, *Nature*, 558, 406
 O’Sullivan, S. P., Machalski, J., Van Eck, C. L., et al. 2018, *MNRAS*, submitted
 Schnitzeler, D. H. F. M., Carretti, E., Wieringa, M. H., et al. 2018, *MNRAS*, submitted
 Taylor, A. R., Stil, J. M., & Sunstrum, C. 2009, *ApJ*, 702, 1230
 Taylor, A. R., Agudo, I., Akahori, T., et al. 2015, *PoS AASKA14*, 113
 Vacca, V., Oppermann, N., Ensslin, T., et al. 2016, *A&A*, 519, A13
 Vacca, V., Murgia, M., Govoni, F., et al. 2018, *MNRAS*, 479, 776
 Vazza, F., Ferrari, C., Bonafede, A., et al. 2015, *PoS AASKA14*, 97
 Vernstrom, T., Gaensler, B. M., Brown, S., Lenc, E., & Norris, R. P. 2017, *MNRAS*, 467, 4914

Capabilities of next generation telescopes for cosmic magnetism

Jeroen M. Stil¹ †

¹Department of Physics and Astronomy, The University of Calgary,
2500 University Drive NW, Calgary, AB, T2N 1N4, Canada
email: jstil@ucalgary.ca

Abstract. The next generation of radio telescopes offer significant improvement in bandwidth and survey speed. We examine the ability to resolve Faraday thick objects in Faraday space as a function of survey parameters. The necessary combination of λ_{\max} and λ_{\min} to resolve objects with modest Faraday thick components requires one or two surveys with instantaneous bandwidth 300 MHz to 750 MHz offered by next generation telescopes. For spiral galaxies, bandwidths in excess of 1.5 GHz are required. Correction for Galactic Faraday rotation must account for common gradients of order 10 rad m^{-2} per degree. How effective a new rotation measure grid is in probing the foreground depends on off-axis polarization calibration.

Keywords. magnetic fields, polarization, techniques: polarimeters, techniques: polarimetric

1. Introduction

Research in cosmic magnetism has entered a transformational period with the commissioning of new and upgraded radio telescopes that have much larger fractional bandwidth and larger field of view than the previous generation of telescopes. Among the new facilities are meter wave telescopes Low Frequency Array (LOFAR) and the Murchison Widefield Array (MWA), and centimeter wave telescopes Australian SKA Pathfinder (ASKAP) and MeerKAT, and large filled-aperture FAST. Existing telescopes that have made major upgrades for broad-band, wide-field imaging are the Jansky Very Large Array (JVLA), the Westerbork Synthesis Radio Telescope (WSRT/Apertif), the upgraded GMRT, eMERLIN, and the Arecibo radio telescope. On the horizon are the Square Kilometre Array (SKA) and the next generation Very Large Array (ngVLA).

Most of these facilities have polarization surveys planned or well underway. Naturally, these surveys are optimized for the main science drivers of the survey, given the capabilities of the observatory with which they are made. Factors that impact the effectiveness of an observatory for cosmic magnetism include the instantaneous bandwidth, operating frequency range, and the spatial frequencies probed over the observed frequency range. Important secondary factors are survey speed and available time for PI-driven follow-up observations. After all, one of the main drivers of a survey is discovery, to be followed by more detailed targeted observations.

Most extragalactic radio emission is synchrotron radiation. Its intensity and polarization contain information on magnetic field strength and structure. High angular resolution is a major factor as polarization angle structure within the beam causes depolarization. On the other hand, as we explore more of the low-surface-brightness universe, short spacing information can become a higher priority for extragalactic magnetism than it

† Present address: Department of Physics and Astronomy, The University of Calgary, 2500 University Drive NW, Calgary, AB, T2N 1N4, Canada.

has been in the past. Interpretation of broad-band polarization observations of well-resolved sources requires careful consideration of the spatial frequencies sampled by an interferometer across observed frequency range.

In this paper, I focus on two aspects of extragalactic cosmic magnetism enabled by the next generation radio telescopes: the ability to resolve a source in Faraday depth, and correction for Galactic Faraday rotation to the extent that it does not dominate the uncertainty in extragalactic Faraday rotation.

2. Resolving structure in Faraday depth

Structure in Faraday depth arises from differential Faraday rotation across the beam and from differential Faraday rotation along the line of sight (see R. Laing, this meeting, for a discussion how higher angular resolution reduces complexity, up to a point). The ability of a survey with continuous data between a minimum wavelength λ_{\min} and a maximum wavelength λ_{\max} to resolve an object in Faraday depth depends on Faraday depth resolution (Brentjens & De Bruyn 2005),

$$\Delta\phi = \frac{2\sqrt{3}}{\lambda_{\max}^2 - \lambda_{\min}^2}, \quad (2.1)$$

and the largest observable continuous Faraday depth range in the source,

$$\delta\phi = \frac{\pi}{\lambda_{\min}^2}. \quad (2.2)$$

Figure 1 shows a diagram of Faraday depth resolution and largest observable Faraday depth scale. A survey occupies a particular locus in this diagram through Equations 2.1 and 2.2. We can now choose a bandwidth, and vary the lowest frequency ν_{\min} (or λ_{\max}), to define a curve that represents all surveys with a set bandwidth. Figure 1 shows four

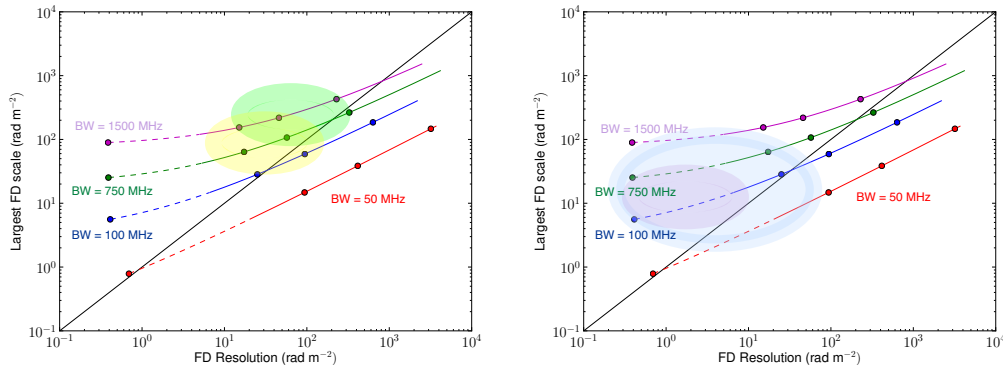


Figure 1. Diagram of Faraday depth resolution and largest observable Faraday depth scale for surveys with total bandwidth 50 (red), 100 (blue), 750 (green), and 1500 MHz (magenta). Dots mark surveys with $\nu_{\min} = 100$ MHz, 600 MHz, 1 GHz and 2 GHz (left to right). Dashed curves (frequency less than 350 MHz) are within the realm of aperture plane arrays, while the continuous curves have frequencies accessible with traditional arrays. The black diagonal line indicates where resolution is equal to the largest detectable Faraday depth scale. In order to resolve an object in Faraday depth, the Faraday depth range of the object must be between the curve and the black diagonal line. In the left panel, the green region marks the approximate parameter space for edge-on galaxies, and the yellow region the same for face-on galaxies. In the right panel, the blue region marks the approximate parameter space for lobes of radio galaxies, and the purple region a fiducial range for relics in galaxy clusters.

curves representing surveys with bandwidths of 50 MHz (red), 100 MHz (blue), 750 MHz (green), and 1.5 GHz (magenta). Dots on the curves mark $\nu_{\min} = 100, 600, 1000,$ and 2000 MHz (from left to right). The black diagonal marks the locations where Faraday depth resolution is equal to the largest detectable Faraday depth scale. We can only resolve objects in a survey with a particular bandwidth if their internal Faraday depth range is between the curve and the black diagonal. Deconvolution of Faraday depth structure below the resolution limit is difficult because both the phase and the amplitude of blended Faraday depth components matter (e.g. Kumazaki *et al.* 2014, Sun *et al.* 2015).

Different classes of objects can now be painted into the diagram, with the horizontal range limited by depolarization on the low-frequency side and the black diagonal on the high frequency side. Disks of spiral galaxies for example depolarize strongly below 1 GHz, but polarization has been detected as low as 350 MHz (Giessübel *et al.* 2013). The green and yellow regions in the left panel of Figure 1 mark approximate loci for diffuse polarized emission from spiral galaxy disks. Lobes of radio galaxies may have little internal Faraday rotation, but a range of Faraday depth may arise from structure in the surrounding medium. Steep spectrum sources such as relics in clusters may be better detectable at lower frequencies, as indicated by the purple region in Figure 1.

Figure 1 shows that in practice, it is easier to resolve objects with a modest Faraday depth range than objects with a larger intrinsic Faraday depth range. The latter require multiple surveys with telescopes with instantaneous bandwidth in the range 300 MHz to 750 MHz. Transformation of wavelength from the observer’s frame to the source frame at redshift z amounts to translation along the black diagonal line in the sense that the same source at high z would be less resolved in Faraday depth.

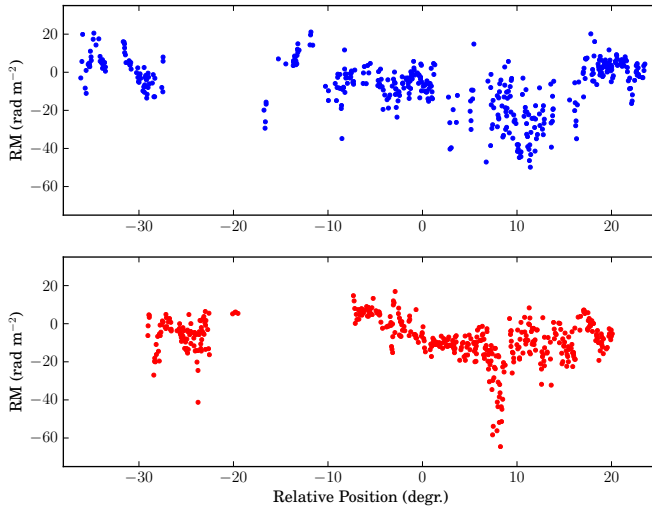


Figure 2. Variation of RM with position from high-latitude diffuse emission in the GALFACTS survey. The panels show two 0.3 degree wide strips, separated by 3 degrees in Galactic latitude in the range 65° to 70° . The horizontal axis is relative separation in the direction of Galactic longitude, corrected for latitude. Only data with strong polarized signal and RM error less than 5 rad m^{-2} are shown. Gaps in the data arise from regions with weaker signal.

3. Importance of off-axis polarization calibration

Arguably the foremost data set that next generation surveys will produce is a dense grid of rotation measures of polarized extragalactic sources across the sky (Beck & Gaensler 2004, Johnston-Hollitt *et al.* 2014). Correcting for Faraday rotation by the Galactic interstellar medium will be the most common application of the RM grid for extragalactic cosmic magnetism. The density of the grid and the quality of the RM data will determine the accuracy of this correction. Far from the Galactic plane, the errors in Opperman *et al.* (2012,2015) are of the order of 10 rad m^{-2} , which constitutes 22° rotation at 20 cm. An error in the Galactic Faraday rotation is magnified by a factor $(1+z)^2$ for the Faraday depth of a screen at redshift z , introducing significant uncertainty in the redshift dependence of Faraday depth (Hammond *et al.* 2012).

Figure 2 shows variation of RM of diffuse Galactic emission at high Galactic latitude from the GALFACTS survey (Taylor & Salter 2010). Although Faraday rotation of diffuse emission does not measure the same Faraday depth as extragalactic sources, we get an impression of the foreground RM structure on angular scales that are not yet accessible otherwise. Gradients of the order of 10 rad m^{-2} per degree and changes in the variance of RM are common on small scales. These small-scale structures cannot be recognized with the current sampling density of ~ 1 polarized source per square degree. The average density of RMs in Figure 2 is ~ 30 per square degree, comparable to the RM grid expected from the POSSUM survey (Gaensler *et al.* 2010, Rudnick & Owen 2014).

Constructing an RM grid that allows for consistent subtraction of Galactic Faraday rotation to the level of 1 rad m^{-2} is within reach of next generation sky surveys. The RM grid relies on sources measured across the field of view, far from the field centre where traditional polarization calibration solutions apply. In the absence of direction-dependent polarization calibration, we can expect residual leakage at the level of a few percent of total intensity at Faraday depth zero that blends with the astrophysical signal, unless the Faraday depth resolution of the survey is much better than 10 rad m^{-2} (Figure 2). This requires frequencies below 600 MHz (see Figure 1). The significance of blending of instrumental polarization with astrophysical Faraday rotation was discussed at this meeting by Y. K. Ma *et al.* Off-axis polarization calibration requires an investment by the observatory in terms of commissioning observations and software (e.g. Jagannathan *et al.* 2017). The performance of next generation telescopes for extragalactic magnetism depends in no small way on their ability to calibrate instrumental polarization across the field of view.

References

- Beck, R. and Gaensler, B. M., 2004, *New Astronomy Reviews*, 48, 1289
 Brentjens, M. A., & De Bruyn, A. G. 2005, *A&A*, 441, 1217
 Giessübel, R., Heald, G., Beck, R. & Arshakian, T. G. 2013, *A&A*, 559, A27
 Gaensler, B., Landecker, T. L., & Taylor, A. R. 2010, *BAAS*, 42, 515
 Hammond, A., Robishaw, T., & Gaensler B. M. 2012, *arXiv* 1209.1438
 Jagannathan, P., Bhatnagar, S., Rau, U., & Taylor A.R. 2017, *AJ*, 154, 56
 Johnston-Hollitt, M., Govoni, F., Beck, R., Dehghan, S., *et al.*, 2015, PoS(AASKA14)092
 Kumazaki, K., Akahori, T., Ideguchi, S., Kurayama, T., & Takahashi, K., 2014, *PASJ*, 66, 61
 Oppermann, N., Junklewitz, H., Robbers, G., *et al.* 2012, *A&A*, 542, A93
 Oppermann, N., Junklewitz, H., Greiner, M. *et al.*; 2015, *A&A*, 575, A118
 Rudnick, L. & Owen, F. 2014, *ApJ*, 785, 45
 Sun, X., Rudnick, L., Akahori, T., Anderson, C. S., Bell, M. R., *et al.* 2015, *AJ*, 149, 60
 Taylor, A. R. & Salter, C. J. 2010, *ASP Conf. Ser.* 438, 402

A fresh view of magnetic fields and cosmic ray electrons in halos of spiral galaxies

Ralf-Jürgen Dettmar¹, Volker Heesen², and the CHANG-ES Team³

¹Fakultät für Physik und Astronomie, Astronomisches Institut (AIRUB), Ruhr-Universität Bochum, Universitätsstrasse 150, 44801 Bochum, Germany; email: dettmar@astro.rub.de

²Universität Hamburg, Hamburger Sternwarte, Gojenbergsweg 112, 21029 Hamburg, Germany; email: volker.heesen@hs.uni-hamburg.de

³Judith Irwin (PI), Dept. of Physics, Engineering Physics, & Astronomy, Queen's University, Kingston, Ontario, Canada, K7L 3N6; email: irwinja@queensu.ca

Abstract. Recent numerical models of the multiphase ISM underline the importance of cosmic rays and magnetic fields for the physics of the ISM in disc galaxies. Observations of properties of the ISM in galactic halos constrain models of the expected exchange of matter between the star-forming disc and the environment (circumgalactic medium, CGM). We present new observational evidence from radio-continuum polarization studies of edge-on galaxies on magnetic field strength and structure as well as cosmic ray electron transport in galactic halos. The findings are discussed in the context of the disk-halo interaction of the interstellar medium. In addition, it is also briefly demonstrated how recent LOFAR observations of edge-on galaxies further constrain the extent of magnetic fields in galactic halos.

Keywords. galaxies: magnetic fields, galaxies: spiral, galaxies: halos, radio continuum: galaxies

1. Introduction

In the context of galaxy formation scenarios various feedback mechanisms (e.g., Silk 2013) have been discussed to explain the observed dependence of the global and long-term star formation efficiency in dark halos of different mass expressed as the ratio of stellar mass to the mass of the dark matter halo (e.g., Behroozi et al. 2013, Moster et al. 2013). For disc galaxies many different processes related to star formation are proposed: besides supernova explosions, stellar winds, and radiation pressure a number of recent papers discuss the possible importance of magnetic fields and cosmic ray pressure as an additional factor for the global dynamics of the interstellar medium (ISM) as well as for the launching of galactic winds (e.g., Girichidis et al. 2016, Pakmor et al. 2016). In the following we discuss the possible evidence for such cosmic ray driven galactic winds as observed by cosmic ray electrons (CREs) propagating in the magnetic fields in galactic halos. Recent progress in instrumentation such as the introduction of broadband multi-channel receivers at all large radio facilities allow for a fresh look at this long standing problem. Progress has also been made with regard to the wavelength coverage: with LOFAR (van Haarlem et al. 2013) it is now possible to observe the emission from CREs at lower energies which are less affected by energy losses. They represent an old population that has traveled furthest from the site of origin in the star forming regions of the mid-plane.

2. Transport models for cosmic ray electrons

The polarized and frequency dependent radio-synchrotron radiation of CREs allows us to constrain the magnetic field strength and structure in galaxies. The frequency depen-

dence of the synchrotron intensity also contains information on the transport processes for the CREs (e.g., Beck 2015). However, the observed emission has to be corrected for the frequency dependent contribution of the thermal radio-continuum which is also strongly correlated with star-formation. Here considerable progress has been made due to the availability of infrared data from satellite observations such as *Spitzer* and *WISE*. The dust emission in the ISM is a very good proxy for the star formation rate and can thus be used to correct for the thermal emission (e.g., Vargas et al. 2018). The clean synchrotron emission at various frequencies can then be used to study the emission by CREs with regard to magnetic field strengths and cosmic ray propagation processes such as diffusion or advection.

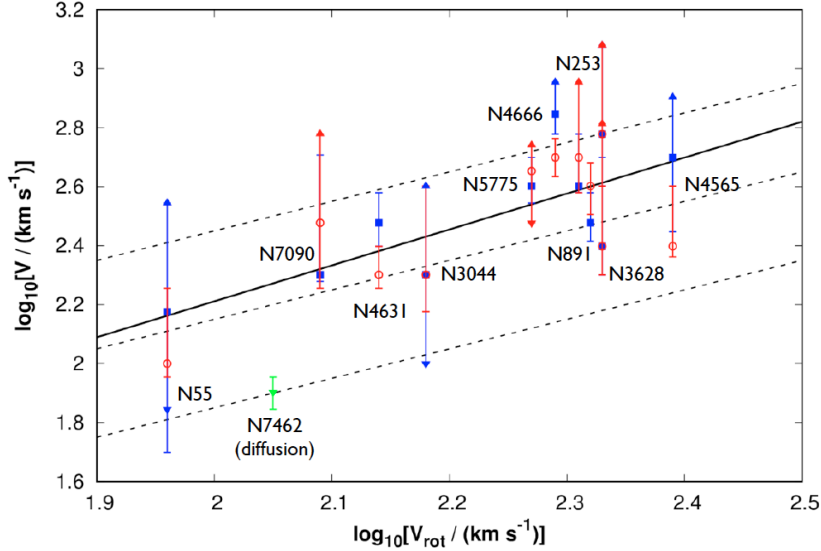


Figure 1. The correlation of the advection speed of cosmic ray electrons with the maximum rotation speed, i.e. total mass, of a sample of galaxies studied by Heesen et al. (2018). Most galaxies in this sample are best described by advective models for the cosmic ray electron propagation.

In a case study of the southern edge-on galaxies NGC 7090 and NGC 7462 based on Australia Telescope Compact Array (ATCA) data, Heesen et al. (2016) demonstrated that advective and diffusive transport of cosmic ray electrons into the halo can be distinguished by fitting a 1-D cosmic ray transport model to the intensity and spectral profiles perpendicular to the galaxy disc. Based on the analysis of archival data from the Very Large Array (VLA) and the Westerbork Synthesis Radio Telescope (WSRT), Heesen et al. (2018) discuss results of a larger sample (Fig. 1) with the conclusion that the radio halos of most galaxies studied so far are best described by advective transport models. For these galaxies the bulk velocity of the cosmic ray electrons correlates with the escape velocity of the galaxies as expected for galactic winds.

3. The CHANG-ES survey: first results

This analysis method is now to be applied to observations from the Karl G. Jansky Very Large Array (VLA) in the context of the “Continuum HALos in Nearby Galaxies – an Evla Survey” (CHANG-ES) project. The CHANG-ES sample consists of 35 edge-on spiral galaxies in the local universe selected by angular size and total flux. The targets

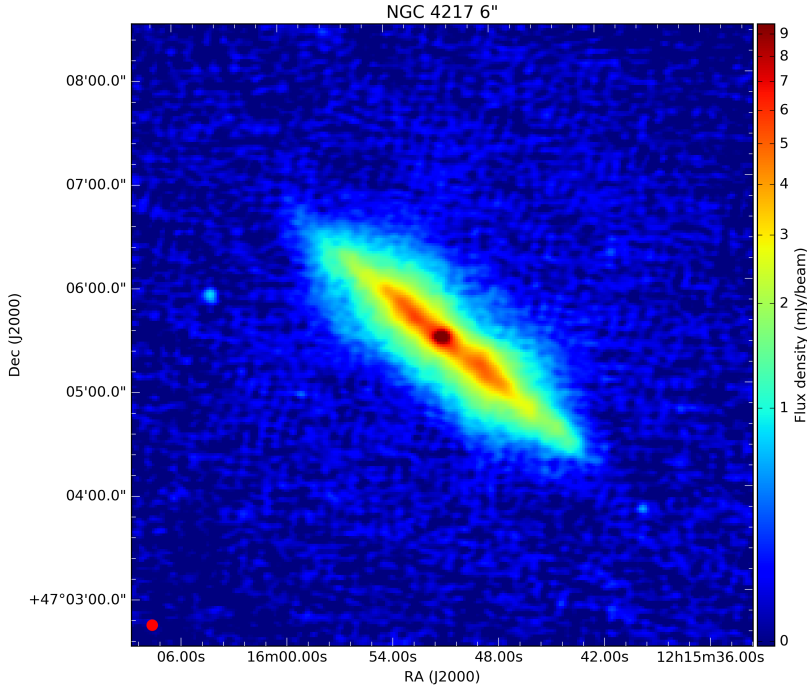


Figure 2. The edge-on galaxy NGC 4217 with a dumbbell-shaped radio-continuum halo is observed by LOFAR at 145 MHz as part of the Data Release 1 of the LoTSS survey (Shimwell et al. 2017, Shimwell 2018). The reprocessing by A. Miskolczi resulted in the reproduced map with a noise level of $\sim 70 \mu\text{Jy}/\text{beam}$ at 6 arcsec resolution.

were observed in the B-, C- and D-array-configurations in C- and L-band (Irwin et al. 2012). First results for the complete sample have been presented by Wiegert et al. (2015) in combination with a first data release of the D-array data products. The study provides an image of an averaged radio-continuum halo or thick disk for the sample. The conclusion that the average edge-on galaxy exhibits an extended radio-continuum halo is different from the finding by Singal et al. (2015) claiming that edge-on galaxies do not possess radio-continuum thick disks or halos that would make the emission look similar to that observed in the Milky Way. Further analyses study general properties of the CHANG-ES sample such as typical scale heights of the radio-continuum disks (Krause et al. 2018) as presented in another contribution to this meeting (Krause 2018). The case study of NGC 4666 based on CHANG-ES data with an indication of a possible reversal of the magnetic field direction in the plane of the disk is also presented elsewhere in these proceedings by Stein et al. (2018). A more detailed description of the CHANG-ES project and of its first results is presented by Stil (2018) at this conference.

4. Magnetic fields in galactic halos

Radio-continuum halos of star-forming disc galaxies frequently exhibit a large scale X-shaped magnetic field as, e.g., described for the prototypical case of NGC 5775 in Tüllmann et al. (2000). The extent of the synchrotron emission itself is proof for the presence of a magnetic field reaching far into the halo. Since the low energy cosmic rays are expected to be transported furthest, studies of the corresponding low frequency emission allow us to probe the magnetic field far into the halo. LOFAR now provides

observations with unprecedented sensitivity and resolution at such low frequencies as, e.g., demonstrated by the study of NGC 891 (Mulcahy et al. 2018). The LOFAR LoTSS survey (Shimwell et al. 2017) will provide a very good base for in depth studies of many more edge-on galaxies. To demonstrate this potential, Fig. 2 shows a map of NGC 4217 observed as part of the LoTSS Data Release 1 (Shimwell 2018). The dumbbell-shape radio halo (or thick disk) results from the combined effect of a radial decline of the magnetic field strength and the energy losses of the CREs transported into the halo (see Heesen et al. 2009a,b for a more detailed discussion).

References

- Beck, R. 2015, *A&A Rev.*, 24, 4
 Behroozi, P. S., Wechsler, R. H., & Conroy, C. 2013, *ApJ*, 770, 57
 Girichidis, P., Naab, T., Walch, S., et al. 2016, *ApJL*, 816, L19
 Heesen, V., Krause, M., Beck, R., & Dettmar, R.-J. 2009a, *A&A*, 506, 1123
 Heesen, V., Beck, R., Krause, M., & Dettmar, R.-J. 2009b, *A&A*, 494, 563
 Heesen, V., Dettmar, R.-J., Krause, M., Beck, R., & Stein, Y. 2016, *MNRAS*, 458, 332
 Heesen, V., Krause, M., Beck, R., et al. 2018, *MNRAS*, 476, 158
 Irwin, J., Beck, R., Benjamin, R. A., et al. 2012, *AJ*, 144, 43
 Krause, M. 2018, *these proceedings*
 Krause, M., Irwin, J., Wiegert, T., et al. 2018, *A&A*, 611, A72
 Moster, B. P., Naab, T., & White, S. D. M. 2013, *MNRAS*, 428, 3121
 Mulcahy, D. D., Horneffer, A., Beck, R., et al. 2018, *A&A*, 615, A98
 Pakmor, R., Pfrommer, C., Simpson, C. M., & Springel, V. 2016, *ApJL*, 824, L30
 Shimwell, T. W., Röttgering, H. J. A., Best, P. N., et al. 2017, *A&A*, 598, A104
 Shimwell, T. W. 2018, *priv. comm.*
 Silk, J. 2013, *ApJ*, 772, 112
 Singal, J., Kogut, A., Jones, E., & Dunlap, H. 2015, *ApJL*, 799, L10
 Stein, Y., Dettmar, R.-J., Irwin, J., et al. 2018, *these proceedings*
 Stil, J. 2018, *these proceedings*
 Tüllmann, R., Dettmar, R.-J., Soida, M., Urbanik, M., & Rossa, J. 2000, *A&A*, 364, L36
 van Haarlem, M. P., Wise, M. W., Gunst, A. W., et al. 2013, *A&A*, 556, A2
 Vargas, C. J., Mora-Partiarroyo, S. C., Schmidt, P., et al. 2018, *ApJ*, 853, 128
 Wiegert, T., Irwin, J., Miskolczi, A., et al. 2015, *AJ*, 150, 81

The Magnetized Disk-Halo Transition Region of M51

M. Kierdorf¹, S. A. Mao¹, A. Fletcher², R. Beck¹, M. Haverkorn³, A. Basu⁴, F. Tabatabaei⁵, and J. Ott⁶

¹Max-Planck-Institut für Radioastronomie, Auf dem Hügel 69, 53121, Bonn, Germany
email: kierdorf@mpifr-bonn.mpg.de

²School of Mathematics and Statistics, Herschel Building, Newcastle University, NE1 7RU U.K.

³Department of Astrophysics/IMAPP, Radboud University Nijmegen; P.O. Box 9010, 6500 GL Nijmegen, Netherlands

⁴Fakultät für Physik, Universität Bielefeld, Universitätsstr. 25, 33615 Bielefeld

⁵Instituto de Astrofísica de Canarias, San Cristóbal de La Laguna Santa Cruz de Tenerife, Spain

⁶National Radio Astronomy Observatory, 1003 Lopezville Road, Socorro, NM 87801, USA

Abstract. An excellent laboratory for studying large scale magnetic fields is the grand design face-on spiral galaxy M51. Due to wavelength-dependent Faraday depolarization, linearly polarized synchrotron emission at different radio frequencies gives a picture of the galaxy at different depths: Observations at L-band (1–2 GHz) probe the halo region while at C- and X-band (4–8 GHz) the linearly polarized emission probe the disk region of M51. We present new observations of M51 using the Karl G. Jansky Very Large Array (VLA) at S-band (2–4 GHz), where previously no polarization observations existed, to shed new light on the transition region between the disk and the halo. We discuss a model of the depolarization of synchrotron radiation in a multilayer magneto-ionic medium and compare the model predictions to the multi-frequency polarization data of M51 between 1–8 GHz. The new S-band data are essential to distinguish between different models. Our study shows that the initial model parameters, i.e. the total regular and turbulent magnetic field strengths in the disk and halo of M51, need to be adjusted to successfully fit the models to the data.

Keywords. polarization, Galaxies: spiral, individual (M51), magnetic fields

1. Introduction

M51 is a nearby face-on grand design spiral galaxy. Modern radio interferometers with high spatial resolution allow us to probe detailed structures of the galaxy in total intensity and linear polarization. Investigating depolarization effects of linearly polarized synchrotron emission at different wavelengths is a powerful tool to put constraints on the magneto-ionic properties of the interstellar medium (ISM) in galaxies. One effect which can cause depolarization is Faraday rotation in magnetized thermal plasma which rotates the plane of linear polarization of an electro-magnetic wave by an angle proportional to λ^2 . The proportionality constant is called the rotation measure (RM) and is measured in units of rad m^{-2} .

By comparing the observed degree of polarization as a function of wavelength with models of depolarization, one can investigate the underlying magnetic field properties (e.g. the regular and turbulent magnetic field strengths in the ISM). In the ISM of spiral galaxies, cosmic rays (CRs) as well as thermal electrons are mixed with magnetic fields in the same spatial volume. This causes emission of synchrotron radiation and Faraday rotation at the same locations. In such a case the polarization plane experiences *differential Faraday rotation* which results in a sinc-function variation of the fractional

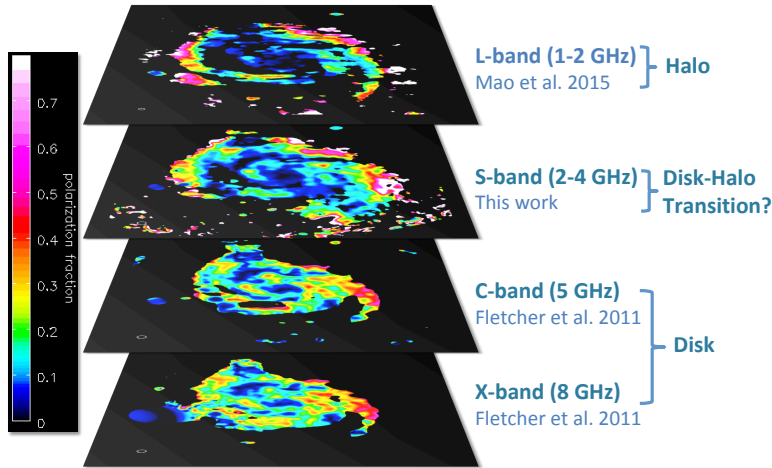


Figure 1. Observed degree of polarization of M51 at different frequencies. All images have the same color scale and are smoothed to the same resolution of 15 arcsec (which corresponds to about 550 pc at the distance of M51). Note that the total intensity images used to calculate the degree of polarization were not corrected for thermal emission.

polarization with λ^2 (Burn 1966). Therefore, at different frequencies one can probe the linearly polarized emission of a face-on galaxy at different physical depths: at high radio frequencies the polarized signal from the disk of the galaxy experiences low Faraday depolarization whereas at low radio frequencies, the polarized signal from the disk is almost completely depolarized. Fig. 1 shows the observed degree of polarization of M51 at frequencies between 1–8 GHz at the same angular resolution and the same color scale. One can see that the degree of polarization decreases with increasing wavelength (from bottom to top). Especially at L-band (top panel of Fig. 1) the central region of M51 is strongly depolarized. A detailed description of the data reduction and analysis and the full result of this work will be included in a forthcoming paper (Kierdorf et al., in prep.).

2. M51’s “unknown” polarization layer

Polarization studies of M51 shows that different configurations of the regular magnetic field exist in the disk and in the halo (e.g. Fletcher et al. 2011). According to Fletcher et al. (2011), the regular field in the disk is best described by a superposition of two azimuthal modes (axisymmetric plus quadrisymmetric), whereas the halo field has a strong bisymmetric azimuthal mode. The clear difference in the magnetic field configuration between the disk and the halo of M51 is still poorly understood. A better understanding will come from observations of the transition region between the disk and the halo. To investigate the “unknown” polarized layer between the disk and the halo we observed M51 in S-band (2–4 GHz, 7.5 - 15 cm) where no polarization data existed previously. We used the Karl G. Jansky Very large Array (VLA) in Socorro, New Mexico operated by the National Radio Astronomy Observatory (NRAO) which provides large antenna separation and wideband receivers resulting in high spatial resolution and wide frequency coverage with high sensitivity. Our new broadband S-band polarization data fill the gap between data observed with the VLA at L-band (1-2 GHz) by Mao et al. (2015), and C-band (4.85 GHz) and X-band (8.35 GHz) by Fletcher et al. (2011). With this combined high quality and broad frequency coverage data set we are able to investigate the magneto-ionic properties in different layers of M51.

3. Faraday depolarization in a multi-layer magneto-ionic medium

Shneider et al. (2014) developed a model of the depolarization of synchrotron radiation in a multilayer magneto-ionic medium. They developed model predictions for the degree of polarization as a function of wavelength for a two-layer system with a disk and a halo and a three-layer system with a far-side halo, a disk and a near-side halo. The model includes differential Faraday rotation caused by regular magnetic fields and internal Faraday dispersion due to random magnetic fields. In the case of a three-layer system, the near and far-side halo have identical properties. Fig. 2 shows the model predictions of the normalized degree of polarization (p/p_0) for a two-layer (left panel) and three-layer (right panel) system, respectively. p_0 is the intrinsic degree of polarization which is assumed to be 70% corresponding to the theoretical injection spectrum for electrons accelerated in supernova-remnants with a synchrotron spectral index of $\alpha_{\text{syn}} = -0.5$ (Shneider et al. 2014). The nomenclature of the different models is as follows: ‘D’ and ‘H’ stands for regular fields in the disk and halo, respectively. ‘I’ and ‘A’ denotes isotropic and anisotropic turbulent fields where the first one is for the disk and the second for the halo. The observed degrees of polarization at X-band, C-band, S-band and L-band are also shown. For the purpose of this proceeding, we consider the total and polarized intensity integrated in a sector with an azimuthal angle centered at 100° and an opening angle of 20° and radial boundaries 2.4–3.6 kpc \dagger . With only the data points at 3.6 cm, 6.2 cm, and L-band (15–30 cm) it is not possible to assess if a two-layer or three-layer system is more likely for M51. Since the model predictions strongly differ within the wavelength range of S-band (7.5–15 cm), our new S-band data are essential to distinguish between the different systems.

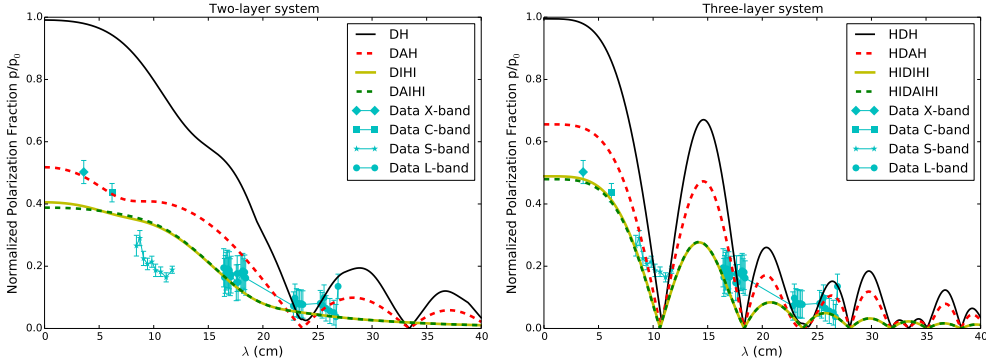


Figure 2. Depolarization models from Shneider et al. (2014) for a two-layer system (left panel) and a three-layer system (right panel) in M51 plotted together with the observed degree of polarization at multiple wavelengths. All model profiles featured have been constructed from a set of the following parameters: a total regular magnetic field strength of $5 \mu\text{G}$ in the disk and halo, a disk turbulent random field of $14 \mu\text{G}$, and a halo turbulent random field of $4 \mu\text{G}$ and a thermal electron density of 0.11 cm^{-3} and 0.01 cm^{-3} in the disk and halo, respectively. For nomenclature and description of the model types appearing in the legend we refer to the text.

By comparing the observed degree of polarization to the models, one can directly rule out models with only regular magnetic fields in the disk and halo (DH) since the observed data deviate most from those model predictions. However, it appears that none of the model predictions with the parameters given in Shneider et al. (2014) are in agreement

\dagger To obtain the non-thermal total flux density at this location, we assumed a thermal fraction $f_{\nu_0}^{\text{th}}$ of 9% at $\nu_0 = 3 \text{ GHz}$ (Tabatabaei et al. 2017) and extrapolated the non-thermal flux densities at frequency ν via $S_\nu = f_{\nu_0}^{\text{th}} \left(\frac{\nu}{\nu_0} \right)^{-0.1} S_{\nu_0}$.

with the observed data at S-band. For the two-layer system, the data points deviate from the model whereas for the three-layer case, some data points are well reproduced by the model predictions but the model drops to zero at $\lambda \approx 11$ cm which is clearly ruled out by the observed data. To investigate the influence of different total magnetic field strengths on the degree of polarization, we developed an interactive tool which allows one to produce model predictions for a range of total regular and turbulent magnetic field strengths in the disk and halo simultaneously. Fig. 3 shows the “best fit” of the model DAH (red dashed line) with regular magnetic fields in disk and halo and anisotropic turbulent magnetic fields in the disk. We explored visually whether any reasonable combination of the free parameters can reproduce the observed degree of polarization. These “best fit” magnetic field strengths and electron densities are listed in the caption of Fig. 3 and are all physically plausible values. For the three-layer system it is not possible to lift up the zero points in the model by changing any parameter. Therefore, this three-layer model can be ruled out. In other words, we do not detect any polarized emission from the far side halo.

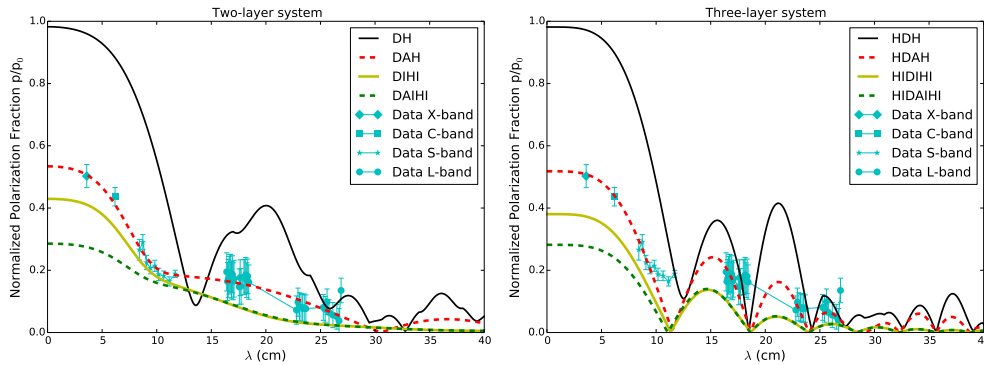


Figure 3. “Best-fit” of the model DAH for a two-layer system (left panel) and a three-layer system (right panel) in M51 to the observed degree of polarization at multiple wavelengths. The “best fit” magnetic field strengths are $10 \mu\text{G}$ and $3 \mu\text{G}$ for the total regular field in the disk and in the halo for the two-layer and three-layer system, respectively. The total random magnetic field strengths in the disk amounts to $14 \mu\text{G}$ and $16 \mu\text{G}$ for the two - and three-layer system, respectively. For the electron density a value of 0.07 cm^{-3} and 0.01 cm^{-3} in the disk and halo fits the data best in both layer systems.

4. Future Work

We show that the comparison of the observed degree of polarization to the wavelength-dependent depolarization models is a powerful tool to put constraints on the magnetic field strengths and thermal electron density in different regions of the galaxy. As a next step, we will apply the same method to other sectors with different azimuthal angles and radii in M51. Consistency between fits to different sectors is a strong indication that the model is physically meaningful. Further, since the different models distinguish between isotropic and anisotropic turbulent magnetic fields, by comparing the observed degree of polarization in different regions of the galaxy with the model predictions, we can investigate turbulent magnetic field configurations in different locations in M51.

References

- Burn B. J., 1966, *MNRAS*, 133, 67
 Fletcher A., Beck R., Shukurov A., Berkhuijsen E. M., Horellou C., 2011, *MNRAS*, 412, 2396
 Mao S. A., Zweibel E., Fletcher A., Ott J., Tabatabaei F., 2015, *ApJ*, 800, 92
 Shneider C., Haverkorn M., Fletcher A., Shukurov A., 2014, *A&A*, 567, A82
 Tabatabaei F. S., et al., 2017, *ApJ*, 836, 185

Techinques and algorithmic advances in the SKA era

V. Vacca¹, F. Govoni¹, M. Murgia¹, T. Enßlin², N. Oppermann³, L. Feretti⁴, G. Giovannini^{4,5}, J. Jasche⁶, H. Junklewitz⁷ and F. Loi⁵

¹INAF - Osservatorio Astronomico di Cagliari, Via della Scienza 5, Selargius, Italy
email: valentina.vacca@inaf.it

²MPA, Karl-Schwarzschild-Str 1, Garching, Germany

³CITA, University of Toronto, 60 St. George Street, Toronto, Canada

⁴INAF - Istituto di Radioastronomia, Via Gobetti 101, Bologna, Italy

⁵DIFA, Università degli Studi di Bologna, Viale Berti Pichat 6/2, Bologna, Italy

⁶Excellence Cluster Universe, TUM, Boltzmannstrasse 2, Garching, Germany

⁷Argelander-Institut für Astronomie, Auf dem Hügel 71, Bonn, Germany

Abstract. The new generation of radio interferometers will deliver an unprecedented amount of deep and high resolution observations. In this proceedings, we present recent algorithmic advances in the context of the study of cosmic magnetism in order to extract all the information contained in these data.

Keywords. magnetic fields, polarization, methods: numerical methods: statistical

1. Introduction

Magnetism in the cosmic web is widely unknown. Magnetic fields have revealed themselves in galaxy clusters in the form of diffuse synchrotron sources and via the Faraday effect on background radio galaxies that indicate strengths of a few μG and fluctuation scales up to a few hundreds of kpc (e.g., Feretti et al. 2012). Beyond galaxy clusters, along filaments and in the voids of the cosmic web, some indication of their presence has been found so far but needs to be confirmed. To shed light on cosmological magnetic field origin and evolution, the analysis of magnetic properties in these environments is crucial. Nowadays, magnetic fields are thought to originate from a seed magnetic field whose strength has been amplified and geometry modified during processes of structure formation. The investigation of non-thermal components in galaxy clusters and in the low density environments between them has the potential to shed light on their evolution and formation. In the following, we give an overview of the effort done by the scientific community in the last years in this direction. In §2 and §3, we respectively describe the progress concerning the study via diffuse synchrotron emission and Faraday effect and in §4 we present the conclusions.

2. Diffuse emission

Diffuse synchrotron sources called radio halos have been observed to permeate the central volume of about 50 galaxy clusters where they reveal μG magnetic fields and ultra-relativistic particles ($\gamma \gtrsim 10^4$). Their emission permits to directly probe the intracluster magnetic field. Magnetic fields fluctuating on scales larger than the resolution of the observations are expected to generate radio halos with disturbed morphology and high degrees of polarization. Magnetic fields with fluctuation scales smaller than the beam could be responsible of regular morphology and no polarized signal (e.g., Vacca

et al. 2010). To date only in three systems a polarized signal likely associated with the diffuse emission of the halo has been detected (e.g., Girardi et al. 2016). Numerical three-dimensional simulations by Govoni et al. (2013) indicate that, at 1.4 GHz, radio halos show intrinsic fractional polarization levels of 15-35% at the cluster center that increase in the cluster outskirts. This level of polarization corresponds to a polarized signal of about $2\text{-}0.5 \mu\text{Jy}/\text{beam}$ for strong and intermediate luminosity radio halos at $3''$ of resolution but, due to instrumental limitations (resolution and sensitivity), it is hard to detect. The JVLA has the potential to detect already polarized emission in high-luminosity radio halos, while for intermediate-luminosity sources only SKA1 can succeed. The detection of faint-luminosity radio halos instead will be very difficult even with the SKA1.

Properly imaging these sources is very important to investigate the magnetization of the medium. However, standard imaging tools as CLEAN (e.g., Högbom 1974) are unsatisfactory since they rely on the assumption of a completely uncorrelated point source sky, while radio halos are diffuse and extended. In the last years new imaging algorithms have been developed based on either compressed sensing (e.g., MORESANE, Dabbech et al. 2015) or Bayesian statistics (e.g., RESOLVE, Junklewitz et al. 2016), capable of exploiting the capabilities of the new generation of radio telescopes to accurately reproduce the complexity of the radio sky in total intensity as well as in polarization. This progress is particularly important in the context of the investigation of faint diffuse emission beyond galaxy clusters, from the filaments of the cosmic web. Recently, we observed a region of the sky of $8^\circ \times 8^\circ$ containing several galaxy clusters of which about ten at $z \approx 0.1$, with the Sardinia Radio Telescope (SRT) at 1.4 GHz (Vacca et al. 2018). The data revealed a field very bright in radio especially crowded at the location of galaxy clusters and between them (Fig. 1). To overcome the limited spatial resolution of $\sim 13'$ and separate possible diffuse emission from embedded discrete radio sources, we combined these data with higher resolution data from the NRAO VLA Sky Survey (NVSS, $45''$, Condon et al. 1998) and subtracted point-sources. In the resulting image,

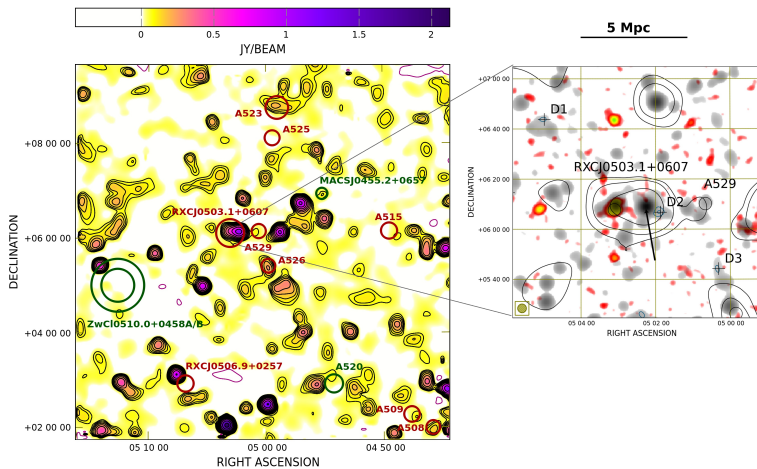


Figure 1. Left: SRT image (angular resolution $13.9' \times 12.4'$) in colors and contours at 1.4 GHz. The circles and labels identify the position of the galaxy clusters in the field of view with known redshift: in red clusters with $0.08 < z < 0.15$, in green clusters with redshift outside this range. Right: Zoom of the central region of the full field of view. SRT contours (negative in magenta and positive in black) and SRT+NVSS after compact-source subtraction contours (in blue, resolution $3.5' \times 3.5'$) overlaid on X-ray emission from the RASS in red colors and radio emission from the SRT+NVSS in grey colors. Images from Vacca et al. (2018).

we identified 28 new diffuse sources with radio emissivity and X-ray emission 10-100 times lower than cluster radio sources. The comparison with magneto-hydro-dynamical simulations suggests that they could represent the tip of the iceberg of the emission associated with the warm-hot intergalactic medium and correspond to magnetic field strengths of $\sim 20\text{-}50\text{ nG}$.

3. Radio galaxies

A complementary and alternative approach to investigate magnetic fields in the cosmic web is given by the analysis of polarimetric properties of background radio galaxies. While crossing the magneto-ionic media in between the source and the observer, their signal suffers a rotation $\Delta\Psi$ of the polarization angle

$$\Delta\Psi = \Psi_{\text{obs}} - \Psi_{\text{int}} = \phi\lambda^2 \quad (3.1)$$

where Ψ_{int} and Ψ_{obs} are respectively the intrinsic and observed polarization angle, λ the wavelength of observation, and ϕ the Faraday depth, related to the magnetic field along the line of sight B_{\parallel} and to the thermal gas density n_e of the magneto-ionic medium

$$\phi = 812 \int_0^{l[\text{kpc}]} n_e[\text{cm}^{-3}]B_{\parallel}[\mu\text{G}]dl \quad \text{rad/m}^2. \quad (3.2)$$

In the case of a screen external to the radio source, the Faraday depth does not change as a function of λ^2 and is defined as Rotation Measure (RM, Burn 1966). If the radio and X-ray plasma are mixed, the Faraday depth is no more constant and the observed polarized intensity may be associated with a range of Faraday depths. In this case more advanced approaches are necessary to properly recover polarimetric properties of the radio sources as QU-fitting, RM Synthesis, and Faraday Synthesis (e.g., O'Sullivan et al. 2012; Brentjens & de Bruyn 2005; Bell & Enßlin 2012).

In case of radio galaxies in the background of galaxy clusters, deep and high resolution polarimetric data at multiple frequencies permit to obtain detailed rotation measure images. When the Galactic contribution is negligible, these images represent a two-dimensional picture of the intracluster magnetic field and can be used to derive its power

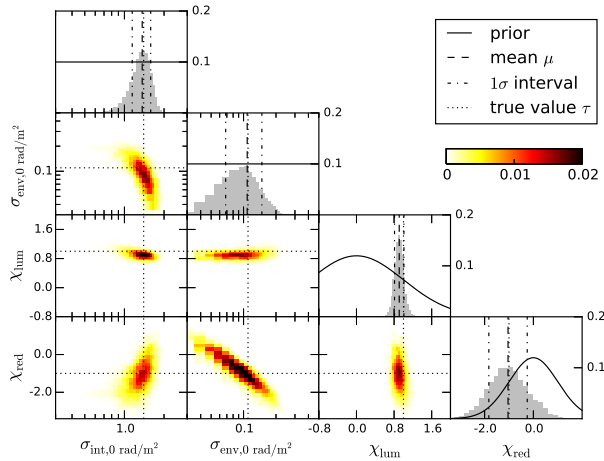


Figure 2. Example of the posterior from the algorithm presented in Vacca et al. (2016) for a mock catalog of Faraday depth values for 3500 sources in the frequency range covered by SKA1-LOW and an overall extragalactic contribution of 0.7 rad/m^2 .

spectrum via the comparison with simulations (e.g., Vacca et al. 2012). Unfortunately, to date detailed Faraday depth images are available typically for one source per clusters, apart from a few exceptions (e.g., Govoni et al. 2006). With the SKA1, we expect a number of several tens of sources for nearby galaxy clusters ($z < 0.1$) allowing us to study the magnetic field over the complete cluster volume (Bonafede et al. 2015).

Thanks to the high sensitivity and resolution of the polarization surveys planned with the SKA precursors and path-finders, the upcoming Faraday depth catalogs will contain several thousands of sources and up to 7-14 million with the SKA1 (Johnston-Hollitt et al. 2015). These data will simultaneously carry out the information of all the structures between the source and the observer (our Galaxy, intervening sources, galaxy clusters, filaments, voids, etc). To isolate the Faraday effect due to the cosmic web different strategies have been developed as, e.g., filtering out unwanted contributions by Akahori et al. (2014). In this context, we recently developed statistical Bayesian approaches to disentangle the Galactic and extragalactic Faraday rotation while properly taking into account the noise (Oppermann et al. 2015) and to further decompose the extragalactic Faraday rotation in the contributions intrinsic to the emitting source, due to any intervening galaxy and associated with different regions of the large scale structure (e.g., galaxy clusters, filaments, voids and sheets, Vacca et al. 2016). We showed that high-quality low-frequency data for a few thousand of sources have the potential to investigate magnetic fields with strengths of ≈ 0.2 -2 nG associated with the large scale structure (Fig. 2).

4. Conclusions

The SKA, its path-finders and precursors are expected to permit a breakthrough in the study of cosmic magnetism, thanks to new data of unprecedented high-quality. To exploit these data and finally uncover the signature of the faint magnetic fields of the cosmic web, advanced and sophisticated techniques of analysis as those developed in the last decades are essential.

References

- Akahori, T., Gaensler, B. M., & Ryu, D. 2014, *ApJ*, 790, 123
 Bell, M. R., & Enßlin, T. A. 2012, *A&A*, 540, A80
 Bonafede, A., Vazza, F., Brüggem, M., et al. 2015, *AASKA14*, 95
 Brentjens, M. A., & de Bruyn, A. G. 2005, *A&A*, 441, 1217
 Burn, B. J. 1966, *MNRAS*, 133, 67
 Condon, J. J., Cotton, W. D., Greisen, E. W., et al. 1998, *AJ*, 115, 1693
 Dabbech, A., Ferrari, C., Mary, D., et al. 2015, *A&A*, 576, A7
 Feretti, L., Giovannini, G., Govoni, F., & Murgia, M. 2012, *A&ARv*, 20, 54
 Girardi, M., Boschin, W., Gastaldello, F., et al. 2016, *MNRAS*, 456, 2829
 Govoni, F., Murgia, M., Xu, H., et al. 2013, *A&A*, 554, A102
 Govoni, F., Murgia, M., Feretti, L., et al. 2006, *A&A*, 460, 425
 Högbom, J. A. 1974, *A&AS*, 15, 417
 Johnston-Hollitt, M., Govoni, F., Beck, R., et al. 2015, *AASKA14*, 92
 Junklewitz, H., Bell, M. R., Selig, M., & Enßlin, T. A. 2016, *A&A*, 586, A76
 Oppermann, N., Junklewitz, H., Greiner, M., et al. 2015, *A&A*, 575, A118
 O’Sullivan, S. P., Brown, S., Robishaw, T., et al. 2012, *MNRAS*, 421, 3300
 Vacca, V., Murgia, M., Govoni, F., et al. 2018, *MNRAS*, 479, 776
 Vacca, V., Oppermann, N., Enßlin, T., et al. 2016, *A&A*, 591, A13
 Vacca, V., Murgia, M., Govoni, F., et al. 2012, *A&A*, 540, A38
 Vacca, V., Murgia, M., Govoni, F., et al. 2010, *A&A*, 514, A71

CMB weak lensing with the primordial magnetic field

Dai G. Yamazaki^{1,2}

¹Ibaraki University, 2-1-1, Bunkyo, Mito, 310-8512, Japan

²National Astronomical Observatory of Japan, Mitaka, Tokyo 181-8588, Japan
email: yamazaki.dai@nao.ac.jp

Abstract. We illustrate that a primordial magnetic field (PMF) suppresses the cosmic microwave background (CMB) B mode from the weak lensing (WL) effect. The WL effect is dependent on the lensing potential (LP) from the matter perturbations. A distribution of the matter perturbations on the cosmological scales is given by the matter power spectrum (MPS). Therefore, the WL effect on the CMB B mode is affected by the MPS. The CMB B mode, provides important information on the background gravitational waves, the inflation theory, the matter density fluctuations and the structure formation in the cosmological scale through the cosmological parameter search. If we precisely research these topics and correctly constrain the cosmological parameters from the cosmological observations including the CMB B mode, we should consider the background PMF correctly.

1. Introduction

Magnetic fields with strength in the order of $1 \mu\text{G}$ ($= 10^{-6}$ G) are observed in the typical subgalaxy to cluster scale by Faraday rotation and synchrotron emission (Neronov and Vovk 2010, Vovk et al. 2012, Feretti et al. 2012). The primary origin of these magnetic fields is the primordial magnetic field (PMF). PMF is assumed to be homogeneous and stochastic with comoving strength in the order of $1a^{-2}$ nG ($1 \text{ nG} = 10^{-9}$ G), where a is the scale factor. If this PMF is generated before the recombination and it evolves into the observed magnetic fields by the isotropic collapse of the density fields in the early Universe, then the observed magnetic fields in the cosmological scales can be explained (Grasso and Rubinstein 2001, Yamazaki et al. 2010a, Kandus et al. 2011, Yamazaki et al. 2012) and PMF parameters have been constrained by using the cosmological observation datasets (Yamazaki et al. 2005, Lewis 2004, Yamazaki et al. 2006a, Yamazaki et al. 2008a, Kahniashvili et al. 2009, Yamazaki et al. 2010b, Kahniashvili et al. 2010, Paoletti and Finelli 2011, Yamazaki and Kusakabe 2012, Shaw and Lewis 2012, Yamazaki et al. 2013, Paoletti and Finelli 2013, Shiraishi 2013, Yamazaki et al. 2014, Planck Collaboration et al. 2016a, Zucca et al. 2017).

There are two kinds of PMF effects on the fluctuations of the CMB and the matter power spectrum (MPS). The first effect is due to the first perturbation source from the PMF in the linear perturbative equations. Therefore, this PMF effect is called “the perturbative PMF effect” in this article. The perturbative PMF effect generates fluctuations of CMB and MPS in smaller scales corresponding to $k \geq 0.1 h\text{Mpc}^{-1}$ (Yamazaki et al. 2006b, Yamazaki et al. 2008b, Yamazaki et al. 2010b, Yamazaki et al. 2011), where h is the Hubble parameter in units of 100 km/s/Mpc.

The second effect is due to the ensemble energy density of the PMF because it is considered a nonperturbative source in linear perturbative theory. Therefore, we call it “the background PMF effect”. The background PMF changes the features of the CMB (Yamazaki 2014) and MPS (Yamazaki 2016). The peak positions of the CMB temperature

fluctuations and the MPS shift to larger scale because of the background PMF (Yamazaki 2014, Yamazaki 2016).

We adopt the flat and Λ CDM model, and assume that the PMF is generated well before the recombination epoch, e.g., the inflation epoch, and that it is stochastic homogeneous, isotropic, and random. A PMF mode in this article is defined by Yamazaki(2018), and the numerical formulation of the PMF spectra from Yamazaki et al. (2008b). We adopt the cosmological parameters determined by the Planck 2016 (TT + lowP + lensing in Table 4 of Planck Collaboration et al. 2016b). We modify CAMB code of Lewis et al. (2000) for computing the lensing potential and the CMB B mode with PMF effects.

2. Lensing potential and weak lensing in the PMF

The WL effect depends on the lensing potential (LP) and the spectrum of the LP $C_\ell^{r\psi}$ depends on the MPS (Lewis and Challinor 2006, Yamazaki 2018). From the PMF effects on the MPS, the LP spectra with the PMF are as shown in panels (a-1) and (a-2) of Fig. 1, where n_B is the spectrum index of the PMF, $B_\lambda = |\mathbf{B}_\lambda|$ is the comoving field strength by smoothing over a Gaussian sphere of radius $\lambda = 1$ Mpc ($k_\lambda = 2\pi/\lambda$). Background PMFs shift the peak positions ℓ_P of the LP spectra to smaller multipoles (larger scales) and suppress the amplitudes for $\ell \gtrsim \ell_P$. The WL effect on the CMB B mode is due to the LP; hence, the PMFs affect the CMB B mode owing to WL through the LP [Panels (b-1) and (b-2) in Fig. 1]. To analyze the WL effect on the CMB B mode owing only to the LP with the PMFs, the CMB B mode spectra of vector and tensor sources are not included in panels (b-1) and (b-2) of Fig. 1. If the background PMF effect for estimating the MPS is not considered, the LP spectra and CMB B mode from the WL effect with the PMF in smaller multipoles remain nearly unchanged like the MPS without the background PMF (Yamazaki 2018). In fact, the overall PMF effect suppresses the PL spectra and the CMB B mode owing to WL for $\ell > 100$ as shown in Fig. 1.

Unlike the MPS and the LP spectrum, the CMB B mode from the perturbative PMF effect has two kind modes: vector and tensor mode. The vector and tensor CMB modes from the perturbative PMF effect directly increase the amplitude of the CMB B mode (Durrer et al. 2000, Mack et al. 2002, Yamazaki et al. 2010b, Yamazaki et al. 2012, Shaw and Lewis 2012). The tensor CMB B mode from the perturbative PMF is much smaller than the CMB B mode from the WL effect, whereas the CMB B mode of the vector mode from the perturbative PMF effect corresponds to the CMB B mode from the WL effect for hundreds of multipoles. In fact, as shown in panel (c) of Fig. 1 for $\ell > 800$, it directly increases the amplitude of the CMB B mode spectra and dominates the spectra. However, because the error bars of the datasets for $\ell > 800$ are large, it is difficult to constrain the parameters of the PMF based on the observation datasets. In addition, the CMB B mode from the perturbative PMF effect for $\ell < 400$, where the observational data points have smaller errors from BK14 (BICEP2 Collaboration et al. 2016), is too small to effectively constrain the PMF parameters. Nevertheless, the background PMF effect suppresses the CMB B mode owing to WL in the effective range of BK14 as shown in panel (c) of Fig. 1. Thus, if we use the observational CMB B mode datasets for $\ell < 400$, the PMF parameters are constrained.

3. Constraints on the PMF parameters

Finally, although preliminary results, we introduce a comparison of constraints on PMF parameters with and without ρ_{PMF} . Using the Planck (Planck Collaboration et al. 2016b) and BK14 data sets and the MCMC method (Lewis and Bridle 2002), the power law

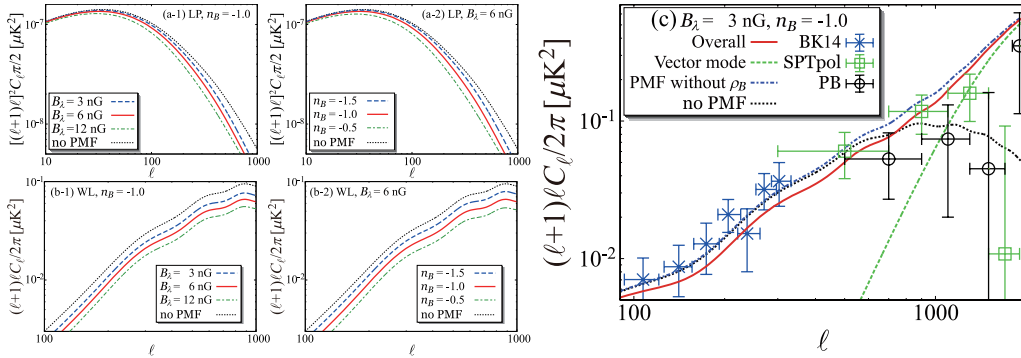


Figure 1. PMF effects on the LP spectra (panels (a-1), (a-2)) and CMB B modes owing to WL (panels (b-1), (b-2)). Panel (c) shows that PMF effects on the CMB B mode for fixed PMF parameters $(B_\lambda, n_B) = (3 \text{ nG}, -1.0)$. All curves are indicated in the legend box in this figure. The tensor-to-scalar ratio r is 0.05. The dots with error bars are the CMB B mode measurements from BICEP2/Keck (BK14) (BICEP2 Collaboration et al. 2016), POLARBEAR (PB) (The POLARBEAR Collaboration et al. 2017), and SPTpol (Keisler et al. 2015), as shown by the legends. The uncertainties of the error bars correspond to 1σ (68.3% confidence level).

index of the PMF with the background PMF is constrained $n_B < -1.8$, which is lower than a result without the background PMF ($n_B < -1.5$). Since the energy density of the background PMF is dependent on the power-law index n_B and becomes much bigger with higher n_B from Eq. (1) in Yamazaki(2018), the effects of the PMF of bigger n_B on the CMB B mode are not negligible for a wider range of multipoles (Fig. 1). Therefore n_B can be constrained more strongly from the CMB B mode with ρ_{MF} .

4. Summary

It has been known that the vector mode from the perturbative PMF effect increases the CMB B mode for large multipoles, e.g., more than hundreds multipoles. In this article, we show that, as in the background PMF effect on the MPS, the background PMF effect suppresses the LP spectrum for wider range of multipole. Since the CMB B mode owing to WL depends on the LP spectrum, the background PMF effect indirectly suppresses it for wider range of multipole. We also show that we expect to strongly constrain the PMF parameters from observational datasets at $\ell < 400$, which have relatively smaller errors, if we correctly consider the background PMF effect on the CMB B mode. The magnetic field affects the physical process at wide scale ranges in the Universe. However, studies of magnetic fields on the cosmological scales are less active because it is difficult to directly observe the magnetic fields in cosmological scales and evaluate theoretical models considering magnetic fields with less observation and results. If we adopt the background PMF effects on the CMB B mode and constrain the PMF parameters in the CMB B mode with observations having smaller errors, we can promote the study of PMF in cosmology.

Acknowledgements

This work has been supported in part by Grants-in-Aid for Scientific Research (Grant No. 25871055) of the Ministry of Education, Culture, Sports, Science and Technology of Japan.

References

- BICEP2 Collaboration, Keck Array Collaboration, P. A. R. Ade, Z. Ahmed, R. W. Aikin, K. D. Alexander, D. Barkats, S. J. Benton, C. A. Bischoff, J. J. Bock, et al., *Phys. Rev. Lett.* **116**, 031302 (2016).
- R. Durrer, P. G. Ferreira, and T. Kahniashvili, *Phys. Rev.* **D 61**, 043001 (2000).
- L. Feretti, G. Giovannini, F. Govoni, and M.urgia, *The Astronomy and Astrophysics Review* **20**, 54 (2012).
- D. Grasso and H. R. Rubinstein, *Phys. Rept.* **348**, 163 (2001).
- T. Kahniashvili, Y. Maravin, and A. Kosowsky, *Phys. Rev.* **D80**, 023009 (2009).
- T. Kahniashvili, A. G. Tevzadze, S. K. Sethi, K. Pandey, and B. Ratra, *Phys. Rev. D* **82**, 083005 (2010).
- A. Kandus, K. E. Kunze, and C. G. Tsagas, *Physics Reports*, **505**, 1 (2011).
- R. Keisler, S. Hoover, N. Harrington, J. W. Henning, P. A. R. Ade, K. A. Aird, J. E. Austermann, J. A. Beall, A. N. Bender, B. A. Benson, et al., *Astrophys. J.* **807**, 151 (2015).
- A. Lewis, A. Challinor, and A. Lasenby, *Astrophys. J.* **538**, 473 (2000).
- A. Lewis and S. Bridle, *Phys. Rev.* **D 66**, 103511 (2002).
- A. Lewis, *Phys. Rev.* **D 70**, 043011 (2004).
- A. Lewis and A. Challinor, *Phys. Rep.* **429**, 1 (2006).
- A. Mack, T. Kahniashvili, and A. Kosowsky, *Phys. Rev.* **D 65**, 123004 (2002).
- A. Neronov and I. Vovk, *Science* **328**, 73 (2010).
- D. Paoletti and F. Finelli, *Phys. Rev.* pp. 123533 (2011).
- D. Paoletti and F. Finelli, *Physics Letters B* **726**, 45 (2013).
- Planck Collaboration, P. A. R. Ade, N. Aghanim, M. Arnaud, F. Arroja, M. Ashdown, J. Aumont, C. Baccigalupi, M. Ballardini, A. J. Banday, et al., *Astron. & Astrophys.* **594**, A19 (2016a).
- Planck Collaboration, P. A. R. Ade, N. Aghanim, M. Arnaud, M. Ashdown, J. Aumont, C. Baccigalupi, A. J. Banday, R. B. Barreiro, J. G. Bartlett, et al., *Astron. & Astrophys.* **594**, A13 (2016b).
- The POLARBEAR Collaboration, P. A. R. Ade, M. Aguilar, Y. Akiba, K. Arnold, C. Baccigalupi, D. Barron, D. Beck, F. Bianchini, D. Boettger, et al., *Astrophys. J.* **848**, 121 (2017).
- J. R. Shaw and A. Lewis, *Phys. Rev. D* **86**, 043510 (2012).
- M. Shiraishi, *JCAP* **11**, 006 (2013).
- I. Vovk, A. M. Taylor, D. Semikoz, and A. Neronov, *Astrophys. J.* **747**, L14 (2012).
- D. G. Yamazaki, K. Ichiki, and T. Kajino, *Astrophys. J.* **625**, L1 (2005).
- D. G. Yamazaki, K. Ichiki, T. Kajino, and G. J. Mathews, *Astrophys. J.* **646**, 719 (2006a).
- D. G. Yamazaki, K. Ichiki, K.-I. Umezu, and H. Hanayama, *Phys. Rev. D* **74**, 123518 (2006b).
- D. G. Yamazaki, K. Ichiki, T. Kajino, and G. J. Mathews, *Phys. Rev.* **D 78**, 123001 (2008a).
- D. G. Yamazaki, K. Ichiki, T. Kajino, and G. J. Mathews, *Phys. Rev.* **D 77**, 043005 (2008b).
- D. G. Yamazaki, K. Ichiki, T. Kajino, and G. J. Mathews, *Advances in Astronomy* **2010**, 586590 (2010a).
- D. G. Yamazaki, K. Ichiki, T. Kajino, and G. J. Mathews, *Phys. Rev.* **D 81**, 023008 (2010b).
- D. G. Yamazaki, K. Ichiki, and K. Takahashi, *Phys. Rev. D* **84**, 123006 (2011).
- D. G. Yamazaki and M. Kusakabe, *Phys. Rev. D* **86**, 123006 (2012).
- D. G. Yamazaki, T. Kajino, G. J. Mathews, and K. Ichiki, *Phys. Rep.* **517**, 141 (2012).
- D. G. Yamazaki, K. Ichiki, and K. Takahashi, *Phys. Rev. D* **88**, 103011 (2013).
- D. G. Yamazaki, M. Kusakabe, T. Kajino, G. J. Mathews, and M.-K. Cheoun, *Phys. Rev. D* **90**, 023001 (2014).
- D. G. Yamazaki, *Phys. Rev. D* **89**, 083528 (2014).
- D. G. Yamazaki, *Phys. Rev. D* **93**, 043004 (2016).
- D. G. Yamazaki, *Phys. Rev. D* **97**, 103525 (2018).
- A. Zucca, Y. Li, and L. Pogosian, *Phys. Rev. D* **95**, 063506 (2017).

Magnetising the Cosmic Web during Reionisation

Mathieu Langer¹ and Jean-Baptiste Durrive²

¹Institut d’Astrophysique Spatiale, CNRS, UMR 8617, Univ. Paris-Sud, Université
Paris-Saclay, bât. 121, 91405 Orsay Cedex, France
email: mathieu.langer@ias.u-psud.fr

²Department of Physics and Astrophysics, Nagoya University, Nagoya 464-8602, Japan
present email: jdurrive@irap.omp.eu

Abstract. Evidence repeatedly suggests that cosmological sheets, filaments and voids may be substantially magnetised today. The origin of magnetic fields in the intergalactic medium is however currently uncertain. We discuss a magnetogenesis mechanism based on the exchange of momentum between hard photons and electrons in an inhomogeneous intergalactic medium. Operating near ionising sources during the epoch of reionisation, it is capable of generating magnetic seeds of relevant strengths over scales comparable to the distance between ionising sources. Furthermore, when the contributions of all ionising sources and the distribution of gas inhomogeneities are taken into account, it leads, by the end of reionisation, to a level of magnetisation that may account for the current magnetic fields strengths in the cosmic web.

Keywords. Magnetic fields, cosmology: theory, large-scale structure of universe

1. Introduction

The Universe seems to be magnetised virtually on all scales. The origin of the cosmological magnetic fields in particular remains unsettled, despite the many models that have been proposed (see [Kulsrud and Zweibel 2008](#); [Ryu *et al.* 2012](#); [Widrow *et al.* 2012](#); [Durrer and Neronov 2013](#); [Subramanian 2016](#)). Many of these rely on beyond-the-standard-model physics possibly operating in the early Universe. In the post-recombination Universe, plasma instabilities (e.g. [Gruzinov 2001](#); [Schlickeiser 2012](#)), the Biermann battery (e.g. [Pudritz and Silk 1989](#); [Subramanian *et al.* 1994](#); [Ryu *et al.* 1998](#)) and momentum transfer effects (e.g. [Mishustin and Ruzmaikin 1972](#); [Harrison 1973](#); [Saga *et al.* 2015](#)) can also generate magnetic fields. Whether all these mechanisms are suitable for explaining the origin of the fields permeating the cosmic web is debated, and will be answered thanks to large radio telescopes (see [Beck 2015](#) and pages 369–597 of [Bourke *et al.* 2015](#)).

We here summarise the basics of an astrophysical mechanism, based on the photoionization of the IGM, that is bound to have contributed to the magnetisation of the cosmic web during the epoch of reionisation. Its principles have been explored in [Durrive and Langer \(2015\)](#), and the resulting, average strength of the field in the Universe by the end of reionisation has been estimated in [Durrive *et al.* \(2017\)](#).

2. Outline of the mechanism

The “recipe” for the generation of magnetic fields is, in principle, simple. First, some mechanism must spatially separate positive and negative electric charge carriers. Second, this separation must be sustained so that a large scale electric field is created. Third, by

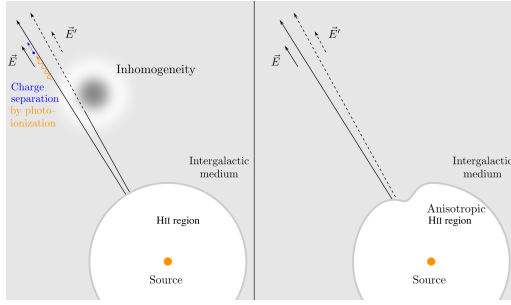


Figure 1. Inhomogeneities at the origin of rotational electric fields.

virtue of Faraday’s law, this electric field must possess a curl. The question of astrophysical magnetogenesis thus essentially boils down to identifying the propitious epochs and environments for such rotational electric fields to emerge.

Cosmological reionisation is one such epoch. The immediate surroundings of luminous sources are ionised forming HII regions. Higher energy photons penetrate beyond the edge of such bubbles into the neutral IGM. There, occasionally, they hit atoms and eject new electrons. As long as the sources shine, the resulting charge separation creates an electric field. Now, in case of perfect local isotropy, the electric field is curl-free. However, local isotropy is broken (see fig. 1). First, the IGM is inhomogeneous. Any overdensity (underdensity) locally enhances (lessens) the process: behind it, the strength of the electric field is smaller (larger) than along photon trajectories that miss density contrasts. The electric field varies *across* photon trajectories, and thus possesses a curl. Second, HII bubbles are aspherical, and the flux of hard photons that escape into the IGM is anisotropic.

In [Durrive and Langer \(2015\)](#), we analysed in detail this mechanism. We obtained the expression for the generated magnetic field, and examined its spatial distribution and strengths. We considered three source types: population III stars, primeval galaxies, and quasars. We modelled a clump in the IGM by a compensated overdensity (see fig. 1 left), and assumed a source lifetime of 100 Myr. Population III star clusters generate relatively stronger fields, on distances (1 – 2 kpc) shorter than half their physical mean separation (~ 10 kpc). These sources thus leave a large fraction of the IGM unmagnetised. Rare, luminous quasars magnetise less but over much larger distances (several Mpc), comparable to half their separation. Primeval galaxies combine modestly high amplitudes, and reasonably large scales (tens of kpc) that are similar to half their separation.

3. Average Magnetic Energy Density seeded in the IGM

We estimated in [Durrive *et al.* \(2017\)](#) the level of global magnetisation thus reached in the Universe by the end of reionisation. The result depends on the distribution of the ionising sources, their spectra, the epochs at which they shine, and on the density clumps in the IGM. We used the [Press and Schechter \(1974\)](#) formalism to model the statistical distribution of sources and overdensities. We focused on primeval galaxies, probably the dominant contributors to reionisation.

The details, illustrated in fig. 2, consist in the following steps:

(a) First, we considered an isolated source and a gas inhomogeneity in its vicinity. We obtained a convenient expression for the magnetic energy density $E_m(D)$ associated to any cloud of mass m at a given distance D of the ionising source.

(b) Second, we summed the effect of all the clouds around the source contained in a

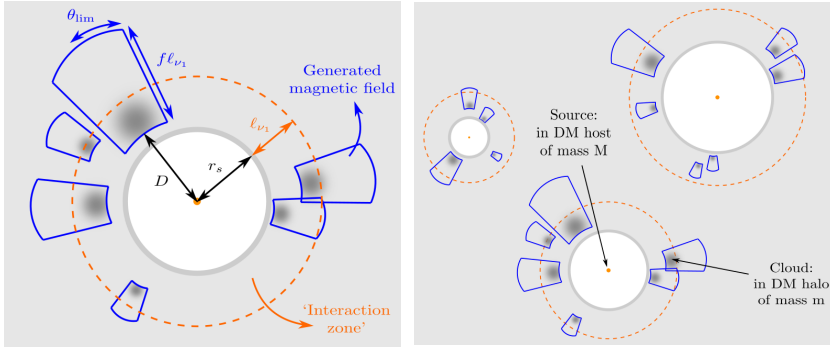


Figure 2. Estimating the global magnetisation level of the IGM. See text for details.

DM halo of mass M . It contributes by injecting a magnetic energy

$$E_M = \int_{r_s}^{r_s + \ell_{\nu_1}} \int_{m_{\min}}^{m_{\max}} E_m(D) d^2P(D, m|M) \quad (3.1)$$

where $d^2P(D, m|M)$ is the probability for a DM cloud of mass m to be in a spherical shell of volume $4\pi D^2 dD$ at distance D . We considered only the clouds within an ‘interaction zone’ set by the photon mean free path ℓ_{ν_1} beyond which the mechanism is not efficient.

(c) Third, we integrated the energy density E_M over the DM halos containing ionising sources. As HII bubbles start to overlap, the efficiency of magnetic field generation decreases as reionisation proceeds. Hence, we weighed the contribution of sources by a factor $1 - Q_i(z)$ accounting for the ionised volume filling factor at redshift z . The mean comoving magnetic energy density finally reads

$$\frac{B_c^2(z)}{8\pi} = \int_z^{z_0} dz' \frac{1 - Q_i}{H(1+z')^5} \int_{M_*}^{M_{\max}} dM E_M g_{\text{gl}} \frac{dn_M}{dM} \quad (3.2)$$

where $\frac{dn_M}{dM}$ is the mass function of the DM halos hosting the sources. The parameter z_0 is the redshift at which the first sources form, and g_{gl} is the rate at which sources switch on.

Figure (3) shows the comoving strength of the generated magnetic field in three different reionisation histories, all consistent with results of the [Planck Collaboration \(2016\)](#). Above $z = 20$ there are no galaxies, and the magnetic field is nil. As galaxies form, their radiation induces magnetic fields that accumulate in the IGM. Once the Universe is fully ionised, the mechanism stops, and a plateau (in comoving units) is reached. Note that in physical units, the strength of the magnetic field by the end of reionisation is a few 10^{-18} Gauss, a suitable seed value for any subsequent amplification by nonlinear processes.

4. Discussion

The model we summarised here can be improved in several ways. In particular, we neglected the contribution of underdense regions, which could multiply the result obtained above by a factor of two. Similarly, we did not take into account the effect of the asphericity of the HII regions. Finally, we assumed that the HII regions have reached their steady state. Whether taking their growing regime into account would increase or decrease the global magnetic field is not obvious. However, nonlinearities develop in the cosmic velocity field as structure formation proceeds (e.g. [Ryu et al. 2008](#); [Greif et al. 2008](#); [Sur et al. 2012](#)). They enter into play when the seed magnetic field has reached its

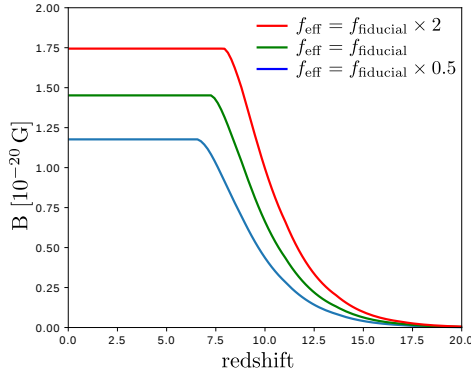


Figure 3. Evolution with redshift of the mean comoving magnetic field strength in the IGM in different reionisation histories. The green curve is the fiducial model assumed in Durrive *et al.* (2017) where f_{eff} is an effective reionisation efficiency. All three considered histories are in agreement with the Planck Collaboration (2016) constraints.

final strength (Langer *et al.* 2005). Magnetic field amplification thus sets in early on, at least within the nodes, filaments and sheets of the cosmic web. The strength shown in fig. 3 thus likely underestimates the actual magnetisation of those structures. In cosmic voids, plasma instabilities might have the potential to amplify rapidly the magnetic seed fields, and bring them above the lower limits suggested by the observation of blazars.

References

- Beck, R. Future Observations of Cosmic Magnetic Fields with LOFAR, SKA and Its Precursors. In *Proceedings of Magnetic Fields in the Universe: From Laboratory and Stars to Primordial Structures*, AIP, 2015, pp. 3–17.
- Bourke, T.L., Braun, R., Fender, R., et al., eds. *Advancing Astrophysics with the Square Kilometre Array – Vol. I*, Dolman Scott Ltd for SKA Organisation, 2015. Available at <https://www.skatelescope.org/books/>.
- Durrer, R., Neronov, A. *A&AR* **2013**, *21*.
- Durrive, J.B., Langer, M. *MNRAS* **2015**, *453*, 345–356.
- Durrive, J.B., Tashiro, H., Langer, M., Sugiyama, N. *MNRAS* **2017**, *472*, 1649–1658.
- Greif, T.H., Johnson, J.L., Klessen, R.S., Bromm, V. *MNRAS* **2008**, *387*, 1021–1036.
- Gruzinov, A. *ApJ* **2001**, *563*, L15–L18.
- Harrison, E.R. *Phys. Rev. Lett.* **1973**, *30*, 188–190.
- Kulsrud, R.M., Zweibel, E.G. *Reports on Progress in Physics* **2008**, *71*, 046901.
- Langer, M., Aghanim, N., Puget, J.L. *A&A* **2005**, *443*, 367–372.
- Mishustin, I.N., Ruzmaikin, A.A. *Soviet Physics JETP* **1972**, *34*, 233–235.
- Planck Collaboration. *A&A* **2016**, *596*, A108.
- Press, W.H., Schechter, P. *ApJ* **1974**, *187*, 425.
- Pudritz, R.E., Silk, J. *ApJ* **1989**, *342*, 650–659.
- Ryu, D., Kang, H., Biermann, P.L. *A&A* **1998**, *335*, 19–25.
- Ryu, D., Kang, H., Cho, J., Das, S. *Science* **2008**, *320*, 909–12.
- Ryu, D., Schleicher, D.R.G., Treumann, R.A., et al. *Space Sci. Revs* **2012**, *166*, 1–35.
- Saga, S., Ichiki, K., Takahashi, K., Sugiyama, N. *Phys. Rev. D* **2015**, *91*, 123510.
- Schlickeiser, R. *Phys. Rev. Lett.* **2012**, *109*, 261101.
- Subramanian, K., Narasimha, D., Chitre, S.M. *MNRAS* **1994**, *271*, L15–L18.
- Subramanian, K. *Reports on Progress in Physics* **2016**, *79*, 076901.
- Sur, S., Federrath, C., Schleicher, D.R.G., et al. *MNRAS* **2012**, *423*, 3148–3162.
- Widrow, L.M., Ryu, D., Schleicher, D.R.G., et al. *Space Sci. Revs.* **2012**, *166*, 37–70.

Small-scale dynamo as a mechanism for excitation of extragalactic magnetic fields

Dmitry Sokoloff

Moscow State University,
Moscow, 119991, Russia and IZMIRAN, Troitsk, Moscow, 142190, Russia
email: sokoloff.dd@gmail.com

Abstract. Presence of magnetic fields in cosmological voids is a challenge for dynamo theory. We argue that these fields can be considered as a result of small-scale dynamo action associated with random motions connected with formation of various structures Universe.

Keywords. magnetic fields, dynamo, Early Universe.

1. Introduction

Magnetic fields of spiral galaxies are believed to be excited by dynamo action based on differential rotation and mirror-asymmetric turbulence in the interstellar medium (e.g. Beck et al., 1996). Corresponding magnetic energy is closed to equipartition with kinetic energy of the turbulence. In this context, estimate for magnetic fields in cosmological voids suggested by Neronov & Semikoz (2009) looks as a challenge for dynamo theory. The point is that both conventional drivers of galactic dynamo, i.e. differential rotation and mirror-asymmetry of turbulence look irrelevant for media of voids.

In principle, origin of magnetic fields in the voids can be directly associated with particle processes in the Early Universe. The point is that differential rotation is a helpful however not obligatory participant in dynamo action and mirror asymmetry alone is in principle sufficient to enhance magnetic fields. Such dynamo is referred as α^2 -dynamo while conventional galactic dynamo is known in this context as $\alpha\omega$ -dynamo. Indeed, violations of mirror symmetry (P-invariance) are known, say, for weak interactions and the media of the Early Universe near electro-weak phase transition. It results in magnetic field excitation at the epoch of electro-weak phase transition. Contemporary, bulk of knowledge concerning electro-weak phase transition gives enough free room to get magnetic field strength comparable with that suggested by Neronov & Semikoz (2009) for magnetic fields in voids (e.g. Vachaspati, 1991; Giovannini & Shaposhnikov, 2000; Semikoz & Sokoloff, 2004). In the framework of this scenario, magnetic fields in voids are immediate imprints of physical processes in the very Early Universe. This scenario presumes that physical process during the epoch of formation of structure of the Universe can be ignored for the magnetic field formation in the voids.

An alternative viewpoint concerning the origin of magnetic fields in voids departs from the idea that magnetic fields of galactic clusters are considered to be excited by a small-scale dynamo action (e.g. Ruzmaikin et al., 1989). In other words, this scenario suggests that magnetic field in the voids is excited by motions of electrically conducting media in the epoch of formation of the structure in the Universe and even at later states of its evolution. This scenario supposes that magnetic structures in the voids do not contain pronounced imprints of particle processes in the Early Universe. Magnetic fields which were created during the electro-weak phase transition or even earlier can contribute in

the seed for dynamo action, however another contribution associated with battery effects may produce the seed even alone.

Of course, these two scenarios are two extremes in the variety of opinions and various intermediate views can be found in the literature.

According to the sense of this focus meeting, we are now at the very early stage of investigation of extragalactic magnetic fields in voids and it looks important to isolate in an explicit form the above options and discuss which one looks more attractive. It is the aim of this contribution.

2. Particle processes and magnetic field in voids

First scenario looked very attractive at the initial stage of research, it obviously deserved investigation and it was addressed in various papers (e.g. Kahniashvili et al., 2011). One can summarize from the above cited papers that it is in principle possible to get sufficient magnetic energy from the particle processes to explain the supposed magnetic field in the voids (we note that Neronov & Semikoz, 2009 give lower magnetic field estimate only). For the first sight, it means that the scenario remains realistic at least until we learn more concerning magnetic field scale in the voids. The point is that Neronov & Semikoz (2009) do not give any estimate on the magnetic field scale.

In fact, however, the epoch of substantial mirror-asymmetry of the medium in the Universe is very short. In order to get substantial magnetic field amplification during this epoch we have to assume that magnetic field growth rate was very high. From the other hand the α^2 -dynamo equations provides a link between the scale of the growing magnetic field and its growth rate. Using this link, we can estimate the present-day scale of magnetic field which was excited in particle processes in the Early Universe and survives until present (see for technical details Tarbeeva et al., 2007). Of course, the estimate is to some extent model dependent, however the figure obtained as the estimate are very low indeed, of order of kilometres only. In spite of the fact that Neronov & Semikoz (2009) avoid to give lower estimate for the magnetic field scale in voids, it is very difficult to believe that magnetic field of this tiny scale could be important for astronomy.

We stress that the magnetic field generated due to mirror-asymmetry of particle process should be referred in the context of dynamo studies as a large-scale magnetic field. Its scale however is bounded from above by the horizon size of the Universe in the epoch of phase transitions which is small in the present-day scales. Because any kind of dynamo is much slower than the light propagation, the actual spatial scale of magnetic field driven by a dynamo acting in the epoch of phase transitions is even much smaller than the horizon size.

The above consideration do not include the case of a strictly homogeneous magnetic field created in an a-causal way just at the instant of Big Bang. Such a magnetic field could be sufficiently weak to avoid observable violations of isotropy of the Universe however sufficiently strong to satisfy lower bound of Neronov & Semikoz (2009), (e.g. Beck et al., 1996). This option was considered at first as early as 1965 by Zeldovich and is very difficult for observational verification (e.g. Ruzmaikin & Sokoloff, 1977). It is however difficult to consider the option at the most attractive one at least for the time being.

3. Small-scale dynamo in voids

Scenario with small-scale dynamo as magnetic field driver in the voids anticipates that magnetic field origin in the voids is more or less the same as that one in galactic

clusters. The difference is that kinetic energy in the voids is lower than that in clusters. Correspondingly, magnetic field strength in voids should be several order of magnitudes lower than that one in galactic clusters.

A weak point in this scenario is that we know almost nothing about possible turbulent flows in voids. From the other hand, it is very difficult to believe that formation of large-scale structure of the Universe was performed by purely laminar flows and did not resulted in any random flows. Fortunately, small-scale dynamo action does not require fully developed turbulent flows. In contrast, the simplest and useful model for small-scale dynamo suggested by Kasantsev (1967) deals with so-called short-correlated flows which contain just one spatial scale only.

Another important point is what does it mean "small scale" in the wording for the dynamo under discussion. The point is that the problem contains two scales, i.e. the scale of random vortexes l and the resistive scale λ . Both scales are referred as small ones in the dynamo studies because they are usually much smaller than the size of the whole magnetized body L . For the voids, the scale l is expected to be more or less comparable with the void scales while λ may be many orders of magnitude lower because dissipation in voids is expected to be very low. In principle, λ might be as tiny as scales discussed in the previous section. Fortunately, investigation of Kasantsev model (e.g. Novikov et al. 1983; Kleeorin et al., 2002) demonstrate that both scales determine the magnetic field correlation function however the magnetic energy at scales l remains substantial.

We note that the small-scale dynamo in the framework of the problem under discussion deserves further investigation. In particular, the random flow driving small-scale dynamo can be purely mirror-symmetric. Then the magnetic field generated is mirror-symmetric in average. However if the flow is still mirror-asymmetric the resulting magnetic field becomes mirror-asymmetric as well (e.g. Boldyrev et al., 2005; Malyshkin & Boldyrev, 2007; Yushkov & Lukin, 2017). Of course, magnetic helicity generated by small-scale dynamo in a mirror-asymmetric flow have to be taken into account in helicity balance for dynamo saturation (Sokoloff et al., 2017).

4. Conclusion and discussion

Comparing the advantages and shortcomings of the above scenario we arrive to an impression that at least on the present stage of research the option that it is small-scale dynamo responsible for the excitation of magnetic fields in voids looks preferable. We note that the general impression from the talks presented at the focus meeting seems to support this opinion.

I am grateful to E.Yushkov and P.Frick for useful discussions. The research is supported by RFBR under grant 18-02-00085.

References

- Beck, R., Brandenburg, A., Moss, D., Shukurov, A., Sokoloff, D. 1996, *ARAA*, 34, 155
Boldyrev, S., Cattaneo, F., & Rosner, R. 2005, *PRL*, 95, 255001
Giovannini, M., & Shaposhnikov, M. 2000, *PRD*, 62, 103512
Kahniashvili, T., Tevzadze, A.G. Ratra, B.P., & Zinner, E. 2011, *ApJ*, 726, 78
Kazantsev, A.P. 1967 *JETP*, 53, 1806
Kleeorin, N., Rogachevskii, I., & Sokoloff, D. 2002, *PRE*, 65, 036303
Neronov, A., & Semikoz, D.V. 2009, *PRD*, 80, 123012
Novikov, V.G., Ruzmaikin, A.A., & Sokoloff, D.D. 1983, *JETP*, 85, 909
Malyshkin, L., & Boldyrev, S. 2007, *ApJ*Letters, 671, L185
Ruzmaikin, A. A., & Sokoloff, D.D. 1977, *A&A*, 58, 247

Dmitry Sokoloff

- Ruzmaikin, A., Sokoloff, D., & Shukurov, A., 1989, *MNRAS*, 241, 1
Semikoz, V.B., & Sokoloff, D.D. 2004, *PRL*, 92, 131301
Sokoloff, D.D., Yushkov, E.V., & Lukin, A.S. 2017, *Geomagnetism and Aeronomy*, 57, 844
Tarbeeva, S.M., Semikoz, V.B., & Sokoloff, D.D. 2007, *Astron. Rep.*, 51, 781
Vachaspati, T. 1991, *Phys. L. B.*, 265, 258
Yushkov, E.V., & Lukin, A.S. 2017, *GAFD* 111, 527
Zeldovich Ya.B. 1965, *JETP*, 48, 986

Large-Scale Diffuse Intergalactic Magnetic Fields Constraints with the Cherenkov Telescope Array

Paramita Barai¹, Elisabete M. de Gouveia Dal Pino¹ (on behalf of the CTA Collaboration)

¹Instituto de Astronomia, Geofísica e Ciências Atmosféricas - Universidade de São Paulo (IAG-USP), Rua do Matão 1226, São Paulo, 05508-090, Brazil
email: paramita.barai@iag.usp.br

Abstract. Magnetic fields of the order of μ -Gauss are observationally detected in galaxies and galaxy clusters, which can be (at least) in part originated by the amplification of much weaker primordial seed fields. These fields should be carried out by strong galactic outflows, magnetically enriching the InterGalactic Medium (IGM). However direct observation of magnetic fields in the IGM is scarce. This talk will give a review of how Intergalactic Magnetic Field (IGMF) can be constrained using gamma-ray observations. High-energy TeV photons emitted by distant blazars can interact with the cosmic extragalactic optical/infrared/microwave background light, producing electron-positron pairs, and initiating electromagnetic cascades in the IGM. The charged component of these cascades is deflected by IGMFs, thereby reducing the observed point-like TeV flux, and creating an extended image in the GeV energy range, which can potentially be detected with γ -ray telescopes (Fermi-LAT, HESS, CTA). Studies (e.g., Neronov & Vovk 2010, Dolag et al. 2011) have put lower limits on the IGMF strength of the order of $10^{-16} - 10^{-15}G$, and filling factors of 60%. This talk will describe the constraints which the Cherenkov Telescope Array sensitivity is expected to give (CTA Consortium 2018).

Keywords. magnetic fields, instrumentation: high angular resolution, methods: data analysis, (galaxies:) BL Lacertae objects: general, intergalactic medium, gamma rays: observations

1. Introduction

Magnetic Fields (MF) of the order of $(1 - 10)\mu G$ are observed (e.g., Berkhuijsen et al. 2003) in galaxies and galaxy clusters. These fields are understood to be created from the amplification of much weaker primordial seed fields, by turbulent dynamo effects and baryonic processes. The origin of these tiny seed fields is unknown (e.g., Widrow 2002). There are 2 classes of concordance models for the generation of primordial seed fields. One is *Cosmological origin*: where the seed fields are produced in the early primordial Universe (e.g., Grasso & Rubinstein 2001). The other is *Astrophysical origin*: where the seed fields are produced by plasma motions from baryonic processes (star-formation, supernovae, black holes) in galaxies (e.g., Ryu et al. 2012).

A potentially relevant component of cosmic MF, of which very little is known yet, is the Intergalactic Magnetic Field (IGMF) existing in the low-density InterGalactic Medium (IGM), or the space between galaxies not related to gravitational collapse. The MFs inside galaxies are dragged out by powerful galactic outflows generated by energy feedback from baryonic processes with time, and dispersed into the IGM. Over cosmological epochs these IGMFs permeate the turbulent IGM, and may be even amplified by turbulent dynamo action (e.g., de Gouveia Dal Pino 2011), at the same time influencing large scale structure formation (e.g., Dolag 2006, Barai 2008).

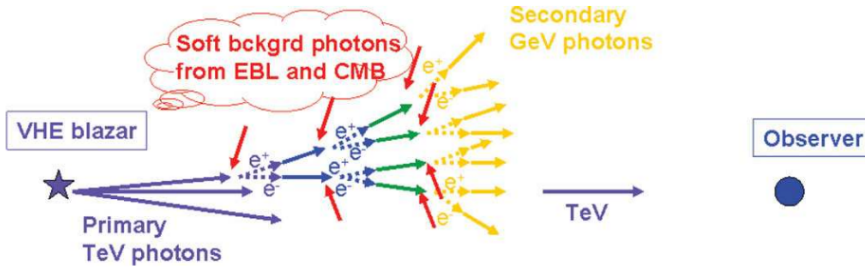


Figure 1. Propagation of VHE primary TeV photons $\gamma_{\text{VHE},1}$ to Earth, and the interactions happening on the way to produce secondary GeV $\gamma_{\text{VHE},2}$ photons. Figure from Sol et al. (2013a).

The knowledge of IGMF distribution is crucial in understanding the *cosmological* versus *astrophysical* origin of cosmic MF. It is challenging to directly observe the IGMF, because they are diffuse and weak in intensity. An upper limit: $B_{IGM} < (10^{-8} - 10^{-9})G$, is provided by standard constraints: Big Bang nucleosynthesis, Cosmic Microwave Background (CMB) anisotropy (e.g., Durrer et al. 1998), Faraday rotation measures of polarized radio emission from quasars (e.g., Pshirkov et al. 2016). Here we will overview how IGMF can be constrained using γ -ray observations, which provide lower limits for it.

2. IGMF Constraints using γ -ray Observations of Blazars

A novel technique to constrain the IGMF's strength and filling factor uses Very-High-Energy (VHE) γ -ray emission from distant blazar sources. Blazars are Active Galactic Nuclei (AGN) with the central supermassive black hole jet pointed toward our line of sight, and present rapid variability (e.g., Aharonian et al. 2007). The observed spectral energy distributions of blazars (e.g., Bonnoli et al. 2015) are fitted to models, where the TeV γ -ray emission comes from the jet base. There, relativistic electrons (e^-) upscatter, by Inverse Compton (IC), lower-energy ambient photons to the TeV. Relativistic protons can also have a contribution, by emitting direct synchrotron radiation, or by the creation of secondary pions, which decay into TeV photons.

The VHE primary TeV photons ($\gamma_{\text{VHE},1}$) emitted by distant blazars undergo the following interactions, as they travel 100s-of-Mpc intergalactic space before reaching Earth:

$$\gamma_{\text{VHE},1} + \gamma_{\text{EBL}} \longrightarrow e^- e^+, \quad e^- + \gamma_{\text{CMB}} \longrightarrow \gamma_{\text{VHE},2} + e^- . \quad (2.1)$$

Firstly, the $\gamma_{\text{VHE},1}$ interact with optical/infrared/microwave Extragalactic Background Light (EBL), and cause e^-e^+ pair production. These very-energetic electrons undergo IC scattering off CMB photons and produce secondary γ -rays ($\gamma_{\text{VHE},2}$) in the GeV energy range, as shown in Fig. 1 (Sol et al. 2013a). The e^-e^+ pair electromagnetic cascades are deflected by IGMF present in the intervening space, and the secondary GeV $\gamma_{\text{VHE},2}$ are strongly attenuated as they appear on Earth. These attenuated secondary GeV components can be detected with our γ -ray telescopes (Fermi-LAT, HESS, CTA), as either:

- **Pair Halo:** Spatially-extended GeV emission around primary TeV $\gamma_{\text{VHE},1}$ signal. These are expected for $B_{IGM} > \sim 10^{-16}G$, and involve imaging analysis searches for extended pair halos around blazars. (Larger IGMFs produce larger deflections, resulting in a weaker pair halo flux, that can make it undetectable with current instruments.)

- **Pair Echo:** GeV emission with a time delay relative to the primary. These are expected for $B_{IGM} < 10^{-16}G$, and involve time-resolved spectral analysis of pair echoes.

Studies usually model the e^-e^+ pair cascade development using Monte-Carlo simula-

tions, compute the simulated **pair halo** and/or **pair echo** assuming some IGMF configuration, compare with observations (e.g. Fermi data on blazars), and derive IGMF constraints (e.g., Alves Batista 2017). However, several studies have inferred a non-detection of secondary components, which nevertheless provide lower limits on B_{IGM} , assuming that the suppression of GeV flux is due to the deflection of e^-e^+ pairs by IGMF. E.g. Neronov & Vovk (2010) found a lower limit of $B_{IGM} \geq 3 \times 10^{-16}G$. Dolag et al. (2011) inferred that IGMF fills at least 60% of space with fields stronger than $B_{IGM} \geq 10^{-16} - 10^{-15}G$. Considering a coherence length > 1 Mpc for the IGMF and persistent TeV emission, Taylor et al. (2011) inferred a $B_{IGM} > (10^{-17} - 10^{-15})G$.

A first hint for the existence of pair halos (extended emission around a point-source) has been found by Chen et al. (2015), by the stacking analysis of 24 blazars at $z < 0.5$ using Fermi-LAT data. It implies a magnetic field strength of $B_{IGM} \sim 10^{-17} - 10^{-15}G$, using a Bayesian statistics.

3. γ -ray Pair Halo to be Observed by the Cherenkov Telescope Array

The Cherenkov Telescope Array (CTA) is a planned next-generation ground-based γ -ray observatory (CTA Consortium 2018). CTA will provide the deepest insight into the non-thermal VHE Universe ever reached, probing the physical conditions of cosmic accelerators like black holes and supernovae. It will consist of an array of around 100 imaging atmospheric Cherenkov telescopes of various sizes. CTA foresees a factor of 5 – 10 improvement in sensitivity in the energy domain (~ 100 GeV – 10 TeV) of current Cherenkov telescopes: HESS, MAGIC, and VERITAS. It is also expected to extend the observable VHE range to below 100 GeV and above 100 TeV, and have unprecedented angular and energy resolution, as well as a wider field-of-view. A Northern site (Canarias Islands) and a Southern site (Chile) are planned for a full sky coverage.

Elyiv et al. (2009) performed Monte Carlo simulations of 3D electromagnetic cascades (described in §2). One of the cases they simulated is a blazar source at a distance 120 Mpc, and $B_{IGM} = 10^{-14}G$. The expected geometry of *Pair Halo* from this blazar is presented in Fig. 2 - left panel. The sky Field-of-View (FoV) of 1.5° is indicated by the blue-dashed circle, which is equal to the radius of the FoV of the MAGIC telescope. And a 2.5° FoV is denoted by the red-solid circle, which corresponds to the size of the FoV of the HESS telescope. These would perfectly fit into the much larger FoV of CTA.

Sol et al. (2013b) estimated the pair halo flux using a theoretical model of differential angular distribution of a pair halo at $z = 0.129$ with $E_\gamma > 100$ GeV (Eungwanichayapant & Aharonian 2009), and assuming an observation time of 50 hours. The pair halo emission is displayed in Fig. 2 - right panel, as the dashed curve. The CTA sensitivity curves are overplotted as the solid lines: the CTA South (North) site is labeled as I (NB). Hence CTA should well observe pair halos in the energy range (0.1 – 5) TeV.

4. Conclusions

The observational detection of IGMF (extremely tiny magnetic fields permeating the cosmos on the largest scales) can shed light on the origin of seed fields in the Universe. Current results of VHE γ -ray astronomy conclude to the existence of a non-zero IGMF: $10^{-17}G < B_{IGM} < 10^{-14}G$, mostly based on the non-detection of expected secondary GeV γ -rays. Future theoretical studies need to take into account possible additional effects in the IGM, e.g. energy losses by cosmic rays, plasma effects. Observationally the positive detection of *Pair Halos* and *Pair Echos* are needed with detailed data on cascade signatures, which the CTA with its improved sensitivity is expected to observe.

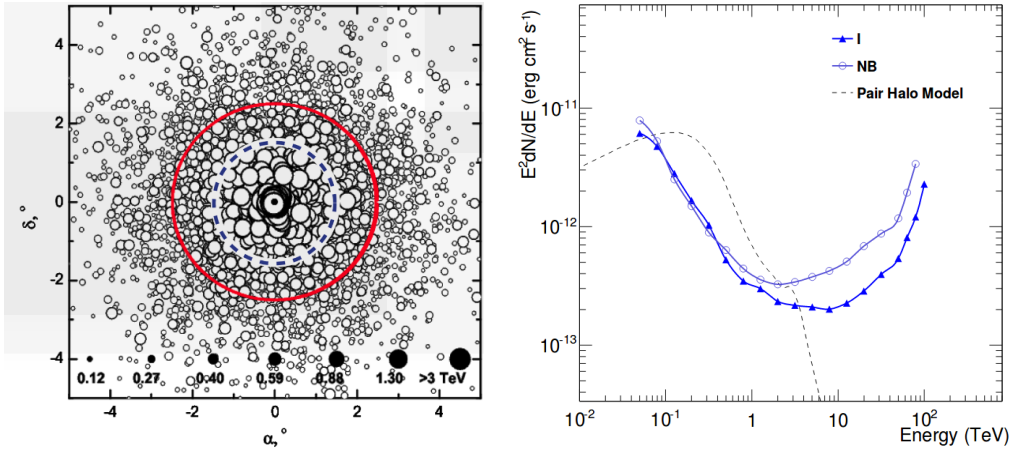


Figure 2. *Left panel:* Open black circles indicate the arrival directions of primary and secondary γ -rays from a blazar (details in §3), with the circle sizes proportional to the photon energies (as labeled in TeV at the bottom of the figure). Sky FoVs of 1.5° and 2.5° are shown by the blue-dashed and red-solid circles. Figure from Elyiv et al. (2009). *Right panel:* Estimated flux for the expected pair halo emission compared to the CTA sensitivity curves for the southern (I) and northern (NB) sites. Figure from CTA Consortium (2018), originally from Sol et al. (2013b).

5. Acknowledgements

This work is partially supported by the FAPESP grants #2016/01355-5 and #2013/10559-5, and by a CNPq grant (#306598/2009-4).

References

- Aharonian, F. et al. 2007, *ApJ*, 664, L71
 Alves Batista, R. 2017, *Il Nuovo Cimento C*, 40, 132
 Barai, P. 2008, *ApJ*, 682, L17
 Berkhuijsen, E. M., Beck, R. & Hoernes, P. 2003, *A&A*, 398, 937
 Bonnoli, G., Tavecchio, F., Ghisellini, G. & Sbarrato, T. 2015, *MNRAS*, 451, 611
 Chen, W., Buckley, J. H. & Ferrer, F. 2015, *Physical Review Letters*, 115, 211103
 Cherenkov Telescope Array Consortium: Acharya, B. S. et al. 2018, eprint arXiv:1709.07997
 de Gouveia Dal Pino, E. M. 2011, in *The Sun, the Stars, the Universe and General Relativity: Proceedings of Sobral 2009*; eds. S.E. Perez Bergliaffa, M. Novello and R. Ruffini, CSP, 37
 Dolag, K. 2006, *Astronomische Nachrichten*, 327, 575
 Dolag, K., Kachelriess, M., Ostapchenko, S. & Tomas, R. 2011, *ApJ*, 727, L4
 Durrer, R., Kahniashvili, T. & Yates, A. 1998, *Physical Review D*, 58, 123004
 Elyiv, A., Neronov, A. & Semikoz, D. V. 2009, *Physical Review D*, 80, 023010
 Eungwanichayapant, A. & Aharonian, F. 2009, *Int. Journal of Modern Physics D*, 18, 911
 Grasso, D. & Rubinstein, H. R. 2001, *Physics Reports*, 348, 163
 Neronov, A. & Vovk, I. 2010, *Science*, 328, 73
 Pshirkov, M. S., Tinyakov, P. G. & Urban, F. R. 2016, *Physical Review Letters*, 116, 191302
 Ryu, D., Schleicher, D. R. G., Treumann, R. A., Tsagas, C. G. & Widrow, L. M. 2012, *Space Science Reviews*, 166, 1
 Sol, H. et al. 2013a, *IAUS (Solar and Astrophysical Dynamos and Magnetic Activity)*, 294, 459
 Sol, H. et al. 2013b, *Astroparticle Physics*, 43, 215
 Taylor, A. M., Vovk, I. & Neronov, A. 2011, *A&A*, 529, A144
 Widrow, L. M. 2002, *Reviews of Modern Physics*, 74, 775

Cosmic-ray propagation in the turbulent intergalactic medium

Rafael Alves Batista^{1,*}, Elisabete M. de Gouveia Dal Pino^{1,†}, Klaus Dolag^{2,3}, Saqib Hussain¹

¹Universidade de São Paulo - Instituto de Astronomia, Geofísica e Ciências Atmosféricas; Rua do Matão, 1226, 05508-090, São Paulo-SP, Brazil

²Max Planck Institute for Astrophysics, Karl-Schwarzschild-Str 1, 85741 Garching, Germany

³Universitäts-Sternwarte München, Scheinerstraße 1, 81679, München, Germany

* email: rafael.ab@usp.br

† email: dalpino@iag.usp.br

Abstract.

Cosmic rays (CRs) may be used to infer properties of intervening cosmic magnetic fields. Conversely, understanding the effects of magnetic fields on the propagation of high-energy CRs is crucial to elucidate their origin. In the present work we investigate the role of intracluster magnetic fields on the propagation of CRs with energies between 10^{16} and $10^{18.5}$ eV. We look for possible signatures of a transition in the CR propagation regime, from diffusive to ballistic. Finally, we discuss the consequences of the confinement of high-energy CRs in clusters and superclusters for the production of gamma rays and neutrinos.

Keywords. magnetic fields, large-scale structure of universe, MHD, galaxies: clusters: general

1. Introduction

Cosmic magnetic fields are ubiquitous in the universe and their intensities span from 10^{-10} G in extended filaments, which are possibly the largest magnetised structures in the universe, up to around 10^{15} G in magnetars. Tiny magnetic fields ($\sim 10^{-17}$ G) can also exist in the vast regions devoid of matter, the so-called cosmic voids (see Barai & de Gouveia Dal Pino 2018, and references therein). Presently little is known about the origin and evolution of these diffuse intergalactic magnetic fields (IGMFs).

CRs are produced via shock and turbulent acceleration processes in active galaxies and even in the more diffuse regions of the intergalactic medium (IGM) like relics and haloes (e.g. Brüggen & Vazza 2015). They are deflected by the pervasive magnetic fields and thus can be used to constrain their strength and coherence lengths.

Strong evidence exists supporting an extragalactic origin of CRs with energies $E \gtrsim 8 \times 10^{18}$ eV (Pierre Auger Collaboration 2017), but it is not clear yet at which energies there is a transition between galactic and extragalactic CRs. Moreover, there are indications of a possible third component comprised of nearby extragalactic sources potentially responsible for the CR spectrum at energies between the second knee ($E \sim 10^{17}$ eV) and the ankle ($E \sim 10^{18.5}$ eV) (Deligny 2014). At energies below $E \sim Z \times 10^{17}$ eV, wherein Z is the atomic number of the cosmic-ray nucleus, it is widely believed that Galactic sources dominate the spectrum as their Larmor radii are about the size of our Galaxy.

A number of authors have performed magnetohydrodynamical (MHD) simulations of large-scale structure formation which were subsequently used for the propagation of CRs, particularly the highest-energy ones (UHECRs). For instance, Dolag *et al.* (2004)

and Sigl *et al.* (2003) have reached diverging conclusions regarding the effects of extragalactic magnetic fields on UHECR propagation. The former concluded that deflections should be small in most of the sky (see also Medina Tanco *et al.* 1998), whereas the latter concluded that they are large, thereby disfavoured the identification of individual sources of UHECRs. In more recent work, Hackstein *et al.* (2016) obtained results that favour small deflections, which is consistent with their later work using constrained MHD simulations (Hackstein *et al.* 2017). A more pessimistic scenario has been studied by Alves Batista *et al.* (2017), who concluded that even if the magnetic fields in cosmic voids, which fill most of the volume of the universe, are high, the deflection of UHE protons with $E \gtrsim 5 \times 10^{19}$ eV would be $\lesssim 15^\circ$ in about 10-50% of the sky, depending on the magnetic power spectrum. This would enable the identification of UHECR sources even in the most pessimistic scenarios.

The distribution of extragalactic magnetic fields is largely uncertain and many differences exist across models. A comprehensive review on the topic was presented by Vazza *et al.* (2017), and a detailed discussion of these uncertainties on UHECR propagation was given by Alves Batista *et al.* (2017). Other properties of the magnetised IGM may also affect the propagation of CRs. This includes magnetic helicity, related to the topology of the magnetic field lines, which can leave an imprint in the large-scale distribution of CR arrival directions for some specific source distributions (Alves Batista & Saveliev 2018), as well as plasma instabilities (Brunetti & Jones 2015).

It is not clear at which energy the transition between the ballistic and diffusive regimes of CR propagation occur. Also, there is an energy below which the flux of extragalactic CRs is strongly suppressed due to magnetic horizon effects, but this depends on the strength and coherence length of the magnetic fields, as well as the distribution of sources. Alves Batista & Sigl (2014) have shown that for sources distributed approximately uniformly, this energy is $E \lesssim 10^{18}$ eV for common extragalactic magnetic field models obtained via MHD simulations. Note, however, that this result depends on the distribution of magnetic fields between the closest sources and Earth, so that magnetic horizon effects may play a role for highly inhomogeneous distributions of sources.

2. Setup of the simulations

Using 3D cosmological MHD simulations done by Dolag *et al.* (2004), obtained with GADGET (Springel 2005), we investigate the propagation of CRs with energies $10^{16} \lesssim E/\text{eV} \lesssim 10^{18.5}$, whose origins are unknown and about which few studies have been done.

We perform a numerical study of the propagation of CRs in the aforementioned MHD background. We employ the CRPropa code (Alves Batista *et al.* 2016). We consider adiabatic energy losses due to the expansion of the universe. Photohadronic and photonuclear interactions between high-energy CRs and photons from the CMB, EBL, and from the clusters are neglected in this first study. Interactions between CMB/EBL photons with CRs are virtually negligible at these energies.

The cosmological simulations we use here have been previously used by Dolag *et al.* (2004) for UHECR propagation studies. They correspond to a volume of $\sim (140 \text{ Mpc})^3$. The initial conditions of the simulation are such that the relative positions between the main structures and Earth are roughly preserved. We select a sample of clusters from the simulation for the analysis, and choose the Virgo cluster to discuss the results.

3. Results

In Fig. 1 the trajectories of three cosmic-ray protons are shown for $E = 10^{17}$ eV and $E = 10^{18}$ eV. One can see in Fig. 1 that the propagation is approximately diffusive near the source, where the intensity of the fields is higher, transitioning towards a rectilinear propagation as energy increases.

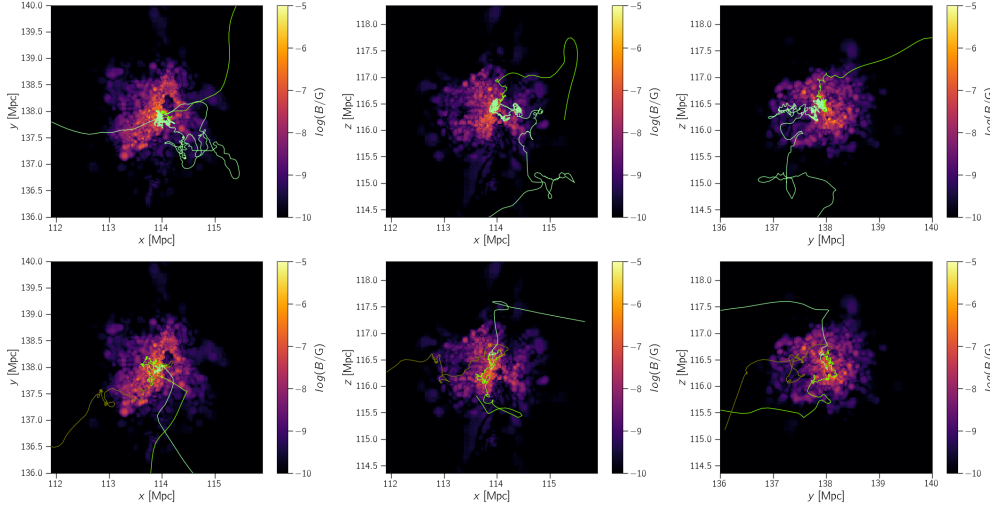


Figure 1. Slices xy (left), xz (middle) e yz (right column) of the simulated volume. The colour scale corresponds to the intensity of the field in these regions. Trajectories of three CR protons are represented through the green lines with different shades. The scenario in the upper row corresponds to $E = 10^{17}$ eV, whereas the lower row is for $E = 10^{18}$ eV.

The diffusion coefficient is energy-dependent and combines two regimes, quasi-linear ($D \propto E^{1/3}$), and non-resonant ($D \propto E^2$). The diffusion coefficient can be written as $D = \langle r^2 \rangle / 6t$, wherein r is the displacement of the CR with respect to its initial position, and t is the time it takes to move a distance r . CRs can escape the cluster if t is less than the age of the cluster, assumed here to be of the order of a Hubble time; and $r \simeq 1$ Mpc, the typical size of a cluster. This implies that for $D \lesssim 10^{27} \text{ m}^2 \text{ s}^{-1}$ the diffusion time is comparable to one Hubble time. The behaviour of the diffusion coefficients for different combinations of energy and distance to the centre of the cluster is shown in Fig. 2.

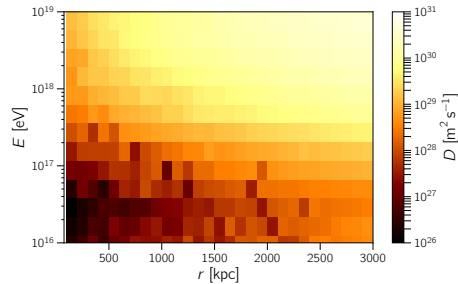


Figure 2. Diffusion coefficient as a function of the cosmic-ray energy and distance to the centre of the cluster for the case of protons with an E^{-1} spectrum leaving the Virgo cluster.

Note that in the central regions of the cluster ($r \lesssim 500$ kpc) the CRs tend to be confined longer compared to those in the cluster outskirts. The energy at which CRs

cease to be magnetically confined is $E \sim 10^{17}$ eV. While this result is somewhat trivial, in the sense that it follows from considerations of the strength of magnetic fields and the size of clusters, it enables us to reach important conclusions. First, all CRs with energies $E \lesssim 10^{17}$ eV should originate within our local supercluster. Second, if our supercluster contains sources of high-energy CRs, the low-energy suppression of the extragalactic CR spectrum should not occur at energies much larger than $\sim 10^{17}$ eV.

4. Conclusions & Outlook

In the present work we have presented preliminary results of a first investigation of the effects of intracluster magnetic fields on CR propagation, using cosmological MHD simulations. We have estimated the diffusion coefficients of CRs in clusters. One of our main results is that below $E \sim 10^{17}$ eV CRs cannot escape the innermost regions of clusters. As a consequence, CRs with $E \lesssim 10^{17}$ eV originate either within the Milky Way or in our local cluster. We have also concluded that at these energies CRs are confined for a time comparable to the age of the cluster.

Thermal UV and X-ray photons produced in the hot ICM may serve as target fields for CR interactions depending on their density; in the central regions of clusters, in particular, this effect may be considerable. Employing the numerical tools here described, we are currently performing a detailed analysis of high-energy CR propagation in galaxy clusters taking into account the photohadronic, photonuclear, and hadronuclear interactions between the CRs and the intracluster gas/photons, which may produce a substantial number of secondary high-energy particles including gamma rays and neutrinos.

Acknowledgements

This work is supported by the São Paulo Research Foundation (FAPESP) grants #2017/12828-4 and #2013/10559-5, and by CNPq grants (#306598/2009-4).

References

- R. Alves Batista and G. Sigl 2014, *JCAP*, 11, 031
- R. Alves Batista *et al.* 2016, *JCAP*, 05, 038
- R. Alves Batista *et al.* 2017, *Phys. Rev. D*, 96, 023010
- R. Alves Batista and A. Saveliev 2018, *Submitted to JCAP*, arXiv:1808.04182
- P. Barai & E. M. de Gouveia Dal Pino 2018, *These Proceedings*
- M. Brüggén & F. Vazza 2015, in: A. Lazarian, E. M. de Gouveia Dal Pino, C. Melioli (eds.), *Magnetic Fields in Diffuse Media* (Berlin: Springer-Verlag), p. 599
- G. Brunetti, & T. W. Jones 2015, in: A. Lazarian, E. M. de Gouveia Dal Pino, C. Melioli (eds.), *Magnetic Fields in Diffuse Media* (Berlin: Springer-Verlag), p. 557
- O. Deligny 2014, *Comptes Rendus Physique*, 15, 367
- K. Dolag *et al.* 2004, *JCAP*, 01, 009
- S. Hackstein *et al.* 2016, *MNRAS*, 462, 3660
- S. Hackstein *et al.* 2017, *MNRAS*, 475, 2519
- R. Jansson and G. Farrar 2012a, *ApJ*, 757, 14
- R. Jansson and G. Farrar 2012b, *ApJ*, 761, L11
- G. A. Medina Tanco, E. M. de Gouveia Dal Pino, & J. E. Horvath 1998, *ApJ*, 492, 200
- G. Müller 2016, *JCAP*, 08, 025
- Pierre Auger Collaboration 2017, *Science*, 357, 1266
- G. Sigl, F. Miniati, T. Ensslin 2003, *Phys. Rev. D* 68, 043002
- V. Springel 2005, *MNRAS*, 364, 1105
- F. Vazza *et al.* 2017, *Class. Quant. Grav.*, 34, 234001

On energy equipartition between cosmic rays and magnetic fields

Amit Seta, Anvar Shukurov, Paul J. Bushby & Toby S. Wood

School of Mathematics, Statistics & Physics, Newcastle University, UK
email: a.seta1@ncl.ac.uk

Abstract. Interpretations of synchrotron observations often assume a tight correlation between magnetic and cosmic ray energy densities. We examine this assumption using both test-particle simulations of cosmic rays and MHD simulations which include cosmic rays as a diffusive fluid. We find no spatial correlation between the cosmic rays and magnetic field energy densities at turbulent scales. Moreover, the cosmic ray number density and magnetic field energy density are statistically independent. Nevertheless, the cosmic ray spatial distribution is highly inhomogeneous, especially at low energies because the particles are trapped between random magnetic mirrors. These results can significantly change the interpretation of synchrotron observations and thus our understanding of the strength and structure of magnetic fields in the Milky Way and nearby spiral galaxies.

Keywords. Cosmic rays, Magnetic fields, Diffusion, Radio continuum: ISM

1. Introduction

Synchrotron emission is one of the main observational probes of galactic magnetic fields. The synchrotron intensity I depends on the number density of cosmic ray electrons $n_{\text{cr}}^{(e)}$ and magnetic field b_{\perp} perpendicular to the line of sight ℓ ,

$$I = K \int_L n_{\text{cr}}^{(e)} b_{\perp}^{(p+1)/2} d\ell, \quad (1.1)$$

where K is a constant, L is the total path length and p is the power-law index of the electron energy spectrum ($p \approx 3$ in spiral galaxies). The determination of magnetic field strength from the synchrotron intensity requires an independent observation of the number density of cosmic ray electrons. In the absence of such information, an energy equipartition between the total cosmic ray (consisting of 90% protons, 1–2% electrons and the rest are heavier particles) and magnetic field energy densities is assumed in order to extract the magnetic field strength. Though there is no convincing theoretical justification or observational evidence to assume point-to-point energy equipartition between cosmic rays and magnetic fields in spiral galaxies, it is widely used to obtain magnetic field strengths from synchrotron intensities (Beck & Krause 2005).

2. Energy equipartition argument: previous tests and our approach

The energy equipartition assumption was first used to study the energy content in cosmic rays and magnetic fields in the jet of M87 using optical and radio emissions from the system (Burbidge 1956). Since then, the energy equipartition assumption has been used to obtain the magnetic field strength in various systems. Duric (1990) suggested that the range of possible magnetic field strengths in spiral galaxies can differ by at most an order of magnitude from the equipartition value. The conclusion is justified as

follows. If the magnetic fields are considerably weaker than the equipartition value then the particles would quickly escape the disk and almost no synchrotron emission would be observed. On the other hand, if the fields are far stronger, then the particles would be confined very close to the sources and strong emission would be observed but only in small regions around the sources. Neither of the above situations is actually seen in spiral galaxies. Also, a weakness of this type of argument is that cosmic ray diffusivity depends not on the magnetic field strength but on the *ratio* of the random to large-scale magnetic field strengths. Chi & Wolfendale (1993) used gamma-ray observations to obtain the proton number density in the Large and Small Magellanic Clouds (LMC and SMC). They showed that energy equipartition does not hold for these irregular galaxies. However, Mao et al. (2012), also using gamma-ray data, concluded that the equipartition seems to hold in the LMC. The radio-FIR correlation studies suggest that the energy equipartition assumption is invalid on scales smaller than a few kpc and may hold on larger scales (Basu & Roy 2013). Yoast-Hull et al. (2016) analyzed the gamma-ray and radio spectra of starburst galaxies and concluded that equipartition does not hold in these dynamic systems. The energy equipartition assumption, when applied on large scales, seems to hold for a number of systems (Beck 2016). However, there are also cases where this is not true. Here, using test-particle and magnetohydrodynamic (MHD) simulations, we test the point-wise or local energy equipartition assumption.

3. Cosmic rays as test particles

Cosmic ray particles gyrate around the magnetic fields lines and are scattered by small-scale magnetic fluctuations, which leads to their diffusion in galaxies (Cesarsky 1980). Such fluctuations can be spatially Gaussian or intermittent. We generate an intermittent magnetic field by numerically solving the induction equation using a chaotic velocity field with the Kolmogorov energy spectrum. The induction equation is solved using a finite difference numerical scheme in a periodic box of dimensionless size 2π (physically equivalent to the driving scale of the turbulence $l_0 \simeq 100$ pc for spiral galaxies) with 512^3 points. Exponentially growing magnetic fields are generated by such a flow via the fluctuation dynamo action. The left-hand panel of Fig. 1 shows that the resulting magnetic field is spatially intermittent being concentrated into filamentary structures. A Gaussian random magnetic field with identical power spectrum is obtained from the intermittent one by phase randomization (Shukurov et al. 2017). For an ensemble of particles in each of these fields, we then solve the particle equation of motion,

$$\frac{d^2\mathbf{r}}{dt^2} = \frac{v_0}{r_L} \frac{d\mathbf{r}}{dt} \times \frac{\mathbf{b}}{b_{\text{rms}}}, \quad (3.1)$$

where \mathbf{r} is the particle's position at time t , v_0 is the particle's speed, r_L is the particle's Larmor radius (a parameter to control particle energy) and \mathbf{b} is the magnetic field assumed to be static at the time scales of interest. Initially, the particles are distributed uniformly in space with randomly directed velocities but fixed speed v_0 . Once the diffusion sets in, we calculate the coordinates of each particle modulo 2π , divide the numerical domain into 512^3 cubes and count the number of cosmic ray particles in each cube to obtain the cosmic ray number density as a function of time and position. Then we average over a long time to obtain the time-independent cosmic ray distribution n_{cr} . Since we neglect any energy losses, n_{cr} represents a cosmic ray proton distribution.

The middle panel of Fig. 1 shows n_{cr} in an intermittent magnetic field. For both the Gaussian and intermittent fields, the magnetic field and cosmic rays are not correlated and the correlation remains close to zero even when both distributions are averaged over

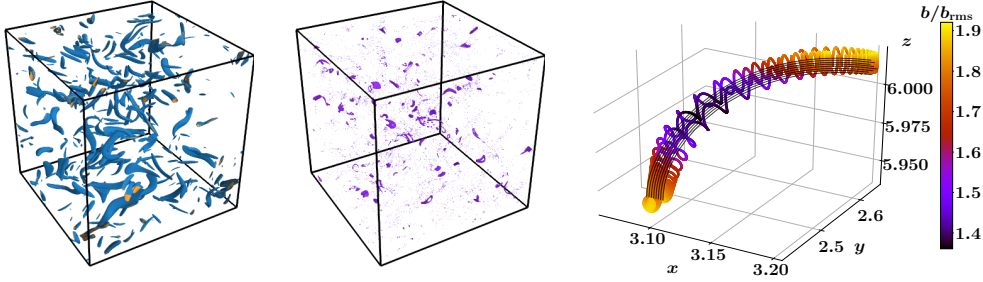


Figure 1. Left: The normalised strength of the intermittent magnetic field $b^2/\langle b^2 \rangle = 12$ (blue), 15 (yellow) from a fluctuation dynamo simulation ($\langle \dots \rangle$ denotes a volume average). Middle: The normalised cosmic ray number density $n_{\text{cr}}/\langle n_{\text{cr}} \rangle = 3.5$ for low-energy particles ($r_L/l_0 = 0.0016$). The magnetic field and cosmic ray number density are uncorrelated and yet there are small-scale structures in the cosmic ray distribution. This is due to magnetic traps which depends on the topology of magnetic field lines rather than the field strength. Right: The trajectory of a trapped particle in the simulation, with the magnetic field strength along the trajectory shown with colour. The dark grey lines show magnetic field lines. The particle moves forward and backward between two magnetic mirrors.

any scale less than the box size. The probability density of n_{cr} in both intermittent and Gaussian magnetic fields is Gaussian at higher energies (particles with $r_L > l_0$) but develops a long, heavy tail at lower energies. The spatial distribution of low-energy cosmic rays ($r_L \lesssim l_0$) is intermittent with numerous small-scale cosmic ray structures (middle panel of Fig. 1). These structures are due to randomly distributed magnetic mirror traps. This is confirmed by the right-hand panel of Fig. 1 which shows a particle trajectory close to one such cosmic ray structures in the domain. The particle follows magnetic field lines (shown in dark grey) but is trapped between two magnetic mirrors. The number of such cosmic rays structures increases when a uniform magnetic field is included and decreases when pitch-angle scattering due to the unresolved magnetic fluctuations is added (Sect. 3.2 in Seta et al. 2018). However, for all cases the cosmic rays and magnetic fields are not correlated at scales smaller than the box size. Furthermore, the magnetic field energy density (b^2) and cosmic ray (n_{cr}) distributions are statistically independent of each other (Appendix C in Seta et al. 2018). Assuming that this also applies to cosmic-ray electrons, this implies that Eq. (1.1) can be written as

$$I = K \int_L n_{\text{cr}}^{(e)} b_{\perp}^2 d\ell = \frac{K}{L} \int_L n_{\text{cr}}^{(e)} d\ell \int_L b_{\perp}^2 d\ell = KL \langle n_{\text{cr}}^{(e)} \rangle \langle b_{\perp}^2 \rangle. \quad (3.2)$$

Thus, one can use synchrotron intensity and the mean cosmic ray number density to obtain the average magnetic field strength.

4. Cosmic rays as a fluid

Cosmic rays exert pressure on the thermal gas which affects the magnetic field, which in turn controls the cosmic ray propagation. To include this nonlinear effect, we solve the MHD equations together with an advection-diffusion equation for the cosmic ray fluid (see Snodin et al. 2006 for equations, parameters and boundary conditions). A random flow is driven at the box scale by an explicit force in the Navier–Stokes equation. Cosmic rays are injected continuously at each time step but can be lost through the domain boundary. The magnetic field is first amplified exponentially, but then saturates due to the back-reaction of the Lorentz force on the flow. The mean cosmic ray energy also

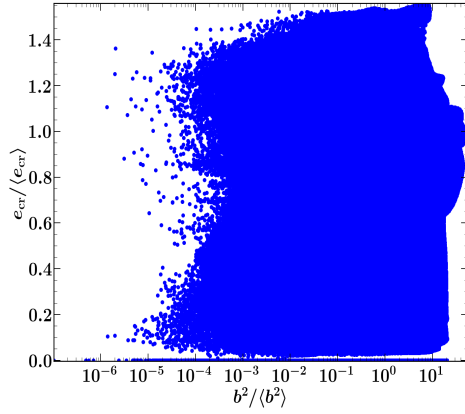


Figure 2. The scatter plot for the normalized energy densities of cosmic rays $e_{cr}/\langle e_{cr} \rangle$ and magnetic fields $b^2/\langle b^2 \rangle$ for the case with $\langle e_{cr} \rangle \approx \langle b^2 \rangle$ at the box scale. Even though both energy densities are equal when averaged over the size of the domain, locally they are not correlated.

increases initially but then settles down to a steady value. We vary the injection rate of cosmic rays such that, in the saturated stage, there are three cases for the relation between the average cosmic ray e_{cr} and magnetic field energy densities b^2 : $\langle e_{cr} \rangle < \langle b^2 \rangle$, $\langle e_{cr} \rangle \approx \langle b^2 \rangle$ and $\langle e_{cr} \rangle > \langle b^2 \rangle$. In all three cases, the cosmic ray energy density is not correlated with the magnetic field energy density. Fig. 2 confirms that the two quantities are uncorrelated even when $\langle e_{cr} \rangle \approx \langle b^2 \rangle$.

5. Conclusions

Using both test-particle and fluid descriptions of cosmic rays, we have shown that the cosmic ray and magnetic field energy densities are not correlated on scales less than the driving scale of the turbulence ($l_0 \simeq 100$ pc in spiral galaxies). Furthermore, the two quantities are statistically independent of each other, so the synchrotron intensity can be expressed as the product of the average cosmic ray number density and average magnetic field strength. The presence of small-scale cosmic ray structures due to random magnetic traps can enhance the synchrotron intensity locally. Such effects must be considered while analyzing high-resolution synchrotron observations of spiral galaxies. Our results do not exclude that energy equipartition may hold at scales larger than l_0 .

References

- Basu, A., & Roy, S. 2013, *MNRAS*, 433, 1675
 Beck, R. 2016, *ARAA*, 24, 4
 Beck, R., & Krause, M. 2005, *AN*, 326, 414
 Burbidge, G. R. 1956, *ApJ*, 124, 416
 Cesarsky, C. J. 1980, *ARAA*, 18, 289
 Chi, X., & Wolfendale, A. W. 1993, *Nature*, 362, 610
 Duric, N. 1990, in IAU Symposium, Vol. 140, Galactic and Intergalactic Magnetic Fields, ed. R. Beck, R. Wielebinski, & P. P. Kronberg, 235
 Mao, S. A., McClure-Griffiths, N. M., Gaensler, B. M., et al. 2012, *ApJ*, 759, 25
 Seta, A., Shukurov, A., Wood, T. S., Bushby, P. J., & Snodin, A. P. 2018, *MNRAS*, 473, 4544
 Shukurov, A., Snodin, A. P., Seta, A., Bushby, P. J., & Wood, T. S. 2017, *ApJL*, 839, L16
 Snodin, A. P., Brandenburg, A., Mee, A. J., & Shukurov, A. 2006, *MNRAS*, 373, 643
 Yoast-Hull, T. M., Gallagher, J. S., & Zweibel, E. G. 2016, *MNRAS*, 457, L29

Simulations of the polarized sky for the SKA

F. Loi^{1,2}, M. Murgia², F. Govoni², V. Vacca², I. Prandoni³, H. Li⁴, L. Feretti³, and G. Giovannini¹

¹Dip. di Fisica e Astronomia, Università degli Studi di Bologna, Viale Berti Pichat 6/2,
I-40127 Bologna, Italy
email: francesca.loi@inaf.it

²INAF-Osservatorio Astronomico di Cagliari, Via della Scienza 5, Selargius, Italy

³INAF-Istituto di Radioastronomia, Via Gobetti 101, I-40129 Bologna, Italy

⁴Theoretical Astrophysics, Los Alamos National Laboratory, Los Alamos, NM

Abstract. It is expected that the Square Kilometre Array will have a huge impact on the study of cosmic magnetism. However, it is not easy to quantify such an impact and to understand how the information about the magnetic fields can be extracted from SKA data. This project aims at answering these questions by realizing full-Stokes simulations of the radio sky at the depth that SKA it is expected to reach.

Keywords. polarization, radio continuum: magnetic fields, galaxies, galaxies: clusters: general, methods: numerical

1. Introduction

Numerical simulations are ideal instruments to forecast the scientific impact of future instrument as well as best suited frameworks to test sophisticated techniques of data analysis. With the advent of the Square Kilometre Array (SKA) we expect to improve our knowledge about the presence and the evolution of magnetic fields in the Universe. In this respect, an all-sky survey in polarization performed with SKA1-MID will be extremely precious since it will yield a Rotation Measure (RM) Grid of about 230-450 RM sources per square degree (Johnston-Hollitt et al. 2015). However, we have to get prepared to manage the huge amount of data that the SKA will collect and also understand how correctly interpret the information from this grid.

With this project we want to answer to these questions using a computational tool which can generate a synthetic radio observation of one or more galaxy clusters in I, U, and Q Stokes parameters, taking into account the contribution of all the radio discrete sources present in the field-of-view of our mock observation. This tool is implemented in the FARADAY software package (Murgia et al. 2004), which has been specifically designed for intracluster magnetic fields studies.

In Sect. 2, we briefly describe the basic models which allow us to produce all the properties of a radio source population distributed in a given slice of the Universe. Moreover, we illustrate the details of the Magneto-Hydro-Dynamical (MHD) simulations used to reproduce the intracluster medium (ICM) characteristics (i.e. magnetic field, thermal density and temperature) of a pair of galaxy clusters; we also show the resulting X-ray surface brightness and the total and polarized radio intensity emission of this system. In Sect. 3, we show the results of the RM Synthesis technique (e.g. Brentjens & de Bruyn 2005, Burn 1966) applied on the simulated U, Q data while the conclusion are drawn in Sect.

4. Throughout the paper, we adopt a Λ CDM cosmology with $H_0 = 71 \text{ km} \cdot \text{s}^{-1} \text{Mpc}^{-1}$, $\Omega_m = 0.27$, and $\Omega_\Lambda = 0.73$.

2. Overview

The emission of a radio source depends on many properties, such as redshift, type, size, luminosity, morphology, spectral properties, and intrinsic polarization. Thus, in order to simulate the I, U, and Q data of a radio source population we have to specify all this features.

We consider the following two families of radio sources depending on the mechanism which feeds the radio emission: active galactic nuclei (AGNs) and star forming galaxies (SFGs). We modeled our radio sources using the radio luminosity functions of Lin & Mohr (2007), Novak et al. (2017), and Smolčić et al. (2017) for what concerns the cluster and the external sources respectively. The size is assigned according to Wilman et al. 2008. The spatial distribution of cluster-embedded radio sources is determined following the profile of Lin & Mohr (2007). To reproduce the morphology and the spectral-polarimetry properties of radio sources we use high-frequency and high-resolution observations of real radio sources of different type or morphology (for example SFGs, type I and type II Fanaroff & Riley 1974 radio galaxies and head-tail radio galaxies).

For the intracluster magnetic field, the thermal plasma density distribution, and the temperature we use a cosmological MHD simulation of a pair of galaxy clusters, where the intracluster magnetic fields are injected by AGNs at $z \sim 3$ while the system is observed at $z = 0.205$. This simulation has been obtained with the ENZO code (Collins et al. 2010) and consists in a set of 3-dimensional cubes of $\sim (6.4 \text{ Mpc})^3$ with a resolution of $\sim 10.7 \text{ kpc}$ containing the ICM physical parameters.

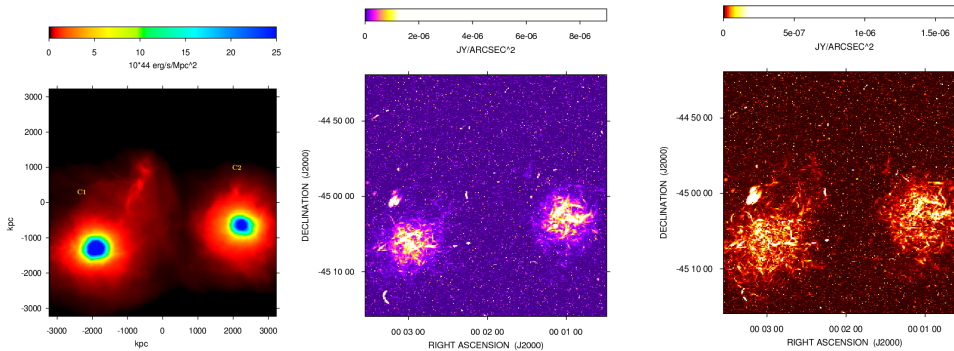


Figure 1. *Left:* X-ray surface brightness of a pair of galaxy clusters at redshift $z=0.205$, in a field-of-view of $\sim 6.4 \text{ Mpc}$ with a spatial resolution of $\sim 10.7 \text{ kpc}$. *Center and right:* total intensity and polarized intensity radio emission between 1.4 GHz of the cluster-embedded, foreground and background discrete radio sources plus the cluster radio halos; the beam $\text{FWHM}=2.5''$.

By using the FARADAY software package, we reproduce the X-ray surface brightness of the system, shown on the left of Fig. 1. By illuminating the cluster magnetic fields with a relativistic particle population, we can also simulate the emission of the radio halos hosted by the clusters (as it has been done in Govoni et al. 2013). The central and the right images of Fig. 1 show the total intensity and polarized intensity associated to the clusters and simulated with FARADAY taking into account the foreground, cluster-embedded, background discrete radio source as well as the hosted radio halos. The signal has been reproduced for a 950-1760 MHz band, with a channel resolution of $\sim 1.46 \text{ MHz}$,

corresponding to Band 2 of SKA1-MID. The field of view is $\sim 0.3 \text{ deg}^2$ and the synthesized beam full-width-at-half-maximum (FWHM) is equal to $2.5''$. We can appreciate the wealth of details of these simulated images: from the fine structure of the discrete radio sources to the large scale filaments of the radio halos. The polarized sky appears bright and rich of discrete radio sources but also the radio halos shine in polarization reaching levels of fractional polarization higher than 10% from distances larger than a few hundreds of kpc from the cluster centers.

We did not add the thermal noise to these mock observations. Indeed, this can be seen as an ideal case since it would be necessary a very long observational time to reach the confusion limit in U and Q. However, as we will see in the next Section, this case is useful to understand how to interpret the results of the RM Synthesis data analysis.

3. The RM Synthesis applied on mock SKA observations

We decided to apply the RM Synthesis technique to three sets of data: the background radio sources, the radio halos, and all the sources together. The interval in Faraday depth explored in our analysis goes from -5000 rad/m^2 to 5000 rad/m^2 with a spacing of 10 rad/m^2 . The resulting transfer function has a FWHM of 40 rad/m^2 .

For the sake of simplicity in Fig. 2 we only show the results from a region centered on the left galaxy cluster of Fig. 1: each row refer respectively to the background radio sources (top), the radio halo (middle), and all the sources in the field-of-view (bottom). From left to right, the first column shows the theoretical RM images as computed from the magnetic field and the thermal density given by the MHD simulations, the central one results from the application of the RM Synthesis to the data, the last column shows the comparison between the theoretical σ_{RM} profile and the one measured in the RM Synthesis images.

We notice that the density of background radio sources is enough to cover the entire cluster area, moreover, the image and the σ_{RM} profile inferred from the RM synthesis reproduce well the theoretical ones. The RM synthesis images of radio halos present micro-structures with respect to the theoretical images; this is due to the fact that the RM synthesis provides us with the RM of the polarized peak of the radio halo filaments, and their position along the line of sight could be different for close lines of sight which share the same theoretical RM value. The σ_{RM} profile presents slightly higher values at less than 500 kpc from the cluster centers. When we consider all the sources together we notice that the behavior of the radio halo dominates. Even if not all the clusters do host a radio halo, we can still have similar effects: indeed multiple radio sources inside the ICM and/or extended Faraday screens can behave like radio halos. Thus, it is important to understand what we observe in order to properly interpret the results.

4. Conclusions

Band 2 observation with the SKA1-MID are potentially very well suited for intracluster magnetic field studies through the measure of the RM. The population of background radio sources composing the RM grid will permit a very precise reconstruction of the "true" cluster RM. Moreover, we notice that radio halos are conceivably useful in the determination of the RM of galaxy clusters through the RM Synthesis technique, although in depth study of this technique is crucial to correctly interpret the results, highlighting the importance of this kind of simulations.

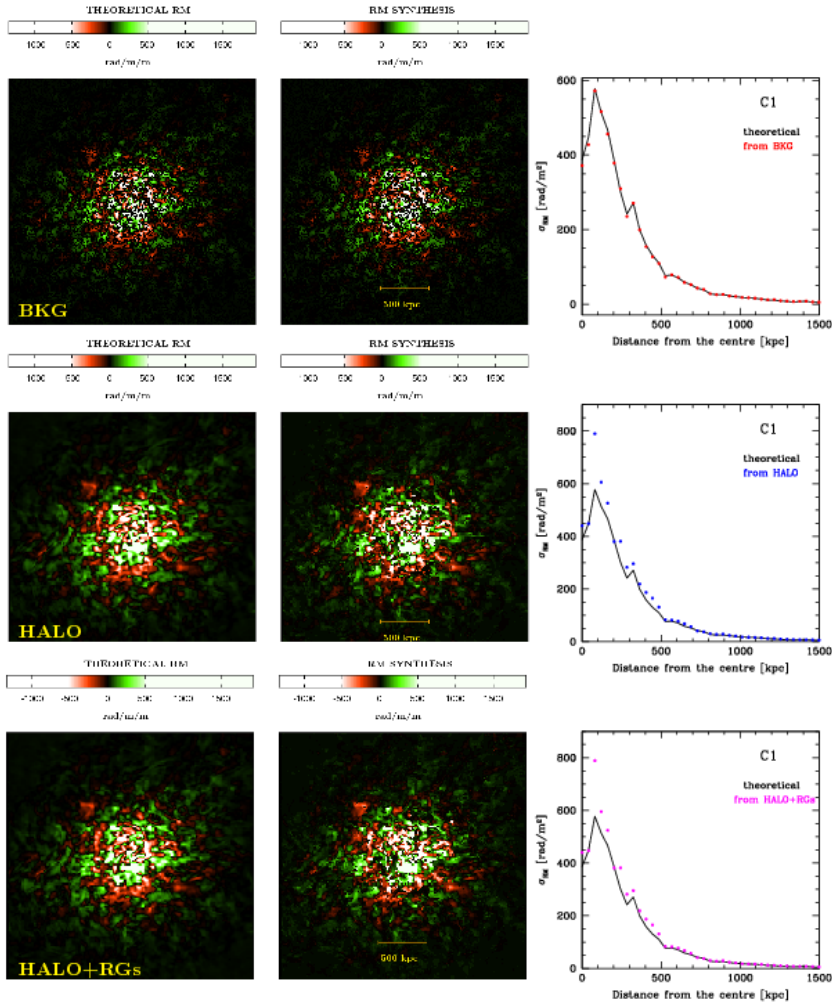


Figure 2. From left to right: Theoretical RM as computed from the MHD cubes, results of the RM synthesis applied on U,Q Stokes simulated cubes, profile of the theoretical RM compared to what measured in the RM Synthesis image for, respectively, the background discrete radio sources (top), the radio halo (middle), and the foreground, background, cluster-embedded diffuse and discrete sources (bottom) of the galaxy cluster on the left in Fig. 1.

References

- Brentjens M. A., de Bruyn A. G., 2005, *A&A*, 441, 1217
 Burn B. J. 1966, *MNRAS*, 133, 67
 Collins, D. C., Xu, H., Norman, M. L., Li, H., & Li, S. 2010, *ApJS*, 186, 308
 Fanaroff, B. L., & Riley, J. M. 1974, *MNRAS*, 167, 31P
 Govoni, F., Murgia, M., Xu, H., et al. 2013, *A&A*, 554, A102
 Johnston-Hollitt, M., Govoni, F., Beck, R., et al. 2015, *Advancing Astrophysics with the Square Kilometre Array (AASKA14)*, 92
 Lin, Y.-T., & Mohr, J. J. 2007, *ApJS*, 170, 71
 Murgia, M., Govoni, F., Feretti, L., et al. 2004, *A&A*, 424, 429
 Novak, M., Smolčić, V., Delhaize, J., et al. 2017, *A&A*, 602, A5
 Smolčić, V., Novak, M., Delvecchio, I., et al. 2017, *A&A*, 602, A6
 Wilman, R. J., Miller, L., Jarvis, M. J., et al. 2008, *MNRAS*, 388, 1335

From the NVSS RM Catalogue to Future Polarisation Surveys

Yik Ki Ma¹ †, S. A. Mao¹, Jeroen Stil², Aritra Basu^{3,1},
Jennifer West⁴, Carl Heiles⁵, Alex S. Hill^{6,7,8}, and S. K. Betti⁹

¹Max-Planck-Institut für Radioastronomie, Auf dem Hügel 69, 53121 Bonn, Germany
email: ykma@mpifr-bonn.mpg.de

²Department of Physics and Astronomy, University of Calgary, 2500 University Drive NW,
Calgary, AB T2N 1N4, Canada

³Fakultät für Physik, Universität Bielefeld, Postfach 100131, 33501 Bielefeld, Germany

⁴Dunlap Institute for Astronomy and Astrophysics, The University of Toronto, 50 St. George
Street, Toronto, ON M5S 3H4, Canada

⁵Department of Astronomy, University of California, Berkeley, CA 94720-3411, USA

⁶Department of Physics and Astronomy, The University of British Columbia, Vancouver, BC
V6T 1Z1, Canada

⁷Space Science Institute, Boulder, CO, USA

⁸National Research Council Canada, Herzberg Program in Astronomy and Astrophysics,
Dominion Radio Astrophysical Observatory, PO Box 248, Penticton, BC V2A 6J9, Canada

⁹Department of Astronomy, University of Massachusetts, 710 North Pleasant Street, Amherst,
MA 01003-9305, USA

Abstract.

With rotation measure (RM) towards 37,543 polarised sources, the Taylor *et al.* (2009) RM catalogue has been widely exploited in studies of the foreground magneto-ionic media. However, due to limitations imposed by observations in survey mode in the narrowband era, the listed RM values are inevitably affected by various systematic effects. With new Karl G. Jansky Very Large Array (VLA) broadband spectro-polarimetric observations at L-band, we set off to observationally examine the robustness of the Taylor catalogue. This would facilitate combinations and comparisons of it with results from current and future polarisation surveys such as Polarization Sky Survey of the Universe's Magnetism (POSSUM), VLA Sky Survey (VLASS), and the eventual Square Kilometre Array (SKA). Our on-axis pointed observations, in conjunction with simulations, allowed us to estimate the impact of off-axis polarisation leakage on the measured RM values. This demonstrates the importance to properly calibrate for the off-axis leakage terms in future all-sky polarisation surveys, in order to obtain high fidelity polarisation information from sources down to low fractional polarisation.

Keywords. galaxies: active — galaxies: magnetic fields — ISM: magnetic fields — radio continuum: galaxies

1. Introduction

Magnetic fields are known to be essential for the astrophysics in, for example, star formation, propagation of cosmic rays, and outflows and evolution of galaxies (see review by Beck & Wielebinski 2013; Beck 2016). One way to probe astrophysical magnetic fields is by quantifying the amount of Faraday rotation experienced by the linear-polarised

† Member of the International Max Planck Research School (IMPRS) for Astronomy and Astrophysics at the Universities of Bonn and Cologne

synchrotron emission from background extragalactic sources (EGSs) in radio regime. This process changes the polarisation position angle (PA; [rad]) by

$$\Delta\text{PA} = \left[0.81 \int_{\ell}^0 n_e(s) B_{\parallel}(s) ds \right] \cdot \lambda^2 \equiv \text{RM} \cdot \lambda^2, \quad (1.1)$$

where ℓ [pc] is the (physical) distance to the background source, n_e [cm^{-3}] is the thermal electron density, B_{\parallel} [μG] is the magnetic field strength along the line of sight (s [pc]; increases away from the observer), λ [m] is the wavelength of the polarised emission in question, and RM [rad m^{-2}] is the rotation measure of the background source. In other words, the average magnetic field strength (and direction) along the line of sight, weighted by n_e , is imprinted in the RM value of the polarised background source. This can be exploited in so-called RM-grid experiments, where RM measurements of numerous polarised background sources are performed to reveal the magnetic field strengths and structures in foreground astrophysical sources (e.g. Mao *et al.* 2008; Mao *et al.* 2010; Harvey-Smith *et al.* 2011; Van Eck *et al.* 2011; Gießübel *et al.* 2013; Kaczmarek *et al.* 2017; Mao *et al.* 2017).

The largest RM catalogue to date is the Taylor *et al.* (2009) catalogue, in which the RM values were determined using narrowband Very Large Array (VLA) data at 1364.9 and 1435.1 MHz (with bandwidths of 42 MHz each) in 1990s from the NRAO VLA Sky Survey (NVSS; Condon *et al.* 1998). With reported values through 37,543 lines of sight north of $\delta = -40^\circ$ (at a source density of about 1 deg^{-2}), the Taylor catalogue allows studies of cosmic magnetism in astrophysical structures with angular sizes larger than several degrees (e.g. Harvey-Smith *et al.* 2011; Stil *et al.* 2011; Purcell *et al.* 2015). While ongoing broadband polarisation surveys such as Polarization Sky Survey of the Universe's Magnetism (POSSUM; Gaensler *et al.* 2010) and VLA Sky Survey (VLASS; Myers *et al.* 2014), as well as the eventual Square Kilometre Array (SKA), will grant us much higher RM densities over the entire sky (see S. A. Mao in this volume), the Taylor catalogue will still remain a unique window to the magnetised Universe by complementing POSSUM and SKA in sky domain and VLASS in frequency domain. Comparisons between the Taylor catalogue and future survey results will also allow studies of polarisation time variabilities over more than 20 years.

Given the significance of the Taylor catalogue, we have investigated its robustness using new broadband data from the Karl G. Jansky VLA. The full results on $n\pi$ -ambiguity and off-axis polarisation leakage in the Taylor catalogue, as well as Faraday complexities and potential RM time variabilities of our target sources, are reported in Ma *et al.* (submitted). In this proceedings, we focus on the implications of the off-axis instrumental polarisation leakage in the Taylor catalogue. The observation details are described in Section 2. The effects of $n\pi$ -ambiguity and off-axis leakage are discussed in Sections 3 and 4. We draw the conclusion and remark on future polarisation surveys in Section 5.

2. New Broadband Observations

From the Taylor catalogue, we selected a sample of 23 sources for our new spectropolarimetric observations. These sources have high RM magnitudes of $\gtrsim 300 \text{ rad m}^{-2}\ddagger$, have Galactic latitude of $|b| > 10^\circ$, and have NVSS flux densities higher than 100 mJy. The unusually high $|\text{RM}|$ values of these sources make them prime $n\pi$ -ambiguity candidates in the Taylor catalogue (see Ma *et al.* submitted).

New broadband data were obtained using Karl G. Jansky VLA in L-band (1–2 GHz)

\ddagger Except for NVSS J234033+133300, which has $\text{RM}_{\text{Taylor}} = +56.7 \pm 6.3 \text{ rad m}^{-2}$.

in D-array configuration on 2014 July 03. The total integration time per source is about 3–4 minutes, with our targets placed on the pointing axis of the antennae to ensure no off-axis instrumental effects are present in our data. Standard flagging and calibration procedures were applied to the data, including one iteration of phase self calibration on the target sources. From this, we formed two sets of Stokes I , Q , and U images — “full band images” utilising the entire usable band, binning 4 MHz of visibility data for each step in frequency, and “NVSS band images” formed with nearly identical frequency coverages as that of the NVSS survey data used by the Taylor catalogue, albeit some flaggings were done to our data in those frequency ranges. On one hand, we use the full band images, combined with the RM-Synthesis algorithm (Brentjens & de Bruyn 2005), to obtain the Faraday depth (FD; the generalisation of RM, see e.g. Brentjens & de Bruyn 2005, Ma *et al.* submitted) of our sources free of $n\pi$ -ambiguity. On the other hand we use the NVSS band images to make direct comparisons with the Taylor catalogue results.

3. $n\pi$ -ambiguity in the Taylor Catalogue

We compared the FD from RM-Synthesis on our full-band images with the RM from the Taylor catalogue ($\text{RM}_{\text{Taylor}}$), and found that the difference between these two sets of values for nine of our targets are consistent with that expected from $n\pi$ -ambiguity in the Taylor catalogue. By comparing the statistical properties of these sources versus that of sources with reliable RM values, we estimate that there may be more than 50 $n\pi$ -ambiguity sources out of the 37,543 Taylor catalogue sources.

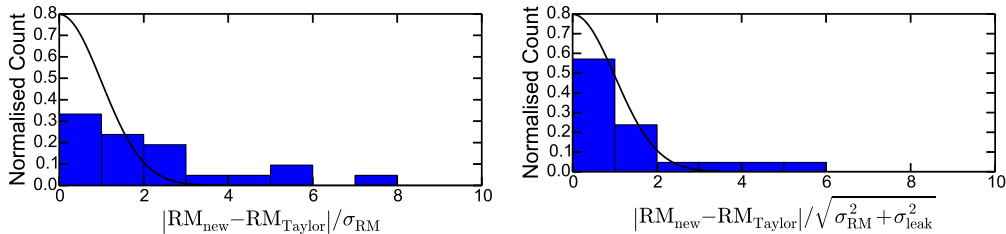


Figure 1. Comparisons between our RM_{new} and $\text{RM}_{\text{Taylor}}$. **(Left)** Histogram of RM differences in units of RM uncertainties of the observations (σ_{RM}); **(Right)** The same histogram as the left panel, except that we have accounted for the extra RM uncertainty due to off-axis leakage (σ_{leak}). The black line in both panels shows a folded normal distribution, which is the expected profile of the histogram if the RM differences are purely due to the included uncertainties.

4. Polarisation Discrepancies due to Off-axis Polarisation Leakage

Through careful comparisons between our results and those from the Taylor catalogue, we noted discrepancies in polarisation properties from the two studies. Firstly, from RM-Synthesis analysis in Section 3, we found that two of our target sources are unpolarised ($\lesssim 0.07\%$ at 6σ), though they are listed as $\approx 0.5\%$ polarised in the Taylor catalogue with signal-to-noise of over 30 in polarisation. Secondly, the RM derived from our new NVSS band images (RM_{new}) and $\text{RM}_{\text{Taylor}}$ do not match within measurement uncertainties (Figure 1 Left), after correcting both for $n\pi$ -ambiguity using the broadband FD obtained in Section 3.

These discrepant polarisation properties are mainly due to off-axis polarisation leakage in the Taylor catalogue. A simulation was conducted to quantify its effect on RM

measurements in the Taylor catalogue. Using the Taylor catalogue listed values (specifically, total intensity, polarised intensity, and $\text{RM}_{\text{Taylor}}$) as inputs, we injected an artificial polarisation leakage signal with amplitudes fixed at 0.5% of the total intensity to the source polarisation signal, and compared the derived RM with and without this leakage effect (see Ma *et al.* submitted for details of the simulation). We found that on average, the effect of the uncorrected off-axis polarisation leakage can be taken into account by increasing the listed RM uncertainties in the Taylor catalogue by 10%. By incorporating this extra RM uncertainty to our sources, we find that the discrepancies between RM_{new} and $\text{RM}_{\text{Taylor}}$ can be mostly explained (Figure 1 Right), except for three sources where significant RM differences still remain. This could be due to true RM time variabilities which will be investigated in a future study (Ma *et al.* in prep).

5. Conclusion and Outlook to Future Polarisation Surveys

In this proceedings, we reported our findings on the robustness of RM values reported in the Taylor catalogue. Our results suggest that the $n\pi$ -ambiguity may affect the RM values of more than 50 out of the total of 37,543 sources in the Taylor catalogue. Furthermore, the uncorrected off-axis polarisation leakage in the NVSS data results in an extra 10% in Taylor RM uncertainties. These effects must be taken into account in future studies utilising this RM catalogue.

We demonstrated the effect of uncorrected off-axis instrumental polarisation on RM measurements in the specific case of the Taylor catalogue. This same instrumental effect can also impact future broadband polarisation surveys, manifested as an artificial signal in Faraday spectrum near 0 rad m^{-2} (see J. Stil in this volume). To ensure high fidelity in Faraday spectra, particularly from sources with low fractional polarisation, current and future polarisation surveys must properly characterise and remove the off-axis polarisation leakage terms.

References

- Beck R. 2016, *A&ARv*, 24, 4
 Beck R., Wielebinski R. 2013, *Planets, Stars and Stellar Systems Vol. 5. Springer, Berlin, Germany, p. 641*
 Brentjens M. A., de Bruyn A. G. 2005, *A&A*, 441, 1217
 Condon J. J., Cotton W. D., Greisen E. W., Yin Q. F., Perley R. A., Taylor G. B., Broderick J. J. 1998, *AJ*, 115, 1693
 Gaensler B. M., Landecker T. L., Taylor A. R., POSSUM Collaboration 2010, *BAAS*, 42, 515
 Gießübel R., Heald G., Beck R., Arshakian T. G. 2013, *A&A*, 559, A27
 Harvey-Smith L., Madsen G. J., Gaensler B. M. 2011, *ApJ*, 736, 83
 Kaczmarek J. F., Purcell C. R., Gaensler B. M., McClure-Griffiths N. M., Stevens J. 2017, *MNRAS*, 467, 1776
 Mao S. A., Gaensler B. M., Stanimirović S., Haverkorn M., McClure-Griffiths N. M., Staveley-Smith L., Dickey J. M. 2008, *ApJ*, 688, 1029
 Mao S. A., Gaensler B. M., Haverkorn M., Zweibel E. G., Madsen G. J., McClure-Griffiths N. M., Shukurov A., Kronberg P. P. 2010, *ApJ*, 714, 1170
 Mao S. A., *et al.* 2017, *Nature Astronomy*, 1, 621
 Myers S. T., Baum S. A., Chandler C. J. 2014, *BAAS*, 223, 236.01
 Purcell C. R., *et al.* 2015, *ApJ*, 804, 22
 Stil J. M., Taylor A. R., Sunstrum C. 2011, *ApJ*, 726, 4
 Taylor A. R., Stil J. M., Sunstrum C. 2009, *ApJ*, 702, 1230
 Van Eck C. L., *et al.* 2011, *ApJ*, 728, 97

New Insights on Galactic Dynamos

Luke Chamandy¹†, Anvar Shukurov²‡ & A. Russ Taylor^{3,4}¶

¹Department of Physics and Astronomy, University of Rochester, Rochester NY 14627, USA

²School of Mathematics, Statistics & Physics, Newcastle University, Newcastle upon Tyne
NE1 7RU

³Department of Physics and Astronomy, University of the Western Cape, Belleville 7535,
Republic of South Africa

⁴Astronomy Department, University of Cape Town, Rondebosch 7701,
Republic of South Africa

Abstract. We argue that pitch angles of the azimuthally averaged large-scale or mean magnetic fields in nearby spiral galaxies inferred from observations can tentatively be explained with simple galactic dynamo models. Agreement is not perfect, but is reasonable considering the uncertainty in dynamo parameters.

Keywords. Dynamo, galaxies: ISM, galaxies: magnetic fields, galaxies: spiral, magnetic fields

1. Introduction

Large-scale (or mean) galactic magnetic fields are observed to be in near-equipartition with turbulent kinetic energy in nearby galaxies, which suggests that the dynamo has likely reached saturation. The most basic properties of the mean magnetic field are its strength B and direction; the latter is characterized by the pitch angle $p = \arctan(B_r/B_\phi)$, with $-90^\circ < p \leq 90^\circ$, where B_r and B_ϕ are the radial and azimuthal components in cylindrical geometry (r, ϕ, z) . The quantity p is arguably more useful for testing galactic dynamo theory than B , for three reasons. Firstly, unlike B , p is insensitive to the extent to which the dynamo instability is supercritical. Secondly, p is insensitive to details of the dynamo non-linearity while B is not. And thirdly, p is more directly and accurately inferred from observation than B .

The analytical expression for the magnetic pitch angle in the saturated (steady) state in the local axisymmetric dynamo model of Chamandy, Shukurov & Subramanian (2014) can be compared with pitch angles inferred from observations (Van Eck 2015 and references therein). Because estimates of the effects of a mean outflow (wind or fountain flow) tend to be too small to significantly affect the dynamo for the galaxies for which data exists to enable such estimates, the formula effectively reduces to

$$p \simeq -\arctan \left[\frac{\pi^2 \tau}{12q\Omega} \left(\frac{u}{h} \right)^2 \right], \quad (1.1)$$

where τ is the turbulent correlation time, Ω is the angular rotation speed, $q = -d \ln \Omega / d \ln r$ with r the galactocentric distance ($q = 1$ for a flat rotation curve), u is the turbulent speed of the largest eddies and h is the scale height of diffuse gas. $p < 0$ for a trailing spiral. Van Eck et al. (2015) found that (i) theoretical values of $|p|$ are much too small compared with observations, and (ii) observational and theoretical values are uncorrelated. In Chamandy, Shukurov & Taylor (2016) we refined their model in three ways:

† lchamandy@pas.rochester.edu

‡ anvar.shukurov@ncl.ac.uk

¶ russ@ast.uct.ac.za

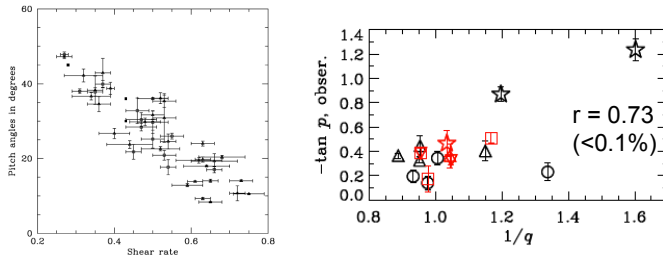


Figure 1. Observational data showing correlations between p_a and q (left, reproduced from Seigar et al. 2006), and p and q (right, adapted from Chamandy, Shukurov & Taylor 2016, with Pearson correlation coefficient and corresponding null probability).

(i) we solved the $\alpha^2\Omega$ local axisymmetric dynamo equations numerically in 1.5D in z , evolving the mean magnetic field up to the steady state, (ii) rather than taking h as a parameter, we modeled $h(r)$ based on the flared HI Milky Way disc model of Kalberla & Dedes (2008) scaled to $h = 400$ pc at $r = 8$ kpc (Ruzmaikin et al. 1988) and scaled radially by the ratio of r_{25} to that of the Milky Way, and (iii) rather than adopting $\tau = 10$ Myr, we took τ to be a free parameter: this leads to a ‘best fit’ value of $\tau \approx 14$ Myr. Like Van Eck et al. (2015) we adopted $u = 10 \text{ km s}^{-1}$, comparable to the sound speed of the warm gas, and used the same compiled observational data for $\Omega(r)$ and $q(r)$.

2. Accuracy and applicability of local axisymmetric solutions

It has been shown that 1.5D axisymmetric saturated solutions and even simplified 0.5D solutions (see Eq. 1.1) approximate accurately 2.5D solutions in (r, z) outside of the central few hundred pc of the galaxy, especially when galactic outflows are weak (Chamandy 2016). A possible objection to our approach is the neglect of non-axisymmetry. While the $m = 0$ azimuthal Fourier mode of the dynamo tends to dominate in axisymmetric discs, non-axisymmetric discs can excite higher order modes (e.g. Chamandy, Shukurov & Subramanian 2015), but non-axisymmetric mean magnetic modes are generally found to be weak (Fletcher 2010). Weak non-axisymmetric modes are expected to exert only a very minor perturbation on the axisymmetric mode (Chamandy, Subramanian & Shukurov 2013). Nevertheless, it has been suggested that since the mean field tends to ‘follow’ the spiral arms, there must be a causal effect. Firstly, the premise is not supported by wavelet analysis which has shown that polarization angles in galaxies are consistently larger than spiral arm pitch angles p_a (Frick et al. 2016, Berkhuijsen et al. 2016, Mulcahy, Beck & Heald 2017). Secondly, even if spiral arm and mean magnetic field pitch angles are correlated (whether this is true is not yet clear), such a correlation does not imply the existence of a causal relationship, and, moreover, a correlation would indeed be expected from their common correlation with the shear rate. This is demonstrated in Fig. 1: the left panel shows a plot of $|p_a|$ vs. $q/2$, from Seigar et al. 2006, while the right panel shows $\tan |p|$ vs. $1/q$ (see Eq. 1.1) from Chamandy, Shukurov & Taylor (2016) (neglecting the galaxy M81 and SB-type galaxies, whose mean magnetic fields are observed to be highly non-axisymmetric; see Krause et al. 1989 and Beck et al. 2005).

3. Results

In Fig. 2, model results for p (middle row, with open (closed) symbols representing numerical (analytical) solutions) are compared with values inferred from observations (top row), along with residuals (bottom row). Galaxies are separated into columns according

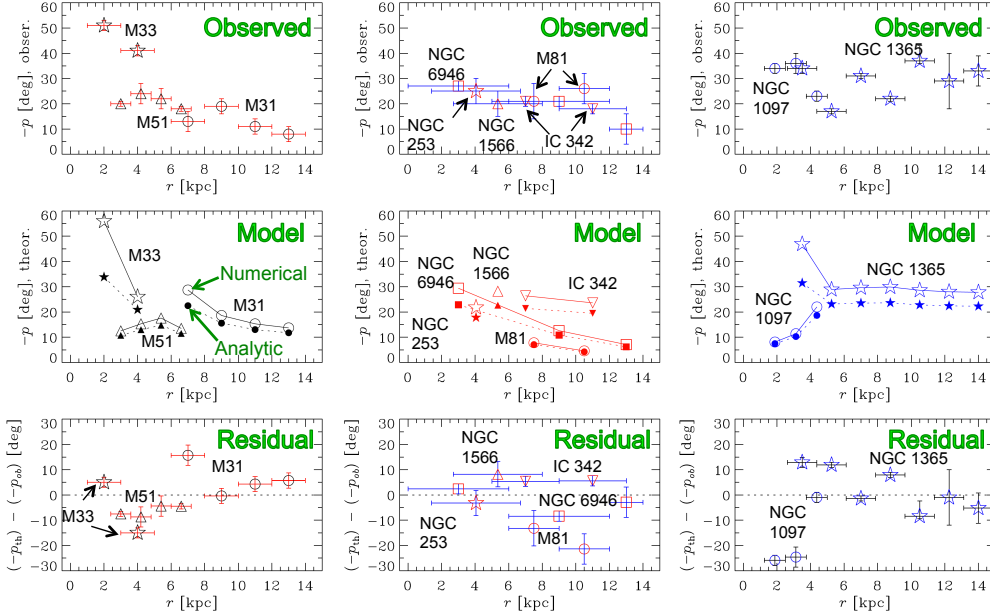


Figure 2. Pitch angle data inferred from observations (top), obtained from our fiducial dynamo model (middle), and their difference (bottom) for three different types of galaxy, organized into columns (adapted from Chamandy, Shukurov & Taylor 2016, see text for details).

to their type and magnetic field observations: the left-hand column contains SA galaxies for which Fourier analysis had been performed on the data (these observational data are the most reliable of those available), the middle column contains those SA or SAB galaxies for which such an analysis had not been performed, and the right-hand column contains SB galaxies. Agreement is not perfect, with $\chi^2_{\nu} \sim 10$ for SA and SAB galaxies, but this is not surprising given that (i) the model is idealized, (ii) inferred values rely on observational modeling and likely have systematic uncertainties, and (iii) we chose to parameterize the model with only *a single free parameter*, τ , even though other parameters are expected to vary between and within galaxies (Chamandy & Taylor 2015). For SB galaxies, which the model is *not* meant to explain, the agreement is worse (especially at small radius where the bar is strong and the magnetic field highly non-axisymmetric) than for unbarred or weakly barred galaxies. Kendall’s rank test can be performed on the pairs of pitch angles within each galaxy and shows that the model agrees with the SA and SAB galaxy data significantly better than a randomly ordered sample.

It is also encouraging that the ‘best fit’ value of τ is of the expected order of magnitude. We also tried a model with $h = \text{constant}$, i.e. an unflared disc, and found that, regardless of the value of h used, agreement between model and data was much worse than with our fiducial flared disc model. We take this as evidence that galactic discs are flared, as would be expected from physical arguments (Rodrigues et al. 2018). Galactic dynamo theory has also been used to point out that the alignment of magnetic spiral *arms* (Beck & Hoernes 1996) with their gaseous counterparts suggests that the latter are winding up and transient, as opposed to rigidly rotating and steady (Chamandy, Shukurov & Subramanian 2015). Thus, magnetic fields can plausibly serve as probes of other phenomena, such as interstellar turbulence, disc flaring and spiral structure and evolution, even in cases where their dynamical influence may be weak or not fully apparent.

Finally, in Fig. 3, we compare our results (excluding M81 and SB galaxies, right panel)

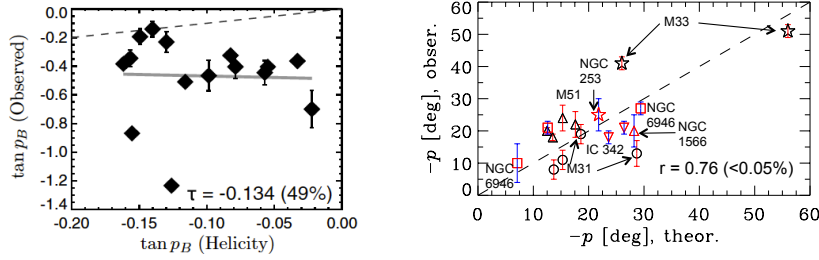


Figure 3. Plot of pitch angles derived from observation vs. values obtained from theory for the models of Van Eck et al. (2015) (left, reproduced from that work) and Chamandy, Shukurov & Taylor (2016) (right, with Pearson correlation coefficient and corresponding null probability).

with those of Van Eck et al. (2015) (left panel), showing that the current state of affairs is not as dire if our more detailed model that includes disc flaring is invoked.

4. Conclusions

Our model can be made to be more realistic by including more physics: the gaseous galactic halo, independent constraints on parameters such as u , and revisiting the roles of outflows and non-axisymmetry. However, given the paucity and heterogeneity of the data, we feel that comparing with results of minimalistic dynamo models is a fruitful approach. There is a need to analyze presently available data as uniformly as possible with modern methods in order to expand and improve the data set. At the same time, there is a need to come up with alternative dynamo models (e.g. Chamandy & Singh 2018), as well as to simulate magnetic properties for large populations of galaxies throughout cosmic time (Rodrigues et al. 2018, see also L. F. S. Rodrigues, this volume).

References

- Beck, R. & Hoernes, P. 1996, *Nature*, 379, 47
 Beck, R., Fletcher, A., Shukurov, A., Snodin, A., Sokoloff, D. D., Ehle, M., Moss, D. & Shoutenkov, V. 2005, *A&A*, 444, 739
 Berkhuijsen, E. M., Urbanik, M., Beck, R. & Han, J. L. 2016, *A&A*, 588, A114
 Chamandy, L. 2016, *MNRAS*, 462, 4402
 Chamandy, L. & Taylor, A. R. 2015, *ApJ*, 808, 28
 Chamandy, L. & Singh, N. K. 2018, *MNRAS*, 481, 1300
 Chamandy, L., Subramanian, K. & Shukurov, A. 2013, *MNRAS*, 433, 3274
 Chamandy, L., Shukurov, A. & Subramanian, K. 2014, *MNRAS*, 443, 1867
 Chamandy, L., Shukurov, A. & Subramanian, K. 2015, *MNRAS*, 446, L6
 Chamandy, L., Shukurov, A. & Taylor, A. R. 2016, *ApJ*, 833, 43
 Fletcher, A. 2010, *ASPSCS*, 438, 197
 Frick, P., Stepanov, R., Beck, R., Sokoloff, D., Shukurov, A., Ehle, M. & Lundgren, A. 2016, *A&A*, 585, A21
 Kalberla, P. M. W. & Dedes, L. 2008, *A&A*, 487, 951
 Krause, M., Hummel, E. & Beck, R. 1989, *A&A*, 217, 4
 Mulcahy, D. D., Beck, R. & Heald, G. H. 2017, *A&A*, 600, A6
 Rodrigues, L. F. S., Chamandy, L., Shukurov, A., Baugh, C. M. & Taylor, A. R. 2018, *ArXiv e-prints*, 1809.10521
 Ruzmaikin, A. A., Shukurov, A. M. & Sokoloff, D. D. 1988, *Magnetic Fields of Galaxies*, Kluwer Dordrecht
 Seigar, M. S. 2006, *ApJ*, 645, 1012
 Van Eck, C. L., Brown, J. C., Shukurov, A. & Fletcher, A. 2015, *ApJ*, 799, 35

The Role of Magnetic Fields in The Evolution of Galaxies

Fatemeh S. Tabatabaei

Instituto de Astrofísica de Canarias, Vía Láctea S/N, E-38205 La Laguna, Spain
Departamento de Astrofísica, Universidad de La Laguna, E-38206 La Laguna, Spain
School of Astronomy, Institute for Research in Fundamental Sciences, 19395-5531 Tehran, Iran
email: ftaba@ipm.ir

Abstract. Magnetic fields constitute an energetic component of the interstellar medium in galaxies and, hence, can affect the formation of galactic structures. Sensitive resolved radio continuum observations together with statistical studies in galaxy samples are performed to investigate the origin and the impact of the magnetic fields. The JVLA cloud-scale survey of M33 unveils strong tangled magnetic field along the spiral arms and in the galaxy center indicating amplification due to compression and local shear in molecular clouds. Studying a sample of non-cluster, non-interacting galaxies, we find that the large-scale ordered magnetic field scales with the rotation speed of galaxies. The total and disordered magnetic fields scales with the star formation rate in normal star forming galaxies. On the other hand, a strong magnetic field in the center of NGC 1097—a massive galaxy undergoing star formation quenching—is found to be responsible for decelerating its massive star formation. Putting these results together, it is deduced that 1) the Universe was highly magnetized short after the peak of the massive star birth at about 1 Gyr after the Big Bang and 2) the strong magnetic field has possibly acted as back reaction after this time, quenching the massive star formation and stimulating the formation of low-mass stars in massive galaxies.

1. Introduction

Cosmic magnetic fields have been present since the very early Universe created through mechanisms such as plasma instabilities and cosmic batteries (e.g., Subramanian 2016). Theoretical studies show that, after the epoch of reionization, these weak seed fields ($\lesssim 10^{-16}$ G) were amplified to stronger fields of $\gtrsim \mu\text{G}$ through various processes such as compression and shear motions (Beck et al. 2013) or small-scale dynamos (e.g., Schober et al. 2013) on time-scales of few to hundreds of Myr . The amplification due to compression and shear occurs because the magnetic field lines are frozen into a fluid and due to the magnetic flux conservation law. The dynamo action, that is based on the energy conservation, converts kinetic energy from turbulence to magnetic energy. Theoretically, both mechanisms can occur in galaxies, and particularly in star forming regions where both supernova-driven turbulence and bulk motions of dense gas are present, however, a general picture of the origin of the field amplification in the interstellar medium (ISM) is missing and awaits sensitive and high-resolution observations in statistically meaningful galaxy samples.

Full polarization radio continuum observations make it possible to measure and map the magnetic field strength and structure in galaxies (see the review by Beck 2015). However, the radio continuum emission needs to be corrected first for contamination by the thermal free-free emission. This is particularly important in high-resolution studies of galaxies even at low frequencies. The dust-unbiased *Thermal Radio Template (TRT)* methods, developed by Tabatabaei et al. (2007), Tabatabaei et al. (2013), and Tabatabaei et al. (2018), map the thermal and the nonthermal synchrotron emission in galaxies

without any assumption about the synchrotron spectrum. These methods are sensitive to the diffuse ISM structures and hence ideal to study the role of the magnetic fields in the energy balance and structure formation in different locations in a galaxy. In addition to the high-resolution studies, surveys in galaxy samples are vital to probe any dependence on galactic properties such as mass, morphology, dynamics, and star formation rate shedding light on the origin and amplification mechanisms of the magnetic fields. Our recent observations in nearby galaxies and their implications for the evolution of galaxies are described as follows.

2. Large-scale magnetic field and galactic dynamics

The observed polarized radio continuum emission from spiral galaxies exhibits a large-scale ordered pattern which is often linked to the mean field $\alpha - \Omega$ dynamo (e.g., Beck 2015) if the observed pitch angles agree with theoretical estimates (Shukurov 2004). However, a global picture connecting the strength of the large-scale magnetic field to dynamics of galaxies have been awaiting further observations to build a statistically meaningful sample. Defining this sample, it is also necessary to take into account the galactic environment as galaxy dynamics can be influenced by interactions and mergers. Putting together the available data of non-interacting, non-cluster galaxies with known large-scale magnetic fields, Tabatabaei et al. (2016) find a tight correlation between the strength of the integrated polarized flux density and the rotation speed v_{rot} of galaxies. This translates to an almost linear correlation between the large-scale magnetic field \overline{B} and v_{rot} assuming that the number of cosmic-ray electrons is proportional to the star formation rate, and a super-linear relation, $\overline{B} \propto v_{\text{rot}}^{1.5}$, assuming equipartition between magnetic fields and cosmic rays (Fig. 1). It is important to note that this correlation is

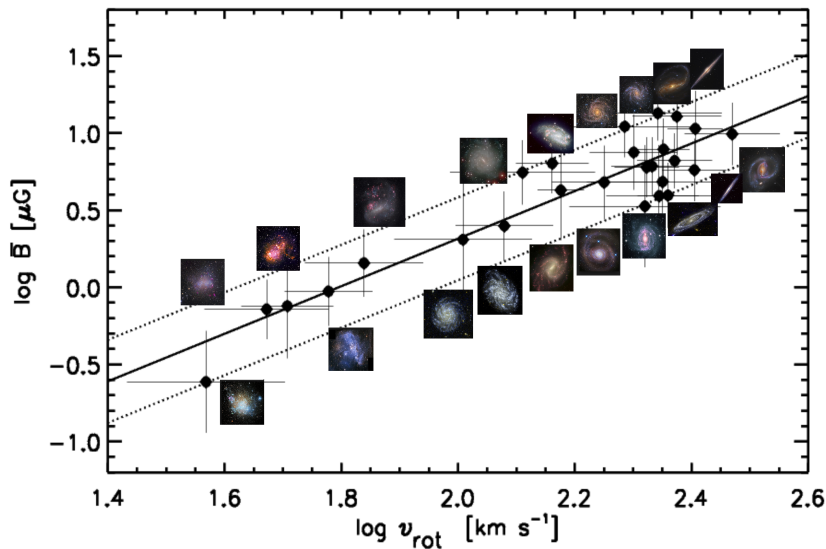


Figure 1. The large-scale magnetic field strength \overline{B} vs. the rotational speed of a sample of nearby non-cluster/non-interacting galaxies with available full polarization radio continuum data (Tabatabaei et al. 2016). Faster rotating and/or more massive galaxies have stronger ordered magnetic fields (with scales of $\gtrsim 1$ kpc). This figure shows the case of the equipartition between the magnetic field and cosmic rays, $\overline{B} \propto v_{\text{rot}}^{1.5}$. A linear correlation holds assuming that the cosmic ray number is proportional to the star formation rate (not shown).

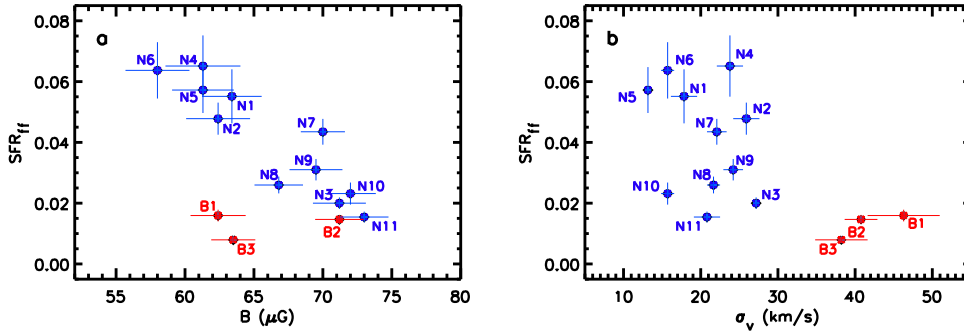


Figure 2. The massive star formation rate per free-fall, SFR_{ff} , of the GMAs decreases with the magnetic field strength B (a) while it is uncorrelated with the turbulent velocity σ_v (b). The blue and red points show the narrow- and broad-line GMAs, respectively. Strong non-circular motions/shocks in the broad-line GMAs can act as additional cause of the low SFR_{ff} in these clouds (Tabatabaei et al. 2018).

not due to the mean field $\alpha - \Omega$ dynamo, as no correlation holds between \overline{B} and the differential rotation (or angular velocity Ω for flat rotation curves). Instead, it shows a coupling between the ordered field and the dynamical mass of galaxies and indicates that gas compression and/or shear is an important mechanism ordering the large-scale ($\gtrsim 1$ kpc) magnetic field in galaxies.

3. Origin of small-scale magnetic field

Only a minor fraction of the observed synchrotron emission from spiral galaxies is polarized (usually $< 20\%$ at 4.8 GHz) meaning that a major part of the emission is due to a field that is varying on scales smaller than observation beam size. This field can be isotropic random and/or non-isotropic tangled field. The maps of the disordered field strength in star forming galaxies shows higher values in massive star forming regions (e.g., $B_{\text{dis}} \propto \Sigma_{\text{SFR}}^{0.16}$, Tabatabaei et al. 2013) indicating possible act of the small-scale dynamo, although the supernovae-driven dynamo predicts a somehow higher power-law index of 0.3 (Gressel et al. 2008). This theoretical index matches better with the global studies of the *KINGFISHER* sample ($B \propto \Sigma_{\text{SFR}}^{0.3}$, Tabatabaei et al. 2017), the *SINGS* sample (Heesen et al. 2014), and a number of dwarf galaxies (Chyży et al. 2011).

The JVLA full-polarization observations of M33 at 6 GHz (5-7 GHz, Tabatabaei et al. in prep.) unveils a totally different view of the magnetized ISM at $9''$ resolution (36 pc, scale of giant molecular clouds). The linearly polarized emission vectors nicely point towards the molecular clouds in star forming complexes and in the spiral arms exhibiting the tangled magnetic field. This field was previously undetected due to depolarization at the large beams of $\gtrsim 120''$ (Tabatabaei et al. 2008). This also shows the importance of the compression/shear in ordering and amplification of the magnetic field on cloud scales.

4. Magnetic feedback controlling ISM structure and star formation

Investigating the ISM energy balance in the central kpc region of the quenching galaxy NGC 1097, Tabatabaei et al. (2018) find a major role of the magnetic field and cosmic rays in controlling the molecular clouds and star formation. Most of the giant molecular cloud associations (GMA) are magnetically supported against gravitational collapse and the star formation rate per free-fall drops with the magnetic field strength, while it is uncorrelated with the turbulence (Fig. 2). This explains the deviations from the star formation laws observed earlier by Hsieh et al. (2013).

5. Implications: magnetic field & quenching of galaxies

The dependency of the magnetic field strength on the star formation rate has an important consequence for the evolution of galaxies. As the cosmic star formation rate peaks at about 1 Gyr after the Big Bang, the magnetic field should also reach its maximum strength through compression and/or small-scale dynamo in a relatively short time scale. Considering that galaxies start to evolve after this time ($t \gtrsim 1$ Gyr), it is then plausible that the magnetic field plays a role in this evolution. Recent discovery by Tabatabaei et al. (2018), shows that the strong magnetic field can decelerate massive star formation and can help the formation of low-mass stars. Hence, magnetic field has possibly acted as a back reaction after the peak of the star formation rate in the Universe, quenching massive star formation and stimulating the formation of big bulges of low-mass stars observed in quenched massive galaxies (e.g., Bell 2008).

References

- Beck, A. M., Dolag, K., Lesch, H., & Kronberg, P. P. 2013, *Monthly Notices of the Royal Astronomical Society*, 435, 3575
- Beck, R. 2015, *The Astronomy and Astrophysics Review*, 24, 4
- Bell, E., F. 2008, *The Astrophysical Journal*, 682, 355
- Chyży, K. T., Weżgowiec, M., Beck, R., & Bomans, D. J. 2011, *Astronomy & Astrophysics*, 529, 94
- Gressel, O., Elstner, D., Ziegler, U., & Rüdiger, G. 2008, *Astronomy & Astrophysics*, 486, 35
- Heesen, V., Brinks, E., Leroy, A. K., Heald, G., et al. 2014, *The Astronomical Journal*, 147, 5
- Hsieh, P., Y., Matsushita, S., Liu, G., Ho, P., T., P., et al. 2013, *The Astrophysical Journal*, 736, 129
- Schober, J., Schleicher, D. R. G., & Klessen, R. S. 2013, *Astronomy & Astrophysics*, 560, 87
- Shukurov, A. 2004, *Mathematical Aspects of Natural Dynamos*, astro-ph/0411739
- Subramanian, K. 2016, *Reports on Progress in Physics*, 79, 6901
- Tabatabaei, F. S., Beck, R., Krügel, E., M. Krause, et al. 2007, *Astronomy & Astrophysics*, 475, 133
- Tabatabaei, F. S., M. Krause, Fletcher, A., & Beck, R. 2008, *Astronomy & Astrophysics*, 490, 1005
- Tabatabaei, F. S., Schinnerer, E., Murphy, E. J., R. Beck, et al. 2013, *Astronomy & Astrophysics*, 552, 19
- Tabatabaei, F. S., Martinsson, T. P. K., Knapen, J. H., Beckman, et al. 2016, *The Astrophysical Journal Letters*, 818, 10
- Tabatabaei, F. S., Schinnerer, E., Krause, M., Dumas, G., et al. 2017, *The Astrophysical Journal*, 836, 185
- Tabatabaei, F. S., Minguez, P., Prieto, M. A., & Fernández-Ontiveros, J. A. 2018, *Nature Astronomy*, 2, 83

Magnetic Fields and Ram Pressure Stripping of Galaxies in Clusters

Craig L. Sarazin¹, Rukmani Vijayaraghavan¹, & Paul M. Ricker²

¹Department of Astronomy, University of Virginia, 530 McCormick Rd.,
Charlottesville, VA 22904, USA

email: sarazin@virginia.edu, rukmani@virginia.edu

²Department of Astronomy, University of Illinois, 1002 W. Green Street, Urbana, IL 61801,
USA

email: pmricker@illinois.edu

Abstract. Numerical magneto-hydrodynamical (MHD) simulations of individual elliptical and disk galaxies undergoing ram pressure stripping in the intracluster medium (ICM) are described. These simulations include isotropic and anisotropic thermal conduction; in the latter case, heat is only conducted along magnetic field lines. Four initial magnetic field geometries are considered, with the field being either continuous or disjoint between the ICM and the galaxy interstellar medium (ISM), and with the large scale field being either parallel or perpendicular to the galaxy-ICM relative velocity. Elliptical galaxies are considered first. Unless thermal conduction is unsuppressed, the elliptical ISM evaporates too quickly to be consistent with the observations of small coronae and stripped gas tails in many large cluster ellipticals. Magnetic fields and anisotropic conduction reduce the effects of evaporation so that gas is stripped at about the same rate as in models with no conduction. The simulations of disk galaxies show that magnetic fields are required to produce stripped galaxies with long, coherent tails, as are observed in many cases. The magnetic fields help to confine the tails, and suppress Kelvin-Helmholtz (KH) instabilities. The structure of the tail depends on the geometry of the magnetic field; fields which are perpendicular to the relative velocity are more effective at confinement than parallel fields.

Keywords. Galaxies: clusters: general, magnetic fields, conduction, MHD, intergalactic medium, galaxies: evolution, galaxies: elliptical and lenticular, cD, galaxies: spiral

1. Introduction

The population of galaxies in clusters differs significantly from that in the field. Clusters primarily contain elliptical and S0 galaxies, which have very little cool gas or current star formation (e.g., Jaffé et al. 2016). One process which contributes to this difference is that gas-rich spiral galaxies which fall into clusters can have their gas stripped as a result of ram pressure as they move rapidly through the ICM. Indeed, tails of hot gas, cooler gas, and recently formed stars are seen behind galaxies falling into clusters (e.g., Sun et al. 2010). These spiral galaxies undergoing stripping are often referred to as “jellyfish galaxies.”

Here, we present the results of numerical hydrodynamical and MHD simulations of individual galaxies undergoing stripping. The ICM is assumed to be uniform at large distances from the galaxy, and the relative velocity is taken to be constant. We use the FLASH 4.3 N-body (dark matter and stars) and MHD adaptive-mesh grid code (Fryxell et al. 2000). In some of the simulations, we include isotropic or anisotropic (only along the magnetic field \mathbf{B}) thermal conduction. We consider four initial magnetic field geometries; at large distances, \mathbf{B} is either parallel or perpendicular to the relative velocity, and the ICM and ISM magnetic fields are either continuous or disjoint. We have also done simulations of stripping of many galaxies in clusters with realistic orbits and

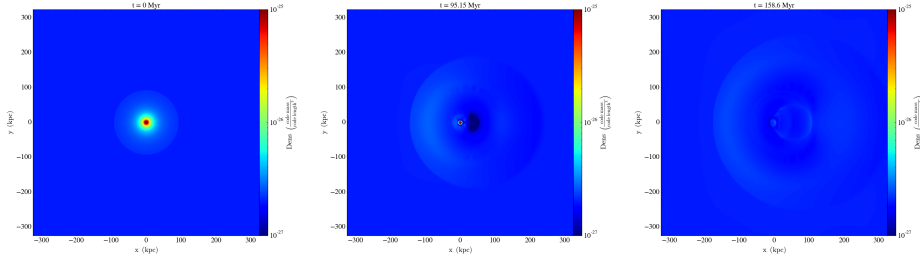


Figure 1. Slices of density in a simulation of ram pressure stripping of a spherical galaxy including full isotropic thermal conduction. The panels are the density initially, after 95 Myr, and after 159 Myr. The ISM evaporates rapidly, before ram pressure can act.

ICM density profiles (Vijayaraghavan & Ricker 2015, 2017), but these are not discussed here.

2. Elliptical Galaxies: Evaporation vs. Stripping

Many large elliptical galaxies in clusters are observed to retain small (~ 3 kpc) coronae of hot gas, which is cooler and denser than the ISM and in near pressure equilibrium (e.g., Sun et al. 2007). The statistics suggest that these galaxies retain this gas for \sim Gyr.

Thermal conduction is expected to be very effective in the ICM due to the high temperatures; unless inhibited, thermal conduction should cause the elliptical coronae to evaporate quickly, typically in $\lesssim 100$ Myr. Figure 1 shows the density distribution in a simulation of a spherical galaxy with ram pressure and full isotropic conduction. Heat is rapidly conducted from the ICM into the ISM, and the ISM expands and evaporates quickly, before ram pressure has time to act. As a result, no ram pressure tail is formed.

The gyroradii of electrons in the ICM magnetic field are very small. As a result, one expects that heat can only be conducted parallel to the field. This can reduce the effects of thermal conduction. If the galaxy is moving through the ICM, the ICM magnetic field lines will be wrapped (“draped”) around the galaxy. This causes the direction of the field to be roughly parallel to the surface of the galaxy and perpendicular to the temperature gradient in many locations along the surface of the ISM, a geometry that greatly suppresses thermal conduction. The same magnetic draping can help to suppress Kelvin-Helmholtz (KH) instabilities due to the shear in the flow at the ICM/ISM interface. Figure 2 shows an MHD simulation with an ICM magnetic field and anisotropic thermal conduction. The galaxy retains a corona for \sim Gyr. Stripped ISM forms a ram pressure tail.

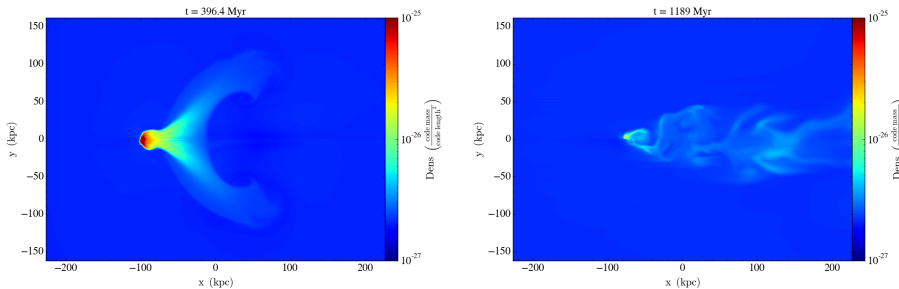


Figure 2. Density for the same galaxy as in Fig. 1 in an MHD simulation including magnetic fields and anisotropic thermal conduction at times of 396 Myr (left) and 1.19 Gyr (right). The spherical galaxy retains a corona for \sim Gyr, and the stripped ISM forms a ram pressure tail.

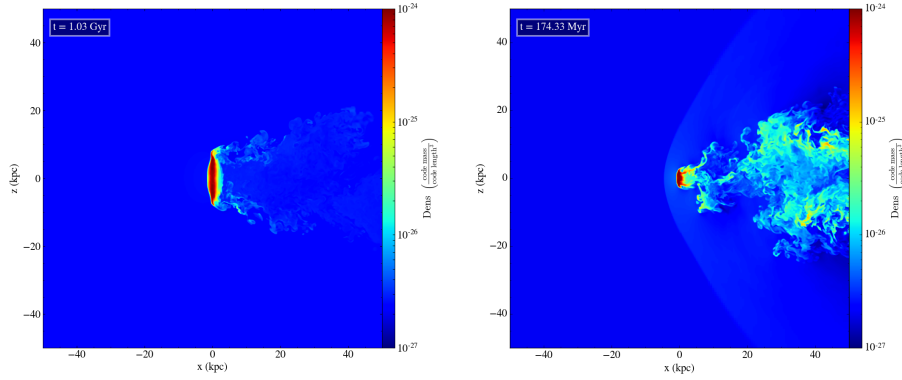


Figure 3. left: Density for a spiral galaxy being stripped by subsonic (610 km/s) motion. There is no magnetic field. right: The same model, but with supersonic motion (2000 km/s).

pressure tail, and the overall stripping rate is similar to that for ram pressure alone. This model is much more consistent with observations of large ellipticals in clusters of galaxies. For more details, see Vijayaraghavan & Sarazin (2017a,b).

3. Stripping of Spiral Galaxies and Jellyfish Galaxies

Figure 3 shows the density in simulations of the stripping of gas from a disk (e.g., spiral) galaxy for either subsonic (610 km/s) or supersonic (2000 km/s) speeds. These simulations have no magnetic fields or thermal conduction. Of course, higher velocities result in higher ram pressures (proportional to v^2), and more rapid stripping. At low speeds, the outer gas in the disk is stripped relatively quickly, but further stripping is a slow process in which gas is gradually peeled from the disk at its outer edge. This results in only a small amount of filamentary gas in the tail. At higher speeds, there is much more material in the tail. However, KH instabilities cause the tail to be filamentary, and it mixes into the ICM fairly quickly.

Magnetic fields of sufficient strength can suppress KH instabilities. Figure 4 shows magnetized simulations of stripping with the same galaxy and velocity as Figure 3 (right). In the left panel, the initial ICM \mathbf{B} is perpendicular to \mathbf{v} . This geometry results in the field being amplified around and draping the tail, and is very effective as suppressing KH instabilities. The result is a long, single, coherent tail.

Figure 4(right) shows the case where the initial field is parallel to \mathbf{v} . The field is not significantly amplified, and is less effective at stabilizing the wake. Although the tail is narrower and more coherent than for the non-magnetic case [Fig. 3 (right)], it is clear that ICM fields which are nearly perpendicular to the galaxy motion are more ideal.

We have derived the mass of gas at various densities and temperatures for the tails in the simulations. In general, the simulations with ICM magnetic fields have more cool, dense gas, with the $\mathbf{B} \perp \mathbf{v}$ case again being best. This suggests that magnetic fields, particularly perpendicular to the motion, are important for generating tails with optical emission line gas, molecular gas, and in situ star formation. However, the “cool” gas in our simulations is generally hotter than 2×10^5 K, and our simulations do not include radiative cooling or star formation. Thus, additional calculations are needed to verify the role of magnetic fields in the formation of cold gas and stars in jellyfish galaxy tails.

For more details on the simulations of stripping from disk galaxies, see Vijayaraghavan & Sarazin (2018).

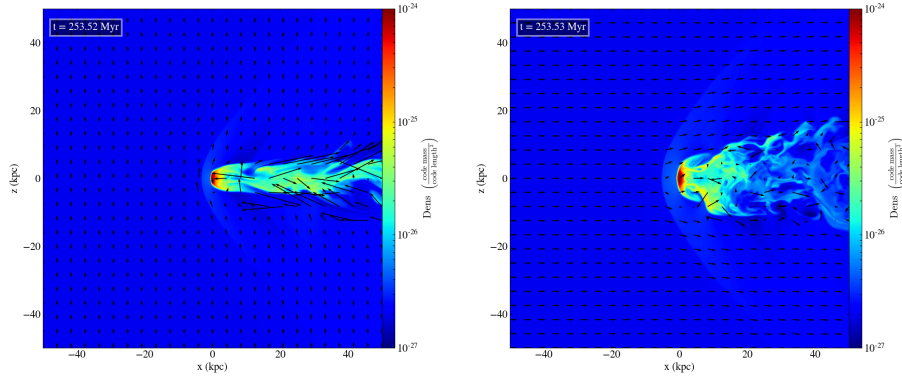


Figure 4. Left: The density for the same spiral galaxy as in Figure 3(right), but with an ICM magnetic field initially perpendicular to the motion. Arrows show the direction and strength of \mathbf{B} . The field drapes the tail and inhibits KH instabilities. Right: The same model, but with the initial magnetic field parallel to the motion. This geometry is less effective at suppressing KH instabilities, and the tail is shorter and less coherent.

4. Conclusions

The results of MHD simulations of the stripping of elliptical and spiral galaxies in clusters were presented. In elliptical galaxies, thermal conduction, if uninhibited, would evaporate their ISM very quickly, in disagreement with the observations of small coronae, and sometimes, stripped tails in large ellipticals in clusters. Magnetic fields drape these galaxies in simulations, and reduce thermal conduction to the level where the stripping rates are similar to those for ram pressure alone.

Low speed (subsonic) stripping of disk galaxies occurs by a relatively gentle peeling of gas from the disk, and does not result in long tails. Combined with the v^2 dependence of ram pressure, this may help to explain why jellyfish galaxies are common in merging clusters, where galaxies from one subcluster fall through gas from another at unusually high speeds.

ICM magnetic fields are required to produce long, coherent tails behind stripped disks, as magnetic forces can suppress KH instabilities. Fields with $\mathbf{B} \perp \mathbf{v}$ are ideal for this, as the magnetic field is amplified and wraps the tail. The stabilizing effect also depends on the energy density of the field. Thus, the structure and length of tails provide an indirect probe of the strength and geometry of magnetic fields in clusters.

The same magnetic field strengths and geometries lead to larger amounts of relatively cool, dense gas in tails. This may supply material for the formation of cold gas and in situ star formation in tails, as is observed in jellyfish galaxies.

References

- Fryxell, B., Olson, K., Ricker, P., et al. 2000, *ApJS*, 131, 273
 Jaffé, Y. L., Verheijen, M. A. W., Haines, C. P., et al. 2016, *MNRAS*, 461, 1202
 Sun, M., Donahue, M., Roediger, E., et al. 2010, *ApJ*, 708, 946
 Sun, M., Jones, C., Forman, W., et al. 2007, *ApJ*, 657, 197
 Vijayaraghavan, R., & Ricker, P. M. 2015, *MNRAS*, 449, 2312
 —. 2017, *ApJ*, 841, 38
 Vijayaraghavan, R., & Sarazin, C. 2017a, *ApJ*, 841, 22
 —. 2017b, *ApJ*, 848, 63
 —. 2018, *ApJ*, submitted

Magnetic fields in simulations of ram pressure stripped galaxies

Mariana Ramos-Martínez¹ and Gilberto C. Gómez¹

¹ Instituto de Radioastronomía y Astrofísica, UNAM, Apartado Postal 3-72, 58089 Morelia, México
email: m.ramos@irya.unam.mx

Abstract. The removal of the interstellar medium (ISM) of disc galaxies through ram pressure stripping (RPS) has been extensively studied in numerous simulations. Nevertheless, the role of magnetic fields (MF) on the gas dynamics in this process has been hardly studied, although the MF influence on the large-scale disc structure is well established. With this in mind, we present 3D magnetohydrodynamic (MHD) simulations of disc galaxies subject to RPS, with different disc inclinations to study the evolution of the galactic MF and its impact on the gas stripping. When the intracluster medium (ICM) wind hits a galaxy, the gas in the disc is compressed, leading to an enhancement of the MF intensity in the upstream side in our simulations. Since the gas is bound by the MF, we observe that in nearly face-on discs, the gas is swept by the wind in ring-like structures, dragging the field lines with it. In the case of nearly edge-on discs, the field lines are compressed in the upstream side and more extended towards the downstream side. The ICM is magnetized in the downstream side from 0.2 to $0.7\mu G$, where nearly face-on discs contribute the most, given that the developed tail is more extended than in nearly edge-on models.

Keywords. MHD, galaxies: ISM, galaxies: magnetic fields, galaxies: evolution, methods: numerical.

1. Introduction

The ram pressure stripping (RPS) is a process in which a galaxy loses its interstellar medium (ISM) through the pressure exerted by the hot intracluster medium (ICM) when the galaxy travels within the cluster. RPS was first proposed by Gunn & Gott (1972) and since then it has been studied in a wide variety of simulations with different methods and techniques (Abadi et al. 1999; Roediger & Brüggen 2006; Vollmer et al. 2006; Tonnesen & Bryan 2009; to name a few). Additionally, several galaxies in clusters have been studied in multiwavelength observations showing that they are good candidates to be experiencing RPS since the galaxies present an asymmetric distribution of gas, that is a truncated gaseous disc and in some cases with tails, while the stellar disc remains unperturbed (e.g. Cayatte et al. 1990; Kenney et al. 2014; Jáchym et al. 2014; Poggianti et al. 2016 and many more).

However, despite the huge variety of RPS models and simulations, the role of the magnetic fields (MF) in the gas dynamics has been hardly explored in this process, although the large-scale disc structure of the MF is well established (Beck 2005; Beck & Wielebinski 2013 and references therein). Some examples of magnetohydrodynamics (MHD) models were carried out by Ruszkowski et al. (2014), where they presented simulations of RPS with a magnetized ICM and found that the MF can affect the morphology of the stripped gas tail, since they observed narrower tails than in purely hydrodynamic (HD) simulations. Pfrommer & Dursi (2010) also showed MHD simulations in which the galaxies are moving in a magnetized ICM. The galaxies in their simulations swept the field lines

where polarized radiation is generated. This is used to map the orientation of the MF in clusters, e.g. Virgo cluster. In these cases, the MF has been implemented only in the ICM and not in the discs. Another case with galactic MF only was performed by Tonnesen & Stone (2014), and they found that MFs do not dramatically change the stripping rate of the gas disc compared to pure HD simulations. Nevertheless, the MF inhibits the mixing of the gas tail with the ICM. Here we present MHD simulations of disc galaxies subject to RPS under the wind-tunnel approximation for different disc inclinations.

2. Model

We performed 3D MHD simulations using the adaptive mesh refinement (AMR) code RAMSES (Teyssier 2002). The gas in the galaxy is set up in rotational equilibrium in a fixed gravitational potential and its density distribution is obtained assuming magnetohydrostatic equilibrium (Gómez & Cox 2002; Ramos-Martínez et al. 2018). The MF has two regimes, in the central region (the bulge) of the galaxy the MF has a random orientation, while in the disc it is azimuthal.

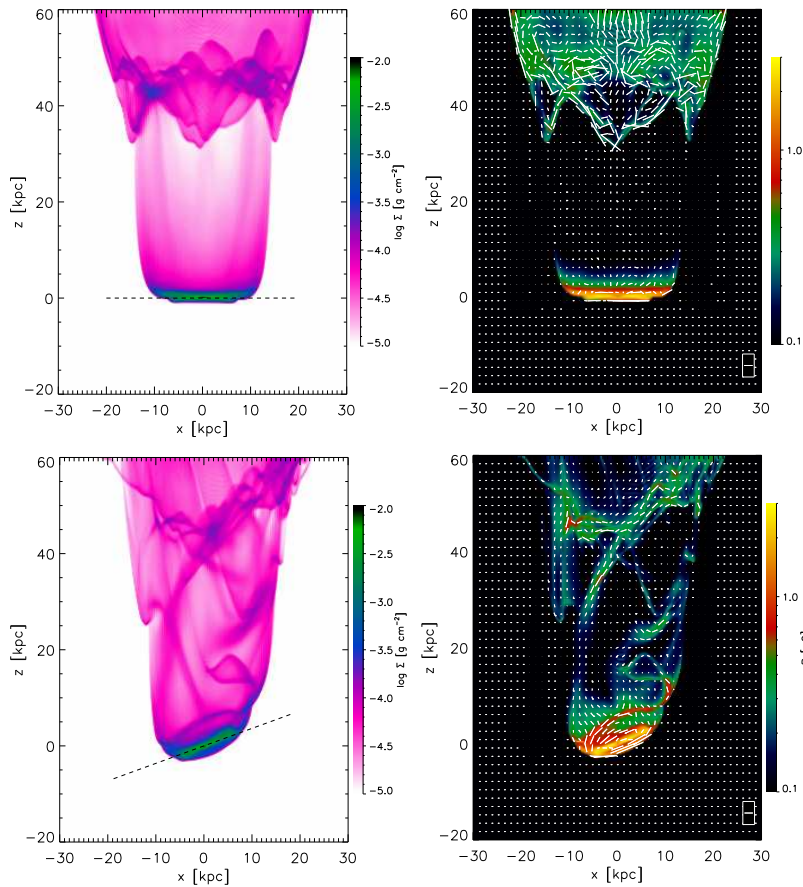


Figure 1. Surface density of the gas (*left*) and magnetic field strength (*right*) for Mod1 (*top*) and Mod2 (*bottom*), projected along the y -axis, both in log-scale at $t = 900$ Myr. The dashed line indicates the original radius of the disc (20 kpc).

The ICM is modeled as a wind and the disc is at rest, simulating the falling of the

galaxy towards a cluster center, that is, the wind-tunnel approximation. The ICM-wind has a constant density with $n_{\text{ICM}} = 10^{-5} \text{ cm}^{-3}$ and a velocity profile that increases linearly in time from 300 km s^{-1} at $t = 0$ to 1000 km s^{-1} in 700 Myr. Additionally, we present four models with different galaxy inclinations with respect to the wind direction. In Mod1 the disc plane is parallel to the $z = 0$ plane, while in Mod2 it is inclined 20° with respect to $z = 0$. In both cases the wind flows up from the bottom of the box (in the $+z$ -direction), that is the interaction with the discs is (nearly) face-on. In Mod3 and 4, the wind flows from left to right ($+x$ -direction), which represents (nearly) edge-on interactions, but Mod3 is a disc inclined 20° with respect to $z = 0$ plane and in Mod4 the disc plane lies in $z = 0$.

3. Evolution of the magnetic field

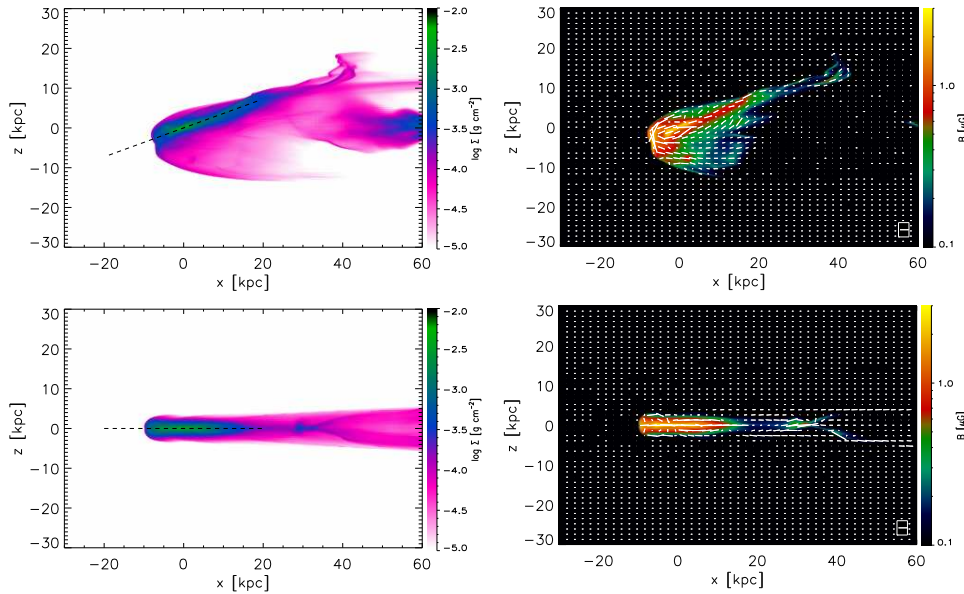


Figure 2. Surface density of the gas (*left*) and magnetic field strength (*right*) for Mod3 (*top* at $t = 570$ Myr) and Mod4 (*bottom* at $t = 900$ Myr), projected along the y -axis, both in log-scale. The dashed line indicates the original radius of the disc (20 kpc).

When the ICM-wind is switched on and hits the galaxy, the compression exerted by the wind enhances the MF strength in all the models a factor of ~ 3 in the shock front. Depending on the geometry of the model, the shocked layer of gas can be present at all radii, as in Mod1 or partially in the disc (Mod2, 3 and 4).

The wind keeps flowing and accelerating, so that it surpasses the gravitational potential of the galaxy and starts to remove the material from the outskirts ($10 \text{ kpc} < r < 20 \text{ kpc}$) where a tail of gas appears in the downstream side. In the cases Mod1 and 2, since the interaction with the wind is (nearly) face-on, the gas is swept from the galaxy in ring-like structures. At $t > 500$ Myr, since the magnetic field is dragged with the gas, it helps to magnetize the downstream side of the tail up to $z \sim 20 \text{ kpc}$ with a strength of $B \approx 0.4 - 0.7 \mu\text{G}$. At $t > 900$ Myr, in Mod1 and 2, the wind moves the rings of gas above and farther away of the galaxy, showing tails of at least 60 kpc in length (fig. 1). Due to the interaction with the accelerated wind, the rings are distorted in the vertical (z) direction giving a filamentary structure to the tail, where the MF is aligned with

these filaments (fig. 1), similar to the results obtained by Ruszkowski et al. (2014). The filaments are the densest structures of the tail ($\sim 10^{-3.6} \text{ g cm}^{-2}$), with MF values ranging from $B \approx 0.3 - 0.4 \mu G$ to $0.7 \mu G$. At intermediate heights of the tails ($z = 15 - 30 \text{ kpc}$) the field strength drops to $\lesssim 0.2 \mu G$ since less gas is swept from the disc and the surface density also decreases.

On the other hand, Mod3 and 4 do not present a very extended tail at $t \geq 500 \text{ Myr}$ as can be observed in an edge-on view of the galaxies (xz -plane, fig. 2). Instead the gas disc shows asymmetries compared to the initial density distribution, being spread out to $x \sim 20 - 40 \text{ kpc}$ but with low densities ($< 10^{-4.5} \text{ g cm}^{-2}$) and truncated for $x < 0$. Additionally, the MF intensity increases a factor of $\sim 2 - 3$ ($B \approx 1.5 - 3 \mu G$) in the upstream side of the interaction ($-10 \text{ kpc} < x < 0$) while in downstream side ($x = 0 - 20 \text{ kpc}$) it shows no dramatic changes, that is $B \approx 0.8 - 1 \mu G$. Even at $t > 900 \text{ Myr}$, Mod4 did not develop a very prominent or extended tail that is poorly magnetized with $B \lesssim 0.2 - 0.3 \mu G$ ($x = 20 - 60 \text{ kpc}$ in fig. 2), compared to the (nearly) face-on models (Mod1 and 2). Also, in Mod3 and 4 the MF lines resemble a water fountain, that is they have a concave shape in the upstream side and wrap around the disc at higher $|z|$ (fig. 2), since the wind flows parallel or nearly to the plane of the disc and sweeps the gas above and below the galaxy more easily than the gas closer to the galactic plane.

At the end of the simulations, in all models we have a remnant disc with size of $r \lesssim 10 \text{ kpc}$ where the MF shows an enhancement by a factor of $\sim 2 - 3$ from $B(t = 0) \approx 0.8 - 1 \mu G$ to $B \approx 2.5 \mu G$ for $t > 500 \text{ Myr}$ in the disc. In the downstream side of the interaction, the tails can magnetize the environment from $B \sim 0.2 - 0.7 \mu G$ and also the distribution of the MF lines changes depending on the disc inclination with respect to the wind.

References

- Abadi, M. G., Moore, B. & Bower, R. G. 1999, *MNRAS*, 308, 947
- Beck, R. 2005 in: K. T. Chyży, K. Otmianowska-Mazur, M. Soida & R.-J. Dettmar (eds.), *The magnetized plasma in galaxy evolution*, Proc. Conf. Held in Krakow, Poland, p. 193
- Beck, R. & Wielebinski, R. 2013 in: G. Gilmore(ed.), *Planets, Stars and Stellar Systems*, Vol. 5 (Springer-Verlag, Berlin), p. 641
- Cayatte, V., van Gorkom, J. H., Balkowski, C. & Kotanyi, C. 1990, *AJ*, 100, 604
- Gómez, G. C. & Cox, D. 2002, *ApJ*, 580, 235
- Gunn, J. E. & Gott, J. R. I. 1972, *ApJ*, 176, 1
- Jáchym, P., Combes, F., Cortese, L., Sun, M. & Kenney, J. D. P. 2014, *ApJ*, 792, 11
- Kenney, J. D. P., Geha, M., Jáchym, P., Crowl, H. H., Dague, W., Chung, A., van Gorkom, J. & Vollmer, B. 2014, *ApJ*, 780, 119
- Pfrommer, C. & Dursi, J. 2010, *Nature Physics*, 6, 520
- Poggianti, B. M., Fasano, G., Omizzolo, A., Gullieuszik, M., Bettoni, D., Moretti, A., Paccagnella, A., Jaffé Y. L., Vulcani, B., Fritz, J, Couch W. & D'Onofrio, M. 2016, *AJ*, 151, 78P
- Ramos-Martínez, M., Gómez, G. C. & Pérez-Villegas, A. 2018, *MNRAS*, 476, 3781
- Roediger, E. & Brügggen, M., 2006, *MNRAS*, 369, 567
- Ruszkowski, M., Brügggen, M., Lee, D. & Shin, M. S. 2014, *ApJ*, 784, 75
- Teyssier, R. 2002, *A&A*, 385, 337
- Tonnesen, S. & Bryan, G. L. 2009, *ApJ*, 694, 789
- Tonnesen, S. & Stone, J. 2014, *ApJ*, 795, 148
- Vollmer, B., Soida, M., Otmianowska-Mazur, K., Kenney, J. D., van Gorkom, J. H. & Beck, R. 2006, *A&A*, 453, 883

Statistical properties of Faraday rotation measure from large-scale magnetic fields in intervening disc galaxies

Aritra Basu,^{1,2} S. A. Mao,² Andrew Fletcher,³ Nissim Kanekar,⁴
Anvar Shukurov,³ Dominic Schnitzeler,² Valentina Vacca⁵ and Henrik
Junklewitz⁶

¹Fakultät für Physik, Universität Bielefeld, Postfach 100131, 33501 Bielefeld, Germany

²Max-Planck-Institut für Radioastronomie, Auf dem Hügel 69, D-53121 Bonn, Germany
email: aritra@physik.uni-bielefeld.de

³School of Mathematics and Statistics, Newcastle University,
Newcastle-upon-Tyne, NE13 7RU, UK

⁴National Centre for Radio Astrophysics, TIFR, Post Bag 3, Ganeshkhind,
Pune 411007, India

⁵INAF-Osservatorio Astronomico di Cagliari, Via della Scienza 5,
I-09047 Selargius (CA), Italy

⁶Argelander Institut für Astronomie, Universität Bonn, Auf dem Hügel 71,
53121 Bonn, Germany

Abstract. To constrain the large-scale magnetic field strengths in cosmologically distant galaxies, we derive the probability distribution function of Faraday rotation measure (RM) when random lines of sight pass through a sample of disc galaxies, with axisymmetric large-scale magnetic fields. We find that the width of the RM distribution of the galaxy sample is directly related to the mean large-scale field strength of the galaxy population, provided the dispersion within the sample is lower than the mean value. In the absence of additional constraints on parameters describing the magneto-ionic medium of the intervening galaxies, and in the situation where RMs produced in the intervening galaxies have already been statistically isolated from other RM contributions along the lines of sight, our simple model of the magneto-ionic medium in disc galaxies suggests that the mean large-scale magnetic field of the population can be measured to within $\sim 50\%$ accuracy.

Keywords. methods: analytical – methods: statistical – ISM: magnetic fields

1. Introduction

The cosmic evolution of magnetic fields on scales $\gtrsim 1$ kpc remains an open question in observational astronomy. In order to constrain cosmic evolution of large-scale magnetic fields in galaxies, it is crucial to measure their redshift evolution. Due to the faintness of distant galaxies, it is a challenging proposition to measure magnetic fields directly through their polarized synchrotron emission. A powerful tool to probe magnetic fields in distant galaxies is provided by statistical studies of the Faraday rotation measure (RM) of quasar absorption line systems, which are tracers of galaxies in the high redshift Universe. The distribution of RM of two quasar samples, with and without absorption line systems, can be statistically compared to infer the properties of magnetic fields in the intervening galaxy population (e.g., Oren & Wolfe 1995; Bernet et al. 2008; Joshi & Chand 2013; Farnes et al. 2014). The sample of quasars with intervening galaxies is

referred to as the ‘target’ sample and the sample without intervening galaxies is called the ‘control’ sample.

Part of the RM measured towards a quasar which has an intervening galaxy arises from the quasar itself (RM_{qso}), the intergalactic medium (IGM; RM_{IGM}) and interstellar medium of the Milky Way (RM_{MW}). Thus, the net RM (RM_{t}) measured in the observer’s frame for a single line of sight in the target sample is given by,

$$\text{RM}_{\text{t}} = \frac{\text{RM}_{\text{gal}}}{(1 + z_{\text{gal}})^2} + \text{RM}'_{\text{qso}}, \quad (1.1)$$

where RM_{gal} is the RM contribution from the intervening galaxy and z_{gal} is its redshift. RM'_{qso} contains RM contributions from rest of the line of sight and is given by $\text{RM}'_{\text{qso}} = \text{RM}_{\text{qso}} (1 + z_{\text{qso}})^{-2} + \text{RM}_{\text{IGM}} + \text{RM}_{\text{MW}} + \delta_{\text{RM}}$. Here, δ_{RM} is the measurement noise and z_{qso} is the redshift of the background quasar.

Similarly, for a line of sight in the control sample, the net RM (RM_{c}) in the observer’s frame is given by,

$$\text{RM}_{\text{c}} = \frac{\text{RM}_{\text{qso,c}}}{(1 + z_{\text{qso,c}})^2} + \text{RM}_{\text{IGM,c}} + \text{RM}_{\text{MW,c}} + \delta_{\text{RM,c}}, \quad (1.2)$$

where the subscript ‘c’ refers to the control sample.

If quasars in the target and the control samples are chosen such that RM'_{qso} and $\text{RM}_{\text{qso,c}}$ have the same statistical properties, then statistical comparison between the distributions of RM_{t} and RM_{c} can yield the excess contribution from $\text{RM}_{\text{gal}} (1 + z_{\text{gal}})^{-2}$. Most of the previous studies where this method is used have attributed statistical differences to turbulent magnetic fields, with the field strengths computed assuming Gaussian statistics for RM_{t} and RM_{c} (e.g., Bernet et al. 2008; Bernet et al. 2013).

Here we investigate the effects of large-scale magnetic fields in the intervening galaxies on the distribution of RM. First, we derive the probability distribution function (PDF) of RM_{gal} analytically for a single galaxy. Then, we consider the statistical distribution of RM_{gal} for an ensemble of galaxies. A detailed treatment can be found in Basu et al. (2018).

2. Magneto-ionic medium in intervening galaxy population

To derive the PDF of RM_{gal} analytically, we have adopted a simple set of assumptions for the magneto-ionic medium in the intervening galaxies: (i) the large-scale magnetic fields in each galactic disc have axisymmetric geometry with magnetic pitch angle p , (ii) both the large-scale magnetic field strength (B) and the free electron density (n_e) decrease exponentially with radius r , (iii) the magnitude and geometry of both magnetic field and electron density do not vary with height from the mid-plane, (iv) the RM contributed by turbulent magnetic fields in the intervening galaxies is insignificant within the three-dimensional illumination beam passing through the galaxies, and (v) the RM contributed by the background quasar has been statistically isolated from RM_{t} .

Under these assumptions, the RM for each line of sight is given as (see Berkhuijsen et al. 1997; Basu et al. 2018),

$$\text{RM}_{\text{gal}} = -0.81 n_0 B_0 e^{-r/r'_0} \cos(\theta - p) h_{\text{ion}} \tan i. \quad (2.1)$$

Here, n_0 and B_0 are the free electron density and the strength of the axisymmetric large-scale magnetic field at the galactic centre, θ is the azimuthal angle, h_{ion} is the thickness of the ionized disc, i is the inclination angle of the galactic disc with respect to the plane of the sky and r'_0 is the radial scale-length of the product $n_e(r) B(r)$.

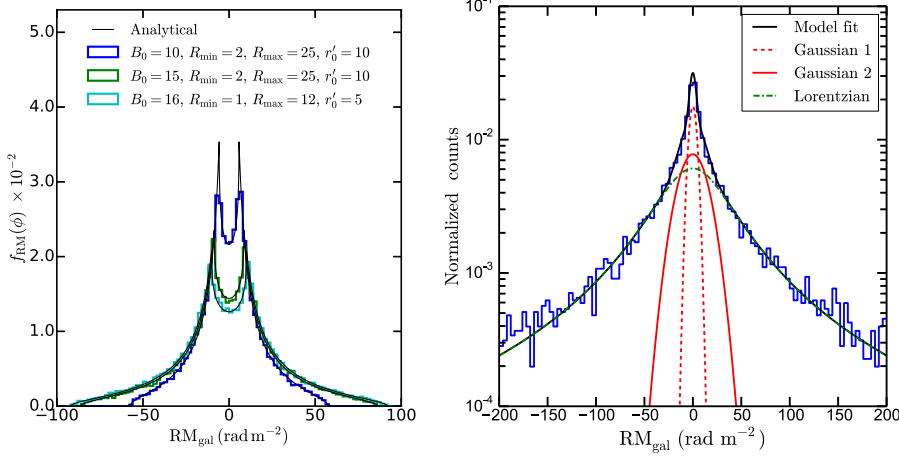


Figure 1. *Left:* Distribution of RM_{gal} for a single galaxy inclined at 30° . The black curves are the analytical PDF given by Eq. (3.1). *Right:* Distribution of RM_{gal} for a sample of 10000 galaxies. B_0 and n_0 of the population have Gaussian distributions with $\langle B_0 \rangle = 15 \mu\text{G}$, $\langle n_0 \rangle = 0.03 \text{ cm}^{-3}$, $\sigma_{B_0} = 5 \mu\text{G}$ and $\sigma_{n_e} = 0.01 \text{ cm}^{-3}$. The distribution is modelled as a sum of one Lorentzian and two Gaussians, which are shown as the different lines.

For an ensemble of intervening galaxies, the quasar sightlines can intersect each galaxy at any radius, inclination angle, and azimuthal angle. For galaxies in the target sample, we assume the galactic discs to be inclined uniformly with i in the range 0 to 90° . The angle θ is distributed uniformly between 0 and 360° . Since it is plausible that the currently available data base of absorption line samples is incomplete in terms of range of radii probed by the background quasars (Basu et al. 2018), we assume that the impact radii are distributed uniformly in the range R_{min} to R_{max} .

3. PDF of RM of intervening galaxy population

Under the assumptions mentioned above, the PDF of RM_{gal} , $f_{\text{RM}}(\phi)$, for a single galaxy has the following analytical form:

$$f_{\text{RM}}(\phi) = \begin{cases} \frac{r'_0}{\pi (R_{\text{max}} - R_{\text{min}})} \frac{1}{|\phi|} \left[\arcsin\left(\frac{|\phi|}{a'}\right) - \arcsin\left(\frac{|\phi|}{b'}\right) \right], & -a' \leq \phi \leq a', \\ \frac{r'_0}{\pi (R_{\text{max}} - R_{\text{min}})} \frac{1}{|\phi|} \arccos\left(\frac{|\phi|}{b'}\right), & \phi \in [-b', -a'] \cup (a', b']. \end{cases} \quad (3.1)$$

Here, $a' = 0.81 n_0 B_0 h_{\text{ion}} \tan i e^{-R_{\text{max}}/r'_0}$ and $b' = 0.81 n_0 B_0 h_{\text{ion}} \tan i e^{-R_{\text{min}}/r'_0}$. The left-hand panel of Fig. 1 shows the analytical PDF of RM_{gal} for a single galaxy with $i = 30^\circ$ (black curve) and, for comparison, the simulated distribution for 10000 lines of sight as histograms.

The right-hand panel of Fig. 1 shows a simulated PDF of RM_{gal} for a sample of 10000 intervening disc galaxies, where we have assumed Gaussian distributions for B_0 (with mean $\langle B_0 \rangle$ and standard deviation σ_{B_0}) and n_0 (with mean $\langle n_0 \rangle$ and standard deviation σ_{n_e}) within the population. We find that the distribution of RM_{gal} can be accurately approximated by the sum of one Lorentzian and two Gaussian components as shown in the right panel of Fig. 1. From Eq. (3.1) and Fig. 1 (left panel), we find that the width of the PDF of RM_{gal} for a single galaxy depends on the parameters a' and b' and, therefore, on B_0 . Thus, we expect the width w of the Lorentzian component to be related to $\langle B_0 \rangle$

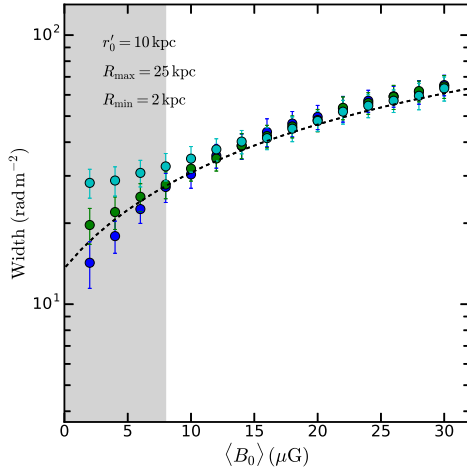


Figure 2. Variation of the width of the Lorentzian component of the distribution of RM_{gal} in the target sample as a function of $\langle B_0 \rangle$. Blue, green and cyan symbols are for $\sigma_{B_0} = 2, 5$ and $10 \mu\text{G}$. The dashed line is the best-fit model given by Eq. (3.2). The shaded region roughly represents the region where $\langle B_0 \rangle \lesssim \sigma_{B_0}$ and the points within were excluded from the fitting.

for a sample of intervening galaxies. In Fig. 2, we show the variation of w with $\langle B_0 \rangle$ for various choices of σ_{B_0} . In the regime $B_0 \gtrsim \sigma_{B_0}$ (the un-shaded area in Fig. 2), the variation of w is approximated by,

$$w(\langle B_0 \rangle) = 13.6 + 1.8 \langle B_0 \rangle - 0.0076 \langle B_0 \rangle^2, \quad (3.2)$$

with $\langle B_0 \rangle$ in μG and w in rad m^{-2} , and is shown as the dashed line in Fig. 2. Thus, w can be used to determine the mean strength of the large-scale magnetic field in a sample of intervening galaxies.

4. Conclusion

Our study suggests that the distribution of RM_{gal} due to axisymmetric large-scale magnetic fields in intervening disc galaxies is non-Gaussian and that the distribution can be empirically modelled as the sum of one Lorentzian and two Gaussian components. The width of the Lorentzian component can be used to estimate the mean large-scale magnetic field strength in a population of intervening galaxies using Eq. (3.2) derived for typical values of the physical parameters, such as, $h_{\text{ion}} = 500 \text{ pc}$, $R_{\text{min}} = 2 \text{ kpc}$, $R_{\text{max}} = 25 \text{ kpc}$ and $r'_0 = 10 \text{ kpc}$. The $\langle B_0 \rangle$ estimated using Eq. (3.2) lies within $\sim 50\%$ of the true value in the absence of additional constraints on the physical parameters.

References

- Basu A., Mao S. A., Fletcher A., Kanekar N., Shukurov A., Schnitzeler D., Vacca V., Junklewitz H., 2018, *MNRAS*, 477, 2528
- Berkhuijsen E. M., Horellou C., Krause M., Neinger N., Poezd A. D., Shukurov A., Sokoloff D. D., 1997, *A&A*, 318, 700
- Bernet M., Miniati F., Lilly S., Kronberg P., Dessauges-Zavadsky M., 2008, *Nature*, 454, 302
- Bernet M. L., Miniati F., Lilly S. J., 2013, *ApJ*, 772, L28
- Farnes J. S., O’Sullivan S. P., Corrigan M. E., Gaensler B. M., 2014, *ApJ*, 795, 63
- Joshi R., Chand H., 2013, *MNRAS*, 434, 3566
- Oren A. L., Wolfe A. M., 1995, *ApJ*, 445, 624

Optimizing Faraday Background Grids

Lawrence Rudnick¹

Minnesota Institute for Astrophysics, University of Minnesota, 116 Church St. SE,
 Minneapolis, MN 55455 USA email: larry@umn.edu

Abstract. Magnetic field strengths in objects ranging from HII regions to cosmological large scale structure can be estimated using dense grids of Rotation Measures (RMs) from polarized background radio structures. Upcoming surveys on the SKA and its precursors will dramatically increase the number N of background sources. However, detectable magnetic field strengths will scale only as $t^{-0.15}$, for an integration time t on a fixed area of sky, so the analysis techniques need to be optimized. A key factor is the difference in the dispersion of intrinsic RMs for different populations, which must be carefully accounted for to achieve the scientifically needed accuracies.

Keywords. magnetic fields, polarization, methods: numerical methods: statistical

1. Introduction

The next generation of radio surveys, including the SKA and its precursors, will dramatically increase the number of detected distant polarized sources. When these sources are viewed through a foreground magnetized plasma, whether it is from an HII region, a galaxy, or cluster of galaxies, or even large scale structure, Faraday effects in that plasma offer a way to explore its magnetic field strength and structure (Johnston-Hollit et al. 2014). Akahori, Gaensler & Ryu (2014) describes the many contributions to the observed rotation measures (RMs), from which the effects of the intervenor must be isolated. The accuracy with which this can be done, as detailed below, depends on the number of background sources and the scatter in their RMs.

Increasing the number of polarized sources is expensive, as seen in Figure 1, since the cumulative number increases only as $P_{det}^{-0.6}$ where P_{det} is the detection limit. This requires that we optimize our techniques for using the limited number of sources that we have; one aspect of that optimization is discussed here.

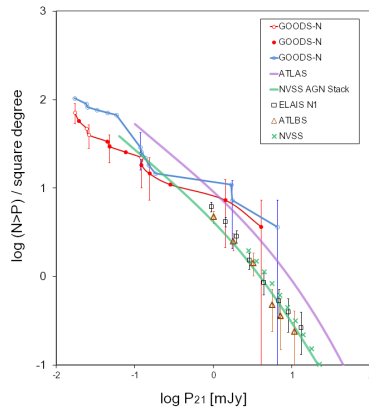


Figure 1. Cumulative polarization counts. Adapted from Rudnick & Owen (2014).

2. Optimizing the figure of merit

In background grid experiments we measure the difference in the variance of RMs seen through a foreground screen to those of a control sample. The sensitivity thus depends on the intrinsic RM variance of individual background sources (the smaller the better), and the number that are available behind the screen (the more the better).

Any such experiment will have multiple populations of background sources. If sources of type j have individual values of $RM_{j,i}$, a sky density of n_j /steradian, and our foreground object of interest covers Ω steradians, then we have $N_j = n_j\Omega$ sources. The population will have a variance in RM, σ_j^2 , and a corresponding uncertainty, of

$$\sigma_j^2 = \langle RM_{j,i}^2 \rangle - \langle RM_{j,i} \rangle^2 \quad \text{and} \quad \delta_j \approx \sqrt{\frac{2}{N_j}} \sigma_j \frac{\text{rad}^2}{m^4}$$

for a Gaussian distribution of N_j sources (Lehman & Casella 1998). δ_j is the error in σ_j^2 , the figure of merit that we would like to minimize. It is important to note, and not generally recognized, that this leads to a minimum magnetic field which scales only as $P_{det}^{0.3}$ or an integration time of $t^{-0.15}$ for observations of a single area on the sky. This general behavior applies whether one is using F -tests or Bayesian statistics, or Monte-Carlo type modeling, etc.

As an example, consider two populations, a and b , with different values of σ_a^2 and σ_b^2 , and the same sample sizes, N . The default procedure is just to average them. Then

$$\sigma_{tot,unwtd}^2 = 0.5 * (\sigma_a^2 + \sigma_b^2) \quad \text{and} \quad \delta_{tot,unwtd} = 0.5 * (\sqrt{\delta_a^2 + \delta_b^2})$$

. However, if we were to weight by the inverse variances of the two populations, then

$$\sigma_{tot,wtd}^2 = \left(\frac{\sigma_a^2}{\delta_a^2} + \frac{\sigma_b^2}{\delta_b^2} \right) / \left(\frac{1}{\delta_a^2} + \frac{1}{\delta_b^2} \right) \quad \text{and} \quad \delta_{tot,wtd} = \frac{1}{\sqrt{\left(\frac{1}{\delta_a^2} + \frac{1}{\delta_b^2} \right)}}$$

To illustrate the difference, assume that $\delta_b = 10\delta_a$, and that the numbers of sources are the same (N) in the two populations, so $\sigma_b \equiv \sigma_0 = \sqrt{10} \sigma_a$. As we will see below, such differences in RM variations between different populations are common. Now,

$$\delta_{tot,unwtd} = 2.3\sigma_0^2/\sqrt{N} \quad \text{and} \quad \delta_{tot,wtd} = 0.48\sigma_0^2/\sqrt{N}$$

Weighting improves the accuracy of the variance by a factor of over 4 in this case. In Figure 2 we show the results of this type of experiment, varying N and varying the ratio of $\frac{\sigma_b}{\sigma_a}$. The $\frac{1}{\sqrt{N}}$ behavior is seen on the left. On the right, we see that when the two population variances are equal, one gets an *improvement* by a factor of $\sqrt{2}$, as expected. But as σ_b rises, even though we are adding more sources, the uncertainty in the unweighted variance goes up. Weighting is critical! This calculation should be redone both for verification and to put in realistic models of the distributions of RMs in different populations, since they are quite unlikely to have Gaussian distributions.

3. Populations and variances

Which source properties will lead to different RM variances? *All of them!*

Galactic location (and especially) latitude is the first major factor. Rotation measures and the scatter among them increase strongly at low galactic latitudes and in the direction of some local Faraday structures. For studies of individual objects, this means that control samples must be done in close proximity to the foreground screen of interest. For studies

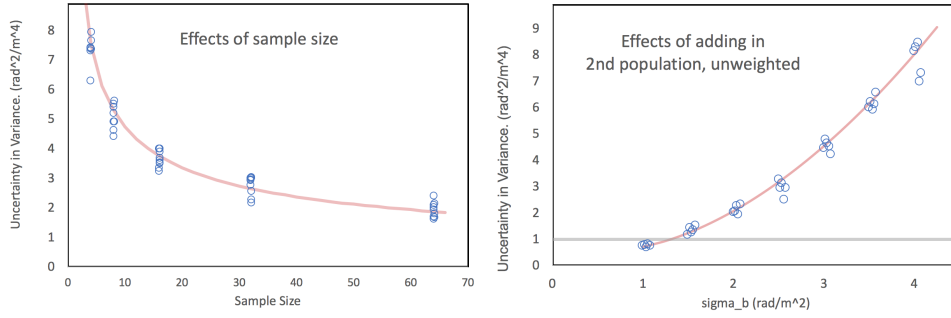


Figure 2. Uncertainty in **variance** for background experiments. Left: Varying the number of sources in each population. Right: **Unweighted** analysis as a function of rms scatter of 2nd population (1st population = 1).

of large samples, the different variances due to screens and background sources at different galactic locations must be properly weighted.

The nature of the optical host leads to very different polarization properties. O’Sullivan et al. (2017) found large differences in the fractional polarizations of radiative-mode and jet-mode AGN, which could be related to Faraday differences (see below).

The spectral index of the background radio source influences its polarization properties. Farnes et al. (2014) shows that the “(fractional) polarization spectral index”, differs for flat and steep spectrum sources. Negative slopes indicate depolarization, i.e., fractional polarization decreasing with increasing wavelength. Often, depolarization will be accompanied by a variation in RM as a function of wavelength. This variation will increase the intrinsic variance in RM within the population. When the polarization spectral index is positive, i.e., the source “re-polarizes” at longer wavelengths; then there will always be a variation of RM with wavelength, and thus an increased RM variance.

3.1. Fractional Polarization

The integrated fractional polarization of a radio source primarily depends on two factors, *i*) variations of the magnetic field direction within the synchrotron emitting source, and *ii*) variations in the Faraday depth either within or across the observed structure of the source. *i*) does not lead to any particular RM behavior, while *ii*) will create strong correlations between fractional polarization and depolarization. Initial indications are that both of these can be important. So fractional polarization is an imperfect indicator of RM variations – a very high fractional polarization implies small RM variations, while a low fractional polarization could be due to either effect. Figure 3 shows the relationship

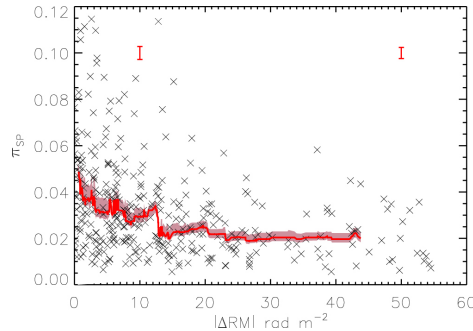


Figure 3. Relation between RM variations and fractional polarization, Lamee et al. (2016).

between RM variations and fractional polarizations of sources selected from the S-PASS survey (Lamee et al. 2016). ΔRM is the difference between RMs measured between a) 1365 MHz and 1435 MHz from the NVSS survey and b) between 1400 MHz and 2300 MHz from the NVSS and S-PASS surveys. As long as $\Delta RM \neq 0$, this will result in an extra contribution to the RM variations in a population. The correlation between fractional polarization and ΔRM shows that low polarization sources are much more likely to have large RM population variances.

Fractional polarization itself is a strong function of both the angular and physical size of the source (work in progress) as well as the total intensity. While this doesn't guarantee that RM variances will depend on these quantities, correcting for any dependencies on size and intensity are likely to be critical.

3.2. Morphology

There is also a strong relation between source morphology and the strength of RM variations across the source, although this has not been systematically investigated to our knowledge. An initial look at this issue has been made by M. Wieber (Minnesota), based on samples of large angular size sources assembled by H. Andernach (Guanajuato) and S. O'Sullivan (Hamburg). These sources are resolved in NVSS, and polarization maps in the two NVSS bands provided by J. Stil (Calgary) were used to characterize σ_{RM} , the variation in RM across the face of the source. Representative groups of the lowest σ_{RM} sources and the highest ones are shown in Figure 4. Color coding has been used to guide the eye, but it is clear that sources with larger values of σ_{RM} are more likely to show structures with bends and other distortions. This relationship is not surprising, given that the distorted sources are interacting with a substantial external thermal medium, with the higher densities (and perhaps fields) leading to higher RMs.

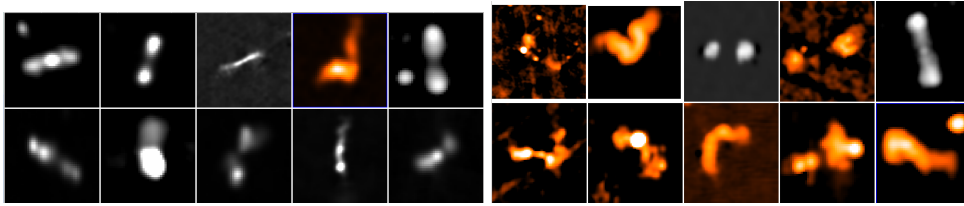


Figure 4. The NVSS structure of low (left) and high (right) σ_{RM} sources.

4. Conclusions

For studies of magnetic fields in foreground screens, using populations of polarized background sources, it is critical to measure the intrinsic variations in the RM distributions of each background population, and properly weight them in the analysis. *This work is supported, in part, by U.S. NSF grant AST17-14205 to the University of Minnesota.*

References

- Akahori, T., Gaensler, B. & Ryu, D., 2014, *ApJ* 790, 123
 Farnes, J., Gaensler, B. & Carretti, E., 2014, *ApJSS* 212, 15
 Johnston-Hollit, M. et al. 2014, *POS-AASKA14*, <https://pos.sissa.it/215/092/pdf>
 Lamee, M., Rudnick, L., Farnes, J. S., Carretti, E., Gaensler, B. M., Haverkorn, M., Poppi, S., 2016, *ApJ* 829, 18
 Lehman, E. & Casella, G., *Theory of point estimation*, Springer-Verlag, New York
 O'Sullivan, S., et al., 2017, *MNRAS* 469, 4034
 Rudnick, L. & Owen, F. N. 2014, *ApJ* 785, 45

Magnetic fields at the epoch of Reionization

B. Ruiz-Granados^{1,2}, E. Battaner^{3,4}, E. Florido^{3,4} and J.A. Rubiño-Martín^{1,2}

¹ Instituto de Astrofísica de Canarias, Vía Láctea, s/n, 38205, La Laguna, Tenerife, Spain
 email: bearg@iac.es

²Dept. de Astrofísica, Universidad de La Laguna, La Laguna, Tenerife, Spain

³ Dept. de Física Teórica y del Cosmos, Universidad de Granada, 18071, Granada, Spain

⁴ Instituto de Física Teórica y Computacional Carlos I, Universidad de Granada, 18071, Granada, Spain

Abstract. We detected magnetic fields with strengths of the order of 1-10 nG at the epoch of Reionization. These were identified by using CMB data to obtain Faraday Rotation at both, the map and the spectrum level. The multipole region of about $\ell < 12$ and the lack of correlations with either, galactic emissions (Faraday rotation, synchrotron and dust) or with CMB anisotropies and lensing, support this identification.

Keywords. Magnetic fields, cosmic microwave background, reionization

1. Faraday rotation of the CMB

A FR signal is detected by using foreground cleaned maps of Stokes' Q and U parameters provided by WMAP9 (Hinshaw et al., 2013) at frequencies 33, 41 and 61 GHz (Ruiz-Granados, Battaner & Florido, 2016). The optical depth of Thomson scattering derived from the bump induced on E-modes due to Reionization is sensitive to the thermal electron distribution n_e and peaks at low multipoles (Zaldarriaga, 1997), being its value $\tau \sim 0.06$ (Planck VI Col., 2018). This is used for computing the rotation measure (RM), which is proportional to n_e , and finally for obtaining the mean-weighted magnetic field strength. RM maps are obtained by minimizing the χ^2 distribution of the polarized angle for the three frequencies. The associated covariance matrices are used for computing the error map (see Fig. 1). Cross-correlations at map level with galactic FR, extragalactic FR, synchrotron and dust polarization are computed and also with CMB temperature, lensing potential and noise maps (see Tab. 1). The angular power spectrum of the observed RM maps is obtained for low multipoles (see Fig. 1 bottom). From the FR power

Table 1. Correlation coefficients between maps in Fig.1 and foregrounds

Maps	r + Δ r	Significance ($ t $)	R^2
CMB temperature	0.009 \pm 0.015	0.62	8.52×10^{-5}
Obs. Galactic RM (1.4-23 GHz)	0.037 \pm 0.024	1.53	1.4×10^{-3}
Obs. Galactic RM (EGRS)	0.024 \pm 0.015	1.60	5.67×10^{-4}
Sim. Galactic RM (23 GHz) halo	0.038 \pm 0.030	1.27	1.4×10^{-3}
U_{23} -galactic	-0.020 \pm 0.015	1.37	4.1×10^{-4}
Q_{23} -galactic	0.019 \pm 0.015	1.27	3.6×10^{-4}
U_{dust} -galactic	0.016 \pm 0.015	1.08	2.6×10^{-4}
Q_{dust} -galactic	0.009 \pm 0.015	0.60	7.95×10^{-5}
ϕ_{dust} -galactic	0.034 \pm 0.015	2.28	1.1×10^{-3}
Noise Q_{CMB}	-0.028 \pm 0.015	1.92	8.2×10^{-4}
Noise U_{CMB}	-0.014 \pm 0.015	0.92	1.8×10^{-4}
Noise ϕ_{CMB}	0.004 \pm 0.015	0.25	1.39×10^{-5}
Lensing potential	0.012 \pm 0.015	0.81	1.45×10^{-4}

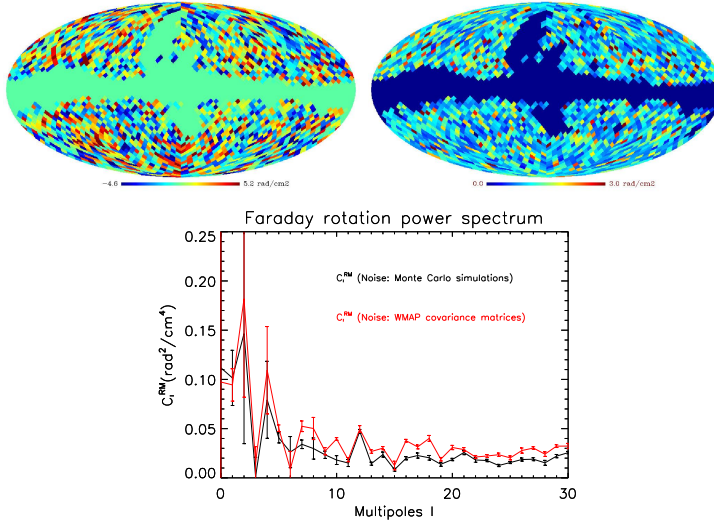


Figure 1. Map of the observational RM (top, left), its error map (top, right) and the power spectrum (bottom) by using WMAP9 at 33, 41 and 61 GHz.

Table 2. Values of the FR at 30 and 70 GHz and the mean-weighted magnetic field strength by computing the mean values between $\ell = 2 - 6$.

FR ($\nu = 30$ GHz)(deg)	FR ($\nu = 70$ GHz) (deg)	$\langle B_{ } \rangle$ (G)
36.0 ± 20.6	6.30 ± 3.72	$6.88 \pm 4.06 (\times 10^{-8})$

spectrum, the mean-weighted magnetic fields strength are deduced by taking the mean value for multipoles $\ell < 12$ (see Tab. 2).

2. Conclusions

The polarized intensity at Recombination are much lower than those of the Milky Way. However, the Recombination interpretation would require magnetic field strengths higher than the limits found by Planck of $B_0 < 3.4 \times 10^{-9}$ G (Planck XIX Col., 2016 & POLARBEAR Col., Ade et al. 2015). No correlation is found with Recombination neither with Galactic foregrounds.

For low multipoles ($\ell < 12$) we find a RM signal derived from the WMAP polarization maps. This multipole range is typical of phenomena taking place at Reionization. The amplitude and shape of the detected feature is consistent with magnetic fields at Reionization of the order of 1-10 nG.

References

- Ade, P. A. R., Arnold, K., Atlas, M., *et al.* 2015, *Phys.Rev.D*, 92, 123509
 Hinshaw, G., Larson, D., Komatsu, E., *et al.* 2013, *ApJS*, 208, 19
 Planck Collaboration, Ade, P. A. R. *et al.* 2016, *A&A*, 594, A19
 Planck Collaboration, Aghanim, N. *et al.* 2018, submitted to *A&A*, arXiv:1807.06209
 Ruiz-Granados, B., Battaner, E. & Florido, E., 2016, *MNRAS*, 460, 3089
 Zaldarriaga, M., 1997, *Phys.Rev.D*, 55, 1822

Propagation of UHECRs in the local Universe and origin of cosmic magnetic fields

S. Hackstein¹, F. Vazza², M. Brüggen¹, J. G. Sorce³, S. Gottlöber³

¹ Sternwarte Bergedorf, Universität Hamburg
Gojenbergsweg 112, 21029, Hamburg, Germany

² INAF, Istituto di Radioastronomia di Bologna, via Gobetti 101, I-41029 Bologna, Italy

³ Université de Strasbourg, CNRS, Observatoire astronomique de Strasbourg, UMR 7550,
F-67000 Strasbourg, France

⁴ Leibniz Institute for Astrophysics Potsdam, An der Sternwarte 16, 14482 Potsdam
email: stefan.hackstein@hs.uni-hamburg.de,

Abstract. We simulate the propagation of cosmic rays at ultra-high energies, $\gtrsim 10^{18}$ eV, in models of extragalactic magnetic fields in constrained simulations of the local Universe. We investigate the impact of different magneto-genesis scenarios, both, primordial and astrophysical, on the propagation of cosmic rays. Our study shows that different scenarios of magneto-genesis do not have a large impact on the anisotropy measurements. The distribution of nearby sources causes anisotropy at very high energies, independent of the magnetic field model. We compare our results to the dipole signal measured by the Pierre Auger Observatory. All our models could reproduce the observed dipole amplitude with a pure iron injection composition. This is due to clustering of secondary nuclei in direction of nearby sources of heavy nuclei. A light injection composition is disfavoured by the non-observation of anisotropy at energies of 4 - 8 EeV.

Keywords. MHD, methods: numerical, ISM: magnetic fields, cosmic rays

1. Introduction

We investigate constrained Magnetohydrodynamical (MHD) simulations of the local Universe for different scenarios of magneto-genesis and probe their influence on the propagation of ultra-high energy cosmic rays (UHECRs). We compare different source models to see what information can be inferred on the extragalactic magnetic field. The MHD simulations used constrained initial conditions (Sorce et al. 2016) and were performed with the MHD code ENZO[†], which is an Adaptive Mesh Refinement (AMR) code for cosmological simulations. The resulting magnetic fields are used with the CRPropa[‡] code to simulate the propagation of UHECRs. The observer is placed at the center of the simulation, the defined position of the Milky Way.

We investigate two major scenarios for magneto-genesis: magnetic fields of primordial origin - prior to $z = 60$, where the MHD simulations start - with several spectral indices of the initial magnetic power spectrum (more info in Hackstein et al. 2018). We compare this scenario to an astrophysical origin, modelled with thermal and magnetic feedback of AGN at several different redshift ranges. We improve on Dolag et al. (2003) by testing these different scenarios and by obtaining the expected B - ρ -ratio from a single consistent MHD simulation. Both scenarios reproduce magnetic fields observed in clusters reasonably well. The main difference is that in the low-density regions, i. e. the voids, the magnetic field strength differs by up to 10 orders of magnitude. The two scenarios are therefore well suited to highlight the influence of the low-density regions.

[†] <http://www.enzo-project.org>

[‡] <https://crpropa.desy.de/>

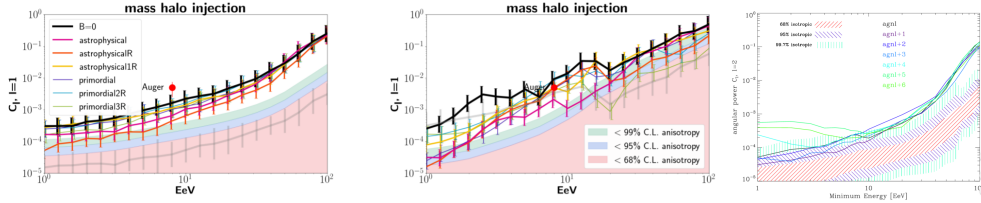


Figure 1. Results for angular power as function of minimum energy of considered events. The coloured bands indicate the confidence level of anisotropy. The dipole observed in the Auger data > 8 EeV is indicated. Left: Dipole from pure proton injection. Center: dipole from pure iron injection. Right: Quadrupole from pure proton injection

2. Results

Anisotropy is measured with the angular power spectrum of spherical decomposition of the full sky of observed UHECR events. We consider as sources the center of viral halos identified in the MHD simulation, where the most energetic objects are most likely to be found. This source density is at the lower bound of allowed densities, $\gtrsim 10^4$ Mpc 3 , as shown by di Matteo & Tinyakov (2017).

Results for the different scenarios of magneto-genesis are pretty converged, the fields in voids have minor influence on the large scale anisotropy signal of UHECRs. It is unlikely that we can identify magneto-genesis scenarios by full-sky observations of UHECR events without prior knowledge on their sources. For light injection composition, in order to reproduce the Auger dipole, a rather extreme source model is needed, that might already be at odds with present constraints. For a heavy composition the contribution of the most nearby sources increases, due to multiple allowed hits of secondary nuclei of the same primary particle. This effect is the strongest at $E = E_{\max}/A$, the maximum energy of secondary protons that can reach the observer only from the most nearby sources.

In another set of simulations, anisotropy occurs at low energies for an increased magnetic field strength, independent of the distribution of sources (results from Hackstein et al 2016). Here, a uniform field dominates around the sources. One can show that anisotropy is indeed expected in that case. The same is true for many fields with pronounced component in vertical direction. This offers the chance to put limits on such fields in the halo of the Milky Way.

3. Conclusions

- (a) light injection composition is unlikely to reproduce the Auger dipole while heavy injection increases multipoles.
- (b) anisotropy at highest energies enables UHECR astronomy
- (c) magneto-genesis scenario unlikely to be distinguished by UHECR observations
- (d) strong vertical magnetic field component introduces quadrupole anisotropy \Rightarrow limit magnetic fields in Milky Way halo.

References

- di Matteo, A. and Tinyakov, P. 2018, *MNRAS*, 476, 715
 Dolag K., Grasso D., Springel V., Tkachev I. 2004, *JETP Lett.*, 79, 583
 Hackstein, S., Vazza, F., Brügggen M., Sigl, G., Dundovic, A. 2016, *MNRAS*, 462, 3660
 Hackstein, S., Vazza, F., Brügggen, M., Sorce, J. G., Gottlöber, S. 2018, *MNRAS*, 475, 2519
 Sorce, J. G. et al. 2016, *MNRAS*, 455, 2078

Statistics and new detections of diffuse radio sources in galaxy clusters

Massimo Cau^{1,2}, Gabriele Giovannini^{1,2}, Alessandro Ignesti^{1,2}

¹IRA-INAF, Bologna IT,
Via Gobetti 101, 40127, Bologna, Italy
email: m.cau@ira.inaf.it

²Dept. of Astronomy & Astrophysics, Bologna University,
Via Irnerio 46, 40126 Bologna, Italy
email: massimo.cau@unibo.it

Abstract. The detection of diffuse radio emission in galaxy clusters (halos, relics and minihalos) is still limited to the nearby clusters ($z \leq 0.3$). Recently, thanks to the improved sensitivity of the largest radio telescopes the number of diffuse radio source at $z > 0.3$ has significantly increased, proving that this class of sources exists at even high redshifts. We obtained L-band observations at the Jansky Very Large Array (JVLA) to study a sample of high redshift massive clusters ($0.3 < z < 0.7$). Our main goal is to investigate the evolutionary history of non thermal properties in galaxy clusters and to determine whether the correlations mostly observed at low redshift evolve with time.

Keywords. galaxies: clusters: general, acceleration of particles, diffusion, turbulence, radiation mechanisms: nonthermal, shock waves, instrumentation: interferometers, methods: statistical, surveys, X-rays: galaxies: clusters.

1. Introduction

Galaxy clusters are the largest gravitationally bound structures of the Universe, formed from density fluctuations and grown hierarchically through the extremely process of merging and mass accretion. They represent very interesting tools to study the cosmology and the evolution of large scale structures. In the last years, most of the detailed knowledge of galaxy clusters has been obtained from the study of thermal X-ray and non-thermal emissions of the intra-cluster medium (ICM). Observational evidences show the presence of a strong correlation between total radio power and X-ray luminosity, suggesting a strict interconnection between non-thermal properties and cluster mass (see Feretti et al. 2012 for review). Diffuse cluster radio sources are not present in all galaxy clusters. The occurrence of radio halos and relics has been studied by Giovannini et al. (1999) in the NVSS sample, finding that is higher in clusters showing high X-ray luminosity. Halos are present in $\sim 20 - 30\%$ while relics in $\sim 25\%$ of clusters with $L_X > 5 \times 10^{44}$ erg s^{-1} but actually we do not know why not all bright massive clusters show a diffuse non thermal radio emission. To understand the physical mechanisms governing the formation processes of diffuse radio sources it is necessary to correlate the non-thermal cluster properties with the cluster evolution. Nevertheless, the discovery of non thermal diffuse emission and consequently the related statistical properties are still limited to low redshifts: up to date the overall average redshift for radio halos is 0.25 and 0.20 for radio relics.

2. Overview and implications

With the purpose to correlate the non thermal cluster properties with cluster evolution, we select an omogeneous sampe of very luminous X-ray clusters, most of them extracted from the Massive Cluster Survey (MACS) presented by Ebeling et al. 2007, 2010 and submitted an L-band (C and D arrays) observational proposal to the JVLA. Our proposal has been accepted with project ID: VLA/17A-025. We obtained the radio images of 36 clusters observed with the C array and 31 clusters observed with the D array. 25 clusters have been observed and reduced both in C and D configurations and therefore we studied the radio emission of 42 different clusters. We have detected diffuse radio emission in 18 clusters corresponding to $\sim 42\%$ of our cluster sample. Among them we found 8 new diffuse radio structures, classified as 6 halos and 2 relics. The other 10 sources have already been discovered and reported in the literature, although most of them at different wavelengths. Reporting the new halos in the $(P_{1.4GHz}, L_{X,500})$ plane and performing a best fit correlation (*Right panel* Fig. 1) we underline the following conclusions:

- the slope of the best fit for the halos hosted in clusters with $z > 0.3$ (blue dotted line) results lower respect to the scaling relation reported in literature for halos with $z < 0.3$ (black dotted line) (e.g. Cassano et al. 2013);
- new halos appear slightly underluminous in the radio band (green dotted line);
- new halos are in agreement with the correlation at $z > 0.3$;

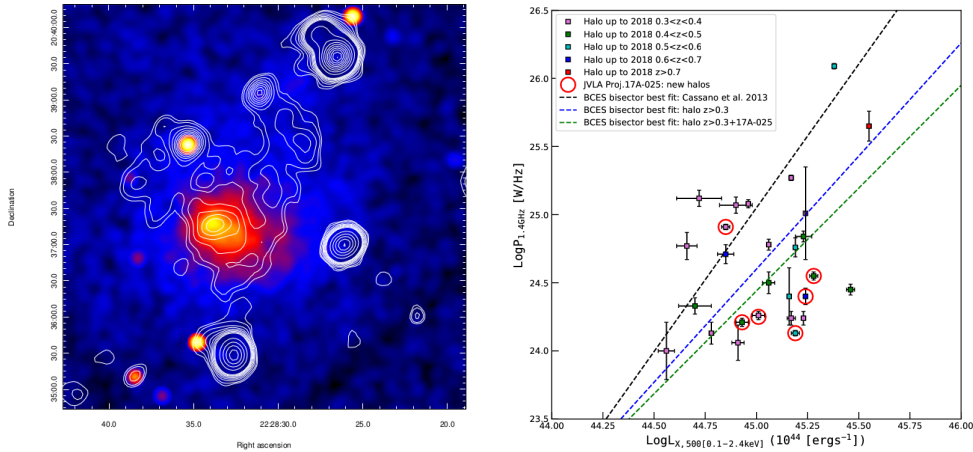


Figure 1. *Left panel* MACSJ2228.5+2036: example new halo detected at high redshift ($z = 0.411$). Radio contours are overlaid to the *Chandra* X-ray image. *Right panel* Distribution of halos with $z > 0.3$ in the $(\log(P_{1.4GHz}), \log(L_{X,500}))$ plane: colored dots are referred to different redshift ranges. Red circled dots are the new halos discovered in Proj. 17A-025. Comparison between scaling relations: literature (black dotted line), updated halo collection at $z > 0.3$ (blue dotted line), updated halo collection at $z > 0.3$ plus new halos (green dotted line).

References

- Cassano, R., Ettori, S., Brunetti, G. 2013, *Astrophysical Journal*, 777, 141
 Ebeling, H., Barret, E., Donovan, D. 2007, *Astrophysical Journal Letters*, 661, L33
 Ebeling, H., Edge, A.C., Mantz, A. 2010, *Monthly Notices of the RAS*, 407, 83
 Feretti, L., Giovannini, G., Govoni, F., & Murgia, M. 2012, *Astrophysics Reviews*, 20, 54
 Giovannini, G. 1999, in *Diffuse Thermal and Relativistic Plasma in galaxy Clusters*, ed. H. Bohringer, L. Feretti, & P. Schuecker, 13

Spectral analysis of magnetic fields in simulated galaxy clusters

Paola Domínguez-Fernández¹, Franco Vazza^{3,1,2} and Marcus Brüggen¹

¹Hamburger Sternwarte, Gojenbergsweg 112, 21029 Hamburg, Germany
email: pdominguez@hs.uni-hamburg.de
email: mbrueggen@hs.uni-hamburg.de

² Istituto di Radio Astronomia, INAF, Via Gobetti 101, 40121 Bologna, Italy

³ Dipartimento di Fisica e Astronomia, Università di Bologna, Via Gobetti 92/3, 40121, Bologna, Italy
email: franco.vazza2@unibo.it

Abstract.

We introduce a new sample of galaxy clusters obtained from a cosmological simulation covering an unprecedented dynamical range. All the clusters in our sample show a clear signature of small-scale dynamo amplification. We show that it is possible to use dynamo theory for studying the magnetic spectrum in the intracluster medium. We study if the intrinsic variations on the spectra depend on the dynamical history of each cluster or on some host cluster properties.

Keywords. galaxy: clusters, general – methods: numerical – intergalactic medium – large-scale structure of Universe

1. Introduction

Galaxy clusters evolve mainly via two mechanisms: accretion of gas and galaxies, and via mergers occurring approximately every few Gyr. These mechanisms directly affect the diffuse, hot, weakly magnetised gas observed in clusters referred as the Intracluster Medium (ICM) (e.g. Kravtsov & Borgani 2012, Brunetti & Jones 2014) by driving shocks through it and therefore, every merger event can be a source of turbulence. In particular, these events effectively affect the structure of the magnetic fields that permeate galaxy clusters.

We know from radio observations that the strength of magnetic fields in the ICM is of the order of μG and the coherence scales are of the order of 10-50 kpc (e.g. Feretti, et al. 2012, Govoni et al. 2017). These coherent large-scale fields indicate that the mechanism which leads to this final structure cannot be solely due to gas compression. In fact, a small-scale dynamo would be a more suitable mechanism to generate observed, large-scale magnetic fields. While the origin of magnetic fields in the Universe remains an open question, a small-scale dynamo seems to play a key role in amplifying magnetic fields in galaxy clusters (e.g. Beresnyak & Miniati 2015), independent of where the seed fields come from.

2. Methods and Results

We studied the formation of seven massive galaxy clusters in a cosmological MHD simulation with the *ENZO* grid code (The Enzo Collaboration; Bryan et al. 2014) using the Dedner cleaning method, and eight adaptive mesh refinement (AMR) levels to increase the dynamical resolution. Each cluster was selected in a comoving volume of $(260 \text{ Mpc})^3$ and further refined in most of the volume in which the clusters form with a maximum spatial resolution of $\Delta x_{\text{max}} = 3.95 \text{ kpc}$ (comoving). We assumed a simple uniform seed field of cosmological origin of 0.1 nG (comoving) at $z = 30$ (for a detailed description see Vazza et al. 2018). In this work, we will only discuss the results from *non-radiative* cosmological simulations to focus on the growth of magnetic fields by the turbulence induced by structure formation processes.

We analyse clusters with different dynamical states at redshift $z = 0$, namely clusters with ongoing mergers, relaxed ones and clusters that have suffered a recent major merger. The baseline model we tested with our cosmological simulation relies on an analytic solution for the magnetic power spectrum derived from dynamo theory (Kazantsev 1967, Kulsrud & Anderson 1992). Our tests (Domínguez-Fernández et al., to be submitted) show that all spectra can be fitted well by an equation which is directly derived from dynamo theory (see Eq. in Fig. 1). In Fig.1 we show the best-fit of the magnetic energy spectra of all of the clusters in our sample.

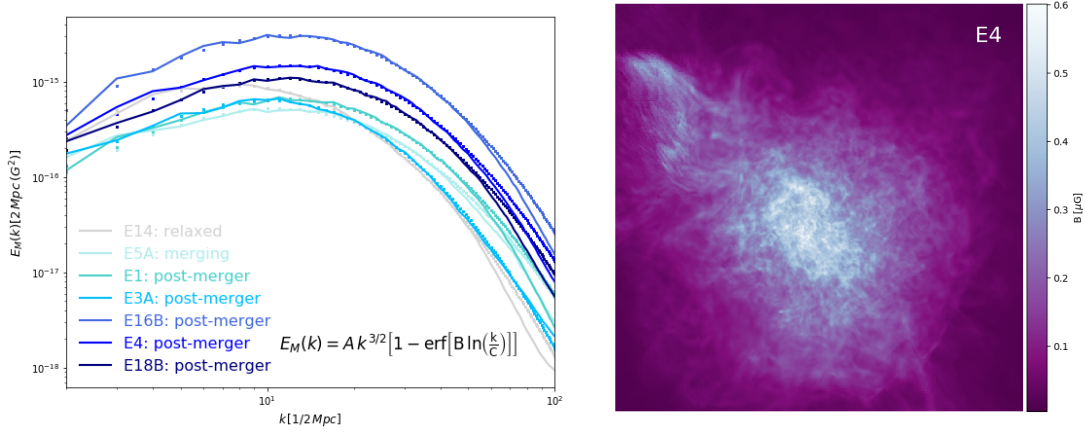


Figure 1. *Left:* Magnetic energy spectra of all of our cluster sample at $z = 0$. The solid lines correspond to the data and the scatter plots show our best-fit. *Right:* Projection of the magnetic field strength in galaxy cluster E4 at Δx_{max}

Discussion

1) Regardless of the dynamical state of each cluster, the magnetic energy spectral shape is in good agreement with dynamo theory. As a first approximation, this indicates that this model can be used for a detailed analysis of a cluster evolution where a small-scale dynamo can be acting in addition to gas compression and shocks.

2) The normalization of the magnetic energy spectrum overall is determined by the dynamical state of each cluster. Relaxed clusters have the highest value for the magnetic spectrum, followed by post-mergers clusters, and then merging clusters. This result is tentatively consistent with the fact that in relaxed system a small-scale dynamo would have to be active for longer dynamical times. Nevertheless, we do not observe a clear dependence on the virial mass of each cluster due to the small number of clusters in our sample.

3) Our analysis shows that the magnetic power spectra does not retain information on the last major-merger, as minor mergers are also injecting turbulence during the formation of each cluster.

4) We refer the reader to the complete work (Domínguez-Fernández et al., to be submitted) where a detailed analysis on the cluster sample is done and where also the evolution of a merging cluster is studied.

5) The resulting power spectrum shows that in general the three-dimensional components of the magnetic field are non-Gaussian. This results from having different magnetic field components being continuously injected by the accretion of substructures (Vazza et al. 2018) rather than from the presence of highly intermittent MHD turbulence (e.g. Shukurov et al. 2017). This has direct consequences for Faraday Rotation measurements and illustrates the importance of reliable simulations of magnetic fields in galaxy clusters for an accurate modelling of future polarisation surveys (e.g. Johnston-Hollitt et al. 2015).

Acknowledgements

Our simulations were performed using *ENZO* and the Supercomputing resources at the Juelich Supercomputing Centre (JSC), under project HHH42. We acknowledge the European Union’s Horizon 2020 program under the ERC Starting Grant ”MAGCOW”, no. 714196.

References

- Beresnyak & Miniati 2015, *ApJ*, 817, 127
 Brunetti, G. & Jones, T. W. 2014, *International Journal of Modern Physics D*, 23, 1430007-98
 Bryan G. L. et al. 2014, *ApJS*, 211, 19
 Feretti, L. and Giovannini, G. and Govoni, F. and Murgia, M. 2012, *A&ARv*, 20, 54
 Govoni, F., et al. 2017, *A&A*, 603, 122
 Johnston-Hollitt et al 2015, *Advancing Astrophysics with the SKA (AASKA14)*, 92
 Kazantsev A. P. 1967, *Journal of Experimental and Theoretical Physics*, 53, 1806
 Kravtsov, A. V. & Borgani, S. 2012, *ARAA*, 50
 Kulsrud R. M., Anderson S. W. 1992, *AJ*, 396, 606
 Shukurov et al. 2017, *ApJL*, 839, L16
 Vazza F., Brunetti G., Brüggen M., Bonafede A. 2018, *MNRAS*, 474, 1672

CHANG-ES: an overview

Jeroen M. Stil¹
on behalf of the CHANG-ES² collaboration

¹Department of Physics and Astronomy, The University of Calgary,
2500 University Drive NW, Calgary, AB, T2N 1N4, Canada
email: jstil@ucalgary.ca

² <http://queensu.ca/changes>

Abstract. CHANG-ES is a survey of 35 edge-on galaxies of total intensity, linear and circular polarization in L band and C band with the Jansky Very Large Array. The goal of the survey is to investigate the origin, extent, and physical conditions of radio halos, and their connection with star formation in the disk. We present an overview of the survey and highlight some results.

Keywords. magnetic fields, polarization, galaxies, galaxy halos

1. Introduction to CHANG-ES

The Continuum Halos in Nearby Galaxies - an EVLA Survey (CHANG-ES) is a survey of 35 nearby edge-on ($i > 75^\circ$) galaxies of all Stokes parameters in L band ($\nu = 1.5$ GHz, $\Delta\nu = 500$ MHz) and C band ($\nu = 6$ GHz, $\Delta\nu = 2$ GHz) with the Karl G. Jansky Very Large Array. The sample was selected for isophotal diameter ($4' < d_{25} < 15'$), $\delta > -23^\circ$, and $S_{1.4\text{GHz}} > 23$ mJy, with three well-known galaxies added just outside these boundaries (Irwin *et al.* 2012). Each galaxy was observed in L band in B, C, and D configuration, and in C band in C and D configuration to provide matching angular resolution up to $4''$, with sensitivity ~ 20 $\mu\text{Jy}/\text{beam}$ (L band) and ~ 4 $\mu\text{Jy}/\text{beam}$ (C band), and sensitivity to angular scales up to $16'$ in L band and $4'$ in C band. Missing short spacings will be filled in with the Green Bank Telescope (Trent Braun *et al.* 2018).

CHANG-ES aims to characterize all aspects of radio halos in spiral galaxies, including their extent, magnetic field, relation to star formation in the disk, and cosmic ray transport. Sensitive, broad-band full-Stokes images from CHANG-ES provide spatially resolved spectral index and Faraday rotation from the disk far into the halo. Now that such data are available for a sample of 35 edge-on galaxies, it is possible to investigate galaxy scaling relations and statistics of halo properties in relation to star formation.

CHANG-ES has so far released D-configuration images with resolution $36''$ (L-band) and $9.6''$ (C-band) for all galaxies (Wiegert *et al.* 2015). These data and future data releases will be made available through the website <http://queensu.ca/changes>.

2. Selected results from CHANG-ES

Edge-on galaxies are particularly suitable for investigation of the vertical structure of the halo and disk-halo interaction. The radio halo extends far above the disk for the median edge-on galaxy (Wiegert *et al.* 2015). Krause *et al.* (2018) found the average scale height of 13 CHANG-ES galaxies to be 1.1 ± 0.3 kpc in C band and 1.4 ± 0.7 kpc in L band. The radio scale height increases linearly with diameter of the galaxy, but there is no correlation with the star formation rate, or the star formation rate per unit area. The frequency dependence of halo scale heights indicates an escape-dominated halo (escape time shorter than cosmic ray life time) with convective propagation for all galaxies.

CHANG-ES measures polarization angle structure and Faraday rotation in the disk and halo. Posters by M. Krause and R.-J. Dettmar at this meeting report large-scale field reversals from Faraday rotation of the diffuse synchrotron emission - a first for edge-on galaxies and in particular galaxy halos. The Virgo cluster galaxy NGC 4388 shows extensions of the magnetic field that indicate a connection between the disk and the halo (Damas-Segovia *et al.* 2016). The polarized structure in the halo in relation to H- α and X-ray emission appears to trace a galactic wind from separate sources in the spiral arms. NGC 4388 experienced recent ram pressure stripping from its motion through the Virgo cluster (Oosterloo & van Gorkom 2005), but the observed symmetry of the polarized halo excludes compression of the halo by ram pressure. A poster by A. Damas-Segovia at this meeting discusses polarization of the AGN outflow in NGC 4388.

The deep radio images from CHANG-ES are combined with multi-wavelength data to investigate the relation between star formation, the magnetic field, and synchrotron emission. Li *et al.* (2016) found that the slope of the mid-IR/radio correlation for CHANG-ES galaxies is super-linear, an indication that galaxies with a higher star formation rate are closer to calorimetric conditions for cosmic ray electrons (see also Yoast-Hull *et al.* 2013). The CHANG-ES data allow separation of diffuse halo emission from disk emission. Vargas *et al.* (2018) used WISE 22 μ and new deep H- α images to derive spatially resolved separation of thermal radio emission for CHANG-ES galaxies.

CHANG-ES also reveals low-luminosity active galactic nuclei in several galaxies. Variability in the unresolved core of NGC 4845 on a time scale of six months between CHANG-ES observations was associated with a tidal disruption event by the super-massive black hole in the nucleus (Irwin *et al.* 2015). The large bandwidth provided single-epoch in-band spectral indices, negative in C band but positive in L-band from synchrotron self-absorption. The peak of the spectrum decreased in brightness as it shifted to lower frequencies over time. The emission was circularly polarized with no detectable linear polarization. Circular polarization from the nucleus was also detected in four other galaxies (Irwin *et al.* 2018). The galaxy NGC 2992 was shown to have kpc sized bipolar outflows that are only revealed in polarization, not in total intensity (Irwin *et al.* 2017).

The galaxy UGC 10288 was included in the sample, but the VLA images showed that most of the radio flux was from a large radio galaxy in the background that crosses the disk of UGC 10288. Irwin *et al.* (2013) analyzed the Faraday rotation of this extended background source and found that the azimuthal component of the magnetic field hints at a direction reversal.

References

- Damas-Segovia, A., Beck, R., Vollmer, B., *et al.* 2016, *ApJ*, 824, 30
 Irwin, J. A., Beck, R., Benjamin, R. A., *et al.* 2012, *AJ*, 144, 43
 Irwin, J. A., Krause, M., English, J., *et al.* 2013, *AJ*, 146, 164
 Irwin, J. A., Henriksen, R. N., Krause, M., *et al.* 2015, *ApJ*, 809, 172
 Irwin, J. A., Schmidt, P., Damas-Segovia, *et al.* 2017, *MNRAS*, 464, 1333
 Irwin, J. A., Henriksen, R. N., Weżgowiec, M., *et al.* 2018, *MNRAS*, 476, 5057
 Krause, M., Irwin, J. A., Wiegert, T., *et al.* 2018, *A&A*, 611, A72
 Li, J.-T., Beck, R., Dettmar, R.-J., *et al.* 2016, *MNRAS*, 456, 1723
 Oosterloo, T., & van Gorkom, J. 2005, *A&A*, 437, L19
 Trent Braun, T., Kepley, A., Rand, R. J., *et al.* 2018, *BAAS* 231, 248.07
 Vargas, C., Mora-Partiarroyo, S., Carolina, S., *et al.* 2018, *ApJ*, 853, 128
 Wiegert, T., Irwin, J., Miskolczi, A., *et al.* 2015, *AJ*, 150, 81
 Yoast-Hull, T. M., Everett, J. E., Gallagher III, J. S., *et al.* 2013, *ApJ*, 768, 53

The QUOCKA Survey: Early Results

George Heald¹ and the QUOCKA Team²

¹CSIRO Astronomy and Space Science, PO Box 1130, Bentley WA 6102, Australia
email: george.heald@csiro.au

²<https://research.csiro.au/quocka/team/>

Abstract. We present early results from QUOCKA: a new polarimetric radio survey aimed at understanding detailed magnetoionic properties of radio galaxies, and enabling the science goals of modern broadband surveys to be carried out with Square Kilometre Array (SKA) pathfinders and precursors. The QUOCKA survey employs the broadband correlator available at the Australia Telescope Compact Array (ATCA), primarily to build on and supplement Early Science observations with the Australian Square Kilometre Array Pathfinder (ASKAP) telescope. Just over 200 sources have been observed so far, and the sample is currently expanding.

Keywords. magnetic fields, polarization, surveys, radio continuum: galaxies

1. Introduction

In this contribution we present early results from a new project using the Australia Telescope Compact Array (ATCA): *QU Observations at Cm wavelength using Km baselines with the ATCA* (the QUOCKA survey). A survey overview has been presented in a companion contribution (Heald et al. 2018a, this volume).

2. Survey progress and plans

To date, the survey has been allocated 494 hours, with 234 hours already observed and the remainder scheduled. QUOCKA has been granted Continuing Status at the ATCA.

The QUOCKA sample is being drawn from polarized sources detected by ASKAP during the telescope’s Early Science period, as described by Heald et al (2018a, this volume). The subsample observed in the first semester was based on sources found in six 30-square degree ASKAP mosaics. As the Early Science period progresses and additional suitable sources are identified, we are growing the list of objects to be followed up with the ATCA. Eventually, our goal is to expand the scope of the QUOCKA project to elucidate and model the broadband polarimetric behaviour of the brightest sources detected by the ASKAP POSSUM survey (Gaensler et al. 2010).

Observations are carried out with ATCA at 1 – 3 and 4.5 – 8.5 GHz, in extended east-west configurations. Several short snapshots over a wide range of hour angle are used to improve the resulting image fidelity. The typical sensitivity is $\sim 100 \mu\text{Jy beam}^{-1}$ in each of the two broad frequency bands.

The QUOCKA team has developed a PYTHON-based data reduction pipeline† that utilizes standard MIRIAD (Sault et al. 1995) procedures. We have performed initial processing of all 201 sources that were observed to date. In addition, 12 highly extended sources have also been observed with the same frequency setup and are being analysed separately (Alexander et al., in prep).

† <https://github.com/gheald/quocka>

3. Data and preliminary results

Here, we present an example of image quality (Figure 1) and broadband polarization response (Figure 2), for a representative QUOCKA source selected at random. Data of similar quality are already available for 200 other QUOCKA sources.

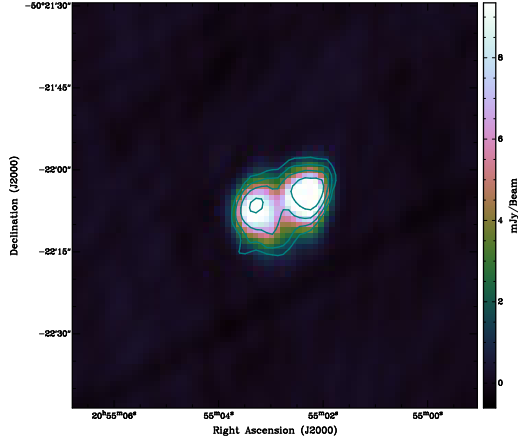


Figure 1. Representative ATCA images of the QUOCKA source J205503-502206. These total intensity images are presented in colourscale for the 4.5 – 8.5 GHz band, and with contours for the 1 – 3 GHz band. Contours begin at $1.5 \text{ mJy beam}^{-1}$ ($\approx 6\sigma$) and increase by powers of two.

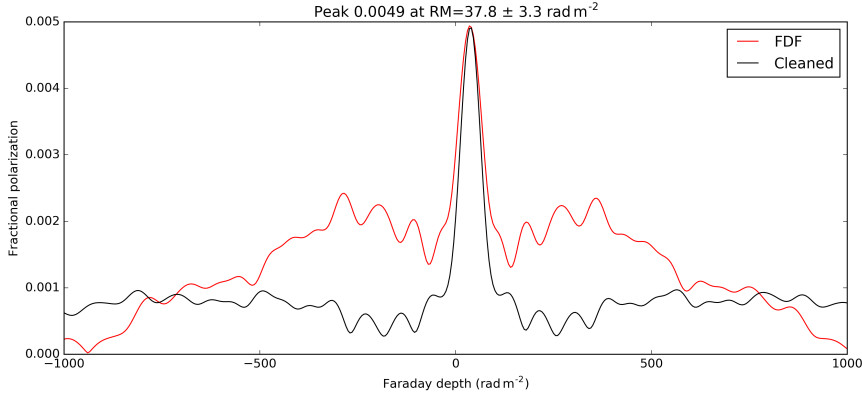


Figure 2. Indicative broadband Faraday dispersion function (FDF) before and after Faraday deconvolution, displayed here for the centre of QUOCKA source J205503-502206. That part of the source peaks at a Faraday depth of $37.8 \pm 3.3 \text{ rad m}^{-2}$. The broadband Stokes $Q, U(\lambda^2)$ data make fitting of detailed magnetoionic models possible (e.g., O’Sullivan et al. 2012).

References

- Gaensler, B. M., Landecker, T. L., Taylor, A. R., & POSSUM Collaboration. 2010, in Bulletin of the American Astronomical Society, Vol. 42, American Astronomical Society Meeting Abstracts #215, 515
- OSullivan, S. P., Brown, S., Robishaw, T., et al. 2012, *MNRAS*, 421, 3300
- Sault, R. J., Teuben, P. J., & Wright, M. C. H. 1995, in Astronomical Society of the Pacific Conference Series, Vol. 77, Astronomical Data Analysis Software and Systems IV, ed. R. A. Shaw, H. E. Payne, & J. J. E. Hayes, 433

Magnetized stars embedded in AGN accretion disks and tori

M. Zajaček^{1,2} and V. Karas³

¹Max-Planck-Institut für Radioastronomie (MPIfR), Auf dem Hügel 69, Bonn, Germany

²Universität zu Köln, Zùlpicher Strasse 77, D-50937 Köln, Germany

³Astronomical Institute, Czech Academy of Sciences, Boční II 1401, Prague, Czech Republic

Abstract. As a result of stellar evolution, a population of magnetized stars is expected to be part of Nuclear Star Clusters (NSCs) residing in many galactic nuclei. In Active Galactic Nuclei (AGN) NSCs are embedded within an accretion disk or a torus near an supermassive black hole (SMBH). The dipole-type magnetic field can significantly influence the gaseous environment in the region of influence around the star, depending on the intrinsic strength of its dipole and parameters of the surrounding medium. We estimate the fraction of the volume in the accretion disk/torus where the structure must be entirely changed by the presence of the embedded magnetized stars, as compared with an unperturbed solution. This is also the case of magnetized, compact neutron stars, where the surface intensity of the magnetic field can reach rather extreme values. In particular, young magnetars are expected to produce inhomogeneities in the external magnetic field of hot corona, scale of which range $\lesssim 100$ SMBH Schwarzschild radii (r_s).

Keywords. galaxies: nuclei, accretion, stars: neutron

1. Summary of the analysis

Most galactic nuclei contain supermassive black holes that are surrounded by nuclear star clusters (NSC) with typical half-light radii of 2-3 parsecs and masses of 10^6 - 10^7 Solar masses (Schödel et al., 2014). The most studied example is the Milky Way, where the center of NSC is associated with the compact radio source of Sgr A* (see Eckart et al., 2017 for a review and references therein). Unlike the case of AGN, the present Sgr A* environment forms a diluted quasi-spherical Bondi-type inflow/outflow solution rather than a standard AGN accretion disk. In fact, based on the near-infrared studies, it appears that Milky Way's NSCs has undergone several episodic star-formation events triggered by an infall of molecular clouds. As a result, the system contains both early- and late-type stars of different masses. They are also expected to contain compact remnants, in particular, magnetized neutron stars that can efficiently interact with the ionized hot accretion flow in the inner $\sim 10^4 R_s$ (Zajaček et al., 2015; Karas et al., 2017).

In the further discussion, we focus on neutron stars and the typical length-scales of their magnetospheres in a mutual interaction with SMBH accretion flow. Let us consider the spin-down energy of neutron stars, which is in the dipole model related to the period, period derivative, and surface magnetic field intensity, $\dot{E} \propto \dot{P}/P^3$ and $\dot{E} \propto B^2 P^{-4}$. As a neutron star passes through the accretion flow, a stationary cavity is formed whose size R_{NS} is determined by the pressure equilibrium between the magnetospheric pressure P_{elmag} of a neutron star on one hand and the ram pressure P_{ram} , the combined gas and magnetic pressure on the other hand. The magnetic pressure of the accretion flow is a fraction δ of the gas pressure, $P_{\text{mag}} = \delta P_{\text{gas}}$, where $\delta \sim 0.1$ (Yuan et al., 2002). One can

thus write,

$$P_{\text{elmag}} = P_{\text{ram}} + P_{\text{gas}}(1 + \delta), \quad \frac{\dot{E}}{4\pi r^2 c} = \rho_a [v_{\text{rel}}^2 + (1 + \delta)c_s^2],$$

$$R_{\text{NS}}^2 = \frac{\dot{E}}{4\pi c \rho_a [v_{\text{rel}}^2 + (1 + \delta)c_s^2]}.$$
(1.1)

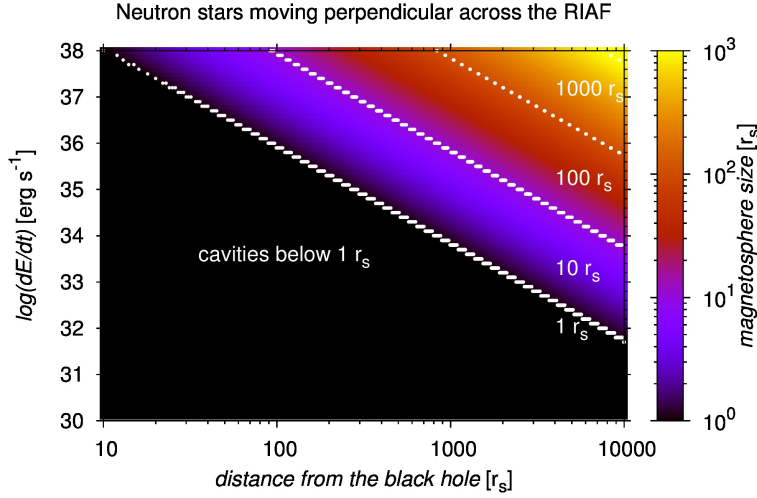


Figure 1. Typical length-scales of magnetospherical interaction of magnetized neutron stars calculated according to Eq. (1.1) as a function of the spin-down energy rate \dot{E} and the distance from the SMBH. For this calculation, neutron stars cross the RIAF solution of Sgr A* and move perpendicular to its motion.

For an exemplary calculation, we consider the density and the temperature profile of the radiatively inefficient accretion flow (RIAF) as inferred for Sgr A*. Neutron stars cross the RIAF perpendicular to its midplane with a Keplerian velocity at a given distance. The distribution of sizes of the neutron-star magnetospheres is plotted in Fig. 1 as a function of the spin-down energy and the distance from the SMBH. We obtain the scaling of magnetosphere sizes with the distance from Sgr A*, in which the typical length-scale of magnetospheres is approximately one order of magnitude smaller than the distance from the SMBH for $\log(\dot{E}[\text{erg s}^{-1}]) = 38$, e.g. $R_{\text{NS}} \approx 100 r_s$ at the distance of 1000 Schwarzschild radii. The length-scale R_{NS} from Eq. (1.1) also represents the typical scale of inhomogeneities of the global magnetic field of the RIAF caused by the population of neutron stars in galactic nuclei. We note that this length-scale is about four orders of magnitude smaller in the standard thin disc due to larger densities. However, since the hot corona is expected to be present beyond the thin disc midplane, a broad distribution of magnetosphere sizes is generally expected in the inner 10^3 Schwarzschild radii.

References

- Eckart, A., Hüttemann, A., Kiefer, C. et al. 2017, *Foundations of Physics*, 47, 553
Karas, V., Kopáček, O., Kunneriath, D. et al. 2017, *CoSka*, 47, 124
Schödel, R., Feldmeier, A., Neumayer, N. et al. 2014, *CQG*, 31, id. 244007
Yuan, F., Markoff, S., and Falcke, H. 2002, *A&A*, 383, 854
Zajaček, M., Karas, V., and Kunneriath, D. 2015, *Acta Polytechnica*, 55, 203

Variability of magnetically-dominated jets in blazars and gamma ray bursts

Agnieszka Janiuk¹, Jeremy Mortier¹ and Konstantinos Sapountzis¹

¹Center for Theoretical Physics,
Polish Academy of Sciences, Al. Lotnikow 32/46, 02-668 Warsaw, Poland
email: agnes@cft.edu.pl

Abstract. The fastly variable accretion flows are found in a number of different types of astrophysical black hole sources. At largest scales, they are present in the cores of active galaxies. In the radio-loud objects, such as blazars, the variability of the inflow can be transmitted to the outflow properties. In these sources, the relativistic jets are pointing to our line of sight. In addition, many similarities are found between the jet physics in blazars and in gamma ray bursts. The latter are observed from extragalactic distances, but operate at smaller scales, within the stellar-mass accreting black holes and in collapsing star's environment. Observational studies have shown an anti-correlation between minimum variability time scale and Lorentz factor of the emitted jet. Motivated by those observational properties of black hole sources, we investigate the accretion inflow and outflow properties, by means of numerical GR MHD simulations.

Keywords. accretion, accretion disks, black hole physics, magnetic fields, hydrodynamics, MHD, gamma rays: bursts, galaxies: jets

1. Introduction

Blazars and gamma ray bursts share the properties of their jets, despite different Lorentz factors and accreting black hole masses (Wu et al. 2015). Launching and collimation mechanisms are common: thick disk or corona, pressure gradient in surrounding wall, external (matter dominated) jet, or toroidal magnetic field. Acceleration of jets occurs due to both magnetic field action field and accretion disk rotation (see Fragile 2008 for a review). The blazar jets are Poynting-dominated, and powered by the Blandford-Znajek mechanism which can extract energy from a rotating black hole. This mechanism is now well known and tested in the purpose of a jet launching, but observations are showing variability in the jet emission. Multiple shocks that collide in the jet, can lead to multiple emission episodes and can account for the fluctuating light curve. A reasonable interpretation of this effect is that the variability observed in the jets can directly reflect the central engine variability. The latter is tightly related to the action of magnetic fields in the center of the galaxy.

We present here the two-dimensional magneto-hydrodynamical models computed in full General Relativity (GR MHD). The numerical scheme is our implementation of the code HARM (Gammie et al. 2003, Janiuk et al. 2013). The properties of magnetic fields and their role in evolution in the flows are studied in detail. Our initial condition assumes the existence of a pressure equilibrium torus, embedded in the poloidal magnetic field which lines follow the isocontours of constant density (Fig. 1 left and middle panel). The Kerr black hole accretes matter from the torus, and the rotation affects the magnetic field evolution. The models are parameterized with the black hole spin, and the initial magnetization of the matter. Code works in GR framework, so dimensionless units are adopted, with $G = c = M = 1$. Hence, geometrical time is given as $t = GM/c^3$, where

M is the black hole mass. In this way, we are able to model the launching and variability of jets in both supermassive black hole environment, and in gamma ray bursts.

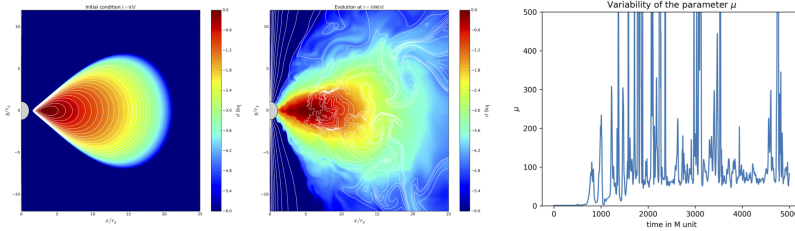


Figure 1. Left: initial configuration of the simulation (logarithm of density, in the code units). Middle: evolved state, after 1000 geometrical time units. Right: Variability of the μ parameter in time.

2. Variability of the jet

Energetic parameter. Variable energy output reflects the MRI instability timescale, which is well resolved through the adequate number of grid cells per MRI wavelength. The total plasma energy flux is given by parameter $\mu = -T_t^r / \rho u^r$. If the Poynting and thermal energy are fully transformed to bulk kinetic, the parameter μ can be interpreted as the Lorentz factor at infinity (Vlahakis & Koenigl 2003). Its value depends on location in the jet.

Correlation between Lorentz factor and minimum variability time scale. The minimum variability timescale, MTS, can be anti-correlated with the bulk Lorentz factor in the jet, if the magnetically arrested (MAD) flow is considered (Lloyd-Ronning et al. 2018). However, in the MAD mode, the flux accumulated at the BH horizon, and the interchange instability rather than MRI governs the minimum timescale of variability. In our simulation the accretion is not in a MAD state, and the Lorentz factor at infinity is given by the μ parameter. Its variability correlates with MRI timescale, interpreted in our model as the origin of the variability in the jet (Fig. 1 right panel).

3. Conclusions

The variable energy output from the central engine implies the varying jet Lorentz factor, which may lead to occurrence of internal shocks, and affect both GRBs and blazars observed variability. Unification of the models across the black hole mass scale, from GRBs to blazars, is not straightforward though. The most uncertain aspect is whether the MAD state drives the jets in both type of sources, or rather halts the GRB emission.

Acknowledgment This work is supported by the grants UMO-2016/23/B/ST9/03114 from the Polish National Science Center and GB 70-4 from the Interdisciplinary Center for Mathematical Modeling

References

- Gammie C.F., McKinney J.C., Toth G. 2003, *ApJ*, 589, 444
 Janiuk, A., Mioduszewski, P., & Moscibrodzka, M. 2013, *ApJ*, 776, 105
 Vlahakis, N., & Koenigl, A. 2003, *ApJ*, 596, 1080
 Fragile, P.C. 2008, *Proceedings of Science*, vol. 39, “Microquasars and Beyond”
 Wu, Q., Zhang B., Lei W.-H., Zou Y.-C., Liang E.-W., Cao X. 2015, *MNRAS*, 455, L1
 Lloyd-Ronning, N., Lei W.-H., Xie, W. 2018, *MNRAS*, 478, 3525

Magnetic Fields and Cosmic Ray Diffusion in M 31

Rainer Beck¹ and Elly M. Berkhuijsen¹

¹ Max-Planck-Institut für Radioastronomie, Auf dem Hügel 69, 53121 Bonn, Germany
email: rbeck@mpifr-bonn.mpg.de

Abstract. Three new, deep radio continuum surveys of the Andromeda galaxy M 31 have been performed with the Effelsberg 100-m telescope. The high degrees of polarization show that the magnetic field in M 31 is exceptionally ordered because an efficient large-scale dynamo operates due to the strong differential rotation and the low star-formation rate. A regular axisymmetric spiral field dominates, indicating that the dynamo operates in its ground mode.

Keywords. galaxies: spiral, galaxies: individual: M 31, galaxies: magnetic fields, cosmic rays

1. Introduction

Synchrotron radio emission is the best tool to study cosmic magnetic fields. The intensity is a measure of field strength, its linear polarization is a signature of ordered fields, and the polarization angle gives the field orientation in the sky plane. Faraday rotation of the polarization angle depends on the square of wavelength, the density of thermal electrons, and the strength of the regular field component along the line of sight; the sign of the Faraday rotation gives the field direction. Ordered fields generated by a large-scale (α - Ω) dynamo reveal a coherent direction and are called regular fields (see Beck 2016 for a review).

The radio emission and magnetic field properties of M 31 have been studied extensively with the Effelsberg 100-m and VLA radio telescopes (e.g. Beck 1982, Berkhuijsen et al. 2003, Fletcher et al. 2004). The polarization and Faraday rotation data, derived from polarization surveys at 6 cm, 11 cm and 20 cm wavelengths, can be well described by a regular magnetic field with an axisymmetric spiral pattern. Such a field is a strong indication of the lowest mode excited by a large-scale dynamo (e.g. Beck et al. 1996). M 31 is the prototype of a dynamo-generated magnetic field.

Polarized emission from strongly inclined galaxies like M 31 at wavelengths of ≥ 6 cm suffers from Faraday depolarization along the line of sight through the disk. Hence,

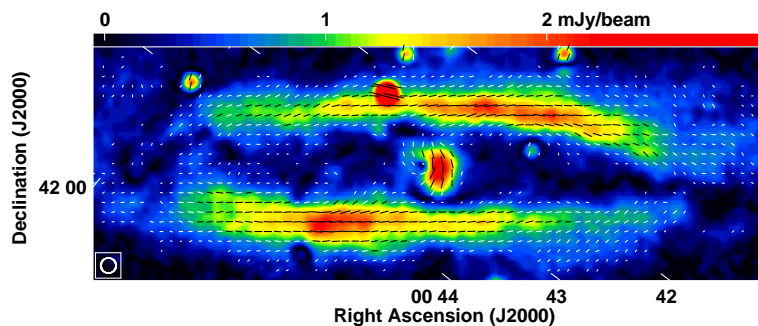


Figure 1. Polarized intensity at 6.2 cm and B-vectors, corrected for Faraday rotation, at $2.6'$ resolution. The degree of polarization reaches 50% in the ring (from Gießübel 2012).

Table 1. New radio continuum surveys conducted with the Effelsberg 100-m telescope.

Central freq. (GHz)	Bandwidth (GHz)	Wavelength (cm)	Resolution ($'$)	Map size ($'$)	Principle investigator
2.64	80	11.4	4.4	196 x 92	Mulcahy (2011)
4.85	300	6.2	2.6	140 x 80	Gießübel (2012)
8.35	1100	3.6	1.4	116 x 40	Gießübel (2012)

observations at shorter wavelengths are needed, which would also provide higher angular resolution. Furthermore, the extension of magnetic fields into the outer disk and halo can be investigated by new surveys with higher sensitivity.

2. New Effelsberg surveys of M 31

Three deep radio continuum surveys of total and linearly polarized emission from M 31 have been conducted in recent years with the Effelsberg telescope (Table 1). At all wavelengths, the total and polarized emission is concentrated in a ring-like structure between about 7 kpc and 13 kpc radius from the center. Diffusion of cosmic rays away from star-forming regions is evident: The ring of synchrotron emission is wider than the ring of the thermal radio emission and the radial scale length of synchrotron emission is larger than that of thermal emission. The diffusion length along the ring, parallel to the disk, is $\simeq 1.5$ kpc and the diffusion coefficient is $D_E \simeq 2 \cdot 10^{28} \text{ cm}^2 \text{ s}^{-1}$. Since M 31 has only a thin radio disk, D_E perpendicular to the disk is smaller by about a factor of 10.

Fig. 1 shows the polarized emission at 6.2 cm with the magnetic field orientations nicely following the ring. RM varies systematically along the ring (Fig. 2). The analysis shows a sinusoidal variation with azimuthal angle along the ring. The phase offset of $7^\circ \pm 1^\circ$ is due to the spiral pitch angle and the RM offset of $-125 \pm 2 \text{ rad/m}^2$ originates in the Galactic foreground. The amplitude of $108 \pm 5 \text{ rad/m}^2$ is a clear signature of an axisymmetric regular magnetic field, confirming the previous results derived from RMs at longer wavelengths (Berkhuijsen et al. 2003). The amplitude is about 10% larger than previously measured, indicating that Faraday depolarization affected the previous data.

References

- Beck, R. 1982, *A&A*, 106, 121
 Beck, R. 2016, *A&A Rev*, 24:4
 Beck, R., Brandenburg, A., Moss, D., Shukurov, A., Sokoloff, D. 1996, *ARAA*, 34, 155
 Berkhuijsen, E.M., Beck, R., & Hoernes, P. 2003, *A&A*, 398, 937
 Fletcher, A., Berkhuijsen, E.M., Beck, R., & Shukurov, A. 2004, *A&A*, 414, 53
 Gießübel, R. 2012, PhD Thesis, University of Cologne
 Mulcahy, D. 2011, MSc Thesis, University of Bonn

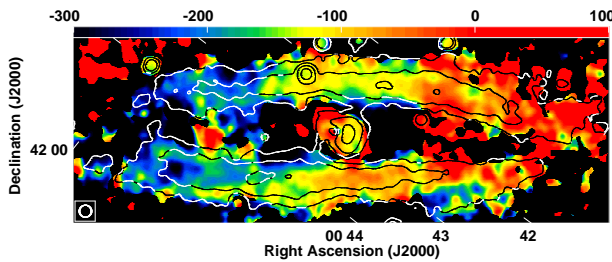


Figure 2. Faraday rotation measures (RM, in rad/m^2), derived from the new surveys at 3.6 cm and 6.2 cm, at $2.6'$ resolution. Contours show the polarized intensity at 6.2 cm.

Reliable detection and characterization of low-frequency polarized sources in the LOFAR M 51 field

C. Horellou¹, A. Neld¹, D.D. Mulcahy^{2,3}, R. Beck³, S. Bourke¹,
T.D. Carozzi¹, K.T. Chyży⁴, J.E. Conway¹, J.S. Farnes⁵, A. Fletcher⁶,
M. Haverkorn⁵, G. Heald^{7,9}, A. Horneffer¹, B. Nikiel-Wroczyński⁴,
R. Paladino⁸, S.S. Sridhar⁹, C.L. Van Eck⁵

¹Chalmers Univ. of Technology, Dept of Space, Earth and Environment, 43992 Onsala, Sweden

²Jodrell Bank Centre for Astrophysics, Oxford Road, Manchester, M13 9PL, U.K.

³Max-Planck-Institut für Radioastronomie, Auf dem Hügel 69, 53121, Bonn, Germany

⁴Astronomical Observatory, Jagiellonian University, ul. Orla 171, 30-244 Kraków, Poland

⁵Dept of Astrophysics/IMAPP, Radboud Univ., PO Box 9010, 6500 GL, Nijmegen, NL

⁶School of Mathematics and Statistics, Newcastle Univ., Newcastle upon Tyne NE1 7RU, U.K.

⁷CSIRO Astronomy and Space Science, 26 Dick Perry Ave, Kensington, WA 6151, Australia

⁸INAF-Osservatorio di Radioastronomia, Via P. Gobetti, 101 I-40129 Bologna, Italy

⁹Kapteyn Astronomical Institute, Univ. of Groningen, Postbus 800, 9700 AV Groningen, NL

Abstract. We present a new source-finding algorithm for linearly polarized sources that we developed and applied to LOFAR data of the M 51 field. The reader is referred to a recently published paper by Neld et al. 2018 for more information.

Keywords. polarization – radio continuum: galaxies – galaxies: magnetic fields – galaxies: individual : M 51 – methods: data analysis – techniques: polarimetric

We have developed a computationally efficient and rigorously defined source-finding algorithm for linearly polarized sources. As the Square Kilometre Array (SKA) approaches completion, it is important to have tools to process large radio continuum datasets and extract reliable polarization information. Polarized extragalactic radio sources are interesting in their own right, and also as background sources to probe the magneto-ionized medium along their lines of sight via Faraday rotation, forming a dense Rotation Measure (RM) grid (e.g. Beck & Gaensler 2004).

We used a calibrated data set from the LOw Frequency ARray (LOFAR) at 150 MHz centered on the nearby galaxy M 51 to search for polarized background sources. The data have been presented earlier along with an analysis of a high-quality 150 MHz radio continuum image of the M 51 galaxy and a first investigation of background polarized sources in the field (Mulcahy et al. 2014). With a new imaging software, we re-imaged the field at a resolution of $18'' \times 15''$ and cataloged a total of about 3000 continuum sources within 2.5° of the center of M 51. We made small Stokes Q and U images centered on each source brighter than 100 mJy in total intensity (201 sources) and used RM synthesis to create corresponding Faraday cubes that were analyzed individually. For each source, the noise distribution function was determined from a subset of the measurements at high Faraday depths where no polarization is expected; the peaks in polarized intensity in the Faraday spectrum were identified and the p -value of each source was calculated. Finally, the false discovery rate method was applied to the list of p -values to produce a list of polarized sources and quantify the reliability of the detections. We also analyzed

sources fainter than 100 mJy but that were reported as polarized in the literature at at least another radio frequency.

Of the 201 sources that were searched for polarization, six polarized sources were detected confidently (with a false discovery rate of 5%). This corresponds to a number density of one polarized source per 3.3 square degrees, or 0.3 source per square degree. Increasing the false discovery rate to 50% yields 19 sources. A majority of the sources have a morphology that is indicative of them being double-lobed radio galaxies, and the ones with redshift measurements from the literature have $0.5 < z < 1.0$. An example is shown in Fig. 1.

In the future, we intend to develop the code further and apply it to larger data sets such as the LOFAR Two-meter Survey of the whole northern sky, LoTSS (Shimwell et al. 2017), and the ongoing deep LOFAR observations of the GOODS-North field. A recent analysis of the first data release region of LoTSS (570 square degrees) at 4.3' resolution resulted in a preliminary catalog of 92 polarized sources (Van Eck et al. 2018); only one polarized source was identified in the M 51 field, while the work presented here yielded six secure detections. This demonstrates that the number of discovered polarized sources at low frequency should increase significantly when the data are imaged at higher angular resolution and new techniques are applied to extract the faint polarized signal.

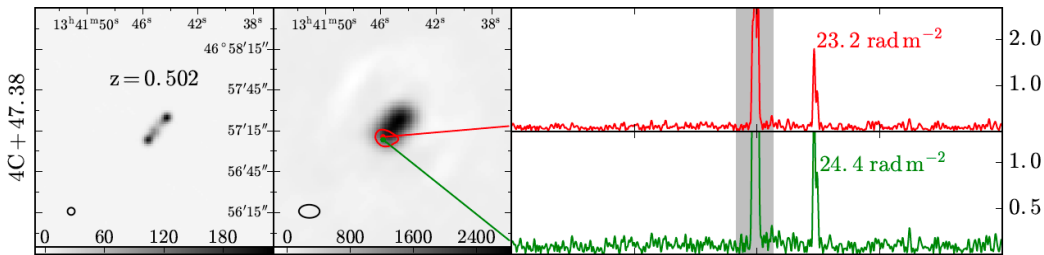


Figure 1. Example of a source (a double-lobed radio galaxy) at redshift $z = 0.502$ detected in polarization in the LOFAR 150 MHz data with a 5% false discovery rate (Neld et al. 2018). *Left column:* $3' \times 3'$ VLA FIRST 1.4 GHz images ($5''$ resolution; Becker et al. 1995). *Middle column:* $3' \times 3'$ LOFAR 150 MHz image ($18'' \times 15''$ resolution). The synthesized beams of the images are displayed in the bottom left corners. *Right column:* The red and green colors are used to show Faraday spectra at two nearby locations in the source. The x -axis (Faraday depth, ϕ) ranges from -100 to $+100 \text{ rad m}^{-2}$. The y -axis shows the polarized intensity in $\text{mJy beam}^{-1} \text{ rmsf}^{-1}$. The grey shading around $\phi = 0$ shows the region of instrumental polarization that was excluded from the analysis.

References

- Beck, R. & Gaensler, B. M. 2004, *New Astronomy Reviews*, 48, 1289
 Becker, R. H., White, R. L., & Helfand, D. J. 1995, *ApJ*, 450, 559
 Mulcahy, D. D., Horneffer, A., Beck, R., et al. 2014, *A&A*, 568, A74
 Neld, A., Horellou, C., Mulcahy, D. D., et al. 2018, *A&A*, 617, A136
 Shimwell, T. W., Röttgering, H. J. A., Best, P. N., et al. 2017, *A&A*, 598, A104
 Van Eck, C. L., Haverkorn, M., Alves, M. I. R., et al. 2018, *A&A*, 613, A58

The evolution of large scale magnetic fields in spiral galaxies

Luiz Felipe S. Rodrigues,¹ Luke Chamandy,^{2,3,4} Anvar Shukurov,¹
Carlton M. Baugh⁵ and A. Russ Taylor^{3,4}

¹School of Mathematics, Statistics and Physics, University of Newcastle,
Newcastle upon Tyne, NE1 7RU, UK
email: luiz.rodriques@newcastle.ac.uk

²Department of Physics and Astronomy, University of Rochester, 454 Bausch & Lomb Hall,
Rochester, NY, 14627-0171, USA

³Astronomy Department, University of Cape Town, Rondebosch 7701,
Republic of South Africa

⁴Department of Physics, University of the Western Cape, Belleville 7535,
Republic of South Africa

⁵Institute for Computational Cosmology, Department of Physics, University of Durham,
South Road, Durham, DH1 3LE, UK

Abstract. We investigate how the large scale magnetic fields in the discs of spiral galaxies evolve through cosmic time. To do this, we couple the galaxy properties computed by a semi-analytic model of galaxy formation to the mean field dynamo equations. These are solved numerically as a function of time and galactocentric radius for a thin disc using the no-z approximation, with imposed axial symmetry, and the dynamical quenching non-linearity. A simple prescription for the evolution of the random (small-scale) magnetic field component and its relation with the mean (large-scale) component is adopted. This allows us to compute radial and time dependent properties of the interstellar medium of discs for a statistical sample of galaxies from $z \sim 7$ until the present. We compute the distribution of the typical magnetic field strength at different redshifts and the dependence of these on galaxy mass. We examine the evolution of the growth rate of the mean disc magnetic fields of galaxies and discuss the steady state assumption. Finally, we analyse what is the sensitivity of our results to specific assumptions and to the galaxy formation model.

Keywords. galaxies: magnetic fields – dynamo – galaxies: evolution – galaxies: spiral

1. Introduction

The Square Kilometre Array and other forthcoming large radio telescopes will significantly increase the number and level of detail of observations of magnetic fields in galaxies, as well as their redshift evolution (e.g. [Taylor et al. 2015](#)). To be able to use these data to constrain both galaxy evolution models and galactic dynamo theory, it is necessary to have dynamo models which account for the variability of galaxies through time and predict the magnetic fields for a statistical sample of galaxies. We developed a framework – thoroughly described in [Rodrigues et al. \(2018\)](#) – to compute magnetic properties of spiral galaxies accounting for the formation history of individual galaxies computed by two versions the GALFORM semi-analytic galaxy formation model ([Lacey et al. 2016](#), [Gonzalez-Perez et al. 2014](#)).

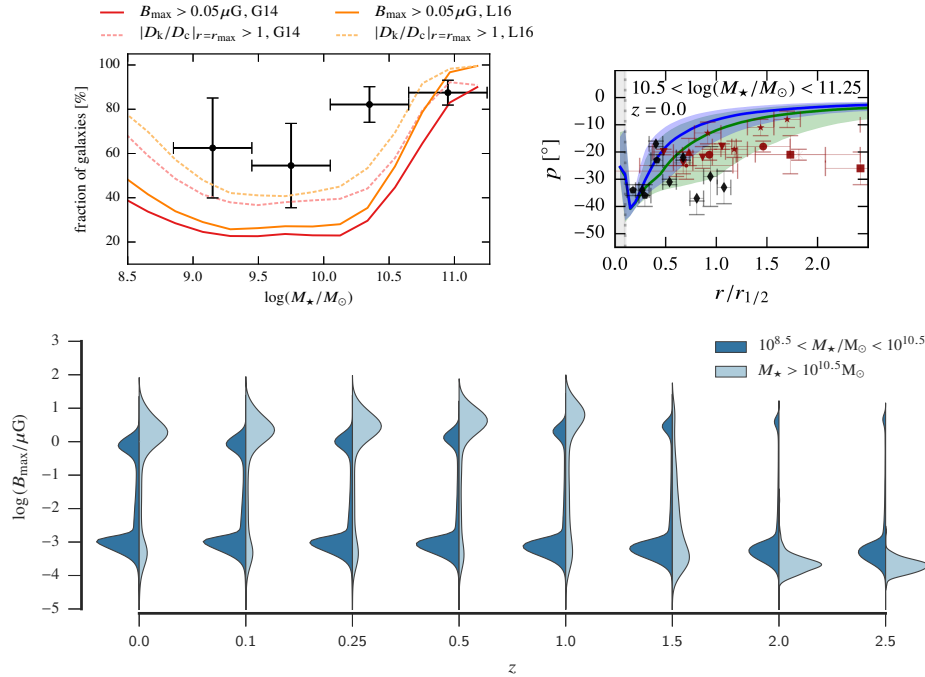


Figure 1. *Top-left.* The mass dependence of the fraction of galaxies containing non-negligible maximum magnetic field strength, $B_{\max} > 0.05 \mu\text{G}$. The black circles with error bars show the fraction of observed galaxies containing large-scale magnetic fields in the compilation of Beck & Wielebinski (2013) and stellar mass data from the S4G catalogue and other sources. *Top-right.* Comparison of the predicted pitch angle profiles of massive galaxies with observations in units of half mass radius, $r_{1/2}$. The blue and green curves show the median pitch angles predicted by the L16 and G14 models, respectively. The shaded areas show the intervals between 15 and 85 percentiles. Points with error bars show observational estimates (Chamandy et al. 2016). *Bottom.* Redshift evolution of the probability density of the maximum large-scale magnetic field strength of spiral galaxies for the L16 model, selected in two stellar mass bins at each redshift.

2. Results

We found that a significant fraction of the galaxies possess no large-scale magnetic field and that this depends on the mass of the galaxy, with a minimum close to $M_* = 10^{10} M_\odot$ (top-left panel in Fig. 1). We find broad agreement with observational data for pitch angle in nearby galaxies (Fig. 1, top-right). The fraction of galaxies containing large-scale magnetic fields decreases with redshift; however if only galaxies which contain significant large-scale magnetic fields are selected ($B \gtrsim 0.1 \mu\text{G}$), the typical field strength increases rapidly with redshift.

Acknowledgements

LFSR and AS acknowledge financial support of STFC (ST/N000900/1, Project 2).

References

- Beck R., Wielebinski R., 2013, *Magnetic Fields in Galaxies*. p. 641, arXiv:1302.5663v6
 Chamandy L., 2016, *MNRAS*, 462, 4402
 Gonzalez-Perez V., et al., 2014, *MNRAS* 439, 264 (G14)
 Lacey C. G., et al., 2016, *MNRAS*, 462, 3854 (L16)
 Rodrigues L. F. S., et al. 2018, *MNRAS* submitted, arXiv:1809.10521
 Taylor R., et al., 2015, *Advancing Astrophysics with the SKA (AASKA14)*, p. 113

The supernova-regulated ISM. Space- and time-correlations

J. F. Hollins¹, G. R. Sarson¹, A. Shukurov¹, A. Fletcher¹ and F. A. Gent²

¹School of Mathematics, Statistics and Physics, Newcastle University, Newcastle upon Tyne, NE1 7RU, UK

²ReSoLVE Centre of Excellence, Department of Computer Science, Aalto University, PO Box 15400, FI-00076 Aalto, Finland

email: j.hollins@newcastle.ac.uk (JFH), graeme.sarson@newcastle.ac.uk (GRS),
anvar.shukurov@newcastle.ac.uk (AS), andrew.fletcher@newcastle.ac.uk (AF),
frederick.gent@aalto.fi (FAG)

Abstract. We apply correlation analysis to determine the correlation lengths of the turbulent magnetic, density and velocity fields in numerical simulations of the Interstellar Medium (ISM). The simulations solve the magnetohydrodynamic (MHD) equations in a shearing, Cartesian box, driven by supernova (SN) explosions. We also estimate the correlation time of our simulations and investigate the anisotropy of the random magnetic field.

Keywords. Galaxies: ISM, ISM: kinematics and dynamics, ISM: magnetic fields, turbulence

1. Introduction

The interstellar medium of a spiral galaxy is a complex, multiphase, random system, driven by the input of thermal and kinetic energy from supernova explosions (SNe) and stellar winds. Statistical analysis of the ISM is complicated by its multi-phase structure: statistical parameters of the ISM vary strongly between the phases. This paper is a summary of the work detailed in Hollins et al. (2017).

2. A Numerical Model of the Multiphase ISM

Our analysis uses data from simulations of the multi-phase ISM based on the Pencil Code (<http://pencil-code.nordita.org/>). These simulations solve the full, compressible MHD equations in a shearing, Cartesian box $1 \times 1 \times 2.2 \text{ kpc}^3$ in size, with a numerical resolution of $\Delta x = 4 \text{ pc}$. The parameters used are those typical of the Solar neighbourhood. Further details are provided in Gent et al. (2013a) and Gent et al. (2013b).

We consider the gas number density fluctuations, n' , and the magnitudes of the random velocity, u' , and random magnetic field, b . We also consider the Cartesian components of the random magnetic field \mathbf{b} . Our analysis focuses on the warm phase of the ISM, which occupies most of the domain (between 80 and 90% of the volume). We also perform calculations in the whole domain to investigate the importance of separating into phases.

3. The Integral and Temporal Scales

Reliable results are obtained for the spatial correlation functions, as shown in Figure 1. The results for n' and b in the both warm phase and where no phase separation is applied are very similar. Thus, the correlation statistics for both n' and b are most

Table 1. The correlation lengths of the fluctuations in gas density, speed and magnetic field for the warm gas and for the total gas at the mid-plane $z = 0$ and $|z| = 400$ pc.

	$ z $ [pc]	l_0 [pc]		
		n'	u'	b
Warm phase	0	53 ± 5	60 ± 3	44 ± 2
	400	37 ± 2	87 ± 3	64 ± 2
No phase separation	0	44 ± 2	74 ± 2	51 ± 1
	400	37 ± 2	117 ± 3	66 ± 1

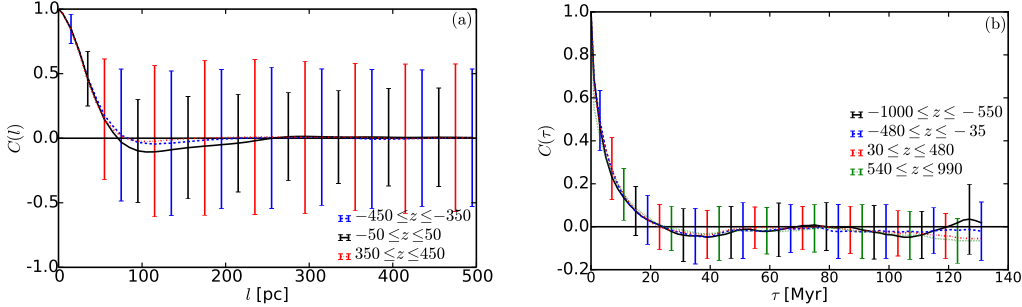


Figure 1. (a) The spatial correlation functions for n' in the warm gas, averaged about $z = -400$ pc (blue, dashed), 0 pc (black, solid), and 400 pc (red, dash-dotted), and (b) the time correlation functions of u' , averaged in layers $-1000 \leq z \leq -550$ pc (black, solid), $-480 \leq z \leq -35$ pc (blue, dashed), $30 \leq z \leq 480$ pc (red, dash-dotted), and $540 \leq z \leq 990$ pc (green, dotted). The error bars denote scatter about the mean.

strongly influenced by the behaviour of these fields in the warm phase. For the non phase-separated u' , the root-mean-square (rms) velocity is roughly 1.5 larger than for the warm phase and the correlation length, l_0 , is roughly 15–30 pc greater at each height, suggesting the hot phase has a larger impact on the correlation statistics for u' .

The correlation time of our simulations, computed from the correlation functions in Figure 1(b), is approximately $\tau_0 = 5$ Myr throughout the domain. We calculate the eddy turnover time using l_0 and the rms value for u' in the warm phase. At the mid-plane, $\tau_{\text{eddy}} \approx 8$ Myr. Thus, τ_{eddy} is a reasonable estimate of τ_0 .

The standard deviations of the turbulent magnetic field components $b_x/b_y/b_z$ have approximate ratios 0.5/0.6/0.6 in the mid-plane, suggesting mild anisotropy in the random magnetic field. The enhanced azimuthal (y) component is a result of the large-scale velocity shear due to differential rotation. The vertical (z) component is amplified beyond isotropy by the stretching of the horizontal magnetic field by the vertical velocity u_z . The polarisation degree of the synchrotron emission due to this level of anisotropy in the random magnetic field, is approximately 15%.

References

- Gent F. A., Shukurov A., Fletcher A., Sarson G. R., Mantere M. J., *MNRAS*, 432, 1396–1423, 2013a
 Gent F. A., Shukurov A., Sarson G. R., Fletcher A., Mantere M. J., *MNRAS*, 430, L40–L44, 2013b
 Hollins J. F., Sarson G. R., Shukurov A., Fletcher A., Gent, F. A., *ApJ*, 850, 4, 2017

Magnetic field effects on the ISM structure and galactic outflows

A. Shukurov¹, C. C. Evirgen¹, A. Fletcher¹, P. J. Bushby¹ and
F. A. Gent²

¹School of Mathematics, Statistics and Physics, Newcastle University, Newcastle upon Tyne,
NE1 7RU, U.K.

emails: anvar.shukurov@ncl.ac.uk (AS), c.c.evirgen@ncl.ac.uk (CCE),
andrew.fletcher@ncl.ac.uk (AF), paul.bushby@ncl.ac.uk (PJB)

²Department of Computer Science, Aalto University, Otaniemi, ESPOO, Finland
email: frederick.gent@aalto.fi

Abstract. The role of magnetic fields in the multi-phase interstellar medium (ISM) is explored using magnetohydrodynamic (MHD) simulations that include energy injection by supernova (SN) explosions and allow for dynamo action. Apart from providing additional pressure support of the gas layer, magnetic fields reduce the density contrast between the warm and hot gas phases and quench galactic outflows. A dynamo-generated, self-consistent large-scale magnetic field affects the ISM differently from an artificially imposed, unidirectional magnetic field.

Keywords. MHD, ISM: kinematics and dynamics, ISM: magnetic fields, ISM: structure, ISM: jets and outflows, galaxies: ISM, galaxies: magnetic fields, galaxies: spiral

Our understanding of global magnetic effects in spiral galaxies remains limited despite a growing appreciation of their significance. Of particular importance is the role of magnetic fields (and of the cosmic rays controlled by them) in galactic outflows and the resulting feedback of star formation on galactic evolution. Studies of magnetic effects in the ISM are hindered by its complex, multi-phase structure and by the complexity of the conversions between kinetic and magnetic energies in random flows (addressed by dynamo theory). Furthermore, observational estimates of magnetic field strength are restricted to the warm and cold ISM phases whereas galactic outflows are driven by the hot gas.

Simulations of the SN-driven ISM have reached a sufficient level of physical adequacy to use them as numerical experiments to explore various effects inaccessible to direct observations. Among such simulations, only a few contain the ingredients (especially differential rotation and stratification) required to simulate large-scale dynamo action (Gressel *et al.* 2008, Gent *et al.* 2013).

We analyse a numerical model of the local ISM, developed by Gent *et al.* (2013), that produces an exponentially growing magnetic field at a scale comparable to the size of the computational domain (1 kpc), starting from a dynamically negligible seed magnetic field and reaching a statistically steady state where magnetic, random kinetic and thermal energy densities are comparable in magnitude. The ISM is represented in three phases separated in terms of specific entropy (or density and temperature) while magnetic field consists of both the mean and fluctuating parts. The SN activity supports a systematic outflow away from the mid-plane. Comparing the ISM properties in the initial and late stages, where magnetic fields are, respectively, negligible and dynamically significant, we can assess the role of magnetic fields in the structure and properties of the ISM. Both stages represent statistically steady states without and with magnetic field, respectively. The most significant magnetic effects are as follows (Evirgen *et al.* 2018).

Table 1. Fits to the outflow speed, of the form (1), at various distances $|z|$ from the mid-plane.

Distance to the mid-plane [kpc]	V_0 [km s $^{-1}$]	ξ	n
$ z < 0.15$	11	4.4	2.7
$0.15 < z < 0.3$	17	2.4	2.4
$0.3 < z < 0.6$	17	3.9	1.9
$0.6 < z < 1.0$	11	2.5	1.5

The multi-phase structure. In agreement with the topological analysis of Makarenko *et al.* (2018), we show that strong local magnetic fields efficiently confine SN remnants, leading to a lower fractional volume of the hot gas (decreasing from 25% to 9% near the mid-plane as magnetic field grows), its lower temperature and higher density (by a factor of 3–10), whereas the total mass of the hot gas varies little. As a result, the density contrast between the warm and hot phases is reduced by almost an order of magnitude.

Outflow speed. As the magnetic field grows, the mean speed of the systematic gas outflow V_z away from the mid-plane decreases from about 20 km s $^{-1}$ for a weak magnetic field to just a few km s $^{-1}$ when magnetic field becomes strong. The decrease is rather abrupt: V_z is only weakly dependent upon the magnetic field when the mean magnetic field B is weaker than that corresponding to energy equipartition with the random gas flow, $B_{\text{eq}} = (4\pi\rho v^2)^{1/2}$, where ρ is the gas mass density and v the root-mean-square random speed. However, it then decreases as a rather high power of B ,

$$V_z \simeq V_0 [1 + \xi(B/B_{\text{eq}})^n]^{-1}, \quad (1)$$

with the values of V_0 , ξ and n given in Table 1. In similar simulations, Bendre *et al.* (2015) also find that the outflow is suppressed by the large-scale magnetic field although they find a weaker dependence of V_z on B with $n = 2$ (and $V_0 \approx 13$ km s $^{-1}$ and $\xi \approx 1.5$ at $|z| = 0.8$ kpc). The value of V_0 depends on the supernova rate ν ; Bendre *et al.* (2015) find $V_0 \propto \nu^{0.4}$. We note that the value of V_0 at large $|z|$ is likely to be sensitive to the size of the computational domain: simulations of Bendre *et al.* (2015) in $|z| \leq 2$ kpc find larger values of V_z at $|z| \simeq 1$ kpc than in our model where $|z| \leq 1$ kpc.

The importance of dynamo action. The sensitivity of the ISM structure and outflow speed to magnetic field is only obtained in simulations that admit large-scale dynamo action (Bendre *et al.* 2015, Evirgen *et al.* 2018). Broadly similar simulations where dynamo action is precluded and a unidirectional magnetic field is imposed (e.g., de Avillez & Breitschwerdt 2005, Henley *et al.* 2015, Girichidis *et al.* 2016) do not reveal any similar magnetic effects. This contradiction requires careful analysis; it suggests rather strongly that dynamo action that produces a large-scale magnetic field responding *self-consistently* to the ISM environment is essential to capture reliably magnetic effects on the ISM.

References

- Bendre, A., Gressel, O., & Elstner, D. 2015, *AN*, 336, 991
de Avillez, M. A., & Breitschwerdt, D. 2005, *A&A*, 436, 585
Evirgen, C. C., Gent, F. A., Shukurov, A., Fletcher, A., & Bushby, P. 2018, *MNRAS*, submitted
Gent, F. A., Shukurov, A., Fletcher, A., Sarson, G. R., & Mantere, M. J. 2013, *MNRAS*, 432, 1396
Girichidis, P., Walch, S., Naab, T., Gatto, A., Wünsch, R., Glover, S. C. O., Klessen, R. S., Clark, P. C., Peters, T., Derigs, D., & Baczynski, C. 2016, *MNRAS*, 456, 432
Gressel, O., Elstner, D., Ziegler, U., & Rüdiger, G. 2008, *A&A*, 486, L35
Henley, D. B., Shelton, R. L., Kwak, K., Hill, A. S., & Mac Low, M.-M. 2015, *ApJ*, 800, id. 102
Makarenko, I., Shukurov, A., Henderson, R., Rodrigues, L. F. S., Bushby, P., & Fletcher, A. 2018, *MNRAS*, 475, 1843

Magnetic fields and CR propagation in the halos of spiral galaxies

Marita Krause¹, Silvia C. Mora-Partiarroyo¹ and Philip Schmidt¹

¹Max-Planck-Institut für Radioastronomie,
Auf dem Hügel 69, D-53121 Bonn, Germany
email: mkrause@mpifr-bonn.mpg.de

Abstract. With CHANG-ES, the Continuum HALos in Nearby Galaxies – an EVLA Survey, we detected for the first time large-scale magnetic fields in the halos of nearby edge-on spiral galaxies. We further determined in a consistent way the vertical radio scale heights of a subsample of 13 spiral galaxies, as a crucial parameter to understand the CR propagation in the halo. Our sample galaxies are consistent with advective CR propagation and we concluded that galactic winds are a widespread phenomenon in spiral galaxies. We discovered a tight correlation of the normalized scale heights with the mass surface density, giving the first observational evidence for a gravitational effect on the CR outflow.

Keywords. galaxies: spiral, galaxies: halos, galaxies: magnetic fields, radio continuum: galaxies

1. Regular magnetic fields in the halo

The magnetic field B in spiral galaxies is usually a composition of a small-scale (up to several 10 pc) random component, an ordered component, and a large-scale regular ($\gtrsim 1$ kpc) component. The ordered component may be the result of compression/shearing of the random component, yielding polarized intensity, however no significant net Faraday rotation along the line of sight. Only the detection of a smooth pattern over several beam sizes in the rotation measure RM is a clear sign of a regular large-scale magnetic field. The sign of the RM (or Faraday depth in case of RM synthesis) gives directly the magnetic field direction along the line of sight.

Usually, the large-scale magnetic field B_{reg} in the disk of a spiral galaxy is an axisymmetric spiral magnetic field (ASS) along the disk (as observed in face-on galaxies) which is thought to be generated by an $\alpha - \omega$ dynamo. In the halo of edge-on galaxies vertical and X-shaped magnetic fields are observed in linear polarization. Only the analysis of the RM pattern in the halo can give information about a possible regular magnetic field there, which is now for the first time revealed by the CHANG-ES observations.

CHANG-ES is a radio continuum and polarization survey of 35 nearby spiral galaxies seen edge-on, performed with the EVLA in C-band (5 - 7 GHz) and L-band (1.3 - 1.9 GHz), using different array configurations (Irwin et al. 2012). Many galaxies of this sample show extended linear polarization in their halos. RM synthesis of these galaxies revealed for the first time large-scale RM patterns in halos, implying, together with the vectors of linear polarization, the existence of regular halo magnetic fields with scales ≥ 800 pc (see Fig. 1, left). In the upper halo of NGC 4631 the regular magnetic fields seem to form large-scale helical magnetic loops (Mora-Partiarroyo et al. 2019). The regular fields in the halo may be former disk fields that were transported into the halo by galactic winds (see below).

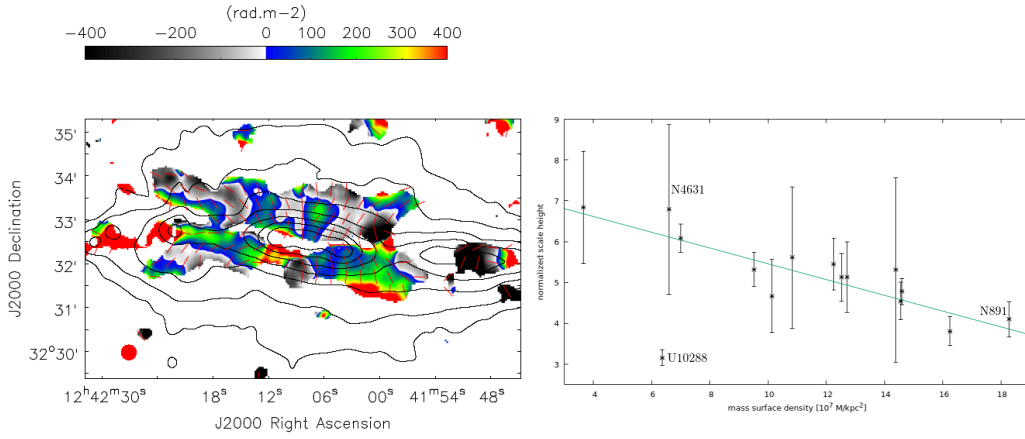


Figure 1. (Left): Distribution of Faraday depth obtained from C-band (D-array) data, overlaid with intrinsic magnetic field vectors, with an angular resolution of $20.5''$ HPBW (Mora-Partiarroyo et al. 2019). (Right): Normalized scale heights in C-band vs. mass surface density.

2. CR propagation in the halo

The halos of spiral galaxies, as the interface between the galactic disk and the IGM, are formed of gas, dust, cosmic rays, and magnetic fields. Their total radio continuum emission is dominated by synchrotron emission due to cosmic ray (CR) electrons in the halo magnetic field. CRs are regarded to be accelerated by supernova shock fronts in the galactic disk. The shape and extent of a radio halo is related to CR propagation (diffusion or advection) from the galactic disk and CR energy losses (synchrotron losses), where the vertical scale height of the radio emission is an important parameter to distinguish between the different processes.

We determined the radio scale heights in C- and L-band in a consistent way for a CHANG-ES subsample of 13 galaxies (smaller than $5'$), having carefully checked for missing spacings effects (Krause et al. 2018). The sample average value for the radio scale heights of the halo are 1.1 ± 0.3 kpc in C-band and 1.4 ± 0.7 kpc in L-band.

We discovered that the radio scale heights h depend mainly on the radio diameter d of the galaxy, implying that smaller galaxies are more spherical in radio emission than larger galaxies. The (absent) frequency dependence of the normalized scale heights \tilde{h} (defined as $100 \cdot h/d$) led us to the conclusion that the sample galaxies are escape-dominated with advective CR propagation, indicating the existence of galactic winds in many spiral galaxies. We could not find any dependence of h or \tilde{h} on star formation rate (SFR) or SFR density, and hence confirmed that the radio scale heights are not simply dictated by star formation in the disk. Moreover, we detected a tight correlation of \tilde{h} with the mass surface density of the galaxies, and hence for a gravitational influence on the CR outflows. This could recently be confirmed also for larger galaxies like NGC 4631 (Mora-Partiarroyo et al. 2019), and NGC 891 (Schmidt et al. 2019), presented together with the CHANG-ES subsample of 13 galaxies (Krause et al. 2018) in Fig. 1, right.

References

- Irwin, J., Beck, R., Benjamin, R.-A., et al. 2012, *AJ*, 144, 44
 Krause, M., Irwin, J., Wiegert, T., et al. 2018, *A&A*, 611, A72
 Mora-Partiarroyo, S.C., Krause, M., Basu, A., et al. 2019, *A&A*, submitted
 Schmidt, P., Krause, M., Heesen, V., et al. 2019, *A&A*, submitted

Magnetic field constraint in the outskirts of spiral galaxies

Ericson Lopez^{1,2} Jairo Armijos¹ Mario Llerena¹ Franklin Aldaz¹

¹Quito Astronomical Observatory, National Polytechnic School,
Box 17-01-165 Quito, Ecuador
email: ericsson.lopez@epn.edu.ec

²Physics Department, Sciences Faculty, National Polytechnic School,
Box 17-01-2759 Quito, Ecuador

Abstract. Based on CO(2-1) public data, we study the monoxide oxygen gas excitation conditions and the magnetic field strength of NGC 2841, NGC 3077, NGC 3184, NGC 3351 spiral galaxies. For their galaxy outskirts, we found kinetic temperatures in the range of 35–38 K, CO column densities $10^{15} - 10^{16} \text{ cm}^{-2}$ and H₂ masses of $4 \cdot 10^6 - 6 \cdot 10^8 M_{\odot}$. An H₂ density 10^3 cm^{-3} is suitable to explain the 2 sigma upper limits of the CO(2-1) line intensity. We constrain the magnetic field strength for our sample of spiral galaxies and their outskirts, evaluating a simplified expression of the magneto-hydrodynamic force equation. Our estimations provide values for the magnetic field strength in the order of 6–31 μG .

Keywords. galaxies: halos, galaxies: magnetic fields, galaxies: spiral.

1. Introduction

In this work, we study the magnetic field strength in the outskirts of four spiral galaxies: NGC 2841, NGC 3077, NGC 3184, NGC 3351, following a different approach to those commonly based on Faraday rotation, dust polarization, synchrotron emission, and so on. To constrain the magnetic field strength of spiral galaxies we will follow the Dotson method (Dotson 1996), i.e., approaching the magneto-hydrodynamic force equation to derive a simple expression that let us to estimate the upper limit of the magnetic field. On the other hand, to estimate the density n and mass M of the sources, we use the carbon monoxide emission as a tracer for the molecular gas H₂ (Neininger et al. 1998). This is because H₂ is invisible in the cold interstellar medium, at temperatures around 10–20 K.

2. Treatment of Carbon Monoxide Data

To carry out this study we use public CO(2-1) data, first published by Leroy et al. (2009), data obtained with the IRAM 30 m telescope located in Spain. To derive n and M from the CO(2-1) data we have selected the spectra by choosing two positions; one located in the nucleus and the second located on the outskirts of the galaxy.

3. Magnetic fields in the galaxies and their outskirts

Gaussian fits to the CO(2-1) lines have been performed. Then, the Large Velocity Gradient (LVG) modeling (van der Tak et al. 2007) is employed to estimate the gas density (n), based on the CO(2-1) line width (ΔV) and the line intensity (I). To estimate CO integrated luminosity (L_{CO}), we use the inner ellipse for the nuclear

Galaxy name	Region	L_{CO} $\times 10^6 \text{ K km s}^{-1} \text{ pc}^2$	r kpc	M_{H_2} $\times 10^7 M_\odot$	$(M_{H_2}+M_{HI})$ $\times 10^8 M_\odot$	B μG
NGC 2841	disk	2.0	8.5	103.0	89.6	$\lesssim 31$
	outskirts
NGC 3077	disk	2.3	0.4	1.3	0.4	$\lesssim 6$
	outskirts	$\lesssim 0.7$	0.8	$\lesssim 0.4$	$\lesssim 0.1$	$\lesssim 7$
NGC 3184	disk	188.0	6.6	103.0	36.8	$\lesssim 14$
	outskirts	$\lesssim 81.1$	13.2	$\lesssim 44.6$	$\lesssim 15.9$	$\lesssim 19$
NGC 3351	disk	226.0	7.1	124.0	32.1	$\lesssim 11$
	outskirts	$\lesssim 109.0$	14.2	$\lesssim 59.8$	$\lesssim 15.5$	$\lesssim 15$

Table 1. Parameters derived for the galaxy sample

region (the L_{CO} will be used later to estimate H_2 masses). To constrain the magnetic field strength for a given galaxy and its outskirts, we use the expression $B < 3.23 \times 10^{-8} \left(\frac{R}{pc}\right)^{0.5} \left(\frac{n}{cm^{-3}}\right)^{0.5} \left(\frac{M}{M_\odot}\right)^{0.5} \left(\frac{r}{pc}\right)^{-1}$ given by Dotson (1996). This relation includes the n_{H_2} , the mass M and radius r of the galaxy, and the radius of curvature R of the magnetic field lines. The n_{H_2} and M were derived using observational data, however the mass that we use here is referred to the dust mass which is obtained by the relation $(M_{H_2}+M_{HI})/100$, i.e. assuming the typical dust-to-gas mass ratio of 0.01. The molecular hydrogen mass (M_{H_2}) for the galaxy disk and its outskirts is derived using the relation $\frac{M_{H_2}}{M_\odot} = 5.5 \frac{R_{21}}{0.8} \left(\frac{L_{CO}}{K km s^{-1} pc^2}\right)$ given by Leroy et al. (2009), where R_{21} is the CO(2-1)/CO(1-0) line intensity ratio equal to 0.8 and L_{CO} is the CO luminosity. In this relation, a CO(1-0)/ H_2 conversion factor of $2 \times 10^{20} \text{ cm}^{-1} (\text{K km s}^{-1})^{-1}$ has been adopted (Leroy et al. 2009).

4. Discussion and Conclusions

In the present contribution, we have estimated the magnetic field strength in the galaxy nuclei and in the outskirts of NGC 2841, NGC 3077, NGC 3184, NGC 3351 spiral galaxies. For that, we have used an approximated expression of the magneto-hydrodynamics to find an upper limit for the magnetic field magnitudes. The magnetic field strength lies within the range of $\lesssim 6-31 \mu\text{G}$, which are in good agreement with the values provided by other author for spiral galaxies. A first good idea about the strength of the magnetic field is possible to obtain directly from the estimation of molecular hydrogen mass and radio of the source, without the necessity of a magneto-hydrodynamic model or using a traditional technique like Faraday rotation or Zeeman line broadening. This is a rough estimation that works if the gas pressure is uniform and the viscosity is neglected. A better approach can be obtained keeping more term in the magneto-hydrodynamics force equation (Dotson 1996) to impede gravitational collapse.

References

- Dotson, J. L. 1996, *ApJ*, 470, 566
 Neininger, N., Gulin, M., Ungerechts, H., et al. 1998, *Nature*, 1998, 395, 871-873
 Leroy, A. K., Walter, F., Bigiel, F., et al. 2009, *ApJ*, 2009, 137, 4670-4696
 Van der Tac, F. F. S.; Black, J. H.; Schier, F. L., et al. 2007, *A&A*, 468, 2, 627-635

The CHANG-ES Galaxy NGC 4666

Yelena Stein^{1,2}, Ralf-Jürgen Dettmar², Judith Irwin³ and the
CHANG-ES Team

¹Observatoire astronomique de Strasbourg, Université de Strasbourg, CNRS, UMR 7550, 11
rue de l'Université, 67000 Strasbourg, France; email: yelena.stein@astro.unistra.fr

²Fakultät für Physik und Astronomie, Astronomisches Institut, 44780 Bochum, Germany;
email: dettmar@astro.rub.de, *presenting author*

³Dept. of Physics, Engineering Physics, & Astronomy, Queen's University, Kingston, Ontario,
Canada, K7L 3N6

Abstract. We investigate the radio continuum radiation of the edge-on spiral galaxy NGC 4666 from the 'Continuum Halos in edge-on spiral galaxies - an EVLA survey (CHANG-ES)'. The radio data in two frequencies (6 GHz, C-band and 1.5 GHz, L-band) are used to analyze the magnetic field structure and the transport processes of the cosmic ray electrons.

Keywords. galaxies: magnetic fields, galaxies: spiral, galaxies: starburst, galaxies: halos, radio continuum: galaxies

1. Introduction

Synchrotron radiation in the radio continuum of edge-on spiral galaxies allow us to determine the magnetic field structure and distribution of the disk and the halo. Additionally, by analyzing the synchrotron intensity, the transport processes of cosmic rays into the halo of edge-on spiral galaxies can be investigated. Here we present first results for the edge-on spiral galaxy NGC 4666 with CHANG-ES radio data. These data will be analyzed in Stein et al. (submitted) in more detail. The CHANG-ES sample contains 35 edge-on spiral galaxies observed with the JVLA in B-, C- and D-configuration in C- and L-band (see e.g. Wiegert et al. 2015). NGC 4666 is a frequently studied starburst galaxy (Lehnert & Heckman 1996) and considered a superwind galaxy with a prominent X-ray halo (Dahlem et al. 1997, Tüllmann et al. 2006).

2. Synchrotron polarizaton

The orientation of the polarized emission follow an X-shaped magnetic field pattern (see Fig. 1), as visible in many edge-on spiral galaxies (Tüllmann et al. 2000), which shows mostly disk parallel vectors within the disk and vertical field components in the halo.

3. 1-D cosmic ray transport model

Transport processes of cosmic ray electrons into the halo (perpendicular to the galaxy disc) are derived using a 1-D cosmic ray transport model with the program SPINNAKER (Heesen et al. 2016, 2018). We used an interactive PYTHON wrapper (Spinteractive, by A. Miskolczi) to apply the model to the non-thermal radio maps. The thermal/non-thermal separation was executed following Vargas et al. (2018). Using SPINNAKER, we find a good solution for advection with an advection speed of 310 km/s, which is a little

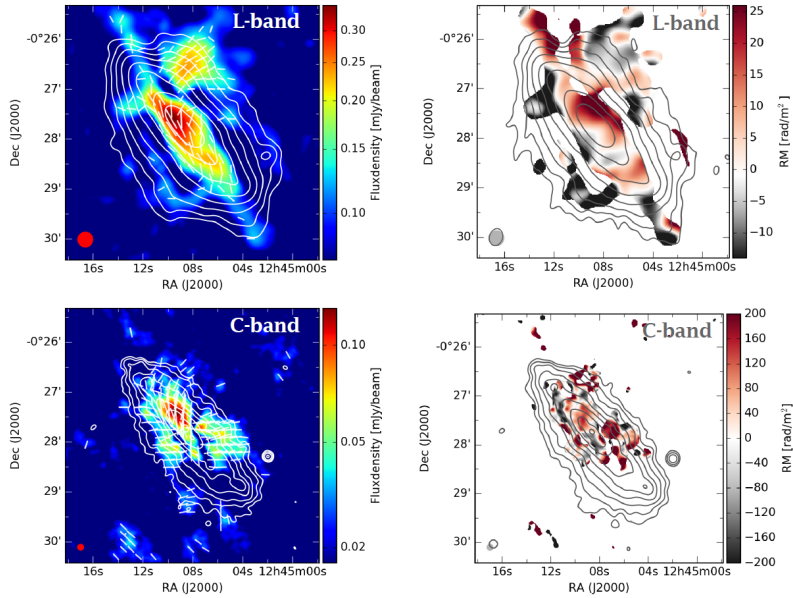


Figure 1. Left column: resulting polarization maps (polarized intensity in color on Stokes I contours and orientation of the polarized emission) from rotation measure synthesis (RM-synthesis). Right column: resulting rotation measure (RM) maps, which represent a measure for the direction of the magnetic field along the line of sight.

higher than the escape velocity. This results and further discussions will be presented in Stein et al. (submitted).

4. Possible magnetic field reversals in the disk field

The analysis of the RM map from C-band indicates magnetic field reversals in the disk field of NGC 4666 (Stein et al. submitted). The analysis of RM values in a rectangular box on the RM map shows in the inner disk the approaching side of the galaxy shows mainly positive RM values, the receding side shows mainly negative RM values. This behavior is expected for the axisymmetric case ($m=0$) with magnetic field vectors pointing inwards. For larger radii ($> 30''$) this behavior of the RM values change into the opposite. The approaching side shows mainly negative RM values whereas the receding side shows mainly positive values. This indicates an axisymmetric field pointing outwards. A sinusoidal fit was applied separately to both sides with a resulting comparable scale length of $75'' \pm 10''$.

References

- Dahlem, M., Petr, M. G., Lehnert, M. D., Heckman, T. M., & Ehle, M. 1997, *A&A*, 320, 731
 Heesen, V., Dettmar, R.-J., Krause, M., Beck, R., & Stein, Y. 2016, *MNRAS*, 458, 332
 Heesen, V., Krause, M., Beck, R., et al. 2018, *MNRAS*, 476, 158
 Lehnert, M. D. & Heckman, T. M. 1996, *ApJ*, 472, 546
 Stein, Y., Dettmar, R.-J., Irwin, J., et al. submitted, *A&A*
 Tüllmann, R., Dettmar, R.-J., Soida, M., Urbanik, M., & Rossa, J. 2000, *A&A*, 364, L36
 Tüllmann, R., Pietsch, W., Rossa, J., Breitschwerdt, D., & Dettmar, R. 2006, *A&A*, 448, 43
 Vargas, C. J., Mora-Partiarroyo, S. C., Schmidt, P., et al. 2018, *ApJ*, 853, 128
 Wiegert, T., Irwin, J., Miskolczi, A., et al. 2015, *AJ*, 150, 81

Faraday rotation from magnetic fields in young galaxies

Sharanya Sur

Indian Institute of Astrophysics, 2nd Block Koramangala, Bangalore - 560034, India
email: sharanya.sur@iiap.res.in

Abstract. In the recent past, Mg II absorption systems probed by a number of authors has revealed the existence of magnetic fields in young galaxies that are of comparable strength to those observed in nearby galaxies. In this contribution we argue that such strong fields can naturally arise due to *Fluctuation* dynamo action. Aided by numerical simulations, we then show that such dynamo generated fields are sufficiently coherent with the rms value of Faraday rotation measure (RM) of the order of 45 - 55 per cent of the value expected in a model where fields are assumed to be coherent on the forcing scale of turbulence. This yields a random RM $\sim 16 - 48 \text{ rad m}^{-2}$ in agreement with observational estimates from Mg II absorption systems. Our results can thus account for the observed RMs in young galaxies.

Keywords. galaxies : high-redshift, magnetic fields, MHD, turbulence

1. Introduction

Mg II absorption systems probed by Bernet *et al.* (2008, 2010), Farnes *et al.* (2014), and Joshi & Chand (2013) reveal that galaxies out to redshifts $z \sim 1$ are magnetized with μG strength fields, comparable to those observed in nearby galaxies. The origin of such strong magnetic fields at an epoch when the Universe was only $\sim 6 \text{ Gyr}$ old remains a challenge. It is plausible that these fields are generated by *Fluctuation* dynamos (Kazantsev 1968) - a process by which weak seed magnetic fields embedded in a conducting fluid are amplified exponentially fast (on eddy-turnover time scales $\sim 10^7 \text{ yr}$ in galaxies) by random stretching of the field lines by turbulent eddies. In the context of young galaxies, the ability of the dynamo to amplify fields on such short time scales together with the fact that its excitation only requires a critical $\text{Rm}_{\text{cr}} \sim (100 - 300)$ makes them an ideal candidate for generating and maintaining fields in these objects. However, from the observational point of view it is crucial to explore if the saturated fields generated by the dynamo are coherent enough and the extent to which the Faraday rotation measure (RM) obtained from such fields compares with observational estimates from Mg II absorption systems. Furthermore, the interstellar medium (ISM) in young galaxies is highly compressible and fields generated by the fluctuation dynamo are intermittent in nature. It is then natural to ask how sensitive is the RM to regions of different field strengths and densities? These issues form the subject of our discussion here.

2. Results

To address our objectives, we adopt a numerical approach focussing on simulations of fluctuation dynamo action in non-helicity forced turbulence using the FLASH[†] code (Fryxell *et al.* 2000). For more details on the setup and initial conditions we refer the reader to Sur *et al.* (2018). Apart from revealing evidence of turbulent stretching, the density snapshots in Fig. 1 (left image, top row) shows the effects of compressibility while field structures (bottom row) appear to be intermittent and less space filling. These 3D volumes are to be thought of as representing a local patch of the ISM containing a few turbulent cells. Since, the fields generated by the fluctuation dynamo are statistically

[†] <http://flash.uchicago.edu/site/flashcode/>

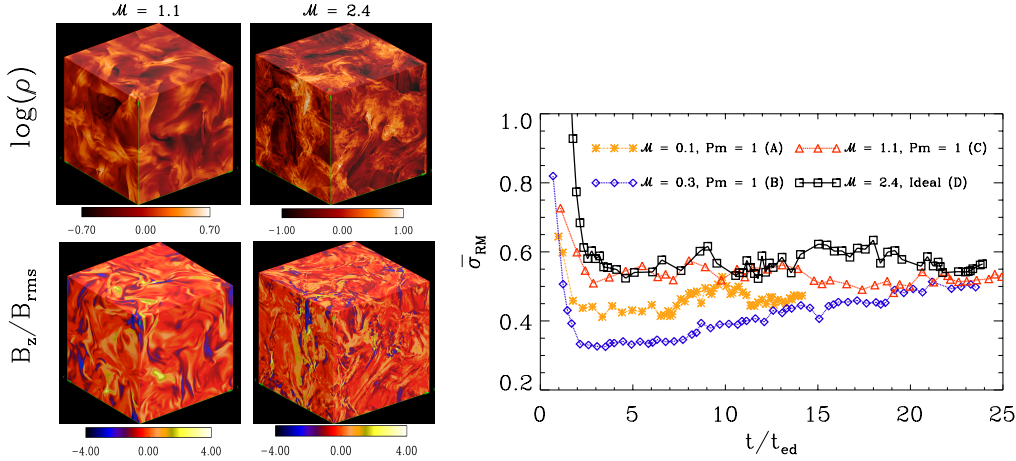


Figure 1. **Left** : 3D volume rendering of the density (top row) and the B_z/B_{rms} (bottom row) for a transonic and supersonic run in the nonlinear phase. **Right** : Evolution of $\bar{\sigma}_{\text{RM}}$ as a function of t_{ed} . See Sur *et al.* (2018) for more details.

isotropic, the mean RM is zero. Therefore, to probe the degree of coherence of the field we compute the time evolution of the normalized standard deviation of RM, $\bar{\sigma}_{\text{RM}} = \sigma_{\text{RM}}/\sigma_0$ by shooting $3N^2$ lines-of-sight (LOS) through these volumes (right plot in Fig. 1). Here σ_0 is the standard deviation of RM obtained by assuming the random magnetic fields to be coherent on the forcing scale of turbulence and N is the number of grid points in each dimension. We find that irrespective of the compressibility of the flow, $\bar{\sigma}_{\text{RM}} = 0.45 - 0.55$ in the saturated state. This implies that the fluctuation dynamo generated fields are sufficiently coherent to obtain a significant amount of RM. The dominant contribution to the RM in the transonic case comes from the general sea of volume filling fields while in the supersonic case, strong field regions as well as moderately over dense regions contribute significantly to the RM (Sur *et al.* 2018).

3. Discussion and Conclusions

Our results show that up to $\mathcal{M} = 2.4$ probed here $\bar{\sigma}_{\text{RM}} = 0.45 - 0.55$ in the saturated state, independent of the Mach number of the flow. Such values of $\bar{\sigma}_{\text{RM}}$ lead to a random RM $\sim 16 - 48 \text{ rad m}^{-2}$ for sightlines passing through the disk. While Faraday RM probes the LOS magnetic field, synchrotron emissivity and its polarization are also useful tracers of magnetic fields in the plane of sky. In a future work, we plan to extend our analysis by exploring these observables which together with the Faraday RM are indispensable for stitching a complete picture of magnetic fields in young galaxies.

Acknowledgements

I thank Pallavi Bhat and Kandaswamy Subramanian for collaborations and discussions.

References

- Bernet, M.L., et al., 2008, *Nature*, 454, 302
- Bernet, M. L., Miniati, F., Lilly S. J., 2010, *ApJ*, 711, 380
- Farnes, J. S., O’Sullivan, S. P., Corrigan, M. E., Gaensler, B. M. 2014, *ApJ*, 795, 63
- Fryxell B., et al. 2000 *ApJS*, 131, 273
- Joshi, R., & Chand, H. 2013 *MNRAS*, 434, 4
- Kazantsev, A. P. 1968 *Sov. J. Exp. Theor. Phys.*, 26, 1031
- Sur, S., Bhat, P., & Subramanian, K. 2018 *MNRAS* (Letters), 475, 1